LES SOFTWARE FOR THE DESIGN OF LOW EMISSION COMBUSTION SYSTEMS FOR VISION 21 PLANTS

Final Report for

October 2000 – December 2004

by
Clifford E. Smith
Steven M. Cannon
Virgil Adumitroaie
David L. Black
Karl V. Meredith

January 2005 **CFDRC Report No. 8321/17**

Contract No.: DE-FC26-00NT40975

submitted to

AAD Document Control, M/S 921-107
National Energy Technology Center
U.S. Department of Energy
P.O. Box 10940
Pittsburgh, PA 15236

Technical Monitor: Mr. Norman T. Holcombe
Contract Monitor: Ms. Crystal Sharp

CFD Research Corporation www.cfdrc.com
215 Wynn Drive • Huntsville, Alabama 35805 • Tel: (256) 726-4800 • FAX: (256) 726-4806 • info@cfdrc.com

DISCLAIMER

ABSTRACT

In this project, an advanced computational software tool was developed for the design of low emission combustion systems required for Vision 21 clean energy plants. Vision 21 combustion systems, such as combustors for gas turbines, combustors for indirect fired cycles, furnaces and sequestrian-ready combustion systems, will require innovative low emission designs and low development costs if Vision 21 goals are to be realized. The simulation tool will greatly reduce the number of experimental tests; this is especially desirable for gas turbine combustor design since the cost of the high pressure testing is extremely costly. In addition, the software will stimulate new ideas, will provide the capability of assessing and adapting low-emission combustors to alternate fuels, and will greatly reduce the development time cycle of combustion systems.

The revolutionary combustion simulation software is able to accurately simulate the highly transient nature of gaseous-fueled (e.g. natural gas, low BTU syngas, hydrogen, biogas etc.) turbulent combustion and assess innovative concepts needed for Vision 21 plants. In addition, the software is capable of analyzing liquid-fueled combustion systems since that capability was developed under a concurrent Air Force Small Business Innovative Research (SBIR) program. The complex physics of the reacting flow field are captured using 3D Large Eddy Simulation (LES) methods, in which large scale transient motion is resolved by time-accurate numerics, while the small scale motion is modeled using advanced subgrid turbulence and chemistry closures. In this way, LES combustion simulations can model many physical aspects that, until now, were impossible to predict with 3D steady-state Reynolds Averaged Navier-Stokes (RANS) analysis, i.e. very low NO_x emissions, combustion instability (coupling of unsteady heat and acoustics), lean blowout, flashback, autoignition, etc. LES methods are becoming more and more practical by linking together tens to hundreds of PCs and performing parallel computations with fine grids (millions of cells). Such simulations, performed in a few weeks or less, provide a very cost-effective complement to experimental testing. In 5 years, these same calculations can be performed in 24 hours or less due to the expected increase of computing power and improved numerical techniques.

This project was a four-year program. During the first year, the project included the development and implementation of improved chemistry (reduced GRI mechanism), subgrid turbulence (localized dynamic), and subgrid combustion-turbulence interaction (Linear Eddy) models into the CFD-ACE+ code. University expertise (Georgia Tech and University of California, Berkeley) was utilized to help develop and implement these advanced submodels into the unstructured, parallel CFD flow solver, CFD-ACE+. Efficient numerical algorithms that rely on *in situ* look-up tables or artificial neural networks were implemented for chemistry calculations. In the second year, the combustion LES software was evaluated and validated using experimental data from lab-scale and industrial test configurations. This code testing (i.e., alpha testing) was performed by CFD Research Corporation's engineers. During the third year, six industrial and academic partners used the combustion LES code and exercised it on problems of their choice (i.e., beta testing). Final feedback and optimizations were then implemented into the final release (licensed) version of the combustion LES software to the general public.

An additional one-year task was added for the fourth year of this program entitled, "LES Simulations of SIMVAL Results." For this task, CFDRC performed LES calculations of selected DoE SIMVAL cases, and compared predictions with measurements from NETL. In addition to comparisons with NO_x and CO exit measurements, comparisons were made to measured pressure oscillations. Potential areas of improvement for combustion and turbulence models were identified.

In conclusion, this program advanced the state-of-the-art in combustion LES analysis, providing a software tool for more accurate analysis as well as the capability of assessing transient combustion events. Some lessons learned (and opinions by the authors) include:

1. Ways to reduce run times are needed before LES can be a practical design and analysis tool. Possible ways to reduce run times include higher order spatial differencing (fourth order or higher on unstructured grids) and adaptive meshing;
2. Chemistry using J.Y. Chen's mechanisms are very accurate, but are too expensive even with ISAT. It is our belief that the chemistry can be simulated using 5-10 step mechanisms with Arrhenius rates, tuned to the conditions of interest. We are currently developing a chemical reactor modeling (CRM) tool that automatically calculates global mechanisms using a detailed chemical mechanism as a starting point. Multiple reactor options are available, including perfectly stirred and/or plugged flow reactors, laminar 1D flame profiles, and opposed diffusion flame.
3. Near-wall models (both velocity and thermal) are needed for practical LES calculations (resolution down to the wall is not practical). CFDRC is developing such models in a Navy Phase II SBIR project.
4. Automatic load balancing is a necessary future in LES calculation with massive parallelization. Parallel division based on number of cells per processor result in significant under usage of certain processors because of stiff kinetics and/or spray.
5. Data storage and processing of data is a large issue. The generation of movies tends to be difficult because large files of data must be manipulated.
6. Pre- and post-processing is a large issue as grids continue to get larger. Parallelization and distributed architecture is needed for pre- and post-processing software.

TABLE OF CONTENTS

LIST OF FIGURES

Page

LIST OF TABLES

1. INTRODUCTION

1.1 Significance of Software

The advanced computational modeling software developed in this DOE project is a supporting technology for the design of Vision 21 plant combustion subsystems. The software focused on the analysis of Vision 21 plant subsystems that burn gaseous fuels such as natural gas, syngas, hydrogen, biogas, etc. In addition, the software is able to address liquid fueled combustion systems since a companion Air Force Phase II SBIR on liquid-fueled combustion has been completed. Combustion systems are important subsystems of the Vision 21 plant, such as combustors in a gas turbine, combustors for indirect fired cycles, furnaces, and sequestrian-ready combustion systems that use oxygen enrichment and CO_2 recycle in order to produce concentrated CO_2 exhaust streams. All of these combustion systems require near-zero NO_x and CO emissions in order to meet Vision 21 plant goals, meaning new, innovative concepts must be developed in a cost-effective manner.

In the past, relatively few combustion designs could be studied and experimentally tested due to the excessive expense of combustion testing. Using today's design/analysis tools, many innovative designs needed for the Vision 21 plant will remain on the drawing board, and only incremental improvements may be realized. The cost of testing gas turbine combustors is especially expensive since Vision 21 plant thermal efficiency goals will require higher pressure ratio engines, and the cost of test facility time grows more than linearly with engine pressure ratio. In addition, combustion instability, seen in most low emissions combustors, is usually not detected until engine testing, and results in excessive test costs to correct, usually at the expense of increasing emissions.

What was needed, and developed in this program, is a new, reliable analysis tool for the design of combustion systems that will significantly reduce development costs. With such a tool, new combustor designs can be easily studied, and only the best designs selected for experimental testing. In addition, since the analysis tool is able to assess various fuels, the effect of fuel type on combustor performance can be easily assessed. This will greatly reduce the test costs to ascertain what gas compositions are suitable for a given combustor design. The software will help to reduce the time-cycle from inception to production, permitting the development of new combustion systems in time to meet Vision 21 timetable goals.

Although the combustion LES code can aid in the design of Vision 21 combustion systems, it will also have utility in the design of other Vision 21 components and subsystems that need time-accurate, unsteady analysis. Some of these components include gas turbine turbomachinery, heat exchangers (to correctly calculate convective heat transfer), cyclone separators, etc.

1.2 Comparison of Current CFD Analysis and LES Analysis

In this project, CFD Research Corporation (CFDRC) developed and validated combustion Large Eddy Simulation (LES) software to design and analyze combustion systems. Combustion LES is the latest CFD methodology for turbulent-reacting flows, providing accuracy and reliability not available from current CFD methods. Current CFD analysis consists of 3D Reynolds Averaged

Navier Stokes (RANS) calculations that use two-equation k-ε models for turbulence, and very simplified chemistry for heat release. The unsteady motions that govern mixing (i.e. countergradient diffusion) cannot be captured by the k-ε turbulence model. Two-step and four-step chemistry (with five or fewer species) is not sufficient to model the minor species that contribute to prompt and nitrous NO_x, autoignition/flashback and lean blowout. With current RANS codes, the effect of turbulence-combustion interaction is approximated by the Eddy Break Up (EBU) or Eddy Dissipation models (Spalding, 1977) which assume the reaction is controlled by either mixing or chemistry, but never a combination of the two. NO_x and CO emissions are very difficult to predict, especially for new designs at sub-10 ppmv levels.

Some manufacturers use RANS simulations to help guide their design efforts, but they only look for relative trends and overall guidance. A typical RANS calculation (Hammer and Roby, 1997) is presented in Figure 1, along with a table showing predicted and measured emissions. It can be seen that agreement is good qualitatively, but the quantitative agreement is not very good. Many manufacturers are highly skeptical of RANS predictions (especially for the prediction of very low emissions), and prefer the expensive "build and bust" experimental approach, meaning innovative designs are seldom explored. The issue of combustion instability, a common occurrence in lean, premixed combustion systems, cannot be assessed by steady-state RANS methods. Likewise, the prediction of lean blowout and autoignition/flashback is not possible.

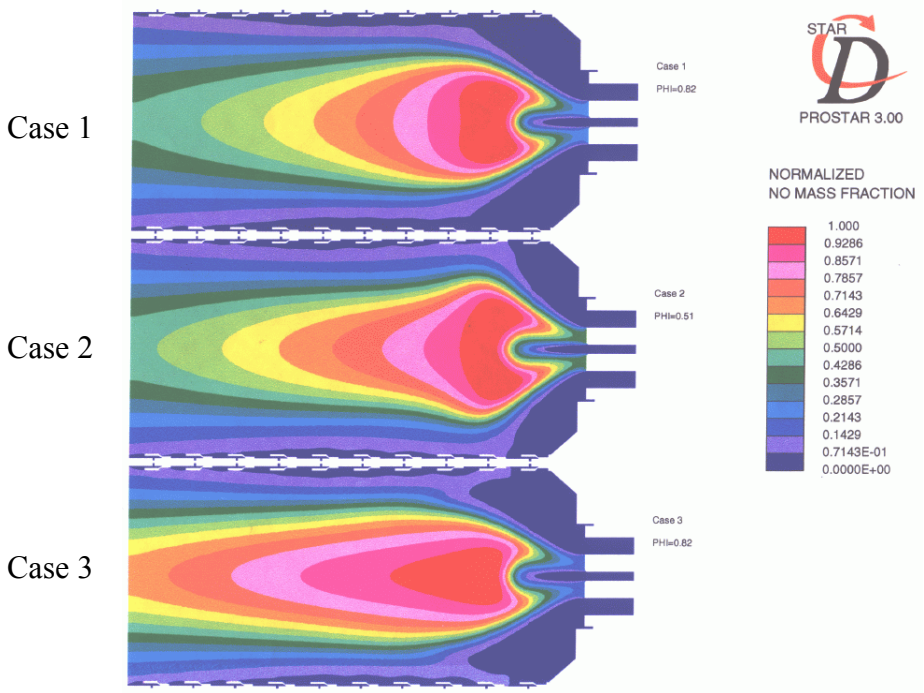

Figure 1. Predicted NO_x Contours of Solar Injector Using 2D RANS Code (StarCD); Three Flow Conditions Are Simulated (Hamer and Roby, 1997)

Table 1. Measured versus Predicted Emissions (Hamer and Roby, 1997)

	Case 1	Case 2	Case 3
Equivalence Ratio	0.63	0.51	**0.82**
Maximum Temperature (K)	1797	1563	**2205**
Measured CO (ppmvd @ 15% O2)	2.39	896	1.42
Predicted CO (ppmvd @ 15% O2)	16.5	2644	22.1
Predicted to Measured CO Ratio	6.9	3.0	15.6
Measured NO (ppmvd @ 15% O2)	36.18	12.3	101.5
Predicted NO (ppmvd @ 15% O2)	26.5	1	950.4
Predicted to Measured NO Ratio	0.7	0.1	9.4
Measured CO2 (%)	3.14	2.44	4.47
Predicted CO2 (%)	3.35	2.27	4.84

The LES method resolves the large scale turbulence numerically, and uses more-universal models for subgrid turbulence and chemistry. This allows a more accurate representation of turbulence, kinetics, and turbulence-combustion interaction not attainable with RANS calculations. It also allows more detailed chemistry to be modeled, including the calculation of minor species needed for accurate prediction of NO_x and CO, lean blowout, and autoignition/flashback. A snapshot of a typical LES calculation performed by CFDRC for the DOE SIMVAL combustor is shown in Figure 2. It can be seen that fine structures in the flowfield are well captured, and the flowfield is much different than its steady-state RANS counterpart in Figure 3. LES methods accurately capture the coupling between unsteady heat release and system acoustics, thus predicting combustion dynamics and limit cycle pressure oscillations.

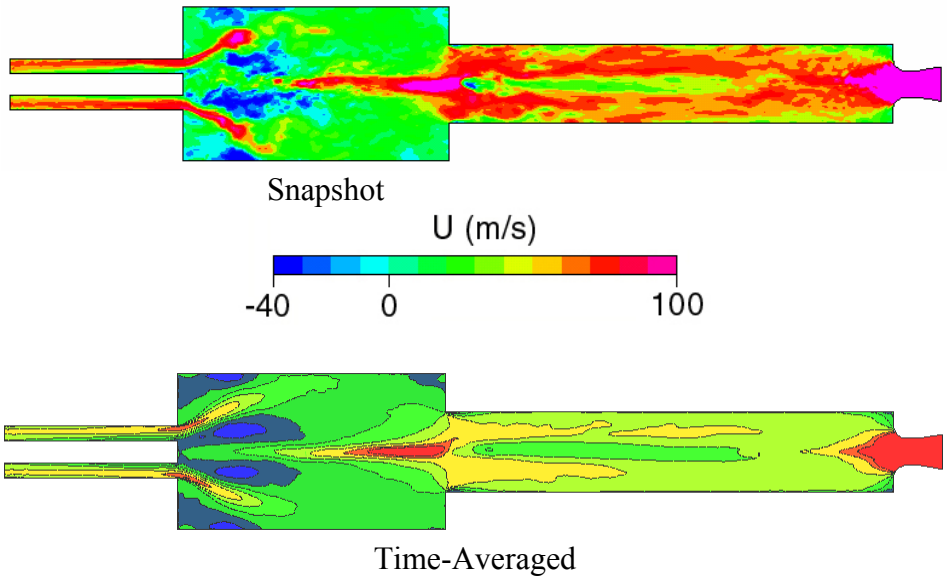

Figure 2. LES Calculation of SIMVAL Combustor, U-Velocity Contours

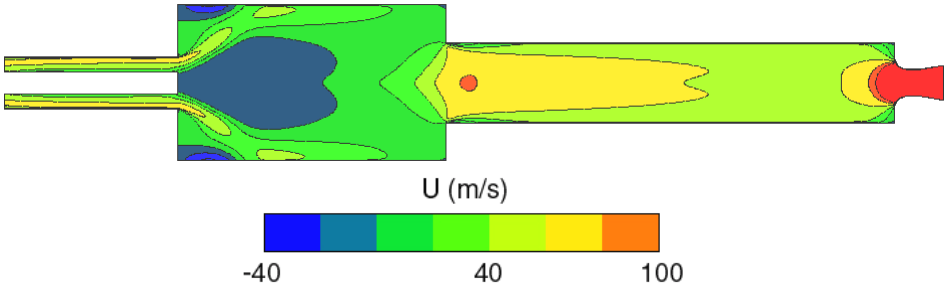

Figure 3. RANS Calculation of SIMVAL Combustor, U-Velocity Contours

Although it is commonly recognized that combustion LES is needed for accurate simulation of turbulent reacting flows, no commercial combustion LES code has been developed to date because of the computer power required for 3D LES. As computers become faster over the next 5-10 years, LES simulation will become feasible, and it will become the principal means of combustion analysis. In the past five years, there have been many aspects of LES methodology that have been developed; these include the development of new turbulence subgrid models, (i.e., Dynamic, Lagrangian Dynamic, etc.). Subgrid chemistry models, such as the Linear Eddy and Conditional Moment Closure, have been proposed for LES combustion methods. In this project, we implemented a number of these models into an advanced CFD code. In addition, we developed and implemented reduced chemistry models from detailed kinetic schemes so that important minor species are accurately predicted. Novel tabulation strategies such as Insitu-Adaptive Tabulation (ISAT) were utilized to allow efficient chemical kinetic solutions

1.3 Industrial Application of Software

The intent of this project was not only to develop reliable CFD software for combustor design, but to also transfer the technology and put the analysis tool to work in the design environment, i.e. the manufacturers of combustion systems for Vision 21 plants. To this end, a LES Combustion Consortium was established that brought together modelers, a software developer and combustor designers with the intent of developing a practical, useful design tool. Models were developed by two of the top university professors in the U.S. and their post-doctoral researchers (J.Y. Chen of University of California, Berkeley, and Suresh Menon of Georgia Tech), and then implemented into the commercial CFD-ACE+ code. The CFD-ACE+ code includes a user-friendly GUI, a grid generator (CFD-GEOM) for structured and unstructured meshes (tetrahedral, prism, and hexahedral cell types are supported), and a graphical post-processor (CFD-VIEW). Combustor designers from all of the U.S. industrial gas turbine companies plus interested manufacturers of burners/boilers were included in the consortium. The industrial partners not only provided guidance into what is needed to make the software practical and usable, but they also served as beta test sites in the development process. Six of the industrial partners exercised the software and performed analysis on relevant combustion systems.

In order for the software to be a practical design/analysis tool, calculations must be performed in a few days or less in this project, with the promise of further reduction in run time (less the eight hours) in the near future. Due to the large number of cells (few millions) required for LES calculations, parallel processing will be utilized. Tens to hundreds of PCs will be clustered

together to give the necessary computing power for practical application. According to Pope (1999), the speed of the fastest computers increases at the rate of a factor of 30 per decade. This expected increase in computing power will make one day or less LES calculations on practical cases a reality in approximately 5-10 years. In order to further reduce run time, LES calculations will only be performed in important locations (e.g. heat release locations, formation/destruction of NO_x/CO species, etc.) and not in nonreacting locations (i.e. upstream of the combustor, external flow around the combustor, etc.).

2. BACKGROUND INFORMATION

2.1 LES Methodology

It was predicted more than a decade ago (Collins and Voke, 1983) that large-eddy simulations (LES) will come to play an important role in modeling complex turbulent flows. Over the last several years, the progress in computer technology and the theoretical developments in turbulence modeling have expanded the envelope of feasible numerical simulations. The general trend at present throughout science and engineering is towards simulations of greater complexity and higher physical fidelity. However, present commercially available tools for simulations of turbulent flows are restricted to turbulence models based on Reynolds average closures, which provide far less information and value than full three-dimensional, time-dependent simulations. A computational environment that will enhance our understanding of the physical mechanisms involved in complex turbulent flows and that is available to the everyday computational fluid dynamics (CFD) user would be of great value.

There is a need for continuing developments of accurate analytical schemes for the numerical description of chemically reacting turbulent flows. Reynolds averaged methods (RANS) augmented by statistical closures (Libby and Williams, 1994) have been the primary means of predicting such flows. In fact, most current engineering predictive procedures are based on such models. In the late 1970s with rapid development of supercomputer technology and the increased number of users of such technology, the method of "direct numerical simulation" (DNS) was introduced into turbulent combustion research (Oran and Boris, 1981). This method has since gained significant popularity; however, within the past decade its limitations in dealing with practical combustion problems have been widely recognized (Givi, 1994). An approach which is regarded somewhere between the two methodologies, DNS and RANS, is large eddy simulation (LES) (Rogallo and Moin, 1984). The attractiveness of LES stems from the capability of this method to provide DNS-like data (large scale statistics) on a much coarser, less expensive grid (an order of magnitude less than the DNS required resolution).

2.2 Development/Implementation of LES Models

In most turbulent flows of practical interest, the motion on the order of the dissipation scale cannot be evaluated explicitly because the available computational resources fail to meet the severe mesh requirements imposed by the physics of the flow. In homogeneous flow simulations, for example, in order to obtain a resolved flow field the number of grid points to be considered is in the range of , where is the Reynolds number based on the Taylor microscale and the root mean square (rms) of velocity fluctuations. To overcome this serious limitation, the governing equations have to be altered in such a way that the activity at the level of unresolved scales is mimicked by a proper model, and only the large-scale fluctuations are explicitly computed. The rationale behind this approach is the fact that the primary momentum transport and turbulent diffusion are sustained by large-scale containing eddies.

A smoothing ("low pass") filter of constant kernel width certainly achieves the separation of scales, decomposing a given field into a resolved component and a residual component (also called sub-grid fluctuations). Compressibility is responsible for complicating the expression for

the governing equations. Straightforward filtering initiates numerous density correlations which are obscure to most modeling considerations. On the contrary, using the density weighted Favré filters, simplicity is attained at the expense of the clarity of physical interpretations for various Favré artifacts.

Operationally, the filtering is described by the convolution:

$$\bar{f}(x,t) = \int_D f(x',t)G(x-x',t,\Delta_f)dx' \tag{1}$$

where $\bar{f}$ represents the filtered value of the field variable f, G denotes the filter, which is a symmetric function with compact support and Δ_f is the filter width (assumed constant in the standard LES formulation). Several types of filters are encountered in the LES approach: the Gaussian filter, the box filter, the sharp-cutoff filter and high-order filters (Aldama, 1990; Najjar and Tafti, 1996; Sagaut and Grohens, 1999). In variable density flows, it is desirable to use Favré (density weighted) filtering:

$$\tilde{f} = \frac{\overline{\rho f}}{\bar{\rho}} \tag{2}$$

With the application of LES Favré averaging procedure to the governing transport equations (continuity, momentum, energy, mass fractions, respectively), we obtain:

$$\begin{aligned}
\frac{\partial \bar{\rho}}{\partial t} + \frac{\partial \bar{\rho}\tilde{u}_i}{\partial x_i} &= 0 \\
\frac{\partial \bar{\rho}\tilde{u}_j}{\partial t} + \frac{\partial \bar{\rho}\tilde{u}_i\tilde{u}_j}{\partial x_i} &= \frac{\partial \tilde{\tau}_{ij}}{\partial x_i} - \frac{\partial T_{ij}}{\partial x_i} \\
\frac{\partial \bar{\rho}\tilde{E}}{\partial t} + \frac{\partial \bar{\rho}\tilde{u}_i\tilde{E}}{\partial x_i} &= \frac{\partial \tilde{\tau}_{ij}\tilde{u}_i}{\partial x_i} - \frac{\partial Q_i}{\partial x_i} \\
\frac{\partial \bar{\rho}\tilde{\phi}_\alpha}{\partial t} + \frac{\partial \bar{\rho}\tilde{u}_i\tilde{\phi}_\alpha}{\partial x_i} &= -\frac{\partial J_i^{\tilde{\alpha}}}{\partial x_i} - \frac{\partial M_i^\alpha}{\partial x_i} - \tilde{\omega}_\alpha
\end{aligned} \tag{3}$$

The filtered equations contain unknown terms such as $\tilde{\tau}_{ij}$ (velocity-velocity correlation) arising from the filtering of nonlinear terms and are known as subgrid scale (SGS) stresses. The closure problem of turbulent flows is omnipresent and in the case of LES can be solved by providing models for the various subgrid scale correlations.

Given the complexity of the practical applications and the advanced capabilities of the CFDRC software, the question of establishing a rigorous LES framework for arbitrary grids has to be answered. We propose to follow the analysis of Ghosal and Moin (1995) in order to implement an LES formalism for non-Cartesian, finite volume, unstructured grids. In a flow with boundaries, the filter width must vary with position to reflect the changing length scales of the characteristic structures in the flow. The variability of the filter width invalidates the conventional derivation of the large-eddy equations written for convolution filters of fixed width. The conditions in which the filtering operation can commute with the operators of differentiation

are related to the accuracy of the numerical scheme. The errors of commutation are of second order, that is of the same order as the spatial discretization employed in CFD-ACE+.

The effect of the numerical scheme on the subgrid scale term has been investigated by several authors (Kravchenko and Moin, 1996; Najjar and Tafti, 1996; Salvetti and Beux, 1998). Although by the current wisdom it is recommended that LES be performed with higher-order schemes, recent studies show that good predictions can be obtained even with low order numerical discretizations, provided the Leonard term is taken into account (Salvetti and Beux, 1998). Of considerable concern is the importance of the truncation error as compared to the SGS term, but scale similarity models such as the one proposed in this project have been shown at least to reduce the modeling error, whereas the truncation error can be reduced by mesh refinement below the minimal mesh resolution for LES (Haworth and Jansen, 1996). Furthermore, LES of high Reynolds complex flows with high order schemes are not affordable presently. On the one hand complex domains cannot be discretized affordably with structured grids (for which cheap high order schemes are available), on the other hand affordable use of unstructured grids is limited to second order schemes. The multi-domain spectral/hp methods on unstructured grids bear great promise for simulating accurately complex geometry turbulent flows when Petaflop machines will be available (Karniadakis, 1999). However, in the mean time, we will be guided by the many successful LES studies done with second order numerical schemes equally on structured (Avva and Sundaram, 1998) and unstructured grids (Haworth and Jansen, 1996; Urbin and Knight, 1999).

SGS Models: The most popular model for engineering applications is arguably the Smagorinsky model (1963), where the eddy viscosity is proportional to the square of the grid spacing and the local strain rate. The constant of the model follows from an isotropy -of-the-small-scales assumption. The standard Smagorisky model gives interesting results in free-shear flows, but fails in the presence of the boundaries and is known for its excessive dissipation. Attempts to determine the model constant in a flow dependent fashion, have produced several generations of the dynamic model since the very interesting paper of Germano, et al. (1991). Using a double filtering technique, the constant arising in the Smagorinsky model is computed as a function of space and time. Problems arise due to local indeterminacies or excessive backscatter (the transfer of energy from the small scales to the large scales) leading to divergent solutions. One remedy has been determined to be the averaging in the directions of homogeneity, but this technique disqualifies the dynamic model for usage in computations of inhomogeneous flows (Lesieur and Metais, 1996).

A priori tests executed by Vreman et al. (1995) have shown that non-eddy viscosity models, e.g. the scale similarity model of Bardina et al, (1980), perform considerably better than the Smagorisky model. However, when implemented in LES, the models hardly dissipate any SGS energy and they have to be combined with an eddy-viscosity type model. Furthermore, several investigations on DNS turbulent fields (McMillan & Ferziger, 1980) have shown that the SGS stress and the large-strain rate tensors are not aligned, or in other words are not correlated, which casts a doubt on the validity of eddy-viscosity type SGS closures.

Given the current state of affairs, we propose to implement two SGS models which have been shown to produce good results in LES. The selective structure-function model (SSF), developed

by David (1993), is an extension of the structure-function model (Metais and Lesieur, 1992) for which

$$\tilde{\tau}_{ij} - \frac{\delta_{ij}}{3}\tau_{kk} = 2C_n\bar{\rho}\nu_t\left(\tilde{S}_{ij} - \frac{\delta_{ij}}{3}S_{kk}\right) - K\left(L_{ij}^m - \frac{\delta_{ij}}{3}L_{kk}^m\right) \quad (4)$$

where $\tilde{S}_{ij}$ is the resolved strain rate tensor, c_n=1., K=0 and ν_t is the eddy viscosity, expressed in terms of the local second-order velocity structure function of the filtered velocity field. The eddy-viscosity in the SSF mode is switched off when the flow does not exhibit sufficient three-dimensionality. When the angle between the vorticity at a given grid point and the average vorticity at the neighboring points exceeds 20 degrees, the eddy viscosity is turned on.

Another selected SGS model is the model of Salvetti and Banerjee (1995) in which the two model constants, C_n and K, are determined dynamically, using a test-filter whose width is set to twice the local grid spacing (volume). The model correlates with the resolved part of the SGS stress, the Leonard tensor $L_{ij}^m = \bar{\rho}\left(\tilde{u}_i\tilde{u}_j - \tilde{\tilde{u}}_i\tilde{\tilde{u}}_j\right)$. This model has been shown to give very high correlation coefficients between the exact and modeled SGS stresses and improves the agreement of LES with direct simulations. Corresponding closures will be employed for the subgrid scale heat and species fluxes.

An alternative closure of the LES momentum equation will be achieved using a new localized dynamic model (developed by Prof. Suresh Menon at Georgia Tech) for the subgrid kinetic energy (Menon, 1999) that has been developed to model the subgrid stresses without a priori specification of the "constants". Although this approach is acceptable for the momentum/energy closure (since the small scales primarily provide a dissipative mechanism for the energy transferred from the large scales), a similar (e.g., subgrid eddy diffusivity) method for the species equations is clearly inappropriate, since, for combustion to occur, the species must first undergo mixing at the small scales, and, then come into contact by molecular diffusion. Since the small scales are not resolved but are critical for the development of the chemical processes, ad hoc and global subgrid models cannot be used for chemical species.

The dependency of the subgrid models on the filter shape and filter discrete approximation have been analyzed in detail by Sagaut and Grohens (1999). They have shown that all the subgrid models exhibit a sensitivity on the discrete test filter, but for dynamical subgrid models the sensitivity is less pronounced. Following their recommendations, for this project we will use a 5-point discrete representation of the box filter, which was shown to produce the best accuracy in a priori tests on a von Karman spectrum.

2.3 Subgrid Chemistry Modeling

PDF Methods: Modeling of scalar fluctuations in RANS has been the subject of intense investigations since the pioneering work of Toor (1962).The aim of statistical moment methods is to provide a closure for these correlations in terms of the mean flow variables. An approach which has proven particularly useful is based on the probability density function (PDF) or the joint PDF of scalar quantities (Pope, 1985; Leonard, 1995). This approach offers the advantage

that all the statistical information pertaining to the scalar field is embedded within the PDF. Because of this feature, PDF methods have been widely used in RANS for a variety of reacting systems (see Dopazo, 1994 for a recent review). The systematic approach for determining the PDF is by means of solving the transport equation governing its evolution. In this equation the effects of chemical reaction appear in a closed form. However, modeling is needed to account for transport of the PDF in the composition domain of the random variables. In addition, there is an extra dimensionality associated with the composition domain which must be treated. An alternative approach is based on an assumed PDF in which the PDF is parameterized a priori in terms of its lower (usually the first two) moments. Obviously, this method is ad hoc but it offers more flexibility than the first approach. Presently the use of assumed methods in RANS is justified in cases where there is strong evidence that the PDF adopts a particular distribution. In spite of the demonstrated capabilities of PDF methods in RANS, their use in LES is limited. The first application of PDF-LES is due to Madnia and Givi in which the Pearson family of PDF's are used for modeling of the SGS reactant conversion rate in homogeneous flows under chemical equilibrium conditions. This procedure was also used later by Cook and Riley (1994) for LES of a similar flow. The extension of assumed PDF models for LES of nonequilibrium reacting shear flows (Figure 5) is reported by Frankel et al. (1993). While the generated results are encouraging, they do reveal the need for more systematic schemes. Most of the drawbacks of these schemes can be overcome by considering the "transport" of the PDF of the SGS variables directly.

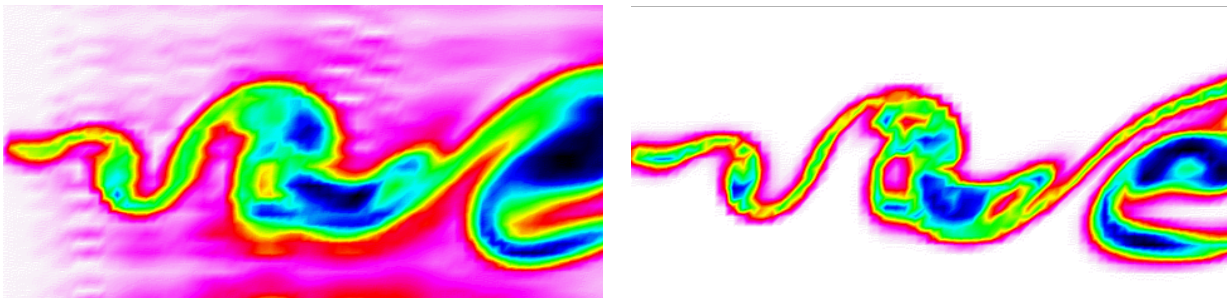

(a) (b)

Figure 5. Contour Plots of Product Mass Fraction From (a) LES and (b) Filtered DNS Results (Frankel et al., 1993)

Referring to the PDF method, the LES is facilitated by introducing the "filtered density function" (FDF), and by providing an effective numerical means to simulate this FDF. Because of the added dimensionality of the compositional variables, solution of the FDF transport equation by conventional finite difference numerical methods is possible in only the simplest of cases. The use of a Monte Carlo PDF method, combined with LES, has been attempted only recently by Givi and co-workers (Colucci et al., 1998). They computed a 3D reacting mixing layer with the Monte Carlo PDF method and using a laminar chemistry assumption. Figure 6 shows the time-variation of the product thickness using DNS and LES with the PDF and laminar subgrid chemistry models. The PDF method included the effects of subgrid fluctuations on the filtered reaction rate and provided a closer agreement with DNS than the laminar chemistry assumption. However, the computational costs associated with the LES-FDF method makes its use prohibitive in practical applications.

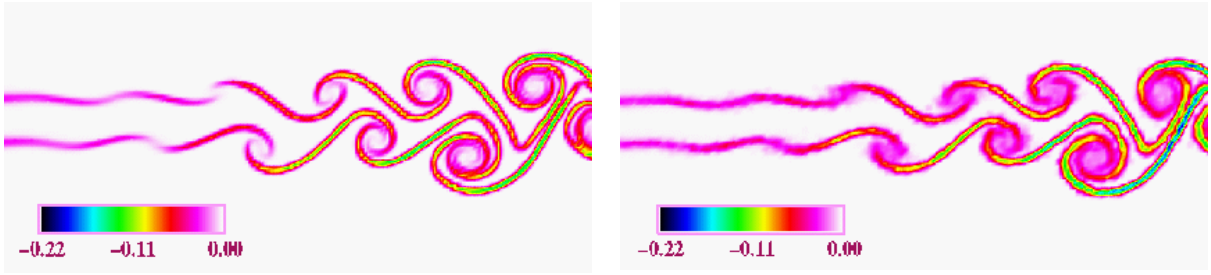

(a) (b)

Figure 6. Contours of the Instantaneous Subgrid Unmixedness for the Spatially Evolving Planar Jet, (a) DNS and (b) FDF (Colucci et al., 1998)

Linear Eddy Model: A less expensive alternative, compared to the LES-FDF method, is the use of the linear eddy model (LEM), developed by Kerstein (1988). The LEM is well suited as a subgrid chemistry model for LES since it provides an exact description of chemical kinetics and molecular diffusion at all length scales of the flow, while modeling the effects of turbulent advection. This is achieved by formulating the model in one spatial dimension. The reaction-diffusion equation for the species concentration is (Frankel et al., 1995):

$$\frac{\partial \phi}{\partial t} = D\frac{\partial^2 \phi}{\partial x^2} + \dot{w}_\phi \tag{5}$$

where ϕ is the species concentration, D is the molecular diffusion coefficient, and $\dot{w}_\phi$ represents the chemical source (sink) term. Turbulent stirring or convection is simulated by making random rearrangement events and the PDF for the size distribution (eddy sizes) must also be provided. Also, a particular rearrangement mapping must be chosen and Kerstein (1991) has shown the triplet map to capture features for high Reynolds number turbulence. As reviewed by Frankel et al. (1995), based on high Reynolds number scaling laws, it can be shown that the following relations must be satisfied (Kerstein, 1991):

$$\frac{L}{\eta} = \mathrm{Re}^{1/p} \tag{6}$$

$$f(l) = \frac{3-p}{L\left[\left(\frac{L}{\eta}\right)^{3-p} - 1\right]}\left(\frac{l}{L}\right)^{p-4} \tag{7}$$

$$\lambda = \frac{27}{3}\frac{p}{p-3}\frac{D\tau}{L^3}\frac{\left(\frac{L}{\eta}\right)^{3-p} - 1}{1-\left(\frac{\eta}{L}\right)^{p}} \tag{8}$$

where L is the integral scale of turbulence, is the Kolmogorov length scale, λ is the stirring frequency, and f(l) is the PDF for the size distribution (eddy size) of the segments of the flow to be rearranged. For high-Re flows, Kolmogorov scaling relations are obtained for p=4/3. McMurtry et al. (1992) have used the LEM as a chemistry subgrid model for a LES of a hydrogen-air diffusion flame. They showed the LEM allowed a realistic description of the scalar field at the smallest scales of the flow. Suresh Menon also has significant experience with the LEM approach.

It is worth reemphasizing that the LEM approach resolves the distinct processes of molecular diffusion and turbulent stirring. Thus, the salient features of small-scale turbulent combustion can be economically captured at high Re and for complex chemistry. To contrast this approach with PDF methods, there are no significant differences in the manner by which small-scale mixing is simulated in PDF and LEM approaches. As in PDF methods, detailed chemistry can be included in the LEM method without any closure problems. However, the key advantage of the subgrid LEM approach when compared to PDF methods is the ability to allow for the deterministic process of molecular diffusion process to continue while small-scale mixing and chemical reactions are occurring. In PDF methods, the scalar particles are discrete, stochastic elements that propagate in distinctly (and random) trajectories determined by the turbulent flow field. As a result, the PDF particles do not have a deterministic local structure which implies that local molecular diffusion process cannot be simulated (it is important to note that molecular diffusion CANNOT be modeled but must be simulated at the requisite time and spatial scales). The subgrid LEM approach addresses this issue by simulating scalar evolution within a deterministic domain (which allows for molecular diffusion effects) while at the same time incorporating the effects of stochastic small-scale mixing and chemical reactions.

Although the full LES-LEM implementation has some obvious advantages, for engineering applications some simplifications are feasible by using the look-up approach (which in turn would reduce the computational effort). In this approach, the LEM simulations for a range of turbulent scales can be carried out off-line for a given chemical mechanism and the data can be stored. This approach is similar to the ISAT approach proposed by Pope except that the table that is generated is for turbulent flow. Thus, in the proposed approach the ISAT capability will be extended to allow for turbulent scales thereby extending the capability of the simulation model. This implementation is proposed in this research for practical applications.

Employing this approach has significant practical advantage when used in LES codes. This is because the expensive chemistry calculation can be decoupled from the spatial flow solution (due to the above noted assumption that scalar decay in time can be used to mimic the spatial evolution of the scalar fields in the flow field). As a result, the PDF can be generated and tabulated once and for all (for a given chemical mechanism) as a function of the lower moments. Subsequently, this table can be used in the LES code to obtain the mean chemical source terms at the various spatial locations.

The key research issues are related to the situation when multi-species processes have to be tabulated. When the number of parameters used for the table increases, the lookup procedure can become expensive. A method recently demonstrated for laminar chemistry is the use of neural networks that are trained on the table has the potential to address this limitation. In this approach,

a neural net is trained on the table and then the neural net is used for the simulations. The research group of Prof. Suresh Menon has already developed this ability to create a neural network that can simulate the laminar chemistry. In the present effort, we will extend this ability to handle turbulent scale parameters. Although this training procedure can take some effort, it needs to be done only once and off-line. Thus, the computational cost for simulating the flow field for design or engineering application will no longer be restricted by the stiffness of the chemical source terms. In fact, in this approach, the time step for the reaction-diffusion equations will be dictated by the advection/diffusion restriction and not be the chemical time step since the reaction source term will be computed and stored for pre-specified time intervals. Note that a similar approach using just the reaction steps (as in laminar chemistry by using CHEMKIN) will not be accurate as has been noted in the past (typically this results in chemistry and fluid dynamics to become decoupled). The key innovation here is that the table is generated assuming that the turbulent flow is affecting the reaction steps - thus, small-scale turbulent stirring (as dictated by the local turbulent velocity and length scales) and molecular diffusion effects are implicitly included in the source term. This unique feature allows the table to provide a 'turbulent' source term (here considered a 'Turbulent CHEMKIN') to the species equations.

Radiative transfer in turbulent reactive flows may be associated either with radiative interactions involving species in a single phase, typically carbon dioxide and water in high-temperature gases, or radiative interactions involving two-phase flow, typically carbon particles in hot gases. The most general formulation for radiative transfer in a flowing medium leads to an expression for the radiation flux vector involving a multiple integral over the spectrum of radiation and over all space involving significant emission absorption or scattering. The integrand depends in a complex fashion on the local and instantaneous temperature and composition. In order to apply the LES formalism one faces the need to average in some fashion the multiple integral, for which significant simplifications are required if useful results are to be realized (Libby and Williams, 1994). This problem is beyond the scope of the study and therefore radiative effects will be neglected. However, it is worth mentioning that the computational platform used in this project, CFD-ACE+, has several relevant capabilities which could be used in the first approximation: non-gray radiation heat transfer (with the Discrete Ordinate Method) and surface to surface radiation.

Conditional Moment Closure: Recently, Bilger (1993) and Klimenko (1990) proposed a new approach for modeling turbulent reacting flows, called Conditional Moment Closure (CMC). The CMC method employs the transport equations of conditionally averaged quantities instead of their spatially filtered counterparts. Variables on which the chemical reactions are known to depend on are chosen to be the conditioning variables. CMC allows the evaluation of the chemical source term in an affordable and sufficiently precise manner.

Besides the Linear Eddy Model approach, for this project we propose to utilize the CMC method in the manner described by Bushe and Steiner (1999), as an alternative to the aforementioned methods for closing the chemical source terms. With the proposed methodology it is not necessary to solve the transport equations in the conditioning space; thus maintaining the solution at a computational affordable level. In its present form the proposed model is devised to provide the filtered means of the chemical source terms needed to close the LES set of equations

in reacting flows. This method has proven its predictive capability in a priori tests using DNS data of turbulent reacting mixing layers.

In non-premixed combustion far from extinction, the reaction rates mainly depend on mixture fraction. Thus, the mixture fraction is clearly an appropriate conditioning variable. In the context of non-premixed combustion, the mixture fraction represents the local fraction of mass originating from the feeding fuel stream. Thus, it is zero in pure oxidizer and one in pure fuel. In the following the conditional average of some quantity f, conditional on the mixture fraction Z having some value ζ, will be denoted by an overline $\overline{f|Z} = \langle F | Z = \zeta \rangle$.

The conditionally averaged reaction term occurring in the conditionally averaged transport equation for the mass fraction Y_i is closed with the first order CMC hypothesis: the conditional average of the chemical source term of some species *i* can be modeled by evaluating the chemical reaction rates using the conditional averages of the composition vector, temperature, and density. Under the CMC method, the level of perturbations from the modeled mean data is reduced by conditional averaging. Thus, $\overline{\dot{\omega}_i(Y_k, T, \rho)|Z} = \dot{\omega}_i\left(\overline{Y_k|Z}, \overline{T|Z}, \overline{\rho|Z}\right)$.

It has been established that the CMC hypothesis, based on a single conditioning variable, provides adequate predictions of reaction rates for flames far from extinction (Bilger, 1993a; Smith 1994). Furthermore, this method takes advantage of the spatial homogeneity of the conditional averages on particular surfaces in the reacting flow field.

The conditional filtered means are defined using the filtered density function (FDF) denoted by P_L (Pope, 1985):

$$P_L(\psi; \mathbf{x}, t) = \int\int\int_{-\infty}^{\infty} G(\mathbf{x}' - \mathbf{x}) \varsigma[\psi, \phi(\mathbf{x}', t)] d\mathbf{x}' \tag{9}$$

$$\varsigma[\psi, \phi(x', t)] = \prod \delta[\psi - \phi(x, t)] \equiv \prod_{\alpha=1}^{N_s} \delta[\psi_\alpha - \phi_\alpha(x, t)]$$

where δ denotes the delta function and y denotes the "composition domain" of the scalar variable. The term $\varsigma[\psi, \phi(x', t)]$ is the "fine-grained" density (Pope, 1985). The equation above implies that the FDF is the spatially filtered value of the fine-grained density.

Evaluations of spatial filtered values of the transport variable are achieved by integrating the FDF. In variable density flows, it is useful to define the Favré FDF, $\widetilde{P}_L = \overline{\rho P_L} / \overline{\rho}$. Thus, the Favré filtered variable is given by:

$$\widetilde{A}(x, t) = \int_{-\infty}^{\infty} A(\psi) \widetilde{P}_L(\psi; x, t) d\psi \tag{10}$$

The density weighted, filtered temperature in each cell can be expressed as

$$\widetilde{T} = \int_0^1 \widetilde{P}_L(Z)\overline{T}\big|\overline{Z}dZ \tag{11}$$

The above equation is an integral equation — a Fredholm equation of the first kind — which, for discrete intervals in Z, can be inverted to yield the conditional average. Similar equations can be written for the density and the mass fractions to obtain $\overline{\rho|Z}$ and $\overline{Y_k|Z}$, respectively. Even in the case of non-homogeneity the inversion would still yield an approximation for the conditional average of the temperature on the surface constituted by the ensemble of LES cells. The conditional average of the chemical source terms can now be obtained using the CMC hypothesis.

In this manner, it should be possible to obtain closure for the sub-grid scale mean reaction rate for any chemical kinetic mechanism. No assumptions have been made regarding the thickness of the regions in which chemical reactions are significant relative to the turbulent length scales. Only the assumption of statistical homogeneity of the conditional averages of temperature, density, and pressure on some surface must be made. As for the FDF of the mixture fraction, a beta PDF with the same mean and variance can approximate the real FDF appropriately.

In premixed systems, a progress variable is usually defined in terms of a reactive scalar such as temperature. Conditional averages of mass fractions and enthalpy will be taken conditional on the progress variable, which will be computed from a transport balance equation. All the above modeling considerations regarding the CMC are also valid in the premixed regime.

It has been reported in the literature that the CMC hypothesis with one conditioning variable gives very good prediction for flames that are far from extinction. In order to improve the predictability of the CMC for local extinctions, autoignition and low NO_x emissions, a second condition variable will be utilized. In the traditional (RANS) CMC approach, this has the drawback of adding two independent variables to the system of equations. However, in the LES formulation the need to have additional equations is circumvented by taking advantage of some spatial homogeneity in the conditional filtered means. Following the procedure reported by Bushe and Steiner (1999), the second conditioning variable will be taken to be the scalar/progress variable dissipation. This will help reduce the conditional variance of temperatures, mass fractions and density and make the chemical closure hypothesis valid even in the presence of autoignition and local extinction. Furthermore, according to Smith (1994) this will also improve the prediction of NO_x formation, especially in combusting systems where instantaneous deviations from conditional means are expected to be large.

2.4 Chemical Kinetics

An adequate chemical description is crucial for predicting flame structure and emissions in advanced combustion systems for Vision 21 power plants. Many reaction mechanisms for describing hydrogen-air or hydrocarbon-air combustion, including provisions for both CO and NO_x, have been developed. These mechanisms range from simple 1- or 2-step models (Westenberg, 1971; Westbrook and Dryer, 1981) to detailed models (276-step, Bowman et al. [1996]). Detailed chemical mechanisms for hydrocarbon fuels are built in a hierarchical manner

and always include submechanisms for H_2 and CO oxidation. Additional species and reaction steps are added to this submechanism as the complexity of the fuel increases. The simple mechanisms incorporate only information for species of interest, such as CO or NO_x, for a limited range of conditions, while the larger mechanisms may describe the chemical behavior for hundreds of species over a broad range of conditions and often include C_2+ chemistry for describing detailed fuel breakdown and ignition.

The use of detailed chemical kinetic mechanisms in multi-dimensional combustion models for industrial fuels is not practical at the present time. The impractical nature of this detailed mechanism approach is largely due to the extremely high computational expense required in integrating the stiff set of chemical kinetic equations. For example, it has been estimated that 6 years of CPU time would be required on an SGI Indigo II workstation to perform the chemical kinetic calculations (16-species, 41-reaction, CH_4-air mechanism) in a multi-dimensional combustor simulation with the Monte Carlo PDF method (Pope, 1997). In addition to computational time, computational memory constraints (on a single processor) limit chemical mechanisms to approximately 20 species. Simplifications in the chemical reaction algorithm (the mechanism and its numerical solution technique) are required before tractable simulations of multi-dimensional combustors can be achieved.

Most current contributions on LES of turbulent reacting flows are via simplified chemistry models (typically of the type: Fuel + Air $\rightarrow$ Products). However, development of computational procedures capable of dealing with turbulent flows involving realistic kinetic mechanisms is in order, especially when numerical treatment of flames such as those in laboratory experiments are attempted. The rigorous means of treating the influence of chemistry in hydrocarbon fuel combustion requires the consideration of detailed mechanisms of elementary reactions. The oxidation mechanism of fuels such as propane requires the consideration of order hundred reactions involving the transport of approximately 30 species for an accurate description of the flame structure. With available computer power, such a consideration is very computation-intensive even for steady laminar flames (Smooke, 1991). The situation becomes substantially worse when turbulent flames are considered.

A remedy for this problem is to systematically reduce the number of equations characterizing the "starting mechanism" to a "reduced system" of equations which are more manageable. The research field of "reduced kinetic schemes" has been actively pursued by chemists for a long time. However, it has been only since the 1980s that these schemes have been systematically utilized in combustion studies (Peters, 1991). Of course the number of steps taken in this approach must be prescribed in such a way that the essential physics of the problem is retained. This is not a frivolous task as the development of reduced kinetic schemes is strongly dependent on the knowledge of the detailed schemes and also on the type of the system being considered. For some of the conventional hydrocarbon flames, the extent of literature on reduced kinetic mechanisms is somewhat rich. Methane is one of the first fuels for which reduced schemes have been developed. In particular, four- and five-step mechanisms are available which are also capable of simulating the mechanism of NO_x formation. Reduced kinetics are also available for some other fuels, *e.g.* acetylene, ethylene and propane.

Reduced Chemical Mechanisms: Fortunately, in chemical kinetic systems there exists a wide range of time scales for chemical reactions. Starting with arbitrary initial conditions in composition space, the concentrations of fast species are soon determined by the concentrations of slow species. This behavior allows for a reduction in the number of species required to describe the combustion chemistry. Simplifications to detailed chemistry often start by establishing a skeletal mechanism (a subset of elementary reactions within the full mechanism) and then a reduced mechanism is developed by applying steady-state assumptions for certain species and partial equilibrium assumptions for certain reactions. This reduction method leads to a coupled set of ordinary differential equations and algebraic equations (steady-state species relationships). These reduced mechanisms are based on a systematic reduction of the detailed mechanism instead of curve fits to limited experimental observations. Peters (1991) points out that the range of application of reduced mechanisms for flames can cover a large range in stoichiometry and pressure. Once the reduced mechanism is developed, the range of application of the reduced mechanisms should be evaluated in simple 1-D or spatially homogeneous reactors. These reduced mechanisms can then be incorporated into current LES software.

While the reduced mechanism approach has been shown to be feasible for systematically reducing detailed kinetic mechanisms, it can be a time-consuming task if done manually. Chen (1988) has developed a general procedure to construct reduced mechanisms in terms of matrix operations so it can be performed by a computer. Computer algorithms have been used to automatically construct reduced mechanisms from detailed CH_4 and NO_x mechanisms (Gottgens and Terhoeven, 1993; Chen, 1997). Using this automated approach, 38 steady-state species assumptions were applied to the 276-step, 49-species, GRI2.11 natural gas mechanism (Bowman et al., 1996) to obtain the following reduced mechanism consisting of four combustion steps and one NO-forming step (Mallampalli et al., 1997):

$3H_2 + O_2 + CO_2 = 3H_2O + CO$ (R1)
$H_2 + 2OH = 2H_2O$ (R2)
$3H_2 + CO = H_2O + CH_4$ (R3)
$H_2 + CO_2 = H_2O + CO$ (R4)
$3H_2 + CO_2 + 2NO = 3H_2O + CO + N_2$ (R5)

The global rates were obtained from linear combinations of the elementary rates in the detailed mechanism and are summarized as follows:

$$w_{R1}=w_4-w_{33}-w_{35}-w_{36}+w_{38}+w_{45}+2w_{46}-2w_{85}+w_{87}+w_{122}+w_{125}+w_{135}+w_{144}+w_{145}+w_{155}-w_{168}-w_{169}-w_{170}+w_{171}+w_{173}+w_{176}+w_{179}-w_{181}+w_{186}-w_{187}+w_{189}-w_{192}-w_{197}-w_{201}-w_{206}-w_{212}+w_{213}+w_{214}+w_{215}+w_{220}+w_{259}$$

$$w_{R2}=w_7+w_{11}+w_{15}+w_{33}+w_{35}+w_{36}-w_{38}+w_{43}-w_{46}+w_{53}+w_{58}+w_{61}+w_{62}+w_{66}+w_{71}+2w_{85}+w_{93}+w_{98}+w_{101}-w_{122}-w_{125}-w_{126}-w_{127}+w_{130}+w_{137}+w_{138}+w_{140}-w_{144}-2w_{155}+w_{158}-w_{160}-w_{166}-w_{167}+w_{169}+w_{170}-w_{173}-w_{176}+w_{180}-w_{183}-2w_{185}+2w_{187}-w_{189}+w_{190}+w_{192}+w_{197}+w_{199}+w_{201}-w_{204}-w_{205}+w_{212}-w_{220}+ w_{222}-w_{227}-w_{240}-w_{246}-w_{247}-w_{248}-w_{256}-w_{259}$$

$$w_{R3}=w_{10}-w_{11}-w_{15}-w_{25}+w_{52}-w_{53}-w_{56}-w_{57}-w_{58}-w_{75}+w_{83}+w_{92}-w_{98}-w_{101}-w_{112}+w_{127}-w_{133}+w_{138}+w_{153}+w_{158}+w_{159}+w_{160}+w_{169}+w_{170}+w_{173}$$

$$w_{R4}=w_{23}+w_{28}-w_{38}-w_{46}-w_{56}-w_{57}+w_{61}+w_{66}-w_{75}+w_{81}+w_{85}-w_{95}-w_{97}-w_{99}-w_{112}-w_{122}-w_{125}+w_{132}-w_{133}-w_{135}-w_{137}-w_{140}+w_{142}+w_{146}+w_{148}+2w_{153}-2w_{155}+w_{169}+w_{170}+w_{180}-w_{183}-w_{185}+w_{187}-w_{189}+w_{190}+w_{192}+w_{197}+w_{199}+w_{201}-w_{220}+w_{222}+w_{224}-w_{240}-w_{246}-w_{247}-w_{248}-w_{249}-w_{250}-w_{251}-w_{255}-w_{256}-w_{259}-w_{262}-w_{268}$$

$$w_{R5}=w_{178}+w_{181}+w_{183}+w_{185}-w_{208}-w_{240}$$

The rate of NO formation from reaction 5 is a function of elementary rates in the thermal, prompt, and N_2O-intermediate pathways, and so all three NO-forming mechanisms, for premixed CH_4-air combustion, are represented. This reduced mechanism, along with a 9-step reduced mechanism) were evaluated in terms of predicting pollutant formation (CO and NO_x) in lean premixed turbulent combustion (Cannon et al., 1998). For example, Figure 7 shows comparisons between predicted mean NO concentrations using the detailed mechanism (GRI2.11) and the 5- and 9-step reduced mechanisms in a spatially homogeneous, Partially Stirred Reactor (PaSR) model. Unlike the Perfectly Stirred Reactor (PSR), the PaSR (Correa, 1993) is a Monte Carlo method that allows for influences of finite-rate mixing and subsequently provides a more realistic and demanding test of reduced chemical mechanisms. The 9-step mechanism predicted mean NO within 3, 1.5, and 0.5 ppm of the detailed mechanism for equivalence ratios of 1.0, 0.8, and 0.65 respectively. The 5-step mechanism was somewhat worse, with 30, 10 and 1.5 ppm discrepancies. The 5-step mechanism performed adequately at the lean conditions. These lean conditions were closer to the conditions used to derive the 5-step mechanism. Overall, the 9-step reduced mechanism provided an accurate representation of instantaneous reaction rates and compositions for a broad region of the accessed composition space in the PaSR.

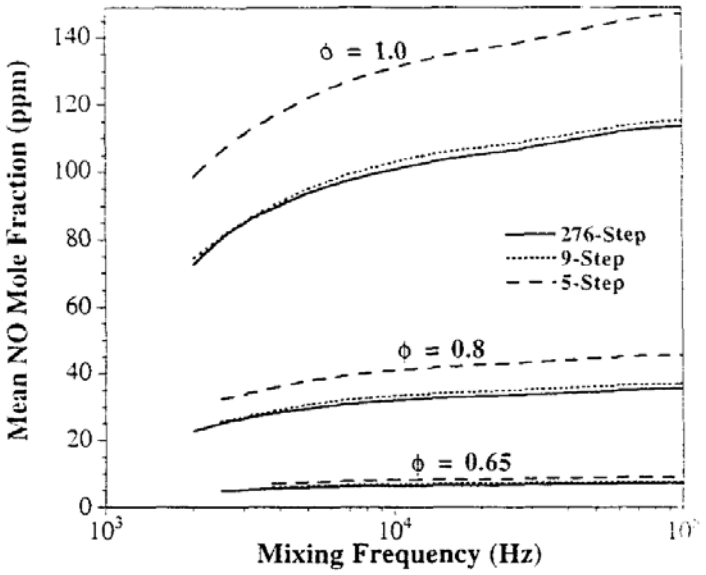

Figure 7. Mean NO Mole Fraction (ppm) vs. Mixing Frequency in the Steady-State PaSR for the Detailed and Reduced Chemical Mechanisms (Cannon et al., 1998)

This same methodology will be used to obtain adequate reduced mechanisms that describe both pollutant emissions and ignition delay. Up to this point, the reduced mechanism approach has only been applied specifically to heat release or specifically to emissions, or specifically at ignition delay, not necessarily at capturing all three phenomena simultaneously with one mechanism. One of the goals of this project will be to develop reduced mechanisms that provide adequate descriptions of ignition delay and pollutant emissions. It is currently determined that ignition delay is most difficult to obtain since not many species are at steady-state. Montgomery et al. (1999), were able to develop a reduced mechanism that adequately described ignition delay. Further reduction in the mechanism by applying more steady-state species was not possible.

Development of accurate reduced chemical mechanisms will be carried out at U.C. Berkeley for different combustion regimes using the most recent detailed methane-air combustion mechanisms. One possible candidate is the GRI3.0 mechanism which contains a detailed NO_x mechanism.

Combustion phenomena of interest to this project include emissions, ignition-delay, and heat release (CO, NO_x, UHC). A Computer Assisted Reduced Mechanism code (CARM) will be used for development of various reduced mechanisms consisting of 8-10 steps suitable for each regime with properly defined mixture, temperature, and pressure. In addition, a slightly large reduced mechanism consisting of 12-16 steps will be developed to cover a wide range of conditions. Validation of reduced chemistry will be critically assessed. It will be carried out by comparison of bench-mark flames including the homogeneous batch reactor, premixed laminar flames, nonpremixed counterflow diffusion flames, well-mixed reactors, and partially mixed transient reactors. The accuracy of reduced chemical mechanisms will be determined through a series of critical tests.

Combustion generated pollutants, such as NO, are formed near the reaction zone. Since the formation rates of pollutant species are relatively slow compared to combustion, the concentrations of pollutant species depend strongly on flow residence time. The steady state assumption made for combustion species is not appropriate for pollutant species; consequently, the pollutant concentrations can not be obtained directly from the steady-state flame library or from the equilibrium chemistry. The NO_x emissions as predicted by our LES methodology will be assessed and compared with the experimental data. The extent to which NO is formed in the flame will be determined by the analysis of data. We will concentrate on the prediction of low NO_x levels as well as high NO_x levels. This will mean all NO_x pathways must be included, i.e., thermal, prompt and nitrous. In addition, other fuel bound nitrogen pathways such as NH_3 (found in syngas) will be included.

The main advantage of the simplified chemistry obtained by the reduced mechanism is that only a few composition scalars are needed to define the thermo-chemical state of the system. A pre-processed look-up table containing reaction information (integrated reaction increment, temperature, density, etc.) can be generated for the allowable composition domain. Once the look-up table is generated, direct integration of the chemical kinetic equations is replaced in the full simulation by a more efficient table look-up and interpolation.

An 8-species, 4-step mechanism can be represented with 6 composition scalars (mixture fraction, enthalpy, and 4 reactive scalars) and then a 6-dimensional table can be constructed for a given chamber pressure. A typical look-up table would contain 20 grid points to discretize the allowable domain for each of the 6 composition scalars with the following information at each point: reaction rate (or reaction increment) for each of the 4 reactive scalars, temperature, density, and specific heat. Grid information consisting of independent composition scalar values and non-uniform grid increments would also be stored. This table would require about 2.3 gigabytes of memory for the general case or about 5.8 megabytes of memory for a perfectly premixed and adiabatic case. Figure 8 shows how the size of the general look-up table would vary with the number of reactive scalars. The storage increases exponentially with each additional scalar and would become too big for a mechanism with more than 4 reactive scalars. This storage problem could be improved if only the accessed composition region of a given flame simulation were tabulated, rather than the whole of the composition space, an idea which is central to the In-Situ Adaptive Tabulation (ISAT) approach.

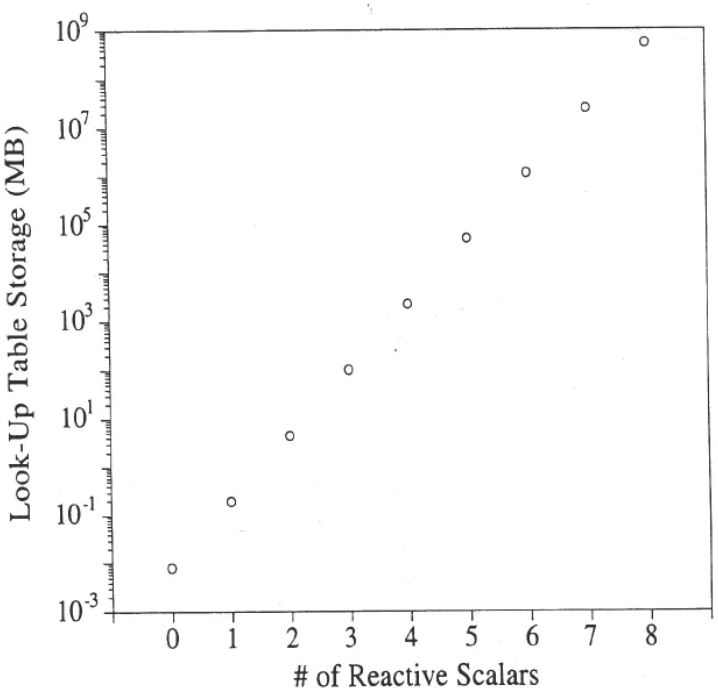

Figure 8. Storage Requirements vs. the Number of Reactive Scalars for a Chemical Look-Up Table with 20 Grid Points per Scalar (including mixture fraction and enthalpy)

In Situ Adaptive Tabulation: An in situ tabulation method, based on the work of Pope (1997), can be used to represent compositions that are accessed during the simulation without requiring storage for unneeded compositions. Since chemical species evolve through composition space along low-dimensional manifolds, table values are needed for only a fraction of the allowed composition space. Figure 9a shows a scatter plot of the steady-state fluid particle compositions in CH_4-CO space during a typical simulation of premixed combustion in a lab-scale gas turbine combustor (Cannon et al., 1997) using a 4-step reduced mechanism. Also shown is the allowable CH_4-CO composition space and the adiabatic equilibrium value for the given lean premixed equivalence ratio (0.8) at the reactor inlet. The actual composition space occupied in the reactor

was significantly less than the allowable composition domain. This actual composition space was defined by the combined effects of reaction, convection, and molecular diffusion for the given reactor simulation with its unique set of boundary conditions.

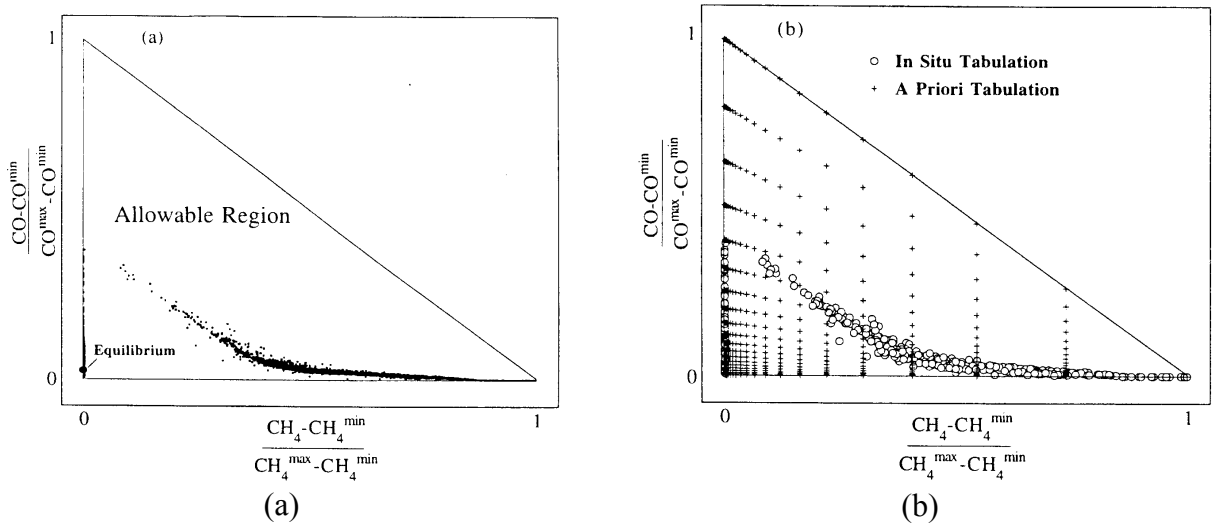

Figure 9. (a) 20,000 CH_4-CO Fluid Particle Properties from Steady-state, 4-step Simulation of a Lab-scale Gas Turbine Combustor, and (b) Representation of Space Required for A Priori and In Situ Tables. (Cannon et al., 1997)

An a priori table is created in a pre-processing stage and must represent reaction information at grid points covering the entire allowable composition domain. The in situ tabulation method, on the other hand, represents reaction information only for the accessed compositions. Figure 9b shows how the a priori table and the in situ tables represent this CH_4-CO composition space for the fluid particle properties in Figure 9a. The in situ table grid points adapt only to the composition region that is obtained during the simulation. The in situ tabulation requires significantly less storage than a priori tabulation, because only a small fraction of the allowable domain is tabulated.

The errors arising from the ISAT retrieval process are controlled with satisfactory success using a procedure based on the concept of regions of accuracy. A simpler version of this method which requires less CPU time and memory uses just the principal directions of the composition space (ISATPD). In the principal directions of the composition space the trajectory of the composition point is essentially restricted to a low dimensional space, despite the fact that the original composition dimension may be very high. This is due to the fact that only the first several principal directions have non-negligible singular values. The retrieval process comprises direct computation (in the early stages of the flow calculation) and search and extrapolation on the elements of the data structure constituted as a binary tree.

In this project, the ISATPD method was used to speed the calculation of the laborious chemical source terms encountered in current reduced mechanisms. For this problem, the binary tree leaves contain a record consisting of a tabulation point and its corresponding reaction source term. The tabulation point is the composition vector mapped into the principal directions of the

composition space (obtained by applying the singular value decomposition). The principal vector is normalized to have a [0,1] region and the tabulation is done in the normalized region. The nodes of the binary tree contain the parameters of a cutting hyper-plane passing through the middle-point between the children (tabulation points) of the parent node and is perpendicular to the line described by the children. This information is used in the search process as detailed below. For a given query composition , the binary tree nodes are used to select the leaf that is likely to be the closest to , by determining the position of query point with respect to each cutting plane. If ___ is within the desired accuracy, then the reaction source term value is returned. Else if the query is outside the desired accuracy, the reaction source term is determined by direct computation and the new query point is entered in the table as follows. The tree leaf with the tabulation point that was referenced in the query is replaced with a node with children ___ and ___. The entries in the tree node are the parameters of the cutting plane between the two new children. It is estimated that speed-up with respect to the direct computation method is about two orders of magnitude for a simulation requiring a million queries.

Currently, at UC Berkeley, a reduced chemistry of methane-air combustion with 12 steps (16 species) has been implemented into ISAT with a significant speed up for applications using Monte Carlo PDF approaches. The memory needed for a total of 20,000 ISAT entries is about 67 MB. As the required memory of ISAT is closely related to the accuracy desired and the total number of scalars, exploration runs will be conducted to determine the optimal balance among these two factors. For CMC applications, the chemical states are expected to evolve gradually in the chemical state space. Hence, the potential speed up with the ISAT for CMC is expected to be greater than applications with the PDF approach.

The ISAT developed at Berkeley follows closely the principles by Pope (1997) but with two additional new features added to enhance the ISAT performance. One of the new features is to allow a variable time interval which is treated as one of the inputs. The second new feature facilitates an automatic trimming of ISAT when the allocated memory is used up. A partially stirred reactor will be used to demonstrate the capability of the combined scheme of reduced chemistry and ISAT. The speed up and accuracy will be assessed by comparison with runs with detailed chemistry. When necessary, improvement on reduced chemistry/ ISAT will be carried to optimize the performances. If necessary, a further demonstration will be carried out for parabolic turbulent jet flames using CMC/ISAT with traditional RANS as such models are feasible with detailed chemistry. These demonstration runs will validate the algorithms developed and provide critical assessment of the accuracy and the computer resources needed for their implementations into LES.

Artificial Neural Network: Recently, artificial neural networks (ANN) have been used to improve computational times and memory for reduced chemical mechanisms (Christo et al., 1996; Blasco, et al., 1998) in full combustor simulations. As described by Blasco et al. (1998), an ANN consists of interconnected layers of non-linear processing elements, which resemble biological neurons. This network stores the information in the neuron interconnections (with weights). A learning algorithm provides a method for adjusting the weights. A popular learning algorithm is the back-propagation scheme (Christo et al., 1996). After the learning phase, the ANN can be used in a recall phase where chemical information needed in the simulation (integrated reaction increments, reaction rate source terms, temperature, density, etc.) can be

obtained efficiently and with small memory requirements. Figure 10 shows the general ANN structure, where the 8 species mass fractions in a CH4-air mechanism are the input at time t, and the integrated reaction increment at t+dt, and temperature and density at time t are the output. The ANN will be used as an alternative to the ISAT algorithm.

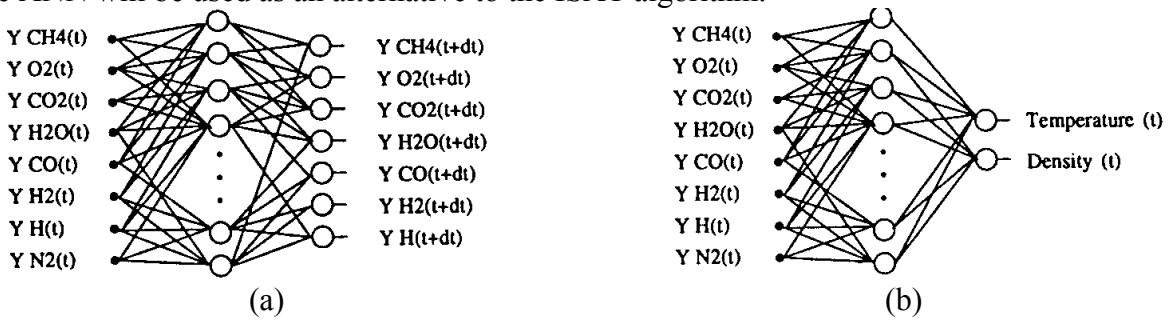

Figure 10. (a) General Artificial Neural Network Structure showing Inputs and Outputs used to Approximate the Reactive-Species Mass-Fractions, and (b) General ANN Structure for Temperature and Density Evaluation (Blasco et al., 1998)

3. TECHNICAL OBJECTIVES

The overall goal of this project was to develop a reliable, user-friendly simulation tool for the design of combustion systems needed for the Vision 21 plant. The specific objectives of the project were:

1. to develop reduced chemical mechanisms that provide accurate representation of emissions (CO and NOx), ignition delay, and heat release;
2. to incorporate the LES formalism with advanced subgrid scale turbulence models into a finite-volume turbulent reacting flow solver on arbitrary grids;
3. to implement advanced subgrid chemistry models (LEM and CMC) into the LES code;
4. to optimize the speed of the LES code by using advanced algorithms (such as ISAT and neural networks) and parallelization;
5. to validate the LES code in benchmark configurations, by comparison with existing numerical or experimental data, for model validation and refinement purposes;
6. to apply the resulting software tool to the design of combustion systems relevant to the Vision 21 program with the direct participation of industry partners; and
7. to package the LES code as a complete commercial software tool that is user-friendly and robust.

All objectives were met during the course of this project, except for objective 3. The CMC subgrid chemistry model was not implemented; only the LEM model was implemented.

4. WORK PERFORMED

In this project, an advanced computational software tool was developed for the design of low emissions combustion systems for Vision 21 clean energy plants. This project was a four-year program. During the first year, the project focused on developing and implementing subgrid turbulence, chemistry, and turbulence-combustion interaction models into an existing time-accurate commercial CFD code, CFD-ACE+. University expertise from Georgia Tech and University of California, Berkeley was utilized to help develop these advanced subgrid models into the unstructured, parallel CFD-ACE+ code. In the second year, the combustion LES code was evaluated and validated using experimental data from lab-scale and industrial test configurations. The code testing (alpha testing) was performed by CFDRC engineers. During the third year, six industrial and academic partners were trained and tested the code on combustion problems of their choice (beta testing). Final feedback and optimizations were then implemented into the code, and the code was released (licensed) to the general public. An additional one-year task was added for the fourth year of this project to analyze the SIMVAL experiments being performed by DoE.

The work performed in each of the four years will be discussed in detail in the sections that follow.

4.1 Year One: Development of Models

Starting Code: The starting point in the development of the LES code was an existing Navier-Stokes solver integrated in a commercial CFD software package, CFD-ACE+ (CFD Research Corporation, 1999). CFD-ACE+ is the culmination of expertise obtained from 16 years of CFD development and commercialization at CFDRC. In 2004, CFDRC spun-off the commercial business unit, and sold the unit to ESI-Group. ESI-Group is now responsible for marketing and licensing the software

CFD-ACE+ is a fluids, heat and mass transfer simulation system based upon a parallel implementation of an unstructured flow solver. This system is comprised of four modules:

- CFD-GEOM: A geometry modeler, mesh generator
- CFD-GUI: A graphical user interface for pre-processing the solver
- CFD-SOLVER: A parallel, pressure-based, polyhedral unstructured solver
- CFD-VIEW: A visualization package/post-processing tool.

These application modules are all integrated via the CFD-DTF common file format and library. This publicly available common file format/library enables many important features in the unstructured flow solver, allowing the treatment of multiple-domained grids containing structured, unstructured and polyhedral-unstructured meshes in a fully implicit manner, as if they were consolidated into a single "virtual" zone.

CFD-SOLVER is a finite-volume, pressure-based, unstructured flow solver. It supports conservation volumes comprised of arbitrary polyhedra, including the more commonly used types, such as hexahedra, tetrahedra, prisms, quadrilaterals and triangles. It uses a fully implicit

procedure based upon the SIMPLE/PISO algorithm, and employs first-, second- and third-order spatial discretizations, as well as first- and second-order temporal schemes. In addition to the traditional Reynolds Averaged Navier-Stokes equations, it is used to solve a wide variety of transport/ conservation equations, including:

- One- and Two-equation Turbulence Models
- Multi-component Diffusion of reacting and non-reacting dilute gases, including PDF models
- Surface Chemistry
- Radiation and Conjugate Heat Transfer

Discretization of the equations is made using a finite-volume formulation, which relates the conservation-law form of the Navier-Stokes equations to a collection of flux integrations over the surfaces of a set of discrete control volumes, or cells. The equations are solved sequentially and implicitly, meaning that each equation, e.g., a momentum equation, is linearized about the current time/iteration level. The Finite-Volume formulation used in developing the flow solver allows it to be applied to meshes of arbitrary polyhedra, permitting the solution on all mesh types, including

- Structured grids
- Unstructured grids of triangles, quads, tetrahedra, pyramids, prisms and hexahedra
- Polyhedral grids, obtained via cartesian mesh, and mesh refinement

Parallel Processing: Given the large number of cells (millions) required for LES calculations, parallel processing is a necessary feature for the LES code in order to obtain practical turnaround times. The CFD-ACE+ flow solver has been parallelized for distributed and SMP architectures using the MPI message passing library and domain decomposition. The parallelization of the code has been performed in such a manner that the convergence rate and robustness of the code is not degraded relative to the serial mode of operation. For parallel processing, ghost cells are filled with data values from cells in the neighboring zones. The data exchange happens on every iteration. In order to maintain implicitness across the entire problem domain, the Conjugate Gradient Solver (CGS) was modified to transfer extra data (ILU factorization and sweep residuals) between neighboring zones on each sweep. This allows the final accuracy of a parallel run to match that of a serial run. The multi-processor computers available at various computational centers will be used to perform the parallelized combustion instability calculations.

1D Acoustic Wave Analyses: In order to accurately predict combustion instability, acoustic waves must be accurately captured by the numerical method. 1D transient analyses with the unstructured flow solver were performed to ensure that pressure wave propagation was accurately captured. The computational grid included structured quad cells and unstructured tri cells. Figure 11 shows the computational domains and grids that covered a length of 0.4 m. The numerical solution was obtained using central or 2^{nd}-order upwind spatial differencing (0.01-0.1 blending factor) and Crank-Nicholson temporal differencing (0.6 blending factor). The simulations were performed at an ambient pressure of 5 atm and an air temperature of 1800 K. The initial conditions were obtained by setting all boundaries to symmetry except for the inlet

where a forced pressure pulse was applied. After the 0.2% pressure pulse was applied for 1e-4 seconds, the inlet boundary was changed to either a mass flow, symmetry, or pressure boundary and the pressure and corresponding velocity wave were allowed to evolve.

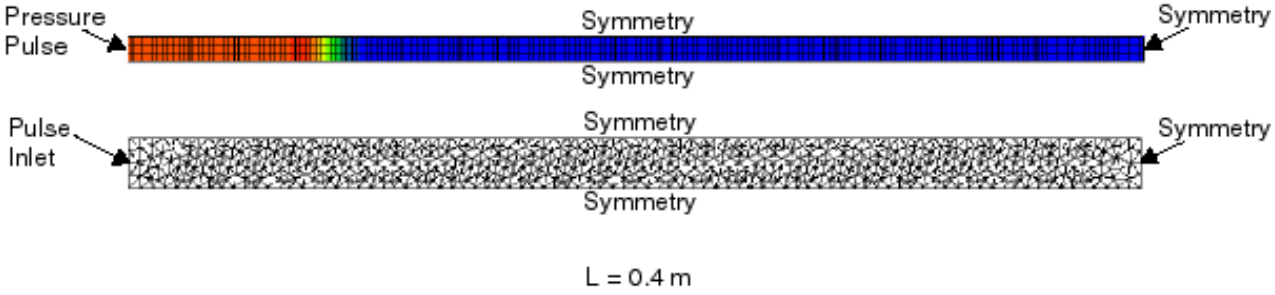

Figure 11. Computational Domain for the 1D, Transient Pressure Pulse Simulation in CFD-ACE+ (Structured and Unstructured Grids)

It was found that the ability of the pressure wave to maintain its amplitude with time was a strong function of the grid size and time step. But the frequency of the wave was not affected by the grid size or time step. Figure 12 shows the pressure history at the midpoint of the domain for the case with an inlet symmetry boundary using various grid sizes and time steps. The predicted frequency (1017 Hz) of the oscillation was within 1% of the expected value (f=c/2L=1027 Hz). The peak pressure amplitude decreased by about 40 and 15% for the 2 and 1 microsecond cases, respectively. The 0.5 microsecond time step cases showed very little loss of the pressure amplitude and indicates that the pressure-based code can capture acoustic waves if the grid sizes and time steps are small enough. LES requires relatively small grid sizes and time steps anyway, so the ability to capture acoustic waves in the combustion instability software should be adequate.

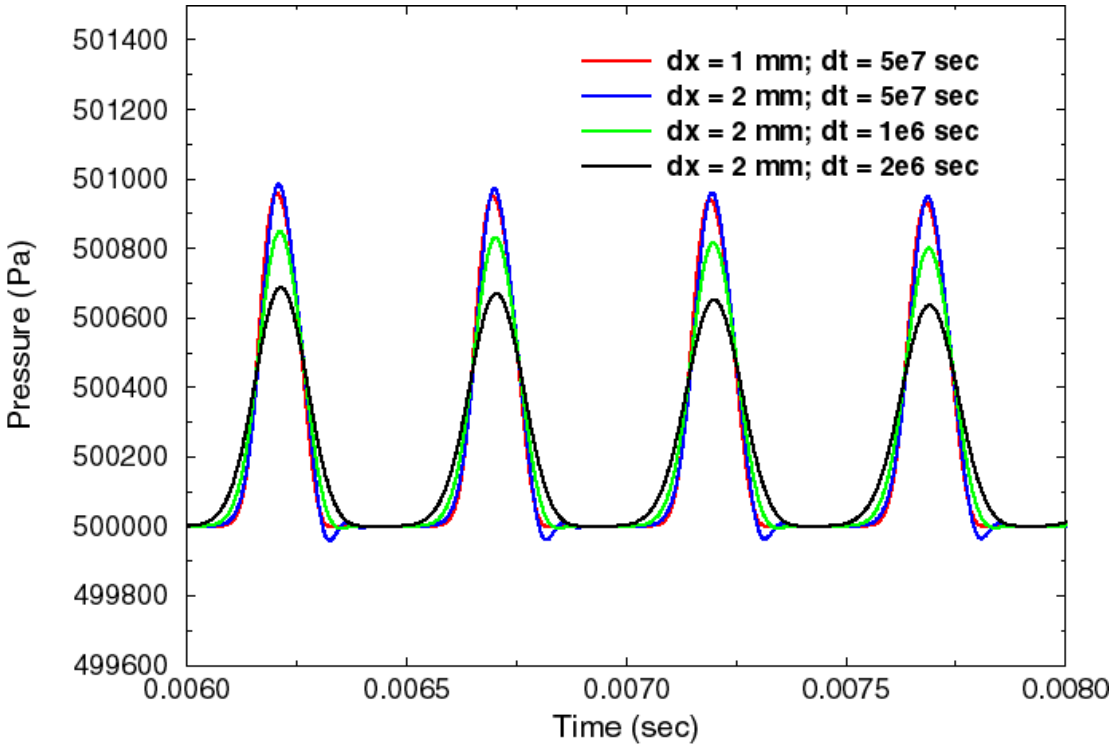

Figure 12. Predicted Pressure History at the Midpoint for the Inlet Symmetry Case (Structured Grid Cases)

Instead of the symmetry boundary at the inlet, cases were also tested with a pressure boundary at the inlet. These cases accurately captured the 4L mode acoustic behavior due to the open/closed boundaries. The CFD-ACE+ boundaries with a fixed mass flow, symmetry, or wall provided a pure reflection to the incoming pressure wave, while boundaries with a fixed pressure provided an inverse reflection of the incoming wave.

Simulations with an unstructured grid were also performed and Figure 13 shows the pressure time history for the acoustic wave at time steps of 1.0 and 0.5 microseconds. These results show very little difference between the unstructured and structured grid solutions. All solutions resulted in a wave frequency of ~1017 Hz, within 1% of the estimated value of 1027 Hz.

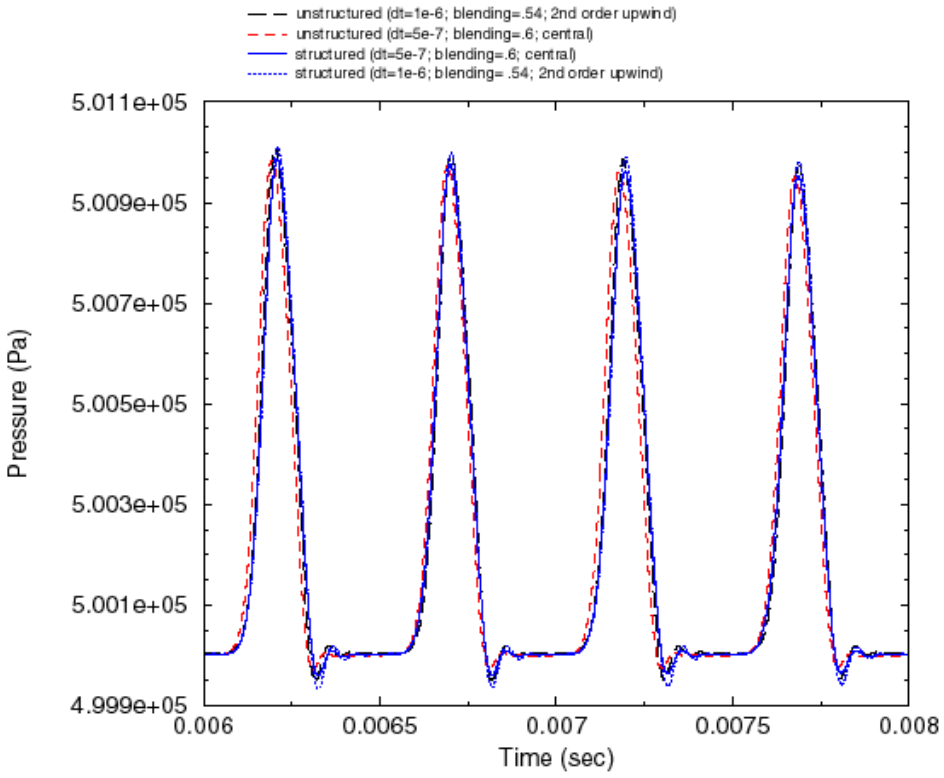

Figure 13. Predicted Pressure History at the Midpoint for Structured and Unstructured-Grid Cases

A final case was also performed that included an overall bulk flow. The grid consisted of 600 cells in the axial direction and covered a length of 1.0 m (see Figure 14). The flow cross-sectional area was slightly decreased with downstream distance so that a pressure gradient could be maintained in the axial direction. A pressure gradient of 1000 Pa provided an overall bulk flow of 140 m/s (M=0.17) at the midsection of the domain. The initial conditions included a converged steady-state solution along with a 0.2% pressure pulse applied at the upstream end for 0.0001 seconds. The upstream boundary was then changed back to the original pressure (501000 Pa) and the pressure and velocity wave were allowed to evolve. The grid size (1.67 mm) and time step (5e-7 seconds) were shown to be sufficient in capturing acoustics in quiescent flow (see Figure 3-2).

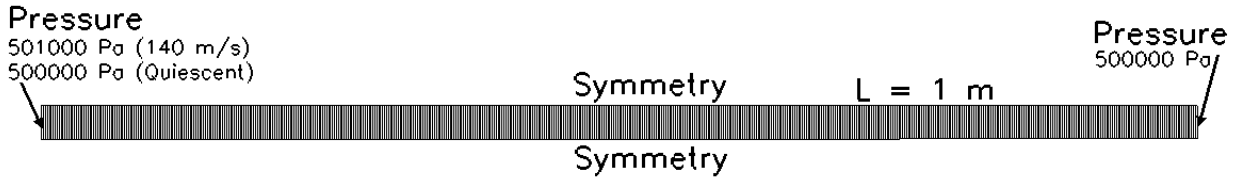

Figure 14. Computational Domain for 1D Acoustic Wave Simulation (with Bulk Flow) in CFD-ACE+

Figure 15 shows the pressure history at the midpoint of the domain for the case with 0 and 140 m/s bulk flow. The bulk flow case shows the pressure pulse amplitude decreases only slightly more than the quiescent case. The amplitude of the pulse has decreased by only ~10% after 8 milliseconds (5 passes through domain including inverse reflections at pressure boundaries). It is likely that some of the amplitude attenuation is due to viscous effects. The speed of the wave for the bulk flow case has slightly decreased compared to the quiescent (and theoretical) case. The acoustic wave speed is ~4% lower for the bulk flow case compared to the quiescent case. Turbulent flame calculations using LES will provide continuous perturbations to the flowfield as vortex structures are formed and evolve. There will be little need to predict small-amplitude pressure waves for much more than 5 reflections and/or 8 milliseconds (as shown in Figure 3-5) during the engineering LES calculations.

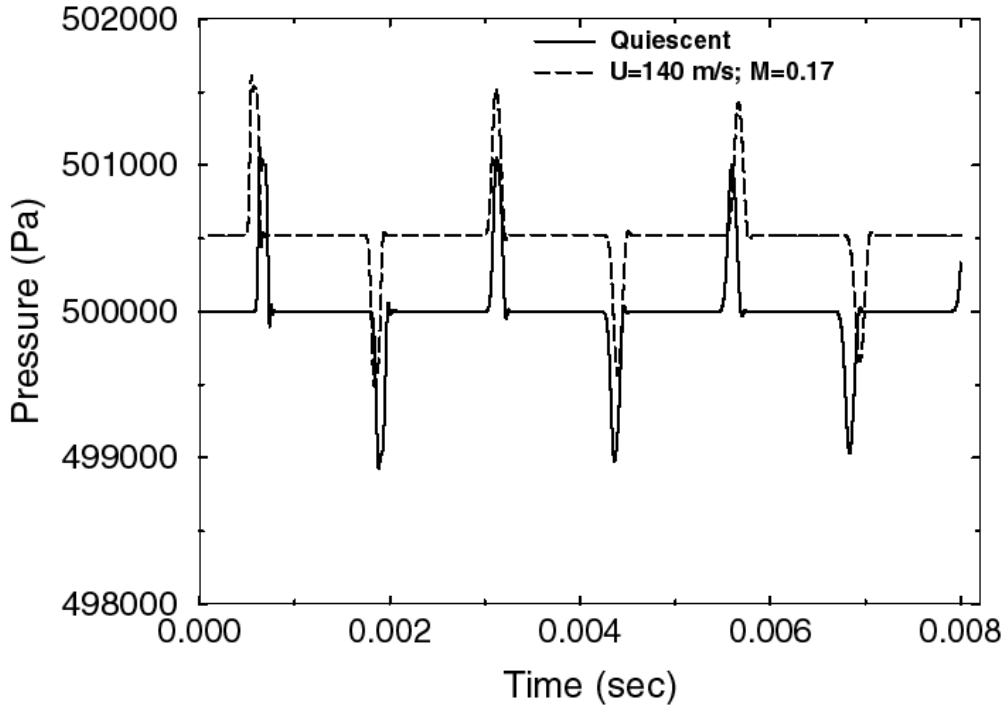

Figure 15. Computational Domain and Predicted Pressure History at the Midpoint for 0 and 140 m/s Bulk Flow

4.1.1 LES Equations

Large Eddy Simulation (LES) is a time-accurate solution to the Navier Stokes equations with grid sizes and time steps that are small enough to resolve the energy-containing scales of a turbulent flow. Subgrid models for turbulent mixing and chemical reaction are needed to resolve the small-scale effects that are more universal and easier to approximate. Each variable in a LES is decomposed into a large-scale component (indicated by an overbar) and a residual component (indicated by a prime),

$$f = \bar{f} + f' \tag{12}$$

The large scale component is obtained by spatially averaging f with a filter function G,

$$\bar{f} = \int f(x')G(x,x')dx' \tag{13}$$

The filter effectively eliminates fluctuations on scales smaller than a specified size. The large scale, or resolved components are time dependent, in contrast to the average components in conventional (Reynolds averaged) turbulence modeling. For variable density flows, CFDRC uses Favre (density weighted) filtering:

$$\tilde{f} = \frac{\overline{\rho f}}{\bar{\rho}} \tag{14}$$

With the application of an LES Favre averaging procedure to the governing transport equations (mass, momentum, energy, species mass fractions, respectively), we obtain:

$$\begin{aligned}
&\frac{\partial \bar{\rho}}{\partial t} + \frac{\partial \bar{\rho}\tilde{u}_i}{\partial x_i} = 0 \\
&\frac{\partial \bar{\rho}\tilde{u}_j}{\partial t} + \frac{\partial \bar{\rho}\tilde{u}_i\tilde{u}_j}{\partial x_i} = \frac{\partial \tilde{\tau}_{ij}}{\partial x_i} - \frac{\partial T_{ij}}{\partial x_i} \\
&\frac{\partial \bar{\rho}\tilde{E}}{\partial t} + \frac{\partial \bar{\rho}\tilde{u}_i\tilde{E}}{\partial x_i} = \frac{\partial \tau_{ij}u_j}{\partial x_i} - \frac{\partial Q_i}{\partial x_i} \\
&\frac{\partial \bar{\rho}\tilde{\phi}_\alpha}{\partial t} + \frac{\partial \bar{\rho}\tilde{u}_i\tilde{\phi}_\alpha}{\partial x_i} = -\frac{\partial \tilde{J}_i^\alpha}{\partial x_i} - \frac{\partial M_i^\alpha}{\partial x_i} - \tilde{\omega}_\alpha
\end{aligned} \tag{15}$$

The filtered equations contain unknown terms such as τ_{ij} (velocity-velocity correlation) arising from the filtering of nonlinear terms and are known as subgrid scale (SGS) stresses. The closure problem of turbulent flows using LES is handled by providing models for the various subgrid scale correlations.

4.1.2 Subgrid Turbulence

Unlike typical steady-state turbulence models, the turbulence models for LES compute an eddy viscosity that is a function of the grid (or filter) size. The larger the grid, the higher the value of the subgrid turbulent viscosity. Thus, as the grid is made finer, the modeled effect of subgrid turbulent mixing becomes less and more scales are then directly computed. The Smagorinsky model (Smagorinsky, 1963) computes the turbulent viscosity from the magnitude of the resolved strain tensor S_{ij}, the grid filter width Δ, and the Smagorinsky constant C_s according to:

$$\nu_t = (C_s\Delta)^2|S|, \text{ where } \bar{S}_{ij} = \frac{1}{2}\left(\frac{\partial \bar{u}_i}{\partial x_j} + \frac{\partial \bar{u}_j}{\partial x_i}\right) \tag{16}$$

where the grid filter width is computed as the cube root of the grid cell volume. This implementation allows LES calculations with arbitrary grid types, including hybrid grid schemes. Various studies have shown that the tunable parameter C_s in the Smagorinsky model is

not a universal constant (Avva and Sundaram, 1998). It has been suggested that the C_s parameter should be flow dependent and should vary from region to region in complex flows. This model was tested in the LES code and results are shown later for instability predictions in the DOE-NETL and Pratt & Whitney combustors.

Another subgrid turbulence model was implemented in the LES code and is called the Localized Dynamic subgrid Kinetic energy model (LDKM). This model was developed by Kim and Menon (1997) to provide subgrid stresses without a priori specification of any constants. The LDKM uses scale similarity and the subgrid-scale kinetic energy

$$k_{sgs} = \frac{1}{2}\left(\overline{u_k u_k} - \bar{u}_k \bar{u}_k\right) \tag{17}$$

to model the unresolved scales. Using k_{sgs} the subgrid stress tensor is modeled as

$$\tau_{ij} = -2C_\tau \bar{\Delta} k_{sgs}^{1/2} \bar{S}_{ij} + \frac{2}{3}\delta_{ij} k_{sgs} \tag{18}$$

with the resolved-scale strain tensor defined as

$$\bar{S}_{ij} = \frac{1}{2}\left(\frac{\partial \bar{u}_i}{\partial x_j} + \frac{\partial \bar{u}_i}{\partial x_i}\right) . \tag{19}$$

In the modeling of the SGS stresses, implicitly the eddy viscosity is parameterized as

$$\nu_T = C_\tau \bar{\Delta} k_{sgs}^{1/2} . \tag{20}$$

The subgrid-scale kinetic energy is obtained by solving the transport equation

$$\frac{\partial k_{sgs}}{\partial t} + \bar{u}_i \frac{\partial k_{sgs}}{\partial x_i} = -\tau_{ij} \frac{\partial \bar{u}_i}{\partial x_j} - \varepsilon_{sgs} + \frac{\partial}{\partial x_i}\left(\nu_T \frac{\partial k_{sgs}}{\partial x_i}\right) \tag{21}$$

which is closed by providing a model for the subgrid dissipation rate term, ε_{sgs}, based on simple scaling arguments

$$\varepsilon_{sgs} = C_\varepsilon \frac{k_{sgs}^{3/2}}{\bar{\Delta}} \tag{22}$$

In these models, C_τ and C_ε are adjustable coefficients determined dynamically using the information from a resolved test-scale field. The test-scale field is constructed from the large scale field by applying a test filter which is characterized by $\ddot{\Delta}$, the test filter width. In the LES code, with arbitrary grids, we are using a test filter consisting of a weighted average of the cells sharing a node with the current cell. This average is biased towards the current cell, with a weight equal to the number of vertices of the cell. The cells that share a face with a current cell have a weight of two.

The application of the test filter on any variable is denoted by the top hat. By definition, the Leonard stress tensor at the test-scale level is

$$L_{ij} = \widehat{\bar{u}_i \bar{u}_j} - \hat{\bar{u}}_i \hat{\bar{u}}_j \tag{23}$$

The Leonard stress tensor and the SGS tensor are known to have high degrees of correlation, which justifies the use of similarity in the derivation of the dynamic model coefficients. The resolved kinetic energy at the test filter level is defined from the trace of the Leonard stress tensor

$$k_{test} = \frac{1}{2}\left(\widehat{\bar{u}_k \bar{u}_k} - \hat{\bar{u}}_k \hat{\bar{u}}_k\right). \tag{24}$$

This test scale kinetic energy is dissipated at small scales by

$$e = (\nu + \nu_T)\left(\widehat{\overbrace{\frac{\partial \bar{u}_i}{\partial x_j}\frac{\partial \bar{u}_i}{\partial x_j}}} - \frac{\partial \hat{\bar{u}}_i}{\partial x_j}\frac{\partial \hat{\bar{u}}_i}{\partial x_j}\right) \tag{25}$$

Based on a similarity assumption and using appropriately defined parameters, the Leonard stress tensor has a representation analogous to the SGS stress tensor

$$L_{ij} = -2C_\tau \hat{\Delta} k_{test}^{1/2} \hat{\bar{S}}_{ij} + \frac{1}{3}\delta_{ij} L_{kk} \tag{26}$$

The least square method is applied to obtain the model constant

$$C_\tau = \frac{1}{2}\frac{L_{ij}\sigma_{ij}}{\sigma_{ij}\sigma_{ij}} \tag{27}$$

where

$$\sigma_{ij} = -\hat{\Delta} k_{test}^{1/2} \hat{\bar{S}}_{ij} \tag{17}$$

Finally, a corresponding approach is used to determine the dissipation rate constant. By invoking similarity between the dissipation rates at the subgrid level and at the test scale level C_ε is determined to be

$$C_\varepsilon = \frac{\widehat{\overbrace{\left(\partial \bar{u}_i/\partial x_j\right)\left(\partial \bar{u}_i/\partial x_j\right)}} - \left(\partial \hat{\bar{u}}_i/\partial x_j\right)\left(\partial \hat{\bar{u}}_i/\partial x_j\right)}{\left[(\nu + \nu_T)\hat{\Delta}\right]^{-1} k_{test}^{3/2}} \tag{28}$$

The coefficients of the LDKM model are Galilean invariable and realizable. This model is also quite simple and efficient, does not rely on any *ad hoc* procedures, and it is applicable to various flow fields without adjustment of the model. The ksgs from the LDKM is needed input for the Linear Eddy subgrid chemistry model.

4.1.3 Subgrid Chemistry

A subgrid chemistry model is required to describe the effects of small-scale turbulent fluctuations on the reaction and diffusion of chemical species. The Linear Eddy Model (LEM) was implemented and tested in the unstructured CFD-ACE+ flow solver. In addition, advanced chemical kinetic mechanisms and efficient tabulation methods were developed and implemented into the software.

Linear Eddy Model: The Linear Eddy Model (LEM), developed by Kerstein (1992), describes the effects of turbulent stirring, molecular diffusion, and chemical reaction at scales down to the molecular level where reaction ultimately occurs. The LEM achieves this by subdividing each LES cell into a smaller one-dimensional domain. Along the one-dimensional domain, molecular diffusion and chemical reaction are treated explicitly according to:

$$\frac{\partial \phi}{\partial t} = D\frac{\partial^2 \phi}{\partial x^2} \tag{29}$$

$$\frac{\partial \phi}{\partial t} = \dot{\omega} \tag{30}$$

where ϕ is the scalar mass fraction, D is the diffusion coefficient, and ω_i is the reaction rate. Since the flow field is resolved in the one-dimensional domain, no modeling is required for molecular mixing and chemical reaction.

The influence of turbulent convection is modeled stochastically by random rearrangement of the scalar field along the domain. Each event involves spatial redistribution of the species field within a specified segment of the linear domain. The rearrangement events are specified by two parameters: λ, a frequency determining the rate of rearrangement events (stirring), and f(l), a pdf describing the size distribution of the segments to be rearranged. For high Reynolds number turbulence described by a Kolmogorov cascade, these parameters can be obtained from (McMurtry et al., 1992):

$$f(l) = \frac{5}{3}\frac{l^{-8/3}}{\eta^{-5/3} - L^{-5/3}} \tag{31}$$

$$\lambda = \frac{54}{5}\frac{\nu Re_L}{L^3}\left(\frac{L}{\eta}\right)^{5/3} \tag{32}$$

where Re_L is the Reynolds number based on the integral length scale, ν is the kinematic viscosity, η is the Kolmogorov scale, and L is the integral scale.

The LEM subgrid mixing and reaction processes are coupled to the large-scale transport in CFD-ACE+ through the LES resolved flux at each grid cell face through splicing events. Portions of the linear eddy domain are transferred to neighboring grid cells, as shown in Figure 16. These splicing events occur at a frequency determined by the large eddy time step and is much greater than the time step governing the convection-diffusion-reaction process in the subgrid. The

individual identity of each LEM segment is stored and not lost during the LES solution. This can lead to high memory usage and requires parallel computing (< 70,000 cells/processor) for modeling practical combustor geometries. This memory requirement is still significantly less than DNS since only a 1D scalar description is required for LEM.

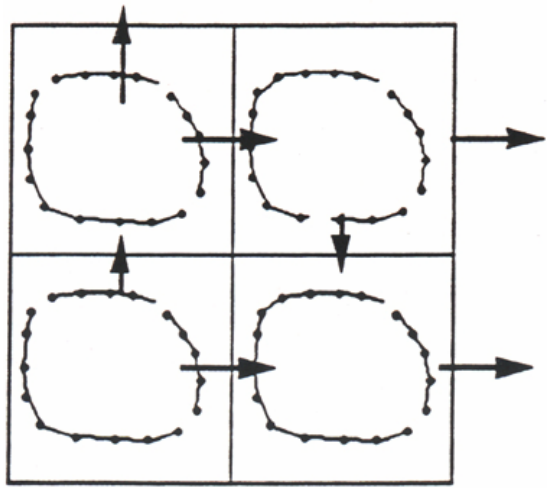

Figure 16. Schematic Diagram of the Linear Eddy Splicing Events

4.1.4 Reduced Chemical Mechanisms

Methane-Air

A reduced chemical mechanism consisting of 15 steps and 19 species was developed by Prof. J.-Y. Chen from the University of California, Berkeley (see Appendix G). This mechanism was provided to CFDRC and incorporated into the LES combustion software. The detailed reaction mechanism used as the starting point for reduction was the GRI 2.11 mechanism and a newly developed mechanism from Miller for NO. The combined mechanism more accurately describes NO emissions at rich conditions compared to the stand-alone GRI mechanism.

An interactive computer-assisted reduction mechanism code (CARM) was utilized to automatically generate the reduced chemistry. CARM uses the following procedure:

(a) A detailed mechanism is used to solve a PSR for certain combustion conditions. The solutions contain information on species concentrations, rates of production, and species sensitivity coefficients.

(b) Quasi-steady-state (QSS) species are selected based on their concentration levels as well as on the rate-of-production analysis.

(c) After selection of the QSS species, a set of independent elementary reaction steps is chosen to eliminate the QSS species in order to permit systematic construction of the reduced mechanism, using the matrix operations proposed by Chen (1988). The subroutine that computes the chemical source terms is automatically generated once the reduced mechanism is constructed.

This subroutine is compatible with CHEMKIN and returns the molar production rates of the species given the pressure, temperature, and mass fractions. A coupled set of nonlinear QSS species equations are numerically solved within the subroutine to provide the necessary elementary reaction rates for the reduced mechanism.

The 19 species mechanism consists of the following 15 global steps:

(1) CH4 + H = CH3 + H2
(2) CH3 + OH = CH2O + H2
(3) CH2O = H2 + CO
(4) C2H2 + O2 = H2 + 2CO
(5) C2H4 + OH = H2 + CH3 + CO
(6) C2H6 = C2H4 + H2
(7) CO + OH + H = H2 + CO2
(8) H2 + O2 = HO2 + H
(9) H2 + HO2 = H2O2 + H
(10) H2 + O2 = 2OH
(11) H2 = 2H
(12) H + OH = H2O
(13) H + O2 + HCN = H2 + CO + NO
(14) H + CO + N2 = NO + HCN
(15) 2H2 + OH + NO = 2H + O2 + NH3

Thirty-one species are assumed to be at steady-state, so their full transport equation is not needed. But, their concentrations must be computed from the tracked (non-steady-state species) in order to compute the elementary rates. This inner iteration requires more computational time than standard Arrhenius mechanisms, but the accuracy is typically better. Also, the reduction in the number of species from 50 to 19 is significant in terms of memory requirements for the LES code and for chemical look-up tables.

Development and Validation of Reduced Chemistry: Several reduced mechanisms have been developed and evaluated for methane-air. These mechanisms were developed to give accurate predictions in ignition delay, flame propagation speed, heat release rate, and pollutant formation, such as CO and NO_x. As the reaction rates in current detailed NO_x mechanisms contain large uncertainties, different NO_x mechanisms for rich and lean combustion were examined. For combustion chemistry, either GRI2.11 or GRI3.0 can be used as the base mechanism. Small differences were found in the predicted results for main flame characteristics. Recent experimental data from Dr. Robert Barlow at Sandia National Laboratories in Livermore have suggested that the NO_x mechanism contained in GRI3.0 gives high NO_x levels roughly by a factor of 2 in partially premixed laminar methane-air flames. GRI2.11 gives reasonable results in lean parts of the flame but under-predicts the NO_x levels in rich parts of the flame. Computed results with a recently modified Miller's mechanism (denoted here as Miller2000) yield much improved NO_x levels for rich parts of the flame where the re-burning process is dominant. Based on the above assessment, Table 2 summarizes the combinations of detailed mechanisms explored during this period for different combustion regimes.

Table 2. Different Combinations of Combustion Chemistry and NO_x Mechanisms

Combustion Chemistry	NO_x Mechanism	Application Regime
GRI2.11	GRI2.11	Lean to stoichiometric
GRI2.11	Miller2000	Rich
GRI3.0	Miller2000	Rich

Calculations were performed for the partially premixed Tsuji flames measured by Barlow and comparisons with the data were made. Figure 17 shows comparisons of measured and predicted NO using the three detailed mechanisms. These results show that the lean side GRI2.1 agrees best with the data. On the rich side, GRI2.1+Miller2000 provided the best agreement with the data. Based on this observation, two 15-step reduced mechanisms with identical species were developed. One from the GRI2.11+Miller2000 and one from GRI2.11. Figures 18 and 19 compare measurements with predictions using the reduced and detailed chemistry. These results show excellent agreement between the reduced and detailed mechanisms.

Figure 17. Comparison of Measured and Predicted NO Using Three Detailed Chemical Mechanisms. GTI2.11 provides better agreement on the lean side, while GRI2.11+Miller2000 provides better agreement on the rich side.

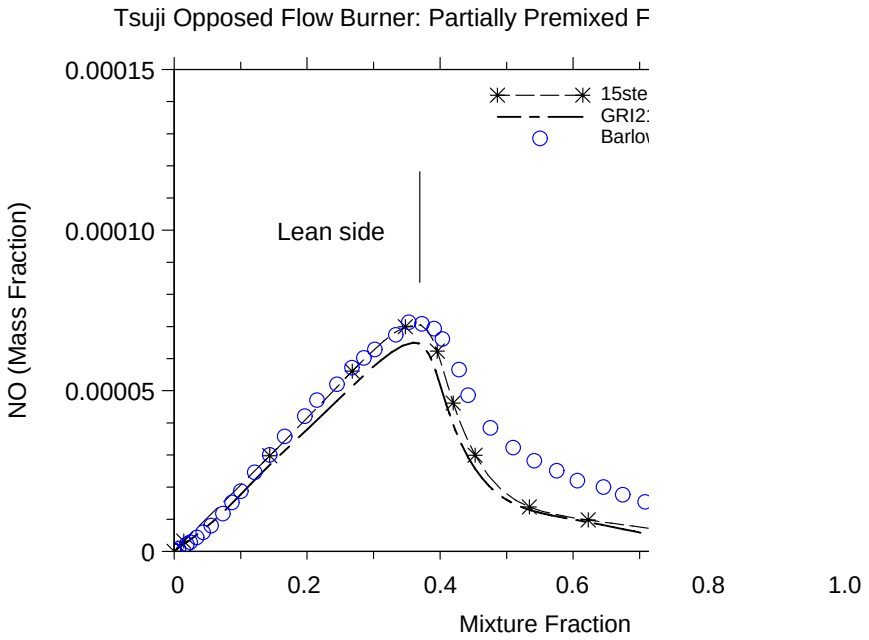

Figure 18. Comparison of Measured and Predicted NO Using GRI2.11 Detailed and 15-step Reduced Chemical Mechanisms. Good agreement is obtained on the lean side.

Figure 19. Comparison of Measured and Predicted NO Using GRI2.11+Miller Detailed and 15-step Reduced Chemical Mechanisms. Good agreement is obtained on the rich side.

Demonstration of Reduced Chemical Mechanism: The 15-step, 19-species reduced chemical kinetics mechanism for methane-air combustion was tested in the CFD code. For this demonstration, 2D, axisymetric unsteady RANS calculations were performed. The transient calculations were started from a steady-state using a 1-step mechanism. CFD-ACE+ allows multi-step chemistry modeling when a species-by-species solution technique is utilized. This species-by-species option requires solution of the transport equation for each of the participating species (19 in this case). The 2D grid was decomposed into 13 domains and parallel computations were performed in parallel on CFDRC's cluster of Linux-based PC's.

Figure 20a shows the unstable limit cycle of pressure inside the combustor. A 6.5% pressure oscillation is observed. The Discrete Fourier Transfer (DFT) of the signal is shown in Figure 20b and clearly indicates a strong oscillation at 258 Hz. Table 3 shows the oscillation results for the experiments compared to predictions using the previous 1-step mechanism and the current 15-step mechanism.

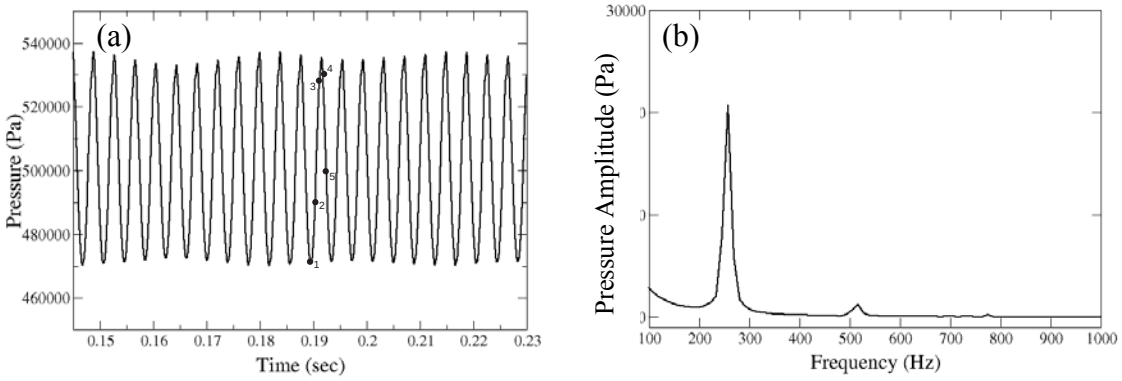

Figure 20. (a) Predicted Combustor Pressure History and (b) Corresponding Spectrum Using 19 Species Chemistry

Table 3. Predicted and Measured Oscillations in the Unstable DOE-NETL Case

	Magnitude	**Frequency**
Measured	6.4%	225 Hz
15-Step Chemistry	6.5%	257 Hz
1-Step Chemistry	6.8%	256 Hz

These results show that the chemistry does not have a strong effect on the predicted oscillation. This is likely due to the strong driving mechanism of a convective time-lag from the fuel injection location to the flame zone. The chemical times are certainly much smaller than the convective transport times and therefore have a very small effect on the predicted instability. The more detailed chemistry will provide superior results if strong extinction/ignition effects are present and if accurate emissions are needed. These results do show that the 15-step reduced

chemistry is implemented correctly in the LES code and that successful convergence can be obtained for this unstable combustion case.

Instantaneous snapshots of pollutant emissions can be observed during the instability cycle. The predicted CO mass fraction during the oscillation cycle is shown in Figure 21, while the NO mass fractions are shown in Figure 22.

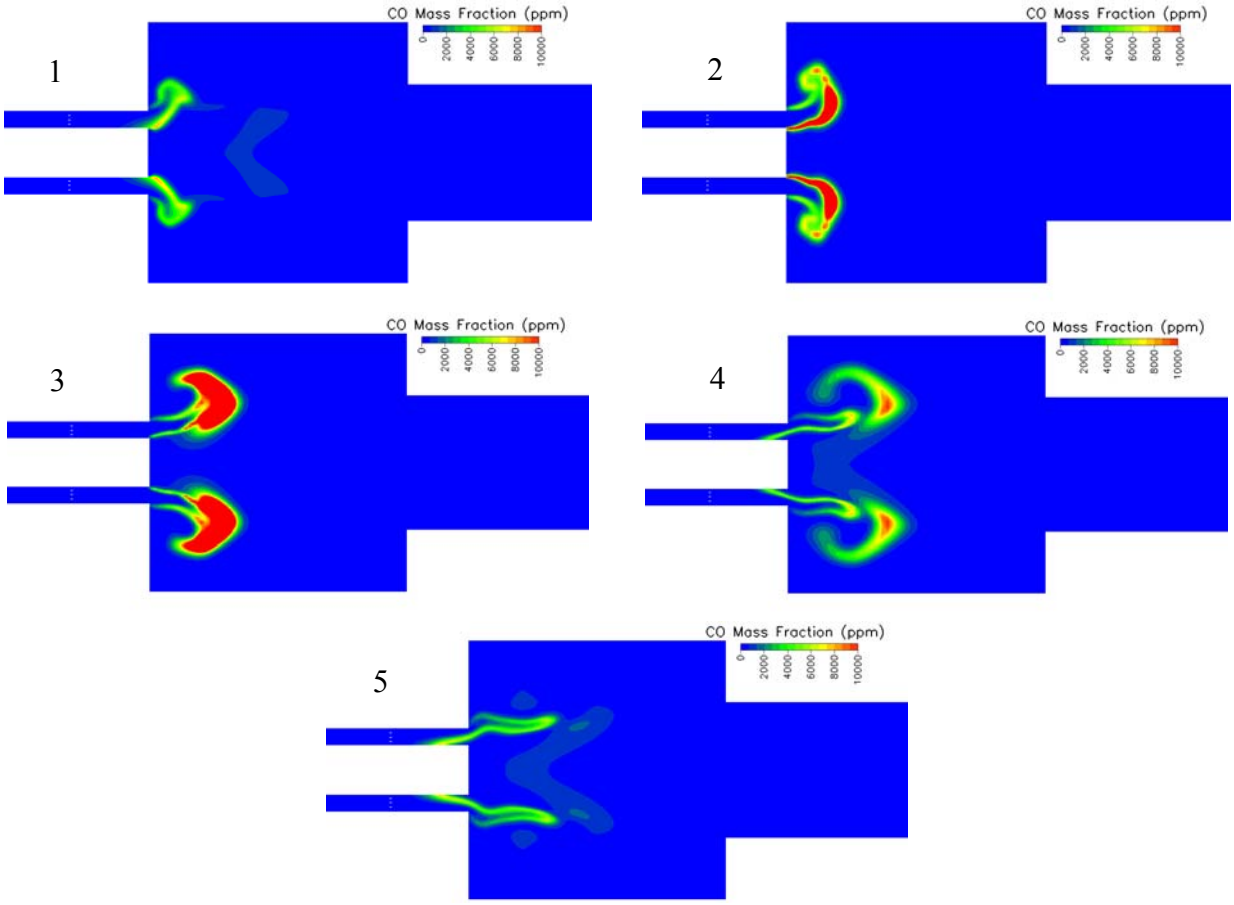

Figure 21. Predicted CO Mass Fractions During the Unstable Cycle [Unsteady RANS with 19 Species Chemistry]

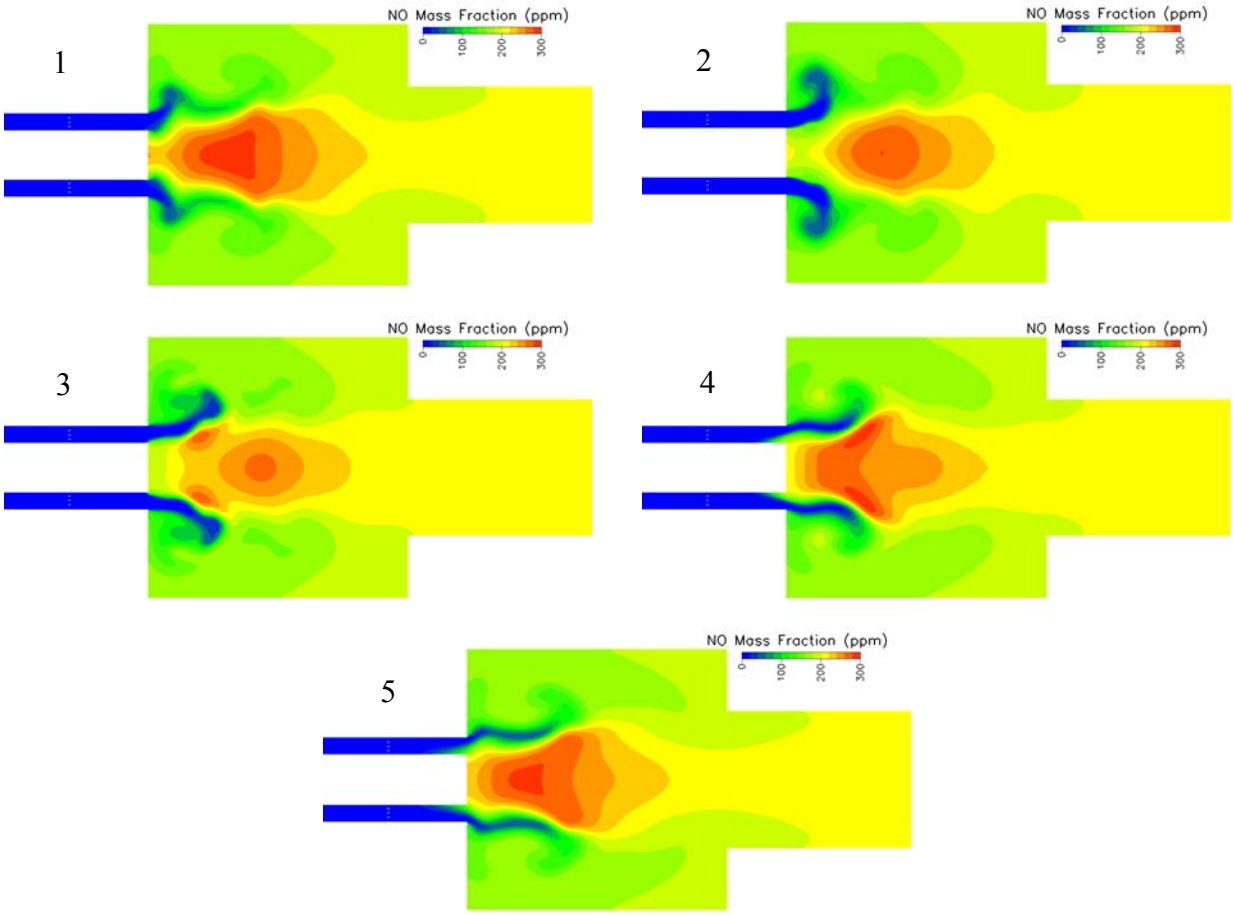

Figure 22. Predicted NO Mass Fractions During the Unstable Cycle [Unsteady RANS with 19 Species Chemistry]

4.1.5 Hydrogen-Air Combustion

For hydrogen-air combustion, a subset hydrogen mechanism of GRI2.11 was used as the base mechanism. The NO_x mechanism taken from Miller, 2000, was added to the base mechanism. A 7-step reduced chemistry was developed with this combined mechanism. Table 4 shows the 7-step (10-species) hydrogen-air mechanism. Figures 23 – 26 assess the performances of the 7-step reduced mechanism showing overall good agreement with results obtained from the detailed mechanism.

Table 4. Reduced Hydrogen Mechanism

(1)	2O = O2
(2)	H + O = OH
(3)	H2 + O = H + OH
(4)	O + HO2 = O2 + OH
(5)	O + H2O2 = OH + HO2
(6)	H + OH = H2O
(7)	O2 + N2 = 2NO

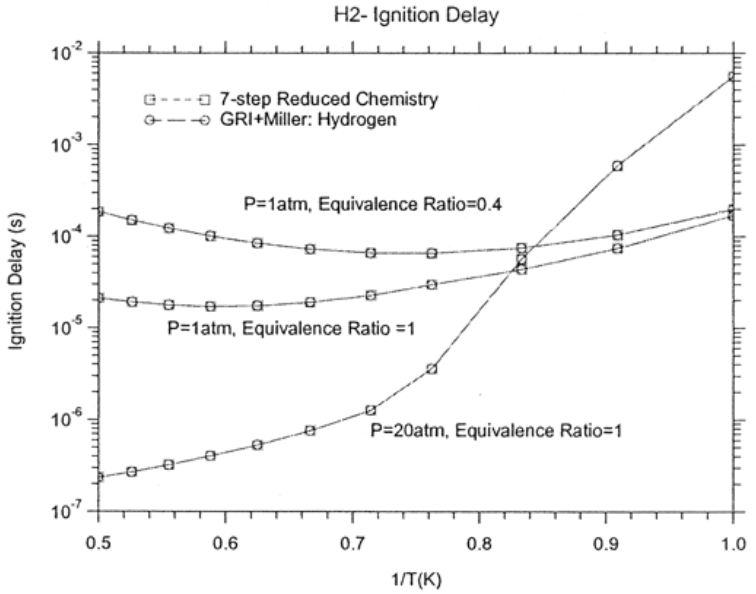

Figure 23. Ignition Delay Times Under Ambient and Elevated Pressures. Test cases include stoichiometric and lean mixture of equivalence ratio of 0.4. The 7-step reduced chemistry of H_2 predicts ignition delay in excellent agreement with those from the detailed mechanism based on GRI2.11 and NO_x mechanism from Miller.

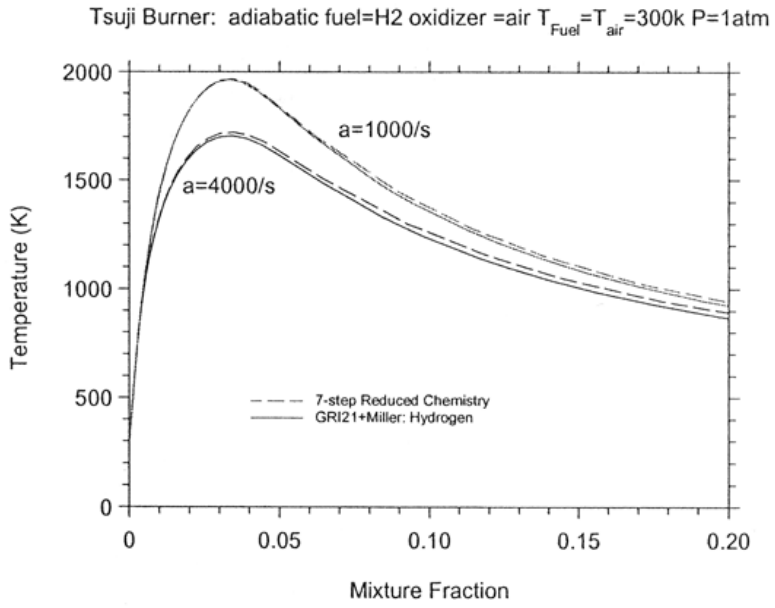

Figure 24. Validation of Hydrogen Reduced Chemistry for Opposed Flow Flames (Tsuji type burner) is Carried at Strain Rates at 1,000/s and 4,000/s and the Extinction Limit is about 12,000/s. The predicted temperatures by the reduced chemistry and the detailed mechanism are in good agreement.

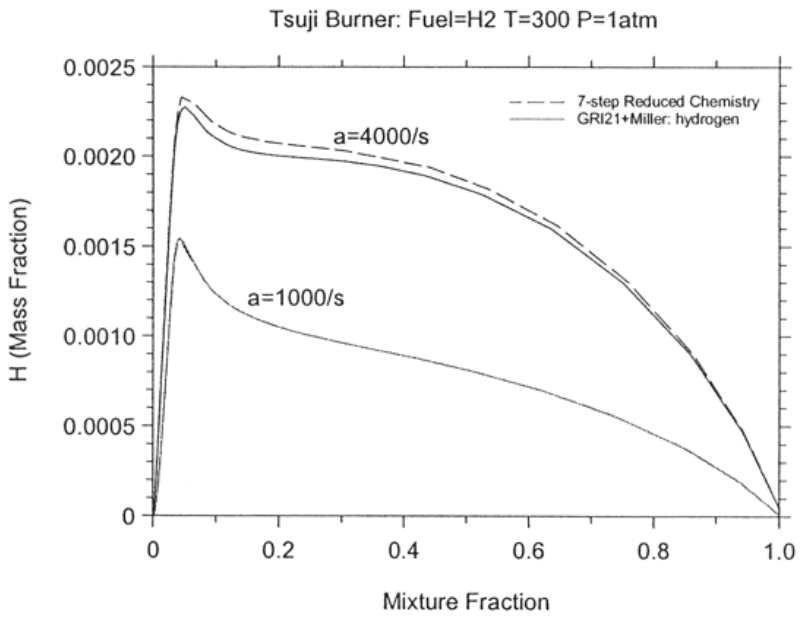

Figure 25. Validation of Hydrogen Reduced Chemistry for Opposed Flow Flames (Tsuji type burner) is Carried at Strain Rates at 1,000/s and 4,000/s and the Extinction Limit is about 12,000/s. The predicted H radical concentrations by the reduced chemistry and the detailed mechanism are in good agreement.

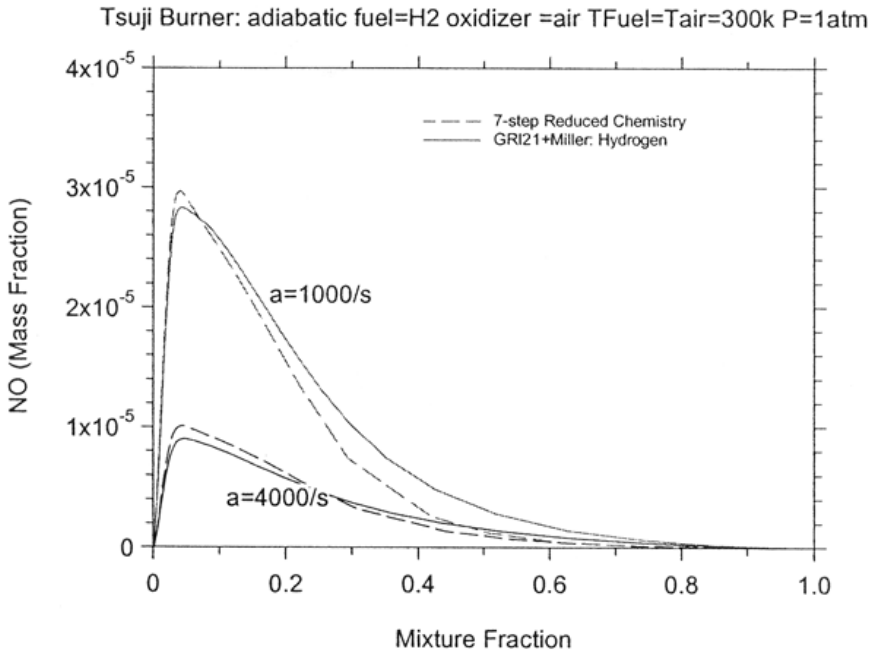

Figure 26. Validation of Hydrogen Reduced Chemistry for Opposed Flow Flames (Tsuji type burner) is Carried at Strain Rates at 1,000/s and 4,000/s and the Extinction Limit is about 12,000/s. The predicted NO concentrations by the reduced chemistry and the detailed mechanism are in good agreement.

Propane-Air Combustion: A detailed propane-air combustion mechanism was compiled by CFDRC based on LLNL propane mechanism with NO_x chemistry. This mechanism was used for development of a 19-step reduced chemistry. Table 5 shows the 19-step mechanism with the GRI2.11 NOx mechanism. Table 6 shows the 19-step mechanism with the Miller NOx mechanism. The performances of this reduced chemistry were assessed first with PSR and results are presented in Figures 27 and 28.

Table 5. Reduced Propane Mechanism (Pitz + GRI2.11 NO_x)

(1)	CH3 + H = CH4
(2)	H + CH4 = CH3 + H2
(3)	CH4 + OH = CH3 + H2O
(4)	CH4 + O = CH3 + OH
(5)	1.33 CH3 + .33 OH + .33 H2O + C2H6 + .67 CH2O = .33 H + CH4 + .67 O2 + C3H8
(6)	.50 H + .50 OH + .50 O2 + CH2O = 1.50 H2O + CO
(7)	OH + CO = H + CO2
(8)	H + O2 = OH + O
(9)	.50 OH + .50 H2O + O + C2H4 = CH3 + .50 H + .50 O2 + CH2O
(10)	.33 CH3 + .67 H + .33 OH + .33 H2O + C2H4 + .67 CH2O = .67 O2 + C3H8
(11)	.67 H2O + .33 CH2O = .33 CH3 + .67 H + .33 OH + .33 O2
(12)	C2H4 = H2 + C2H2
(13)	1.33 H + .67 O2 + C3H6 = .33 CH3 + .33 OH + .33 H2O + C2H4 + .67 CH2O
(14)	.67 CH3 + .33 H + 2O + .67 O2 + .33 CH2O + C3H8 + 2NO = H2 + 2.33 OH + 1.33 H2O + 2CO + C2H4 + N2
(15)	CH3 + C2H2 = H + C3H4P
(16)	H + C3H4A = CH3 + C2H2
(17)	.50 H + .50 O2 + C3H4A = .50 OH + .50 H2O + C3H3
(18)	O + NO + HCN = OH + CO + N2
(19)	H + CO + NH3 = H2 + OH + HCN

Table 6. Reduced Propane Mechanism (Pitz + Miller NO_x)

(14)	1.5 H + CO + .5 O2 + CH2O + N2 = .5 OH + .5 H2O + C2H2 + 2NO
(17)	02 + C3H3 + NO + HCN = H2 + CO + CO2 + C2H2 + N2
(18)	O2 + NO + HCN = OH + CO2 + N2
(19)	1.50 OH + .5 H2O + HCN = .5 H + CO + .5 O2 + NH3

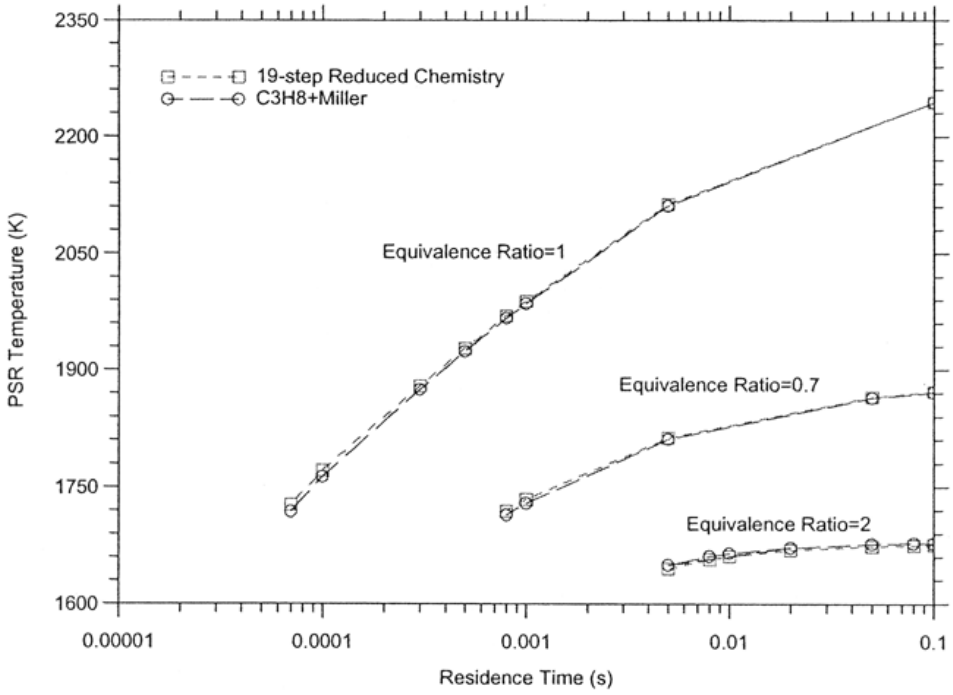

Figure 27. Comparison of Predicted Temperatures from a Perfectly Stirred Reactor Versus Residence Time for Three Different Mixtures. The 19-step reduced chemistry gives temperatures within 10% of those from the detailed propane mechanism (from LLNL) and Miller's NO_x mechanism.

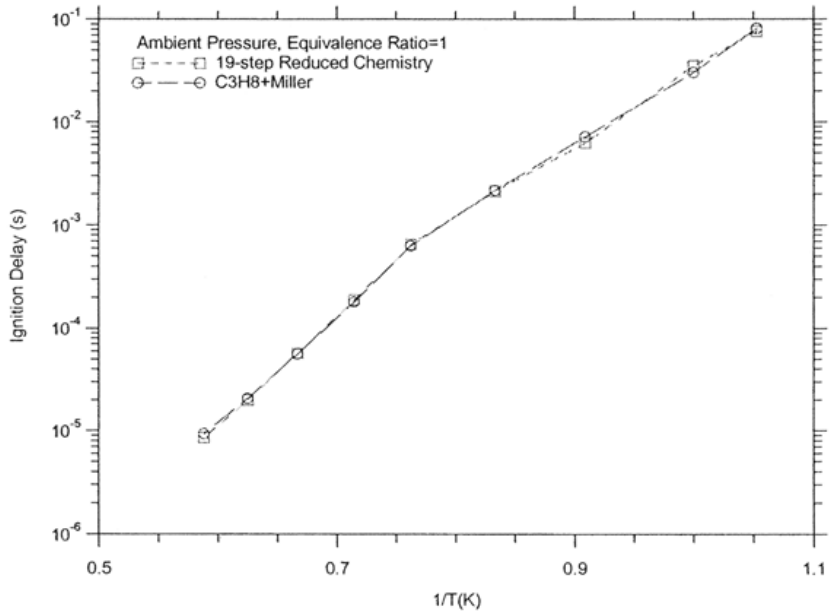

Figure 28. Comparison of Predicted Temperatures from a Perfectly Stirred Reactor Versus Residence Time for Three Different Mixtures. The 19-step reduced chemistry predicts NO_x level reasonable agreement with those from the detailed propane mechanism (from LLNL) and Miller's NO_x mechanism. The worst case is send fro the rich mixture of equivalence ratio of 0.7; however, the NO_x level is below 1ppm which is of negligible significance.

It is concluded from the comparisons that the 19-step performs very well for PSR over a wide range of residence times and equivalence ratios. Next, the reduced chemistry is tested for its accuracy in predicting autoignition delays. A detailed comparison is presented in Figures 29 and 30 showing good agreement with detail chemistry.

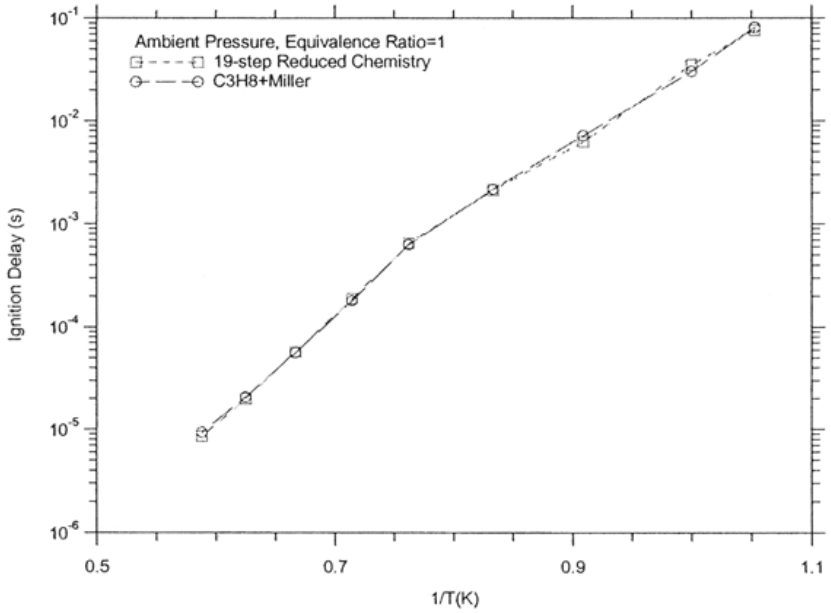

Figure 29. Comparison of Ignition Delay at Ambient Pressure Versus Temperature for Stoichiometric Mixture. The 19-step reduced chemistry predicts ignition delay in very good agreement with those from the detailed propane mechanism (from LLNL) and Miller's NO_x mechanism.

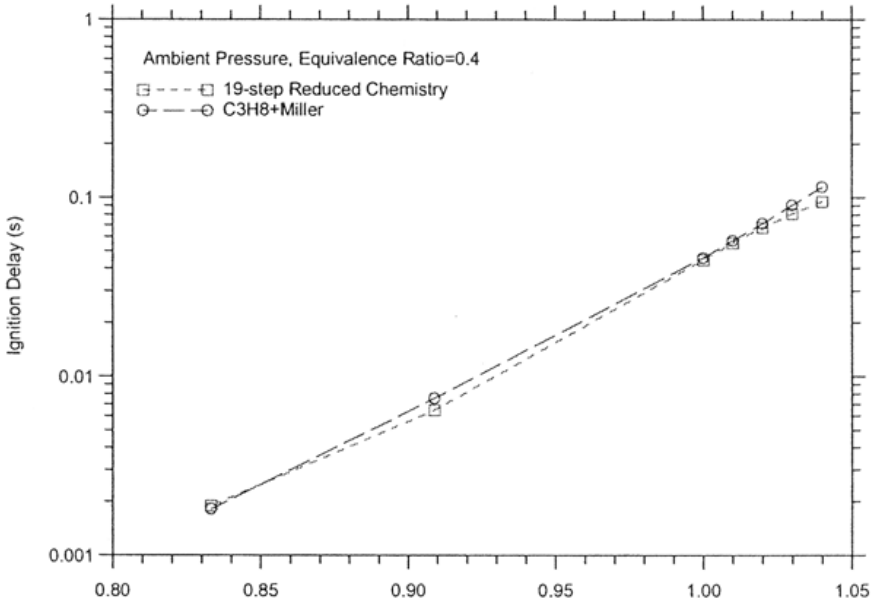

Figure 30. Comparison of Ignition Delay at Ambient Pressure Versus Temperature for a Lean Mixture of Equivalence Ratio of 0.4. The 19-step reduced chemistry predicts ignition delay in good agreement with those from the detailed propane mechanism (from LLNL) and Miller's NO_x mechanism.

In-Situ Adaptive Tabulation: The In-Situ Adaptive Tabulation (ISAT) method, developed by Pope (1997), was implemented in the LES code to efficiently store and retrieve reaction rates and/or integrated reaction increments. The ISAT method utilizes a binary tree data structure to store reaction information at compositions that are accessed during the LES calculation. Fast retrievals are used for revisited compositions. Three ISAT methods were implemented in CFD-ACE+. ISAT type 1 stores compositions in a table, where the tolerance is a function only of the input composition. First-time compositions are used in the future for queries that are close in composition space. No extrapolation or interpolation is used. ISAT type 2 performs linear extrapolation from existing composition points in the table. ISAT type 2 does not track growth of composition cells in the table, therefore the extrapolation may be inaccurate for large tolerance bands. ISAT type 3 allows each node in the binary tree to grow based on the local ellipsoid of accuracy (EOA). The EOA is computed from a Singular Value Decomposition (SVD) and allows linear extrapolation within a compositional node.

Test cases were performed to help validate the ISAT Type 3 method. The test cases included the DOE-NETL SimVal perfectly premixed combustor (Maloney, 2001) and the DOE-NETL partially premixed combustor (Richards and Janus, 1997). Comparisons of accuracy and cpu time between direct integration and ISAT were made. In addition, calculations were performed with staggered chemistry and non-staggered chemistry. The staggered chemistry approach computes integrated reaction rates only once per time step, while the non-staggered approach computes rates every time step within the iteration. The transient calculations required 8 iterations per time step for the premixed combustor case.

The reduced mechanisms, with steady-state species, can only be handled with the operator-splitting solution technique. Operator splitting only works for transient runs and uses a stiff ODE solver to solve the coupled set of species chemical kinetic equations. An average reaction rate (over the global time step) is then used in the overall conservation equation for each species mass fraction. For an initial steady-state condition, 1-step chemistry without operator splitting is used. Then, the mechanism is switched to the required multi-step mechanisms and the transient run is initiated. An overall time step of 1e-5 seconds was used for the premixed combustor case. Figure 31 shows the steady-temperature location using the 1-step chemistry and the 5-step and 15-step chemical mechanisms after 100 time steps. These results show that all three mechanisms predict a different flame location. This is somewhat surprising for the 5- and 15-step mechanisms since they were both derived from the full GRI mechanism. Further work is required to understand why the 5- and 15-step mechanisms give different predicted flameshapes. The shorter flamezone predicted by the 5-step mechanism allows instability to develop, while the longer flame does not. The weaker coupling for the longer flame is due to a greater distribution in the heat release zone.

ISAT results for the various different mechanisms are presented in Table 7. The ISAT results were obtained by setting the maximum tree records to 20,000 for the 5-step mechanism and 40,000 for the 19-step mechanism. When the maximum tree records were reached, then the tree is dumped and reinitiated from scratch. Another option to store multiple trees, each with a distinct temperature range, may also be utilized. For these tests, only 1 tree for the entire temperature range was used. The results show that a speedup can be achieved with the 5-step, 9-species mechanism. The computational times are reduced by a factor of 2.3 for the staggered

chemistry case. Compared to the direct integration/non-staggered case, the ISAT/non-staggered speedup is 4.4.

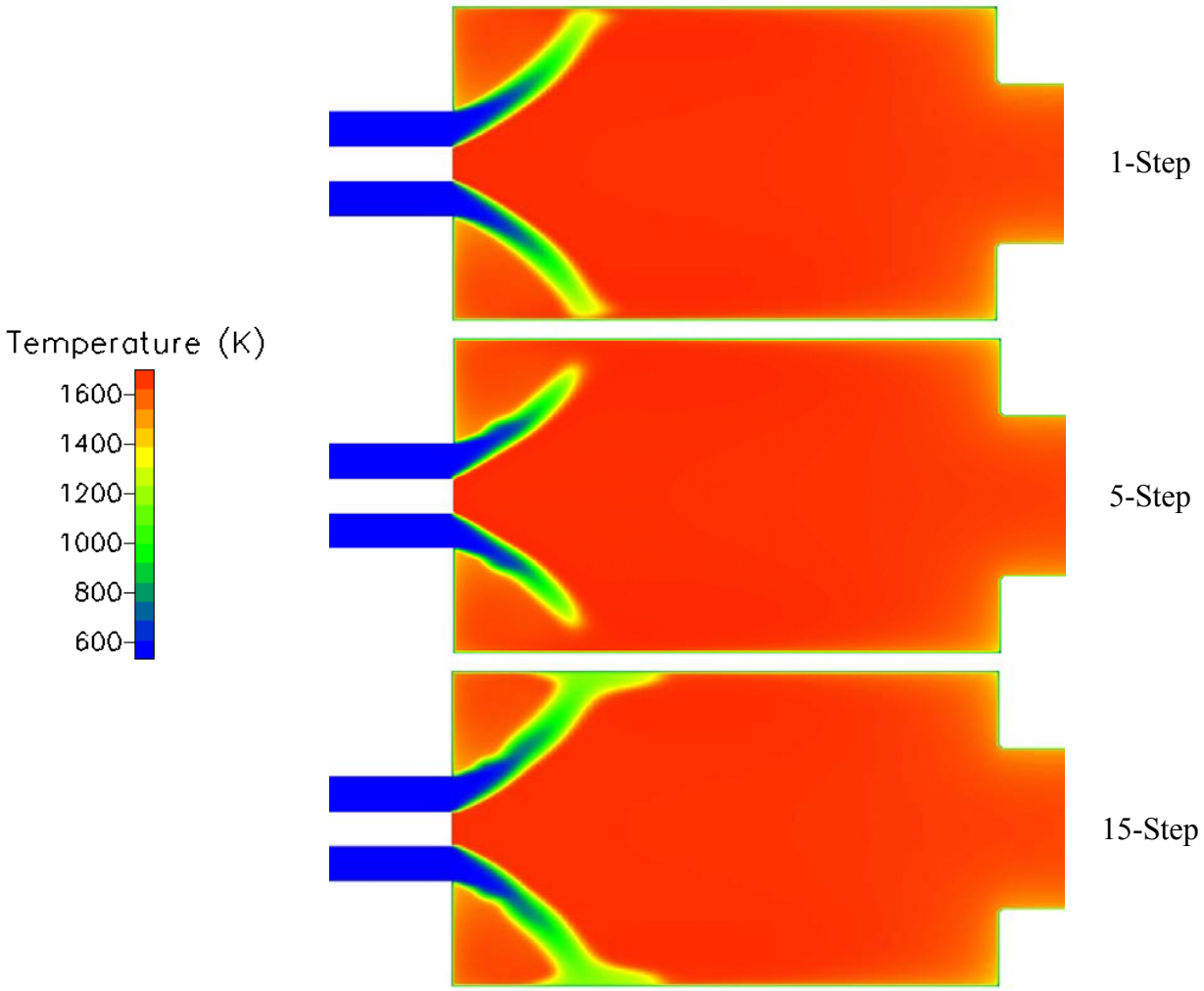

Figure 31. Temperature Predictions Using the 1-step, 5-step, and 15-step Chemistry

Table 7. Direct Integration and ISAT Results for Transient Combustor CFD Calculations

Premixed Case Mechanism	Kinetics Solution	Error Tolerance	% Retrieves	CPU Time
5-step	DI/Non-Staggered	—	—	400 min.
5-step	DI/Staggered	—	—	39 min.
5-step	ISAT/Non-Staggered	1e-4	88	91 min.
5-step	ISAT/ Staggered	1e-4	82	17 min.
5-step	ISAT/ Staggered	1e-4 (tighter radicals)	73	22 min.
15-step	DI/Staggered	—	—	45 min.
15-step	ISAT/ Staggered	1e-4	35	66 min.
1.Partially Premixed Case				
5-step	DI/Staggered	—	—	45 min.
5-step	ISAT/ Staggered	1e-4	70	32 min.

Figure 32 shows predicted transient pressure results with ISAT and direct integration. Good agreement is found when using an ISAT tolerance of 1e-4 (82% retrieves). Figure 33 shows predicted radial profiles of OH, and NO mass fraction using direct integration and ISAT with various tolerance levels. The tighter tolerance (73% retrieves) ISAT was needed to predict the OH and NO concentrations in the central recirculation zone. It appears that long residence time fluid is more sensitive to the ISAT tolerance. Comparisons of major species and temperature were excellent between direct integration and ISAT for either tolerance level. Figure 34 shows the entire flame zone comparisons between direct integration and the 73% retrieve ISAT. Good agreement was obtained.

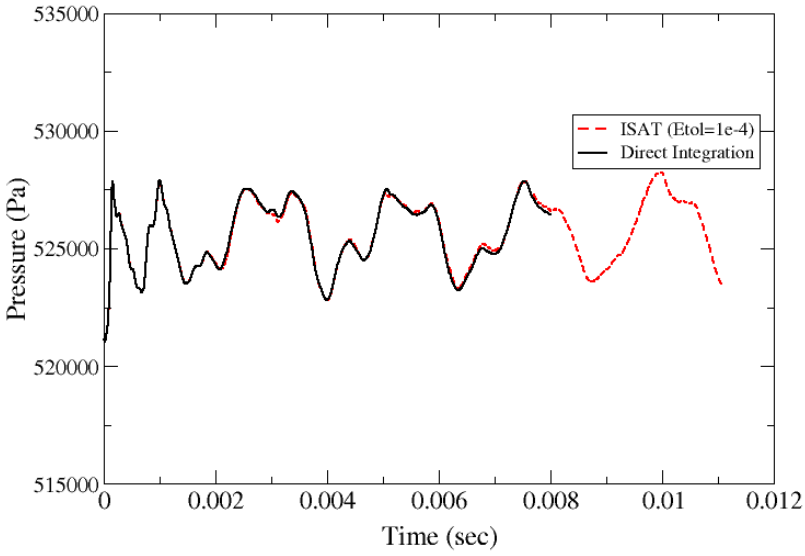

Figure 32. Comparison of Combustor Pressure History Using Direct Integration and ISAT for the 5-step, 9-species Chemistry

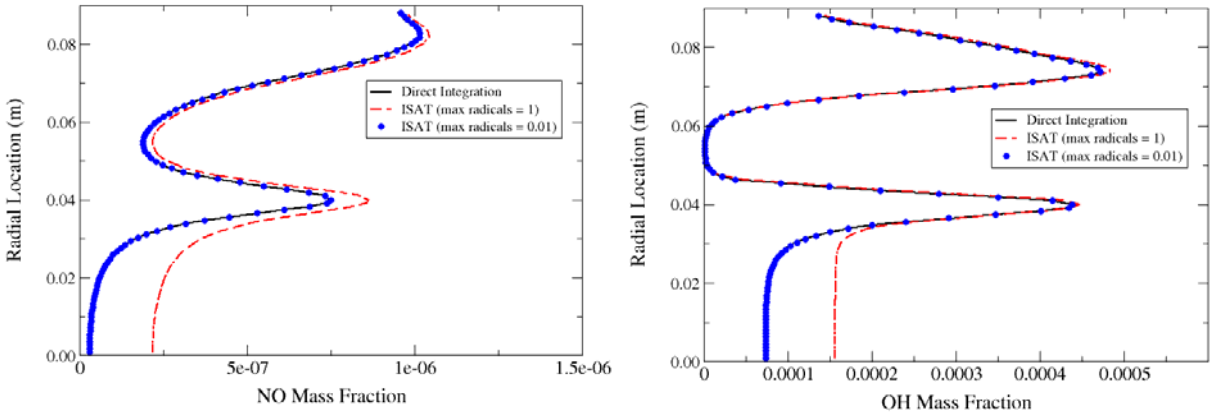

Figure 33. Comparisons of Predicted Radial Profiles of NO and OH Using Direct Integration and ISAT with Different Tolerance Levels

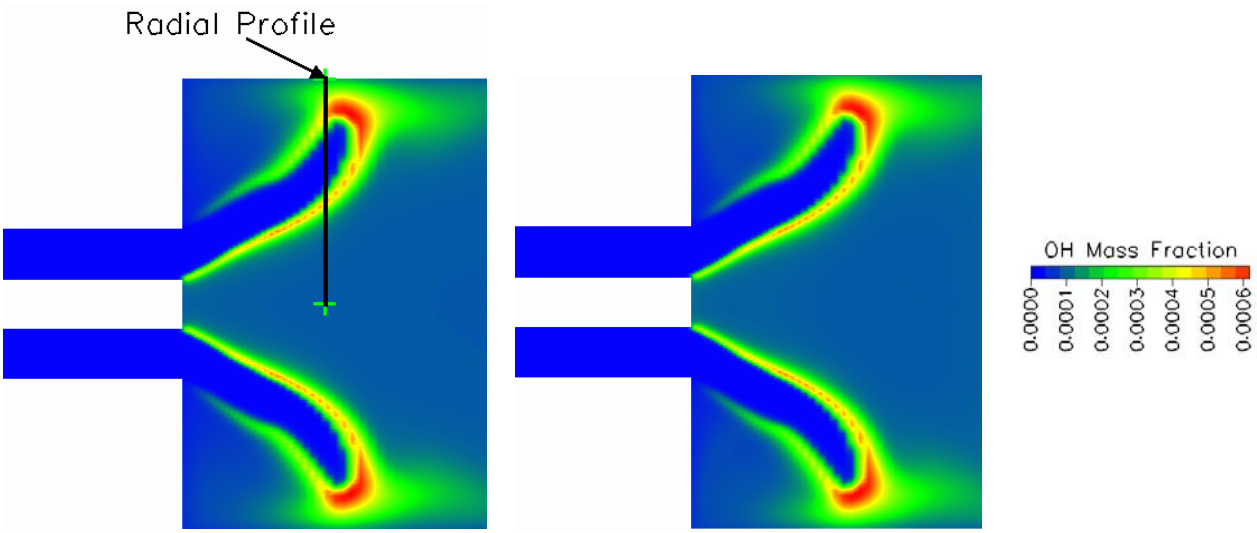

Figure 34. OH Contour Predictions at 6 msec Using Direct Integration and ISAT (73% retrieves)

For the 15-step chemistry, a speed-up was not achieved with ISAT, even though 35% of the computations were retrievals. These results show that for more detailed chemistry, the retrieval process is fairly expensive - even more than direct integration. Pope and coworkers have reported speedups of 10-100 for Monte Carlo PDF calculations. To achieve this speed-up, ~99% of the chemical kinetic calculations would need to be fast retrievals. Approaches for improving the ISAT method need to be investigated, including: multiple tree storage, more accurate mapping gradient solution, more accurate and/or efficient singular value decomposition, and a more efficient tree structure (PK-tree).

Artificial Neural Networks: An artificial neural network (ANN) method was developed by Georgia Tech for speeding up the chemical kinetic calculations in comprehensive turbulent reacting flow codes. The full final report from Georgia Tech (Kapoor and Menon, 2003) is included as an addendum to this final report. A summary from this report on the ANN method and results will be reported here.

An ANN is a structure of several interconnected nonlinear elements that function like biological neurons with an ability to learn from a set of input-output parameters. When the ANN is subjected to a new sample set the predicted output should be within a sufficient level of accuracy. The information in the ANN is stored in the form of weights and biases, which are computed iteratively in the learning phase of the network training. Once the ANN is trained, fast recall kinetic calculations can be performed and only a small amount of memory for storing the weights and biases is required.

Figure 35 shows a multilayer perceptron network that is typical of a three layer neural network that has been used by Georgia Tech for representing laminar chemistry. The inputs are the mass fractions and temperature, while the outputs are the new mass fractions and temperature after

reaction for a given time step. The accuracy of the network when used in the combustion LES code will depend most strongly on the initial dataset used to train the ANN. The learning algorithm utilized is of lesser importance in terms of the overall ANN accuracy. Georgia Tech used both a three-layer scaled conjugate gradient (SCG) back propagation network (Christo et al., 1996) and a Levenberg-Marquardt back propagation network (Blasco et al., 1998). Tests were also performed to determine the optimum input-output range and transformations for the ANN. Due to the highly non-linear reaction rates, a logarithmic transformation was needed. Several mechanisms and tests were performed to demonstrate the validity of the ANN approach. These tests included methane-air mechanism with a 5-species laminar ANN (LANN), 8-species LANN, 9-species (CH4-air) LANN, and 5- and 9-species turbulent ANNs.

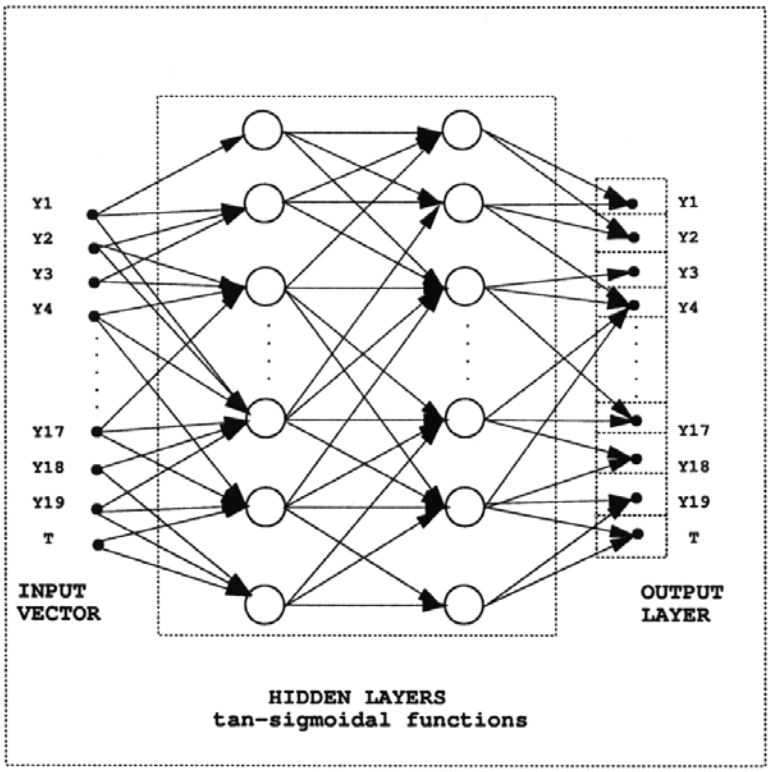

Figure 35. A Three-Layer Neural Network Structure used in the LANN Method

A single-step global mechanism (Westbrook and Dryer, 1981) involving 5-species was first used to test the LANN approach. A 2D DNS (400x400 grid points) simulation with a stationary premixed flame positioned in the center was used as the initial test. The simulations used a finite-volume scheme based on the explicit MacCormack predictor-corrector method, being 2^{nd} order in both space and time. An inflow velocity (with a 1.77 m/s rms) is set equal to the laminar flame speed of the stoichiometric methane-air mixture. An isotropic turbulent field was initialized in the domain. Figure 36 shows instantaneous results using the LANN, as well as a comparison of 1D profiles using LANN and direct integration (DI). The ANN results are in excellent agreement with the direct integration results.

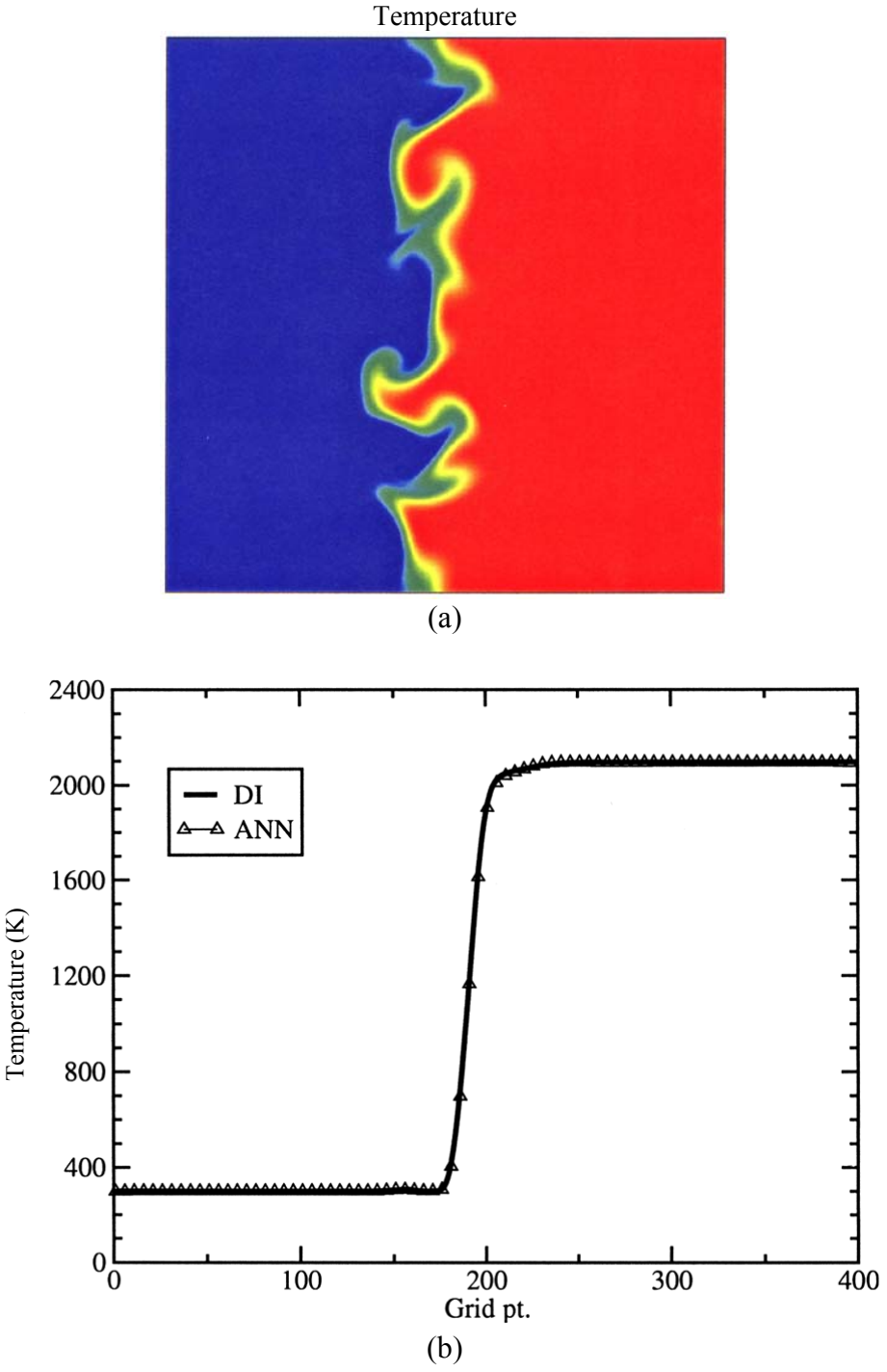

Figure 36. (a) Instantaneous LANN Results and (b) Comparisons of Time-averaged LANN and DI Profiles [5-species, single-step kinetics]

Similar calculations with 8-species and 9-species mechanisms were also performed. These mechanisms were developed using steady-state species assumptions, as described earlier. These mechanisms include the following major reaction steps, as shown below.

8-species Mechanism

$$CH_4 + 2H + H_2O \Leftrightarrow CO + 4H_2$$
$$CO + H_2O \Leftrightarrow CO_2 + H_2$$
$$2H + M \Leftrightarrow H_2 + M$$
$$O_2 + 3H_2 \Leftrightarrow 2H + 2H_2O$$

9-species Mechanism

$$4OH \Leftrightarrow O_2 + 2H_2O$$
$$2OH + 0.33CH_4 \Leftrightarrow 1.67H_2O + 0.33CO$$
$$H_2 + 0.33CO \Leftrightarrow 0.33H_2O + 0.33CH_4$$
$$H_2 + 4OH + 0.33CO + N_2 \Leftrightarrow 2.33H_2O + 0.33CH_4 + 2NO$$
$$2OH + CO \Leftrightarrow H_2O + CO_2$$

The ANNs produced for these mechanisms were similar to the one for the 5-species mechanism, though a larger number of ANNs were required to account for more reactive scalars. Figure 37 shows a comparison of instantaneous CO and temperature contours using DI and LANN, along with a comparison of time-averaged profiles of CO and temperature for the 8-species mechanism. These results show that the LANN approach is able to do fairly well for the major species and temperature but does a poor job for intermediate minor species. It was determined that different transformations were needed for major species and minor species. For most of the major species, the logarithmic transformation was used, but for some of the minor species, a linear transformation in some of the non-active temperature bins was used.

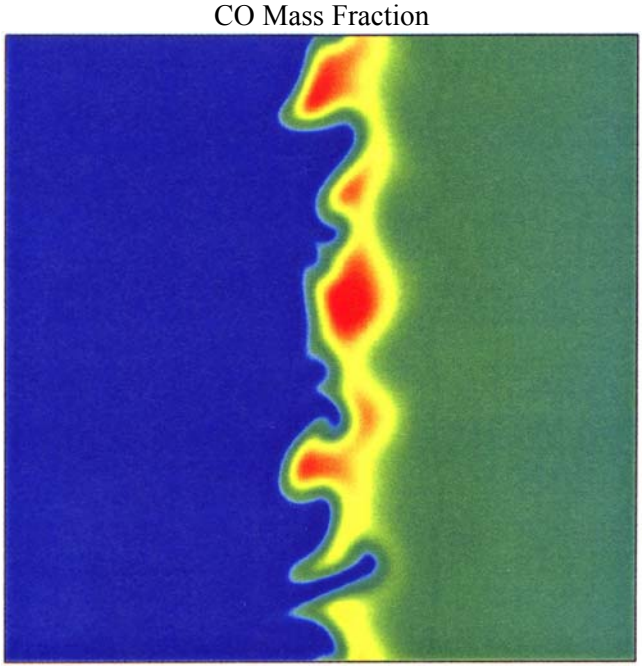

(a)

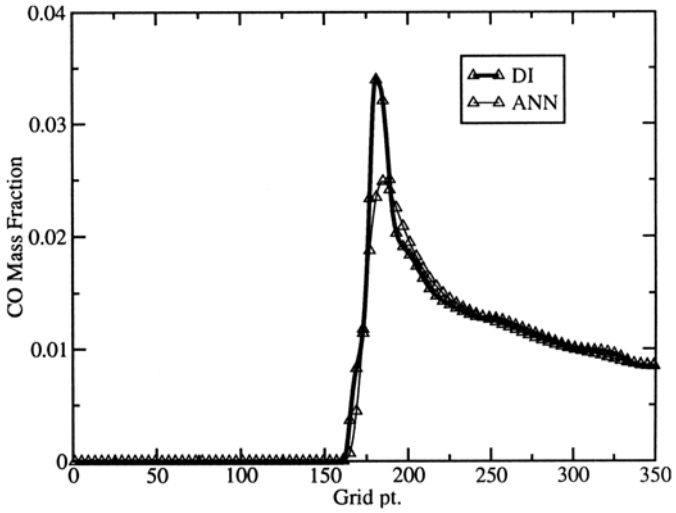

(b)

Figure 37. (a) Instantaneous LANN Results and (b) Comparisons of Time-averaged LANN and DI Profiles [8-species, 4-step kinetics]

Figure 38 shows time-averaged profile comparisons for temperature, major species, and minor species using the 9-species mechanism and using the new transformation for the LANN. These results show excellent agreement using the new LANN method. A proper mapping of the scalar-temperature space and appropriate transformations are required for the LANN method with multi-step chemistry. These LANN studies have demonstrated an approach that can handle both major and minor species.

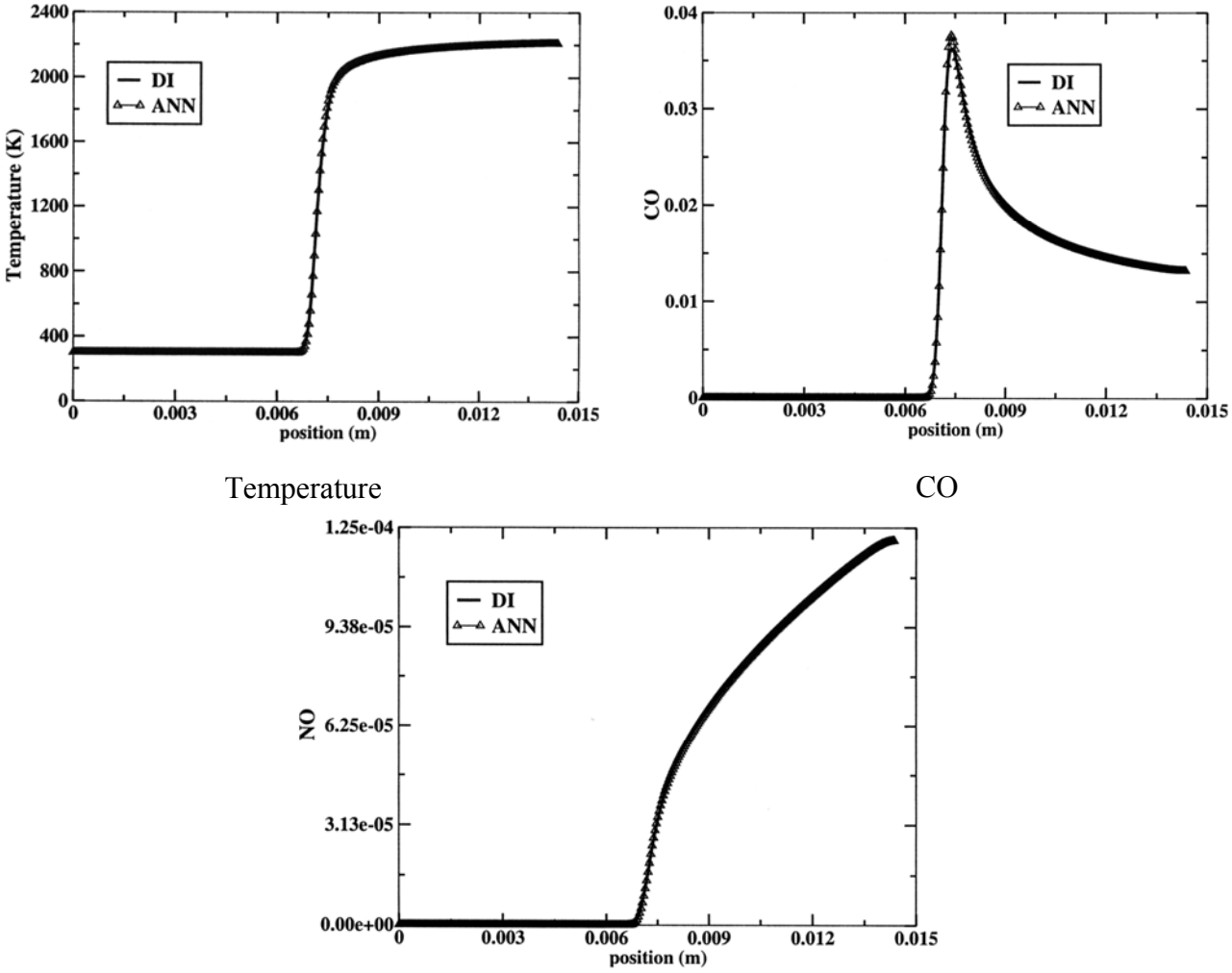

Temperature CO

NO

Figure 38. Time-averaged Profile Comparisons for the New LANN and DI Using the 9-species and 5-step Kinetic Mechanism

The computational speed-up of the LANN method compared to DI was determined for these chemical mechanisms. Table 8 shows the computational cost using LANN is between 10 and 20 times lower than DI. The actual gain is more in case of the single-step reaction since the ANN structure is less complicated compared to the 4- and 5-step mechanisms. Georgia Tech claims that cost reduction is expected to become even higher for a larger chemical mechanism and when simulations are performed for multiple flow-through times.

Table 8. Speed-up Obtained Using LANN [CPU Time Per Step (sec)]

	DI Cost (x)	**ANN cost (y)**	**Speedup (x/y)**
5-species, 1-step	1.50	0.073	20
8-species, 4-step	4.76	0.48	10
9-species, 5-step	4.31	0.37	11

The ability to generate a turbulent ANN (TANN) using turbulence intensity and length scale as additional input variables was also investigated. This TANN approach would be needed to eliminate the need to do DNS and take the place of a subgrid chemistry model in LES. This would produce further computational savings compared to the LANN method. The 5-species global mechanism was used to generate the TANN using 2D DNS on a 353x353 grid. Simulations were carried out for a range of u' in a range $0< u'/SL < 10$. This should account for the turbulent scales that will be lost when a coarser LES grid is used. This considers the flame-turbulence interaction problem as a generic subgrid domain to develop the training set, and is assumed to be applicable to all fine-scale premixed flame-turbulence interactions. This assumption remains to be confirmed and will be the focus of future studies. Results from preliminary calculations are shown in Figure 39. Here a coarser 177x177 LES grid was used. The results show that the TANN is able to capture the overall flame-turbulence behavior, though further investigation is needed to determine the reason for minor discrepancies that are observed.

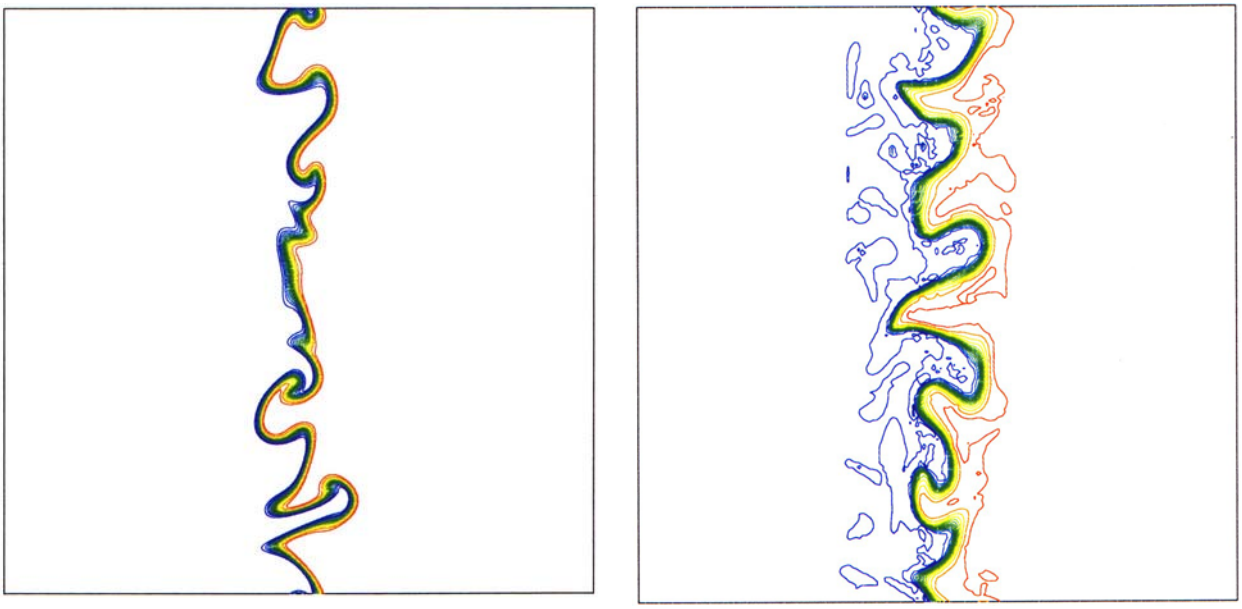

(a) 1912K-533K, DI

(b) 1911K-533K, TANN

Figure 39. Comparison of Instantaneous Temperature Using DI (DNS) and TANN (LES) for the 5-species, Single-step Kinetics

The LANN method was implemented in CFD-ACE+ for the 5-species, 1-step mechanism. The DOE SimVal baseline case was used to test the method. The SimVal case includes perfectly premixed inlet conditions (ϕ=0.6) and an inlet temperature of 533 K and combustor pressure of 5.1 atm. Georgia Tech provided the LANN routines to CFDRC at these appropriate conditions. Figure 40 shows the predicted instantaneous temperature using LANN and DI. The results show that the global features of the flame are similar, but detailed features are not captured with the LANN. It is unclear why the LANN method does not better match the DI results. Attempts to modify the way Georgia Tech generated the LANN were tried, including holding the temperature constant during the reaction increment, similar to the way CFD-ACE+ handles the reaction. These attempts did not provide any improvement. Further work is needed to resolve the LANN

implementation in CFD-ACE+ and the usefulness of the method for a full combustor simulation. It is possible that the limited data used to train the LANN was insufficient for the composition ranges experienced in a combustor CFD simulation. The mixing levels covered a broader range in the CFD simulation compared to the 2D DNS training data and therefore different compositions were experienced during the reaction process. Improvements to the LANN recall accuracy or to the training data itself will likely be needed.

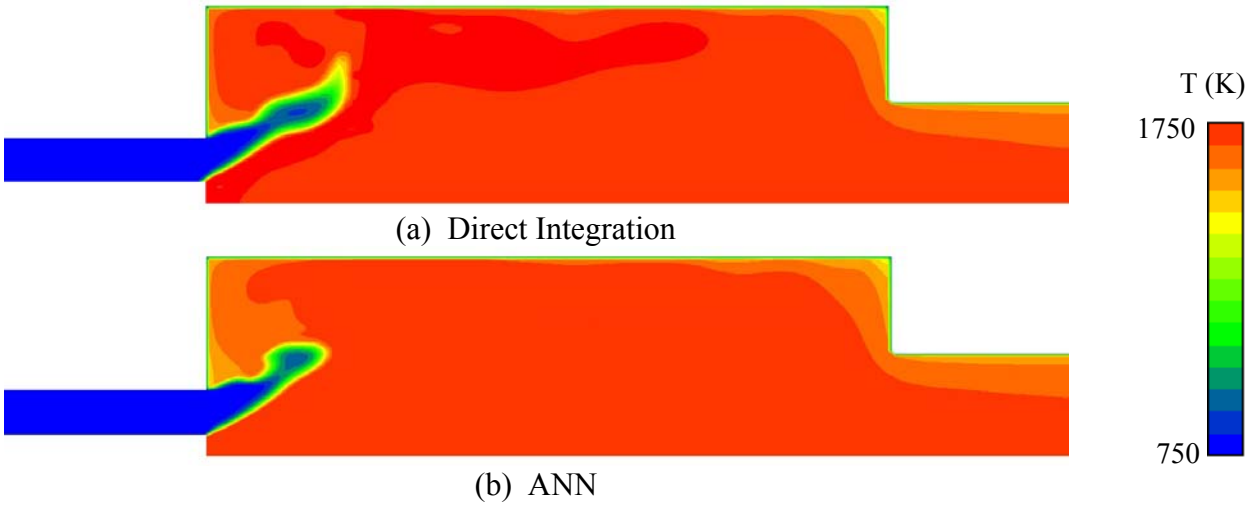

Figure 40. Instantaneous Temperature Prediction of DOE SimVal Combustor Using DI and LANN [5-Species, Single-step Mechanism; ϕ=0.6, T_{in}=533 K, P=5.1 atm]

4.1.6 Parallel Performance

The parallel performance of the LES code has been tested on a cluster of 64 PC's with the Redhat 6.2 Linux operating system. The cluster of PC's are composed of: 8-800 MHz, 8-900Mhz, 16-1000Mhz, and 32 1200 MHz AMD Athlon Processors. Each processor is connected through a 100BASE-TX Ethernet Fully Connected Network Topology. A set of 16 PC's are connected to one 3Com SuperStack II Switch. A total of 4 switches are needed for all the PC's. The four switches are connected to a 3Com matrix module creating one virtual switch between all 64 processors. A characterization of the processor to processor communication performance in conjunction with the Message Passing Interface (MPI) was performed.

The transfer time plotted against data size is shown in Figure 41. For data sizes less than 1 klb, the time to transfer is approximately equal to the communication latency time (minimal time to transfer a given amount of data) of about 5.0e-5 seconds. The transfer time grows exponentially for data sizes between a klb and 10 klb. Then the transfer time becomes linear for data sizes greater than a megabit, where the throughput is maximized. This simply shows that it is more efficient to transfer one large array than to transfer several smaller arrays. Figure 42 show the throughput curve for a processor to processor communication. This shows the maximum throughput attainable is 90 mgb/s.

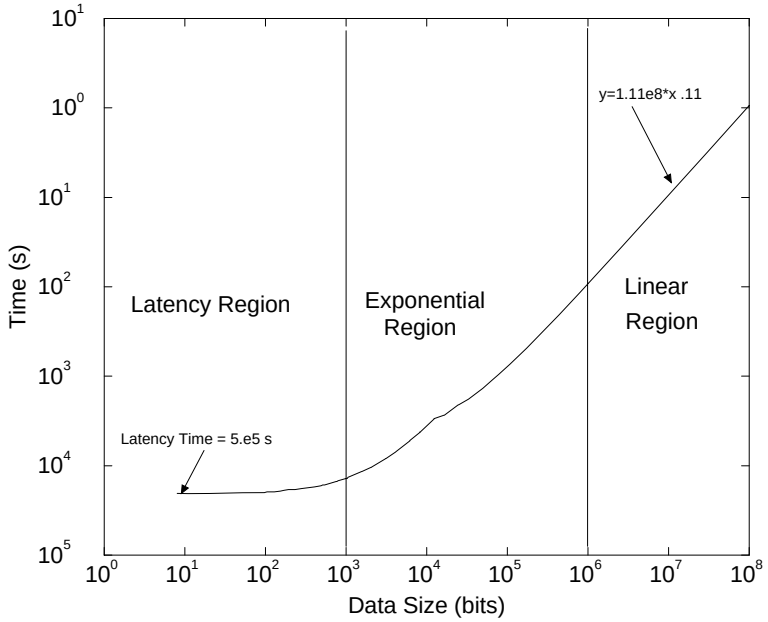

Figure 41. Transfer Time vs. Data Size

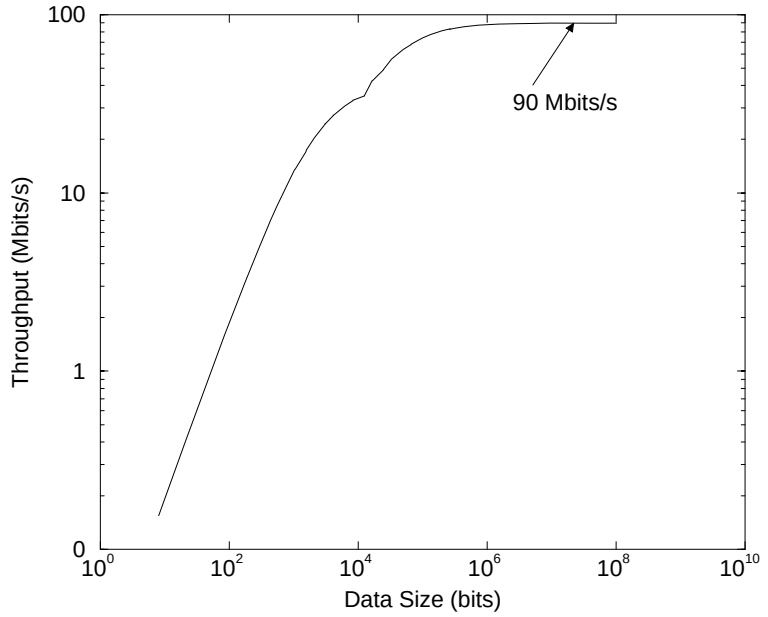

Figure 42. Throughput vs. Data Size

Load balancing of the communication domain, data buffering, synchronization, and communication to computational domain size ratio are parallel issues that have been found to affect the parallel performance of the CFD-ACE+ software as applied on the Linux cluster at CFDRC. The parallel performance of CFD-ACE+ was investigated and optimized for transient flow calculations.

The communication for a given LES problem can be minimized by either decreasing the amount of data to be transferred between processors or by increasing the computational domain size. Greater parallel scalability can be achieved as the domain surface to volume ratio becomes smaller. This gives LES a large potential in scalability due to the large computational domain usually involved.

Load balancing of the communication domain must be considered when using a large number of processors. Large synchronization times can develop if the number of neighboring processors differs for a given processor. For example, a processor with 3 neighbors will have to wait on a processor with 6 neighbors. The k-way partitioning implemented in Metis (domain decomposition software use in CFD-ACE+) minimizes the amount of transfer data but doesn't balance the number of neighboring processors. This is difficult to accomplish in a graph decomposition, but can be achieved through geometrical decompositioning. If a partitioning along an orientation axis can be achieved, then the number of neighbors for each domain will be load balanced (excluding end domains). The significant improvement in parallel performance for an x-cut (or sliced) decomposition versus an arbitrary (k-way) decomposition is shown in Figure 43. A 33% improvement in clock time was obtained with the x-cut decomposition of a 32 processor reacting backstep case.

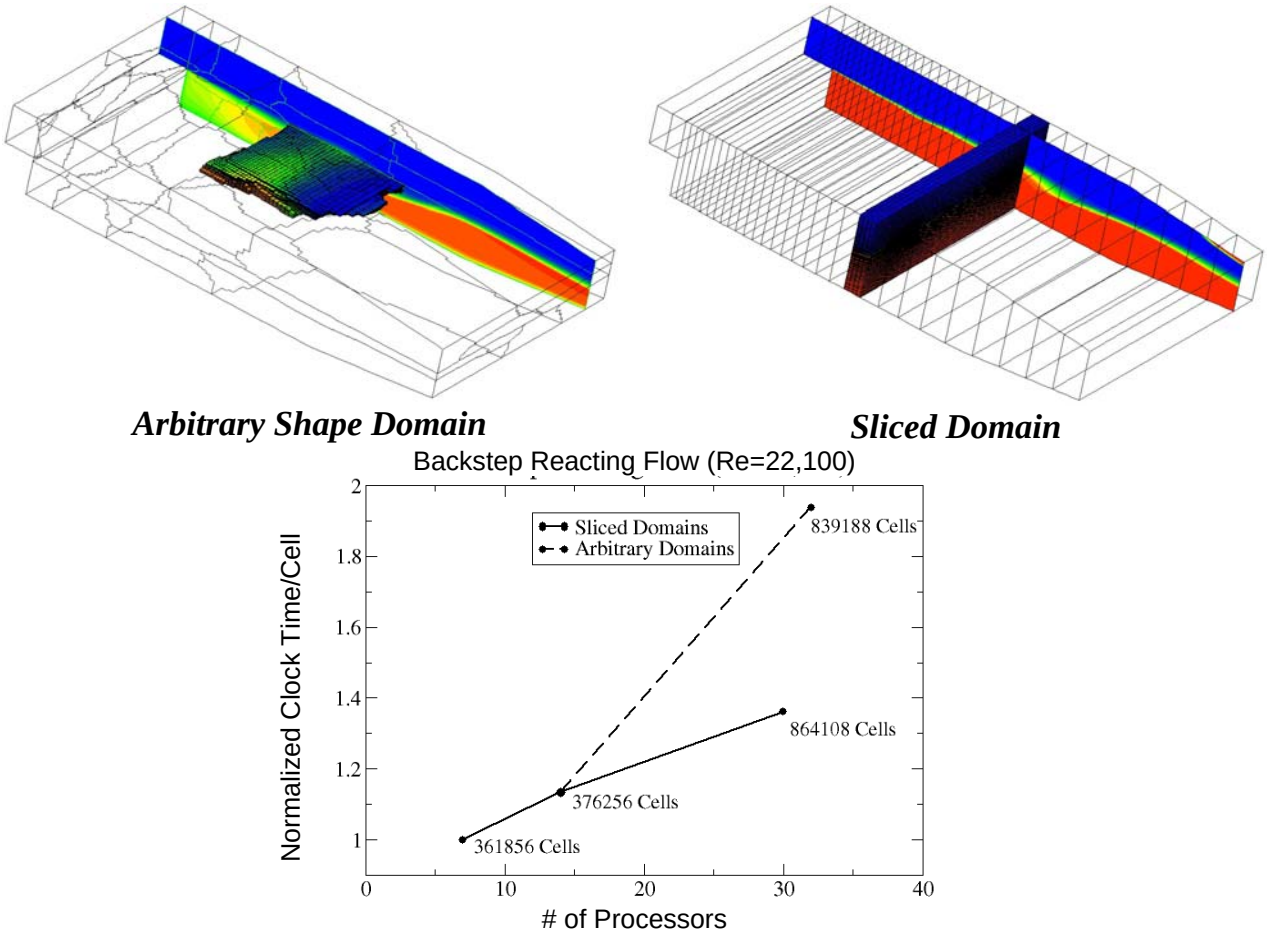

Figure 43. Normalized Clock Times per Cell for Arbitrary and X-cut Decompositions in a Reacting Backstep Cases

Other methods for improving the parallel performance were also tested. The packing of ghost cell data was improved by storing a map of the ghost cell position. This increases the required memory slightly but decreases the extent of the packing loop. The loop now goes over the surface of ghost cells rather than over the total volume of cells. This has a greater effect for domains with a small surface to volume ratio.

Typical LES runs require 5-10 sweeps on the pressure correction equation for each iteration. Also, a time step will require 5-10 iterations to obtain convergence. This zonal implicit method was employed with the CGS numeric solver. This slightly decreases accuracy of the solver, but for transient calculation with small time steps (as needed for LES), the convergence can be maintained with no more than double the number of iterations per time step.

These parallel improvements were applied to a transient simulation of a three-dimensional incompressible lid driven cavity. In order to assess parallel performance the number of time steps, iterations, and sweeps were held constant for all runs to maintain a constant computational load. A structured grid with dimensions 191x191x95 was created for the lid driven cavity investigated by Prasad and Koseff with a SAR ratio of 0.5 (discussed in the next section). Figure 44 shows the speedup of compute time on the LES cluster. The transfer time of ghost cell data remains constant for all cases since geometrical partitioning was used to decompose the domain along the x-axis. This type of decomposition creates a y-z plane of ghost cells in the interior of the domain. Since the computational grid size in the y-z plane is constant in the x direction, the number of ghost cells will also be constant, independent of the total number of processors. The parallel efficiency of the 8 processor case was 98% (i.e., 2% of the total time was spent in parallel transfer). Therefore, the wall clock time here can be used as a base for the speedup comparisons for the 16, 32, and 64 processor cases. The 8, 16, and 32 processor cases were run on 1200 MHz machines. The 64 processor case is obviously distributed over a non-homogeneous network. The speedup of the 64 processor case was limited by the slowest processor speed. To account for this, the 8 processor case was run on the 800 MHz processors as well. The ratio of the two 8 processor case times was used to scale the 64 processor case. It was found that the 800 MHz machines were 1.24 times slower than the 1200 MHz machines for this case. The speedup obtained for the 64 processor case was 52 which is about an 80% efficiency. The efficiency of the original parallel method (fully implicit) in CFD-ACE+ was only 60% for the same 64 processor case. The significant improvements in the parallel speedup is crucial for performing practical engineering LES.

4.1.7 First Consortium Meeting

In November 30, 2000, the first meeting of the Combustion LES Consortium was held at CFDRC. The agenda of the meeting is shown in Figure 44. The purpose of the consortium was: (1) to guide and direct software development and validation, and (2) to transfer the LES Software to industry. The consortium members are shown in Figure 45. All organizations were present except Siemens-Westinghouse, Precision Combustion, and NASA GRC.

Welcome	Cliff Smith	9:00 - 9:05
CFDRC's Perspective	Ashok Singhal	9:05 - 9:10
DOE's Perspective	Tom O'Brien	9:10 - 9:15

Project & Consortium Overview	Cliff Smith	9:15 - 9:40
Starting Code: CFD-ACE+	Milind Talpallikar	9:40 - 10:00
Background/Current Status	Steve Cannon	10:00 - 10:30
BREAK		10:30 - 10:35
Planned Code Development		
- LEM Model & Neural Nets	Suresh Menon	10:35 - 11:10
- Reduced Chemistry	J.Y. Chen	11:10 - 11:40
- CMC Model	Virgil Adumitroaie	11:40 - 12:00
LUNCH		12:00 - 12:30
Validation Cases/Alpha Testing	Steve Cannon, Others	12:30 - 1:15
Discussion / Feedback	All	1:15 - 2:30
Opportunity for Post-Processing Funding	Cliff Smith	2:30 - 2:40
Written Feedback / Questionnaire	All	2:40 - 3:00

Figure 44. Agenda of the First Combustion LES Consortium

Industrial Consortium

Charter Members

1. Rolls Royce-Allison
   M.S. Anand
2. Honeywell
   Jurgen Schumacher
3. Solar Turbines
   Alan Kubasco
4. Coen
   Paul Matys
5. McDermott Technologies
   Alan Sayre
6. Siemens-Westinghouse
   Rich Valdes
7. Pratt & Whitney
   Jeff Lovett
8. GE Power Systems
   Anil Topaldi
9. Woodward FST
   Geoff Myers
10. Vapor Power
    Tanh Tran

Non-Charter Members

1. Precision Combustion
   Hasan Karim
2. Virginia Tech
   Uri Vandsburger
3. Parker Hannifin
   Erlendur Steinthorsson
4. RamGen Power
   Jon Tonouchi
5. John Zink
   Carol Schnepper

Government Members

1. DOE-NETL
   Tom O'Brien
   George Richards
   Dan Maloney
2. Air Force
   Balu Sekar
3. DOE-ANL
   Tom Obot
4. NASA GRC
   Nan-Suey Liu

Figure 45. Combustion LES Consortium Members

At the end of the meeting, a questionnaire was filled-out by each consortium member. Many useful comments were received. Some of the common themes in the questionnaire were:

1. Everyone seemed to be excited about the consortium, and the possibility of getting combustion software that can model instability, flashback, lean blowout, emissions, etc.

2. Everyone seemed to like our approach.

3. It was important to have a validated code that was efficient and easy-to-use.

4. It was important to have at least one validation case that closely resembles an industrial combustor.

5. The feasibility of one-day LES calculations should be established.

6. The need of LES calculations versus unsteady RANS calculations should be determined.

7. Part of the validation exercise should include comparison with other codes, e.g. FLUENT.

8. It would be nice to have spray included (editors note: will be covered under an Air Force Phase II SBIR Program).

9. Software should be portable to computer platforms other than PC-Linux clusters.

10. Software should be provided earlier to consortium members (i.e., do not wait until start of third year of project).

11. More discussion is needed to decide what validation cases should be selected. The NETL case should definitely be one of the validation cases.

12. Next meeting should be longer (i.e., 1 ½ - 2 days rather than one day).

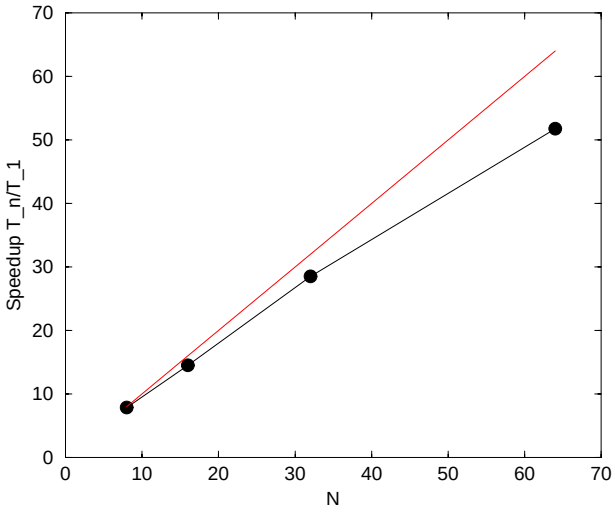

Figure 46. Speedup vs. Number of Processors

4.2 Year Two: Validation (Alpha Testing)

In Year Two, the combustion LES code was validated against data to determine its ability to efficiently and accurately capture turbulent combustion in gaseous-fueled combustors. The validation cases included: 1) Lid-Driven Cavity, 2) the Loughborough non-reacting combustor port flow, 3) a non-reacting and reacting back-step, 4) lean premixed bluff-body experiment, 5) the DOE-NETL lean premixed combustor, and 6) the DOE-HAT lean premixed combustor.

4.2.1 Lid-Driven Cavity Case

Measured data from a lid-driven cavity experiment was used to validate the LES code. The Localized Dynamic Subgrid-scale Model (LDKM) was described last quarter and was used in the LES. Three-dimensional cavity flows are highly non-homogeneous with complicated flow patterns; consisting of a primary vortex and several corner vortices. The localized SGS model, such as LDKM, should be capable of predicting these flows (Kim and Menon, 1997). An experiment of a rectangular lid-driven cavity with benchmark quality data was performed by Prasad, et al. (1988). Their experiments show that local and global three-dimensional features are present in the flow. The cavity with an SAR (SAR = L/B) of 0.5:1 and a Reynolds number equal to 10,000 ($Re=U_bB/v$) was used for the validation of the LDKM model with LES (see Figure 47 for dimensions).

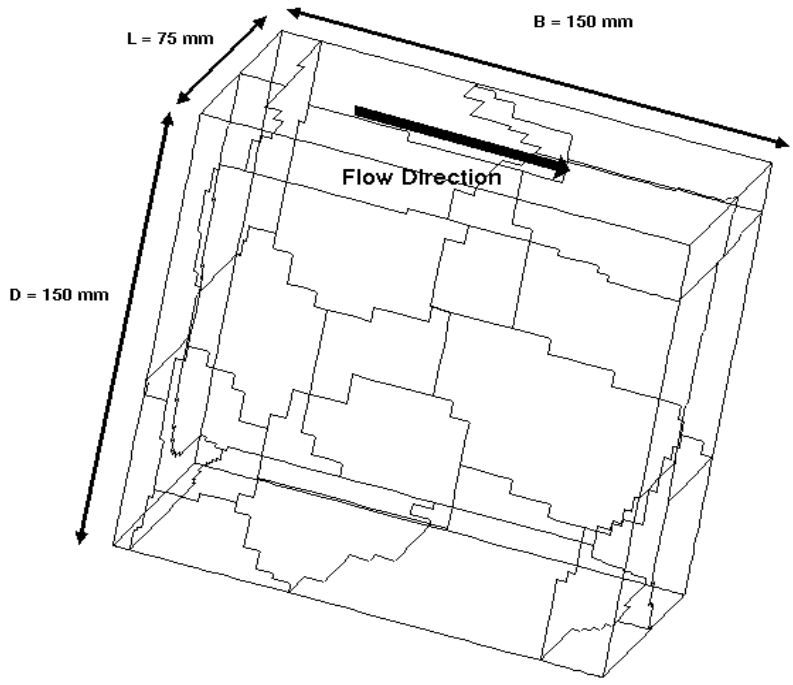

Figure 47. Lid-Driven Cavity Dimensions

The resolution of the computational grid was 64x64x32 (123039 cells). The grid was uniform in the Z direction and stretched towards the walls in the X and Y directions. A hyperbolic tangent distribution was used for the X-Y stretching with a 3.14e-4 meters spacing at the walls. The computational grid in the X-Y plane of the cavity is shown in Figure 48. The following flow conditions were specified as:

U_b = .06 m/s
T = 298.15 K
ρ = 997 Kg/m^3
Cp = 4184 J/Kg-K

Isothermal boundary conditions were used for all the walls including the lid. The U_b was imposed on the top wall to simulate the moving wall in the experiment.

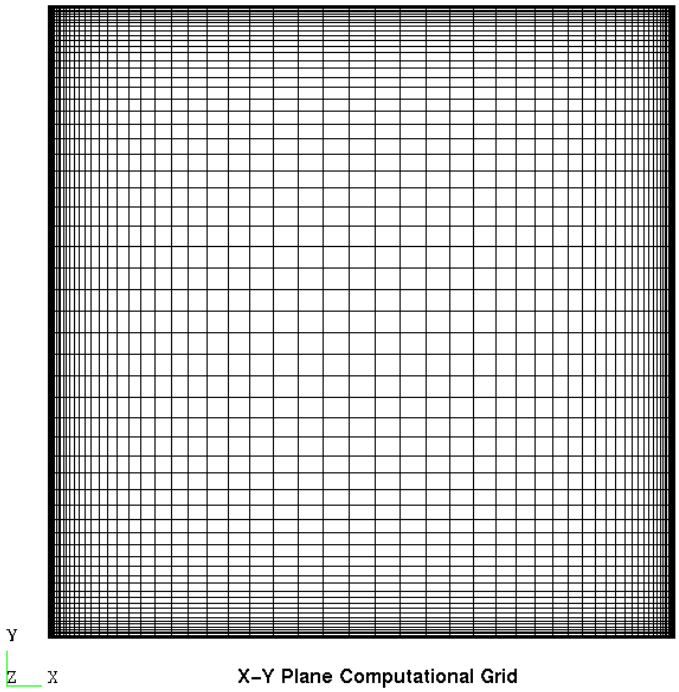

Figure 48. X-Y Computational Grid at Z = 37.5 mm

First a steady RANS solution was obtained and used as the initial condition for the unsteady RANS and LES calculations. The R grid parameter at the X-Y midplane is shown in Figure 49. This parameter is a measure of the quality of the grid for LES. A value less than zero implies that the filter or resolved scale is larger than the local energy containing scales, while a value greater than 1 implies that the resolved scales are smaller than the energy containing scales. Figure 47 shows that most of the grid is suitable for the LES calculation. The parameter is a function of the turbulent kinetic energy and is therefore dependent on the turbulence model. The parameter near the walls becomes less accurate for the RNG turbulence model used for this steady calculation. The grid parameter suggests more resolution is needed near the walls and along the top wall where large strain occurs due to the imposed velocity. Currently a 192x192x96 grid is being simulated to address this resolution issue.

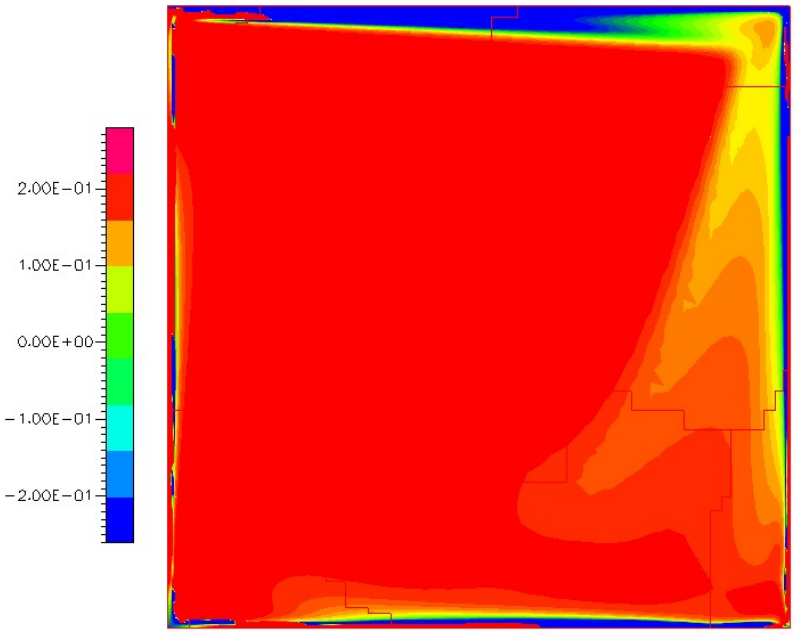

Figure 49. LES Grid Parameter

The RNG k-ε turbulence model was used for the unsteady RANS calculation and the LDKM with dynamic coefficients was used for the subgrid closure in the LES calculation. Figure 50 shows the normalized mean U-velocity along the Y-centerline.

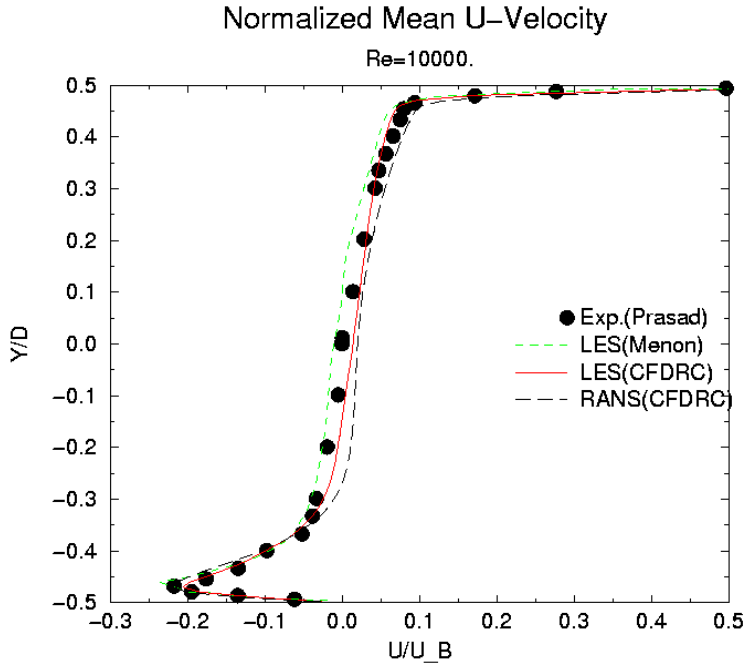

Figure 50. Normalized Mean U-Velocity

Both the LES and RANS calculations capture the mean velocity at the lower boundary wall. The LES predicts the mean velocity in the core flow and along the top wall better than the RANS calculation. This LES calculation is consistent with the LES calculation performed by Kim and Menon. Good comparisons were obtained for the mean V-velocity shown in Figure 51.

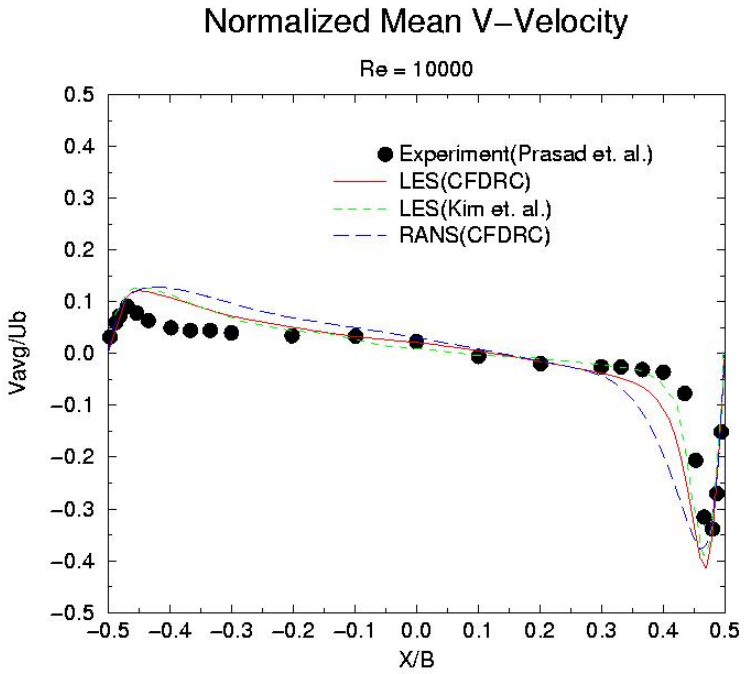

Figure 51. Normalized Mean V-Velocity

The RANS calculation over predicts the mean V-velocity at the end walls. The LES by CFDRC better predicts the overall mean V-velocity but does not show as good agreement as Kim et al. near the location of X/B = .375. Both LES models over predict the peak mean V-velocity values. The Normalized U-RMS is shown in Figure 52.

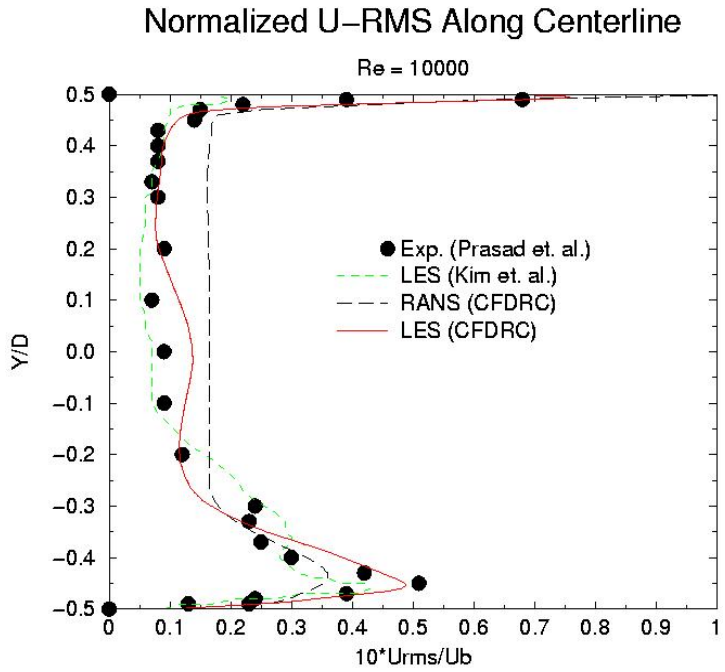

Figure 52. Normalized U-RMS Along Y-Centerline in Midplane

The LES simulations by CFDRC better predicts the U-RMS at the bottom wall compared to the LES by Kim et al., and the RANS simulation by CFDRC. It also compares better to data near the lid than that of Kim. The U-RMS near the center peaks at .15 for the LES-CFDRC simulation. This was not observed in the experiment or calculations by Kim (1997). This indicates that a longer compute time may be needed to average out the effects of the initial conditions provided by the RANS solution. Also the second peak was not captured at Y/D = -0.3. This second peak on rms could be due to the "coherent" structures described by Prasad (1989). Figure 53 shows the average U-velocity and vectors in the X-Y plane located at Z=.0375 meters and t=234 s. This shows the primary vortices and the secondary corner vortices located along the lower boundaries. A monitor point was placed 5 mm from the lower wall boundary layer to compare the U-velocity spectrum with experimental data shown in Figure 54.

The Kolmogorov -5/3 law was observed in the experiment in the inertial subrange, where the transfer of energy is dominant. The LES calculation predicts the -5/3 law observed in the experiment, which is crucial for LES calculations. The roll off in the viscous range was predicted by CFD-ACE+ at the frequency of about 0.5 Hz. The roll off is greater for the LES calculation than observed in the experiment. This indicates that higher frequency structures are dissipated more than observed in the experiment. Larger simulation times are needed to properly get statistics for the lower frequencies. This shows that LES with the subgrid scale model LDKM in CFD-ACE+ can be used to capture complex flows of three-dimensional cavity-driven flows where coherent structures may exist.

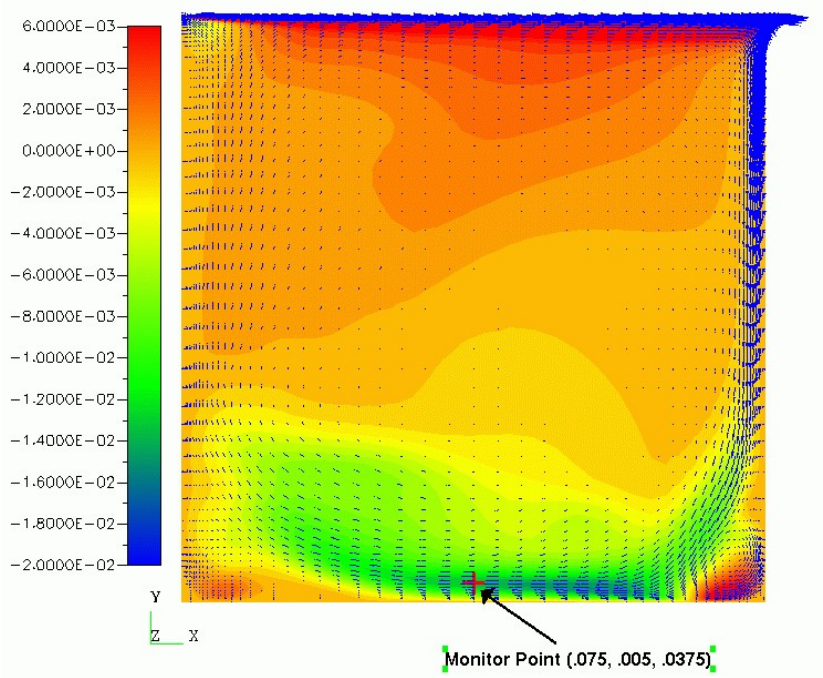

Figure 53. Average U Velocity Contours and Vectors

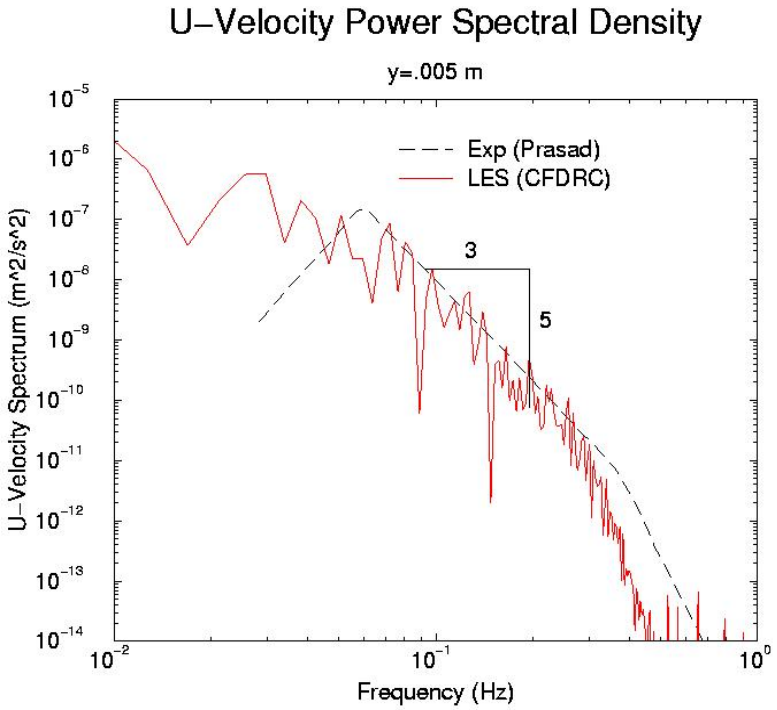

Figure 54. U-Velocity Power Spectrum

4.2.2 Loughborough Non-Reacting Combustor Port Flow

Experimental data from a combustor port flow at Loughborough University was used for validation of the combustion LES code. Adrian Spencer, assistance professor at Loughborough University, was responsible for acquiring the data and was at CFDRC during the summer of 2002 to do the validation work. At Loughborough University studies have been carried out on generic combustor port flow scenarios. These studies include water flow rigs which are scaled to match typical jet Reynolds numbers found in combustors. The use of water is advantageous for various reasons, but in particular it was chosen for the ease in which measurements can be made using optically based techniques. The test case is comprised of two concentric pipes. The inner pipe has a row of 6 equi-spaced ports which allows flow from the annulus feed to enter the inner pipe, or core, see Figure 55. By using various valves it is possible to set the following parameters; jet Reynolds number, annulus bleed flow fraction and jet to core flow velocity ratio. These three bulk flow parameters fully define the test condition, and may be varied to represent primary zone or dilution zone type port flows. Measurements of an impinging flow are available for a jet to cross flow ratio of 5 and an annulus bleed flow of 50%, with a jet Reynolds number of around 24000. It is this case that was simulated using LES.

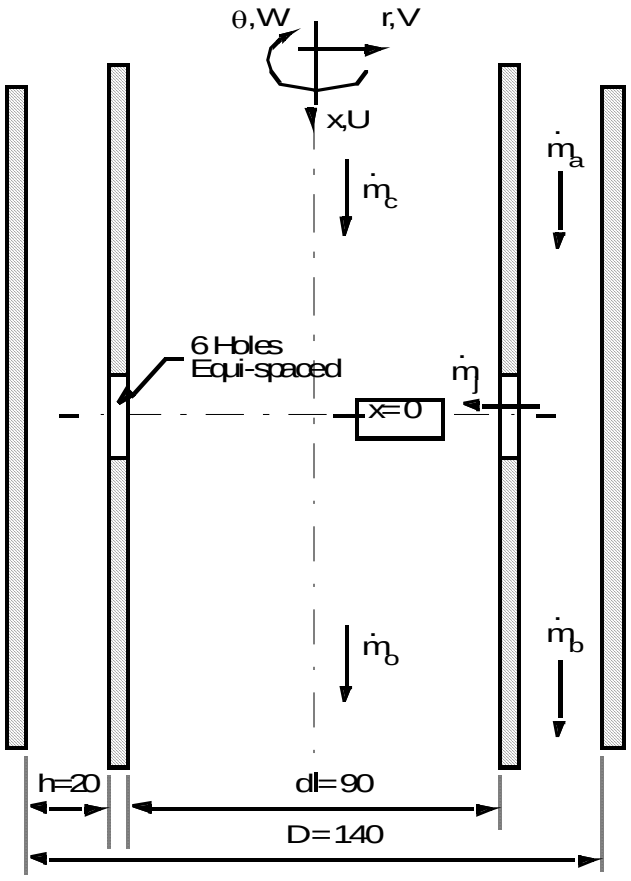

Figure 55. Co-Ordinate System Used for the Test Section

LDA measurements are available for the inlet planes of the rig and these are shown in Figure 56. The given axial velocity profiles were scaled to give the correct inlet mass flow rates and the

other inlet velocity components were set to zero. Random Gaussian fluctuations were specified, having a uniform rms value representative of a mass weighted average value available from the LDA measurements. The annulus exit velocity was fixed to set the correct bleed flow and the core exit plane was specified as constant pressure.

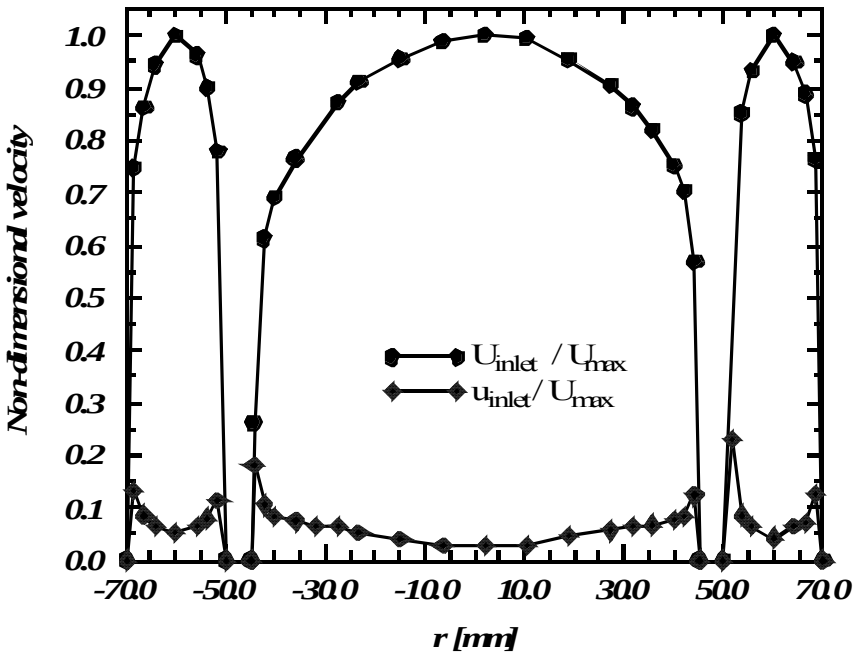

Figure 56. Inlet Axial Velocity Profiles

The solid model of the computational domain is shown in Figure 57. Flow enters left and exits right, the area reduction at the exit planes was used to ensure that no back flow occurred through these planes, and the core inlet and exit planes were extended as far as possible from the impingement point. The downstream extension was used to reduce any effects of the constant pressure boundary condition on the impingement. PIV measurements of the flow show that reverse flow can penetrate to x = -150mm instantaneously thus the upstream extension was employed to x = -200mm.

The grid density was chosen based on previous RANS grid refinement studies. It was found that 100,000 cells for a grid independent RANS calculation required 2,200,000 cells for a full 3D LES study at a similar grid density. Here, in Figure 57, a butterfly grid is used in the core and an O-grid in the annulus. Each port contains 15x15x5 cells connecting the core and annulus domains. The LES modeling utilized the Smagorinsky model for subgrid turbulence and a time step of 2.5e-4 seconds. The calculations were performed on CFDRC's 16 PC Linux cluster.

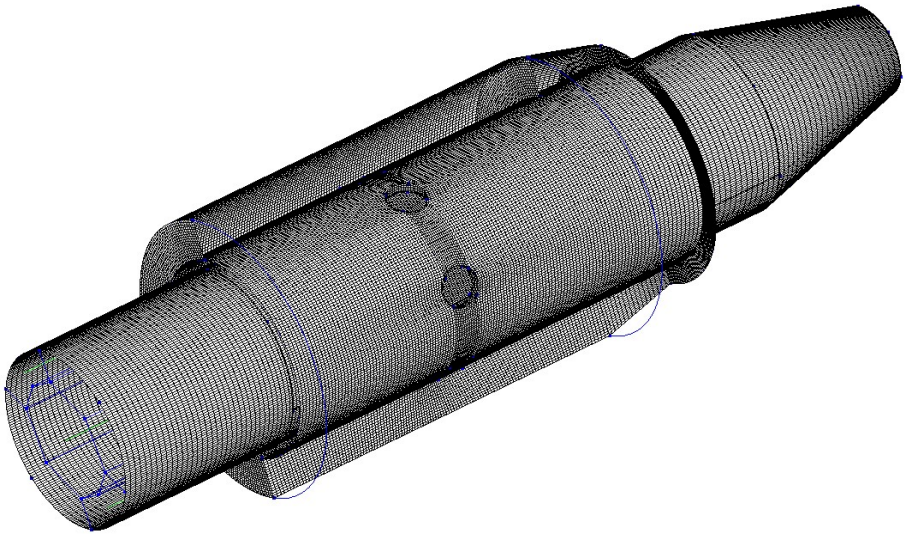

Figure 57. Surface Grid

Figure 58 shows one instantaneous snapshot of the velocity vectors in-line with the jets. The velocity vectors are colored by a passive scalar to indicate the origin of the fluid. It can be observed that the jet fluid penetrates a significant distance upstream of the ports. This upstream penetration is in agreement with experimental data as indicated by the black x. Random turbulent structures are observed throughout the flowfield.

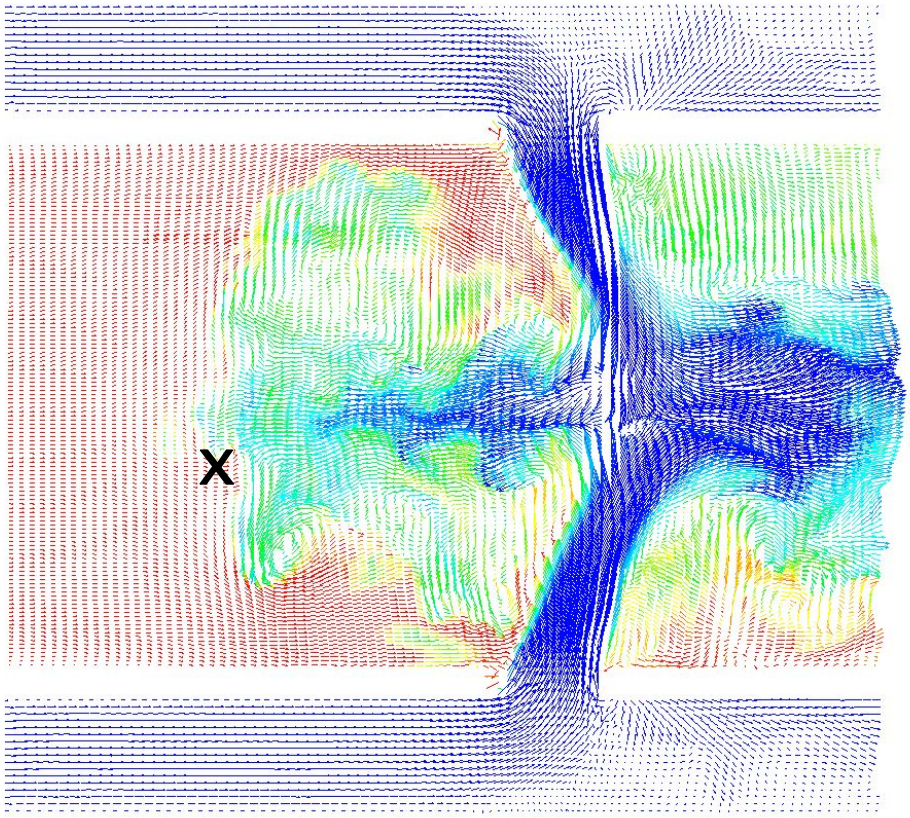

Figure 58. Instantaneous LES Snapshot of Combustor Port Flow

A comparison of predicted and measured mean velocity profiles are shown in Figure 59. The radial profile location is indicated in the velocity vector plot. Here it can be seen that LES is much better at capturing the higher negative u-velocity on the centerline compared to RANS. It is likely that the symmetric nature of the RANS calculation prevents the back-and-forth movement of flow about the combustor centerline. This movement about the centerline, as captured with LES, is needed to predict the higher backflow rates.

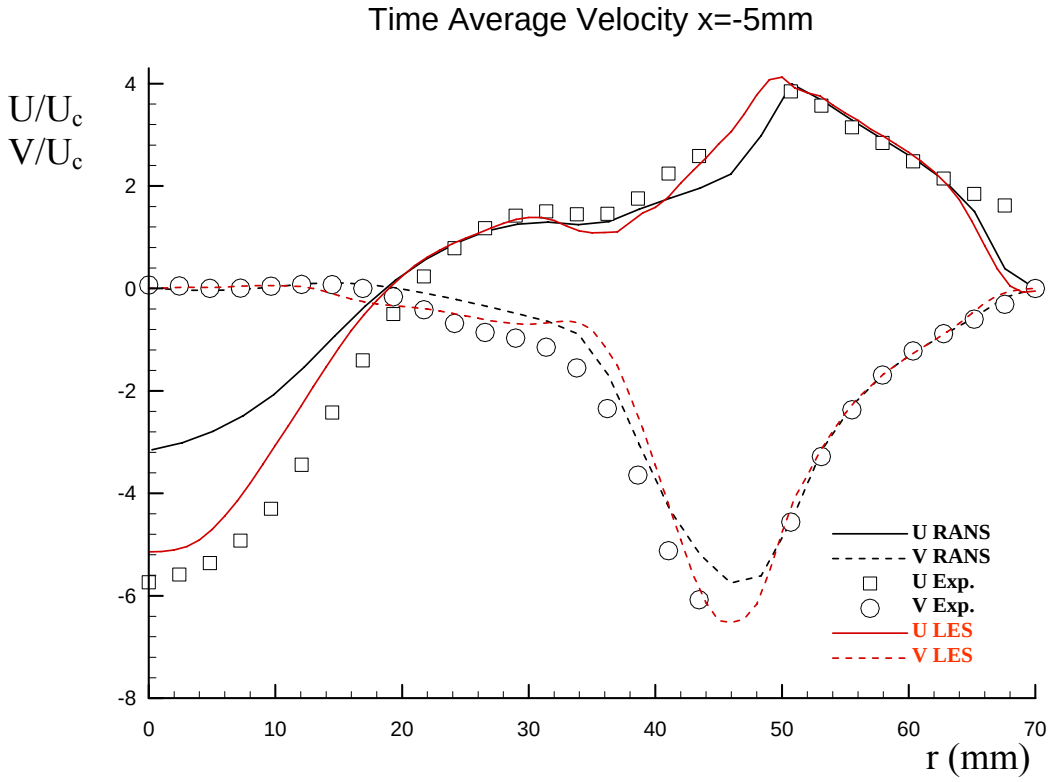

Figure 59. Comparison of Measured and Predicted Profiles of Mean U and V-Velocity in Combustor Port Flow

A comparison of RMS velocity results are shown in Figure 60. Here, it is clear that the RANS greatly under predicts the rms levels of both the U- and V-components. LES does a much better job at predicting the rms values. Some discrepancies do exist along the shear layer of the jet up near the port where higher frequency vortices were observed experimentally. These high frequency vortices were not captured with the LES and would require more grid resolution. These smaller structures don't seem to have a large impact on the mean flowfield.

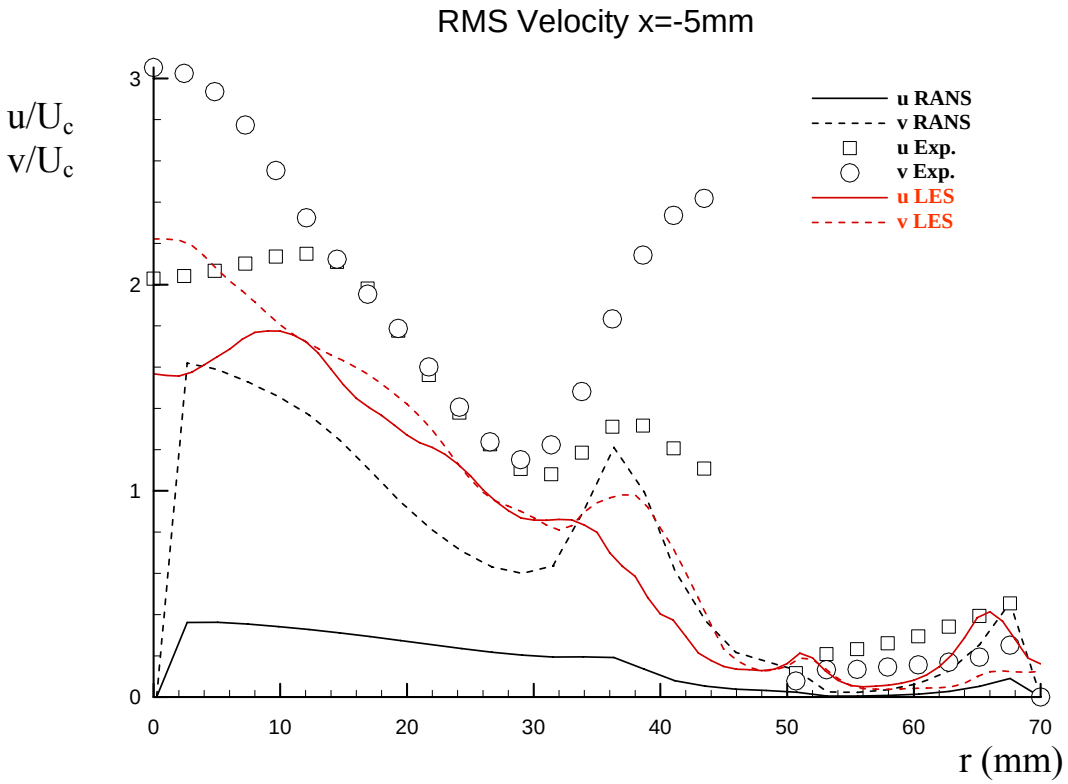

Figure 60. Comparison of Measured and Predicted Profiles of rms U and V-Velocity in Combustor Port Flow

The predicted and measured U-velocity PDF is shown in Figure 61 at the upstream penetration location at the centerline. The LES does a good job of predicting the velocity PDF. Possibly more time steps are needed to smooth out the PDF since only 2 seconds of data have been used (versus 82 seconds for the experiments). Overall, the LES with Smagorinsky subgrid turbulence modeling has produced good results, showing significant improvements over steady RANS analysis.

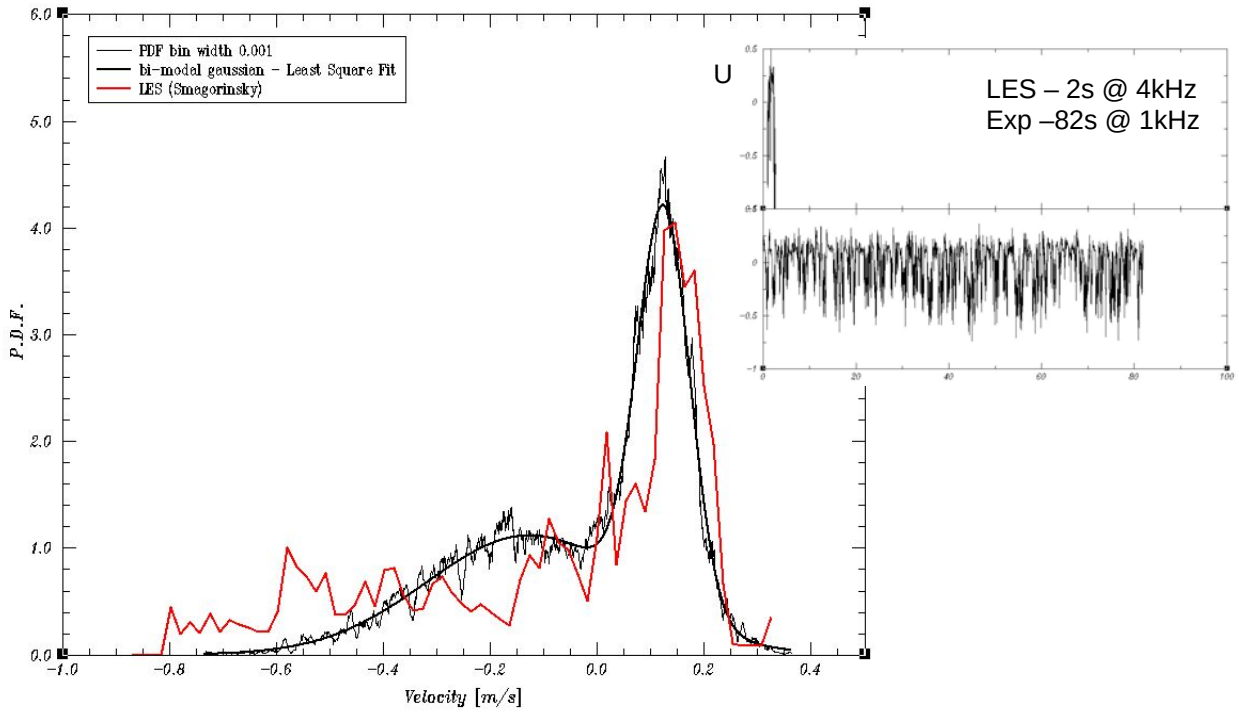

Figure 61. Comparison of Measured and Predicted U-PDF at Upstream, Centerline Location

4.2.3 Non-Reacting and Reacting Back-step

The combustion LES software was evaluated for predicting isothermal and reacting shear layers formed at a rearward facing step. LES results were compared with the experimental data taken from Pitz and Daily (1983). The experimental configuration consists of a rectilinear section followed by a smooth contraction to one half of its height, a step expansion into the test section, and a converging exit region. The computational domain is shown in Figure 62. The tests were conducted at atmospheric pressure and the mean velocity and temperature at the inlet are 13.3 m/s and 293 K. These conditions give a Reynolds number of 22,100 using the step height as the characteristic length.

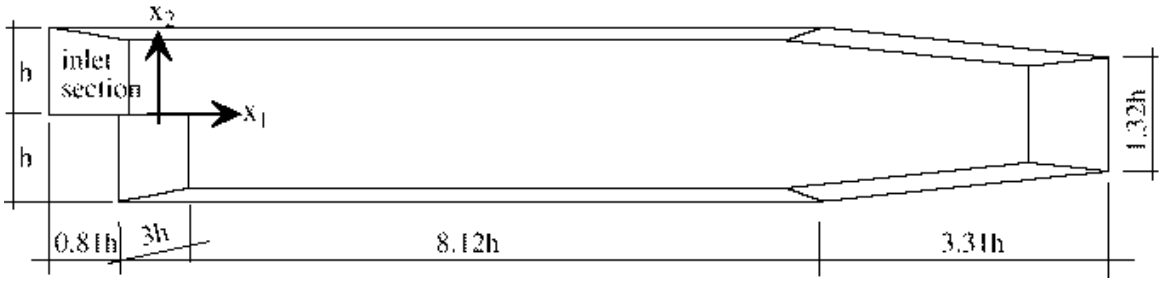

Figure 62. Computational Domain for the Backward Facing Step (Weller et al., 1998)

The computational grid consisted of 376,256 cells decomposed into 15 domains. Cells were clustered near the shear layer and towards the wall. Figure 63 shows the computational grid. The nondimensional y^+ values were between 10 and 20 along the top wall and between 1 and 8 along the bottom wall. Wall functions were used for RNG k-ε steady-state calculations and Van Driest Damping was utilized for the near-wall, Smagorinsky LES calculations. A fixed velocity and pressure were imposed at the inlet and outlet boundaries, respectively. Random fluctuations were imposed on the velocity at the inlet. Periodicity was assumed at the streamwise boundaries. Second order differencing in space (Central) and time (Crank-Nicholson) were utilized. The transient simulations were performed with a time step of 1.6e-5 seconds (maximum Courant number of 0.22) for a total of 0.504 seconds (~12 flow through times). Statistics were collected after the initial perturbation had settled out at approximately 5 flow through times. Mean and rms velocity profiles were obtained and compared to experimental data.

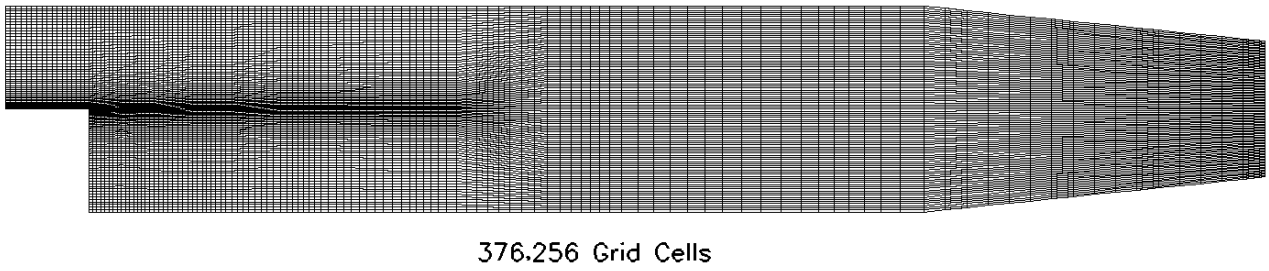

Figure 63. Grid Resolution for the Back-step Case

The inlet 13.3 m/s flow forms a shear layer downstream of the dump. Velocity and pressure oscillations occur in this shear layer as indicated in Figure 64. It is interesting to observe the high frequency oscillations in pressure that are not observed in the velocity. Low amplitude pressure oscillations (+/- 0.037%) occur, while high amplitude velocity fluctuations of +/- 6 m/s (~ 67%) are experienced. Figure 65 shows a snapshot of axial velocity at 0.496 seconds. The formed structures are irregular and 3-dimensional in nature.

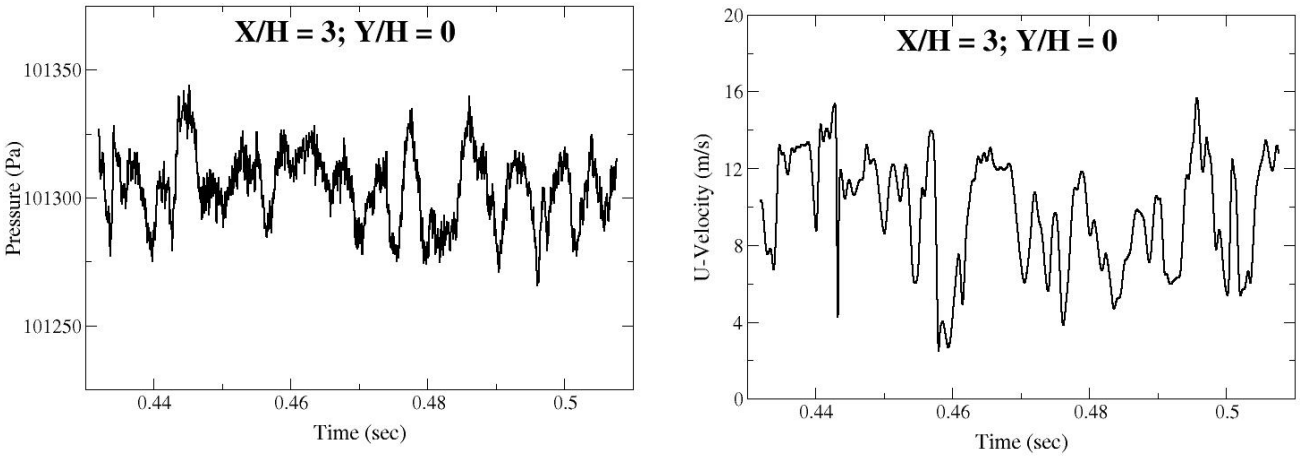

Figure 64. Predicted Pressure and Axial Velocity History at X/H=3 and Y/H=0 Using LDKM

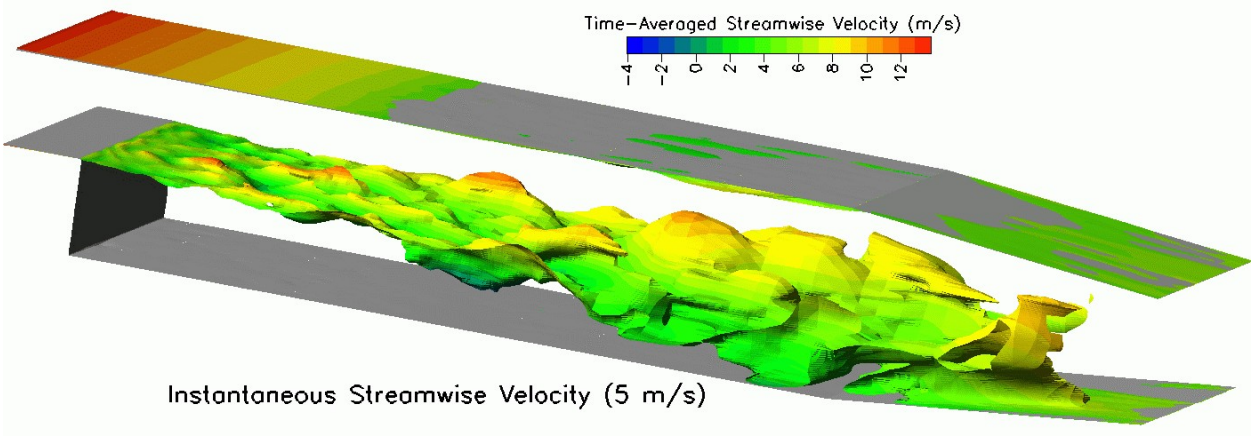

Figure 65. Predicted Instantaneous Streamwise Velocity (5 m/s) at 0.496 Seconds Using LDKM

The measured length of the recirculation zone extends 7-step heights from the dump. The LDKM predicts a reattachment length of 6.91, the Smagorinsky predicts 6.84, and the unsteady RANS (RNG k-ε) predicts 6.93. What is most interesting is that unsteady RANS does not predict any unsteady motion (i.e., unsteady RANS produces a steady-state solution), yet there is little difference between LES and unsteady RANS results for this nonreacting back-step case. Figure 66 shows comparisons between measured and predicted axial velocity profiles at various X/H locations. These results show reasonable agreement with all three models for the mean velocity profiles. All three models underpredict the spreading rate of the shear layer. At the furthest downstream location, separation occurs at the top wall using the Smagorinsky model. The RNG k-ε and LDKM models do a better job of predicting the flow at this downstream, top wall region.

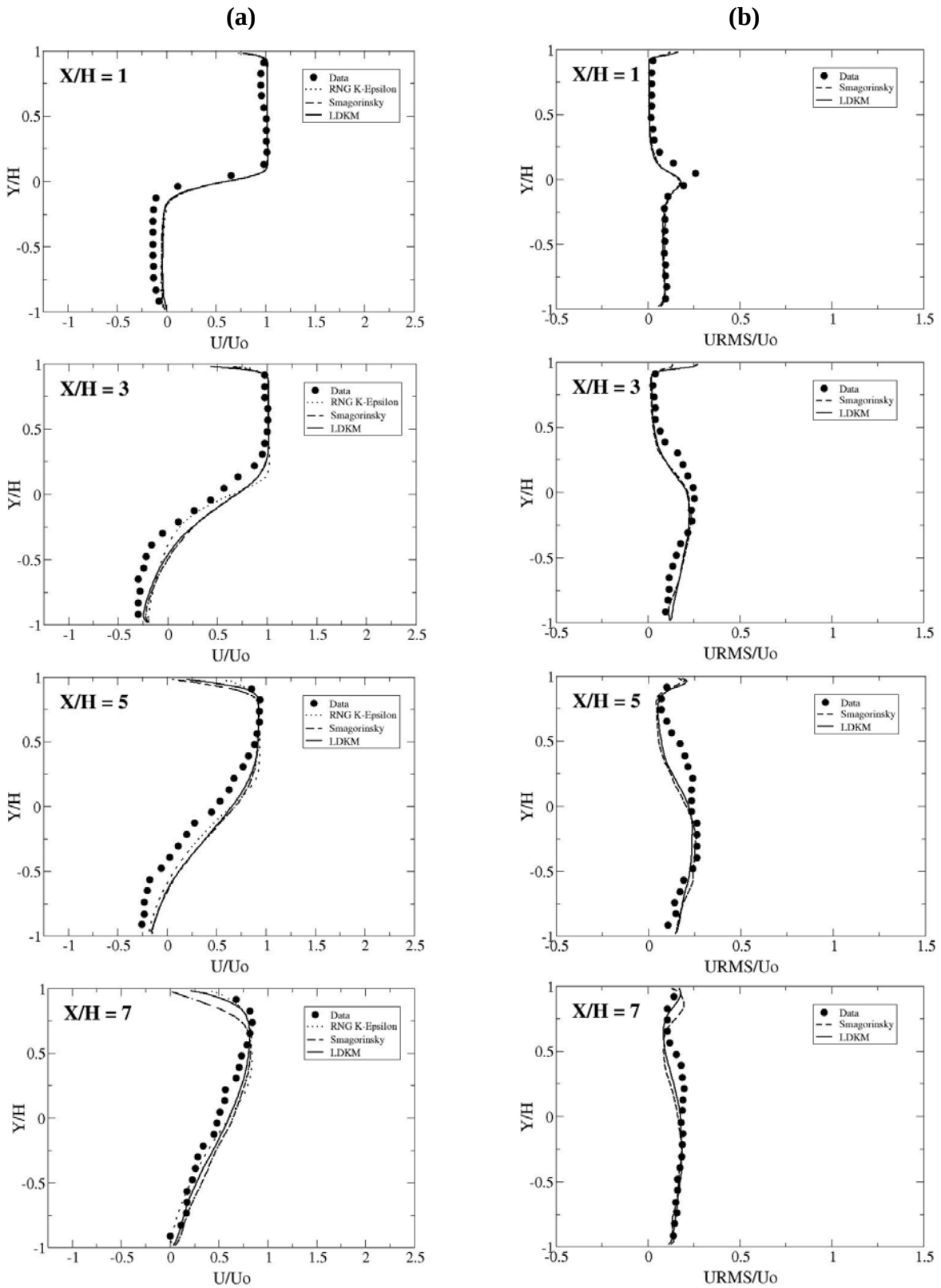

Figure 66. Comparison of Time-averaged Velocity Profiles of Streamwise (a) mean and (b) rms Velocity at Various Axial Locations

A similar LES study, performed earlier by Weller et al., (1998), showed better agreement with experimental data. They used a similar grid, with similar subgrid models and numerical accuracy. It is unclear why the LES results, in our study, are not as good as Weller et al, (1998).

After further investigation of the experimental data, it was learned that the flowfield was not 2-D since the endwalls damped the negative recirculation region, allowing higher negative flows along the centerline (Z/H=0). This endwall damping was believed to be due to a thick laminar boundary layer at the lower half of the duct where negative recirculation occurs. A full 2,200,000 cell case with endwalls was performed. Unfortunately, the LES calculations still did not match the experimental data. Y+ values in the LES simulation were less than 5. The grid may need to be even finer to fully resolve the turbulent boundary layer near the wall, or more appropriate LES subgrid near-wall modeling may be needed.

The combustion LES code was also validated against the experimental data from the reacting back-step case. The reacting flow case utilized a premixed propane-air flame with an equivalence ratio of 0.57. The conditions were identical to the non-reacting conditions.

Reacting flow simulations were carried out using a 1-step propane-air reaction with LEM. The LDKM subgrid turbulence model was used to close the momentum equations at the LES grid level and the subgrid tke provided necessary input for the LEM. For computational efficiency, these initial predictions utilized a 2D planar geometry. A total of 10,132 cells were used with clustering in the shear layer. Wall temperatures were specified according to the experimental data. A converged steady-state solution was utilized as the initial condition for the LES calculations.

The predicted instantaneous flame shape strongly depends on the subgrid chemistry model assumptions. Figure 67 shows instantaneous Schlieren images for LES predictions using laminar chemistry and LEM and the measured Schlieren image. The laminar chemistry assumption did not account for subgrid stirring events and was not able to predict large-scale mixing. The LEM results showed significantly more large-scale mixing, in reasonable agreement with the experimental data. The very fine-scale structures do not show up in the predictions since their effects were described with the subgrid turbulence model.

Laminar Chemistry

LEM Subgrid Chemistry

Measured Schlieren Image

Figure 67. Schlieren Images for LES Predictions and Measurements

In this reacting case, the incoming fluid contains cold premixed reactants which mix with hot combustion products in the initial shear layer behind the step prior to burning. The high turbulent strain rates (modeled in the subgrid) should delay the heat release, allowing the development of a Kelvin-Helmholtz instability. With laminar chemistry, the flame speed is independent of strain rate, and strong chemical reaction is allowed to take place immediately after the cold premixture contacts the hot products. The heat release in the shear layer inhibits the growth of the instability, resulting in a near smooth flame surface with very little wrinkling. The LEM includes subgrid turbulent stirring effects and allows the development of a Kelvin-Helmholtz instability. Figure 68 shows the instantaneous chemical reaction rates for the laminar chemistry and LEM predictions. Not only is the reaction zone delayed downstream of the dump plane for the LEM, but also the reaction flame zone is much wider at certain points and broken in certain points due to subgrid turbulent stirring.

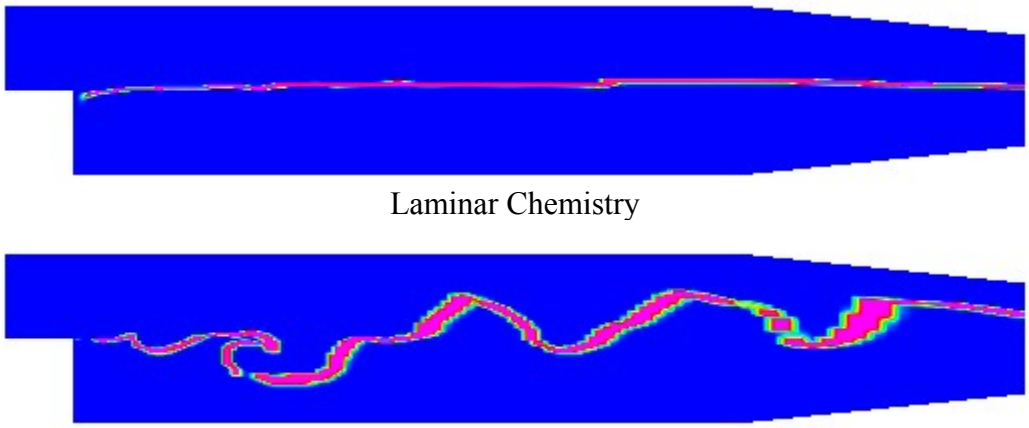

Laminar Chemistry

LEM Subgrid Chemistry

Figure 68. Predicted Chemical Reaction Rates

The reattachment length for the reacting flow is much less than the non-reacting case. Figure 69 shows the predicted reattachment length for the laminar chemistry and LEM predictions. The LEM case predicts a value of 3.6H, near the experimental value of 4.5H. The laminar chemistry prediction shows a reattachment length of almost 7.4H. The development of the shear layer vortices are required so the large-scale structures can close down the recirculation zone. These results show the need for accurate subgrid chemistry modeling, particularly in regions where strain rate extinction can occur. It is likely that richer premixed reactants would provide a more stable situation and the laminar chemistry approximation may be more appropriate.

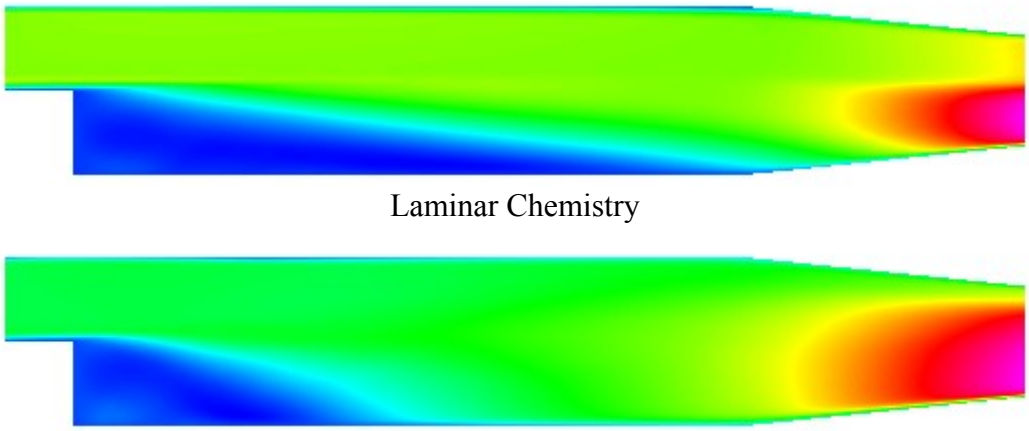

Laminar Chemistry

LEM Subgrid Chemistry

Figure 69. Predicted Axial Velocity Contours Showing Reattachment Lengths using Laminar Chemistry and Linear Eddy Model

The computational times for the LEM subgrid and laminar chemistry models were similar. One reason for the relatively fast LEM is due to computing subgrid chemistry once per time step, instead of at each iteration (7/time step) for the laminar case. These calculations were performed with a fixed LEM cell number (32) in each LES cell. Overall these results are very promising.

The reacting back-step case was also performed using the 3D geometry. Figure 70 shows a calculated axial velocity isosurface for the (a) isothermal and (b) reacting flow cases. The recirculation zone has been properly predicted, with the length of the recirculation region X=7.2H for isothermal and X-3.8H for reacting flow. The LEM was needed assumption did not allow a Kelvin Helmholtz instability to develop and thus large-scale vortex structures downstream of the back-step were not formed and a much longer reattachment length (7H) was predicted.

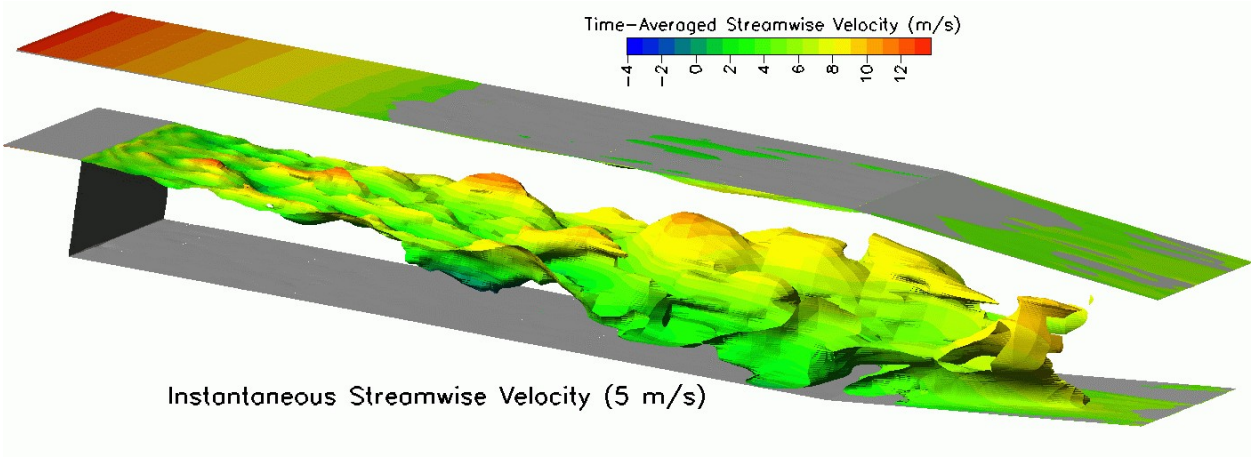

(a) Isothermal Flow

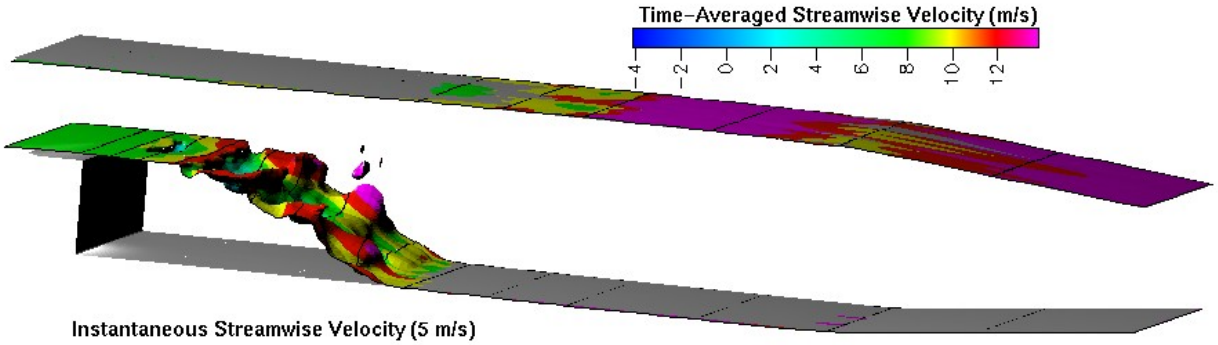

(b) Reacting Flow

Figure 70. Predicted Axial Velocity Iso-Surface for (a) Isothermal Flow and (b) Reacting Flow

Detailed comparisons of experimental and predicted (using LEM) profiles of the mean axial velocity and temperature are shown in Figures 71 and 72. These results show good agreement between measurements and predictions. Radiative heat transfer was required in the model to obtain good agreement with measured peak temperatures downstream of the back-step. The most significant discrepancy was found for the velocity in the recirculation region at X=3H. At this location, the negative flow is underpredicted and was also observed in the non-reacting simulations.

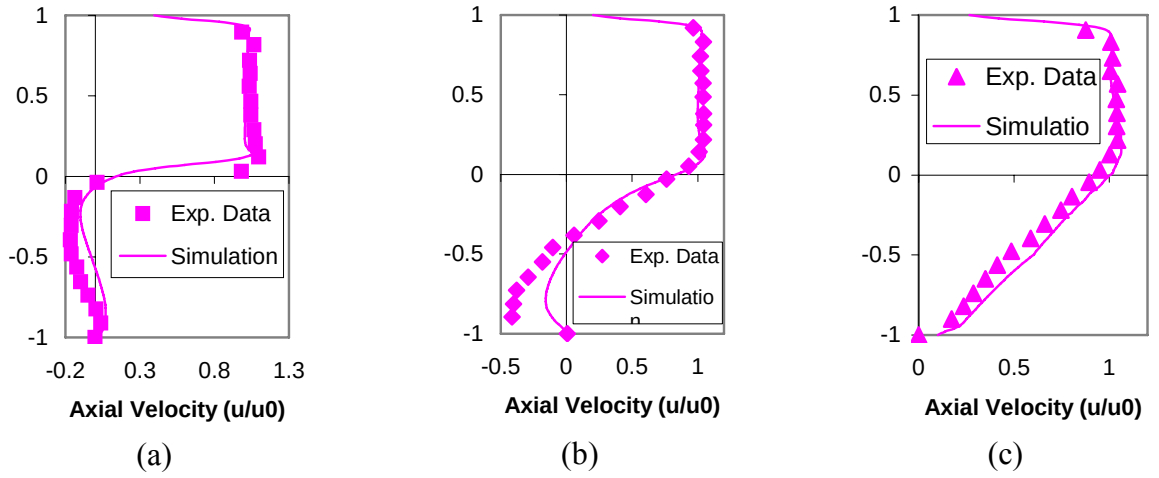

Figure 71. Mean Profiles of Axial Velocity at (a) X=H, (b) X=3H, and (c) X=5H for the Reacting Back-step Case (simulations with LES+LEM)

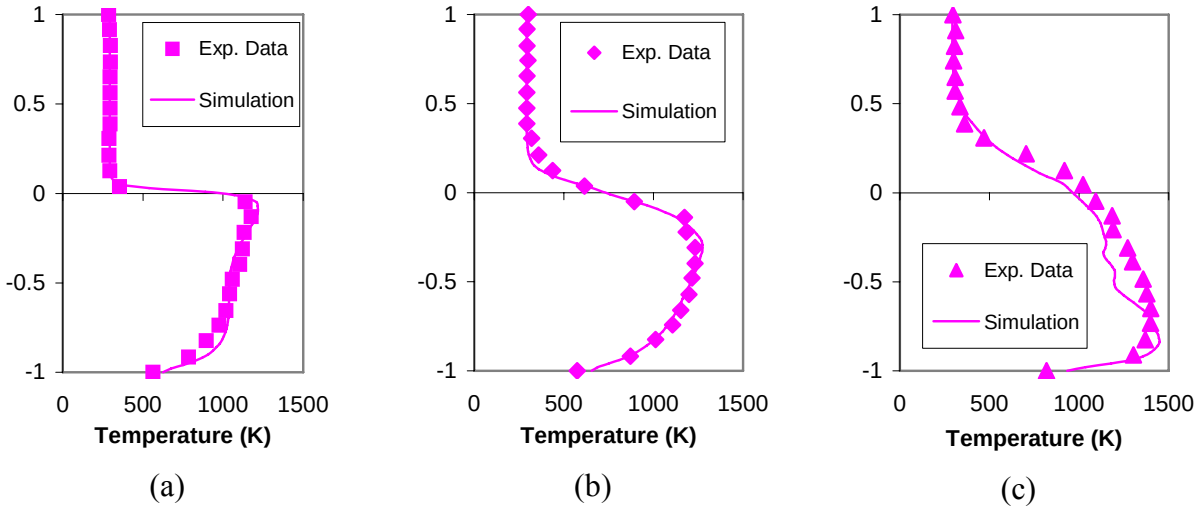

Figure 72. Mean Profiles of Temperature at (a) X=0.4H, (b) X=1.2H, and (c) X=3.5H for the Reacting Back-step Case (simulations with LES+LEM)

4.2.4 DOE-NETL Lean Premixed Combustor

The unstable lean premixed fuel injector/combustor from Richards and Janus (1997) was modeled using the CFD-ACE+ LES code. The combustor had previously been modeled using 2D and 3D unsteady RANS. The calculation domain for the simulation can be important in allowing proper acoustic predictions. Previous 2D axisymmetric predictions of this DOE combustor included an inlet plenum and a long exhaust duct as shown in Figure 73a. For computational efficiency, it was decided to eliminate the inlet plenum and most of the exhaust duct. The smaller 3D domain is shown in Figure 73b and started at the swirler vane discharge and ended downstream of a shorter exhaust duct exit. The smaller domain required a total pressure boundary at the swirler vane discharge instead of a fixed mass boundary since mass flow variations through the swirler must be allowed during large amplitude pressure oscillations. The full domain case, with a fixed mass boundary at the inlet to the plenum, automatically

allowed for variable mass flow rates through the premix barrel due to the compressibility of the gas in the plenum. The use of swirl source terms in the computational domain were also not needed in the smaller domain case. Since the unsteady heat release was likely coupling to a bulk Helmholtz mode, the lengths associated with the inlet plenum and exhaust duct were found not to be critical.

(a) Full Domain

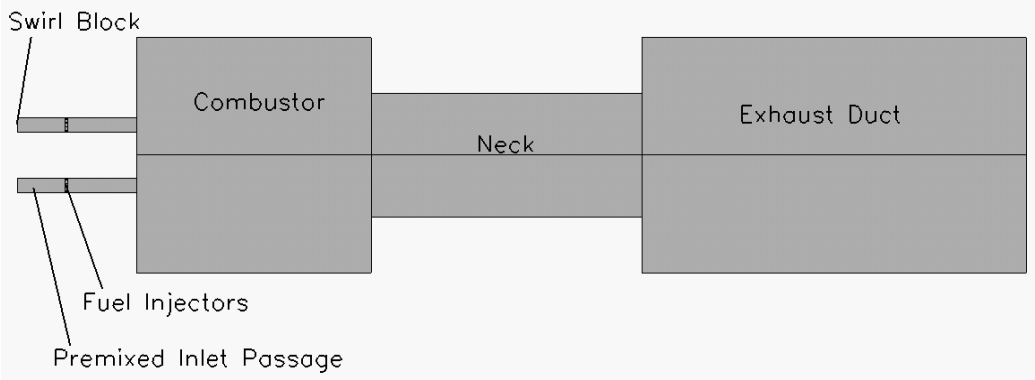

(b) Shortened Domain

Figure 73. Computational Domain for Combustion Instability Test Case

The 3D axial-radial-tangential grid resolution in the combustor is shown in Figure 74. Two different grids were analyzed and the grid lengths at the premix dump correspond to 1.6 and 0.6 mm lengths in the axial and radial directions respectively. The tangential size of the cells were 1.9 mm at the premix dump and 9.7 mm at the outer wall of the combustor for the 394,000 cell case. The tangential sizes for the 796,000 cell case were approximately half those of the coarser grid. As described in Cannon et al. (2000), the finer grid size should resolve the energy containing scales for 3D LES of this case.

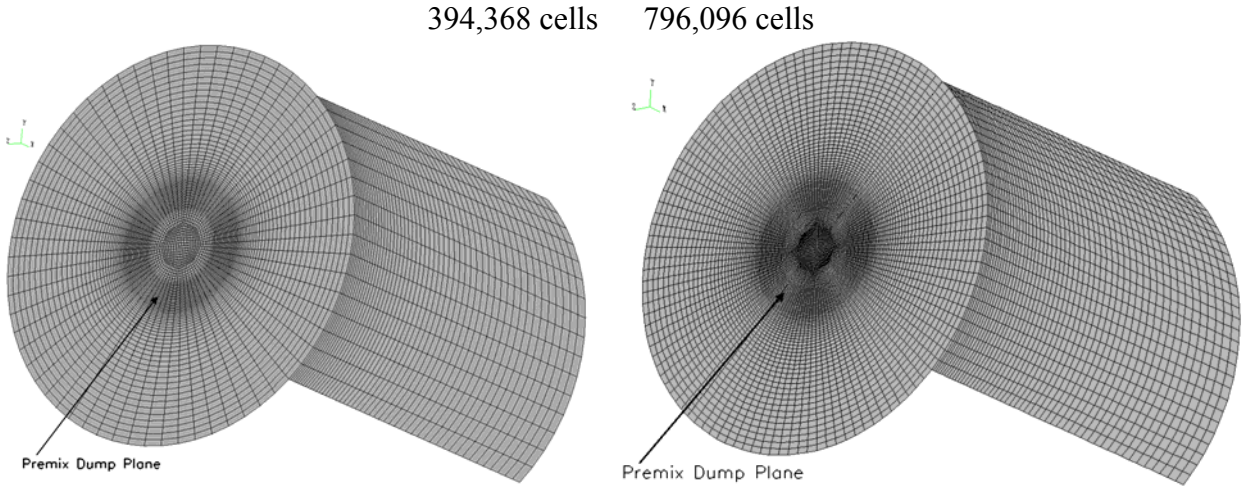

Figure 74. Combustor Grid Resolution for 3D Geometry (394,368 cells and 796,096 cells)

Unsteady RANS and LES calculations were performed at the unstable conditions. The perturbations associated with starting up the 2nd order time-accurate solution method were enough to allow unsteady heat release and pressure oscillations to grow if sufficient coupling is present. For the 3D LES calculations, random fluctuations were also superimposed on the steady-state flowfield which allowed a reasonable initial flowfield with sustained turbulence levels. The predicted pressure history in the combustor is shown in Figure 75a for the 2D unsteady RANS calculations. The results show that a large amplitude oscillation builds up within 40-50 msec and reaches peak-to-peak values of +/- 5% at a frequency of approximately 280 Hz. The measured limit cycle of combustor pressure is shown in Figure 75b and is similar in amplitude though at a lower frequency of ~225 Hz. The difference in frequency between the predictions and measurements could be due to deficiencies in the submodels (laminar/1-step chemistry, RNG k-ε unsteady RANS), solution techniques (2nd-order spatial and temporal differencing), or geometry/boundary conditions (2D axisymmetric, simplified swirler and fuel injector, no exhaust cooling water). In this study, the 2D axisymmetric geometry was rotated through 360 degrees to perform full 3D simulations with an unsteady RANS turbulence model and an LES subgrid turbulence model. A better description of vortex stretching that is inherent in all turbulent flows can now be included and its effect on the modeled instability for this test case was investigated.

Unsteady RANS and LES calculations of the full 3D geometry were performed using the same boundary conditions from the 2D axisymmetric case. The 800,000 cell 3D calculations were performed using 8 PC's and required approximately 10 days of computational time to reach a limit cycle after 70 milliseconds. Figure 76 shows the predicted combustor pressure from the 3D unstable runs. The results indicate a faster buildup in pressure oscillations compared to the 2D unsteady RANS case, but nearly identical amplitude and frequency were obtained with the 3D unsteady RANS and LES. This is interesting, given the differences found in instantaneous flowfield snapshots between the predictions.

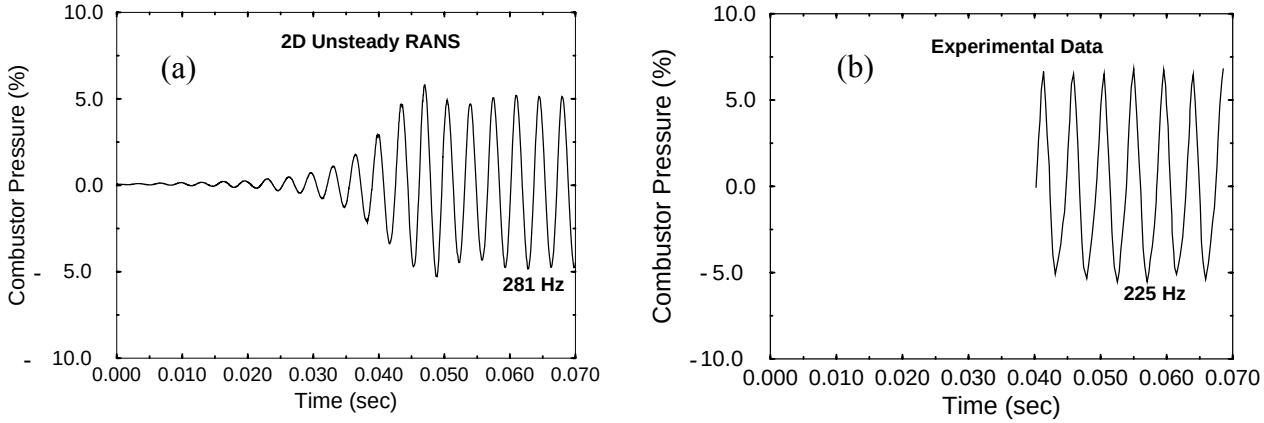

Figure 75. Combustor Pressure History for Unstable Case (a) 2D Unsteady RANS, and (b) Experimental Data

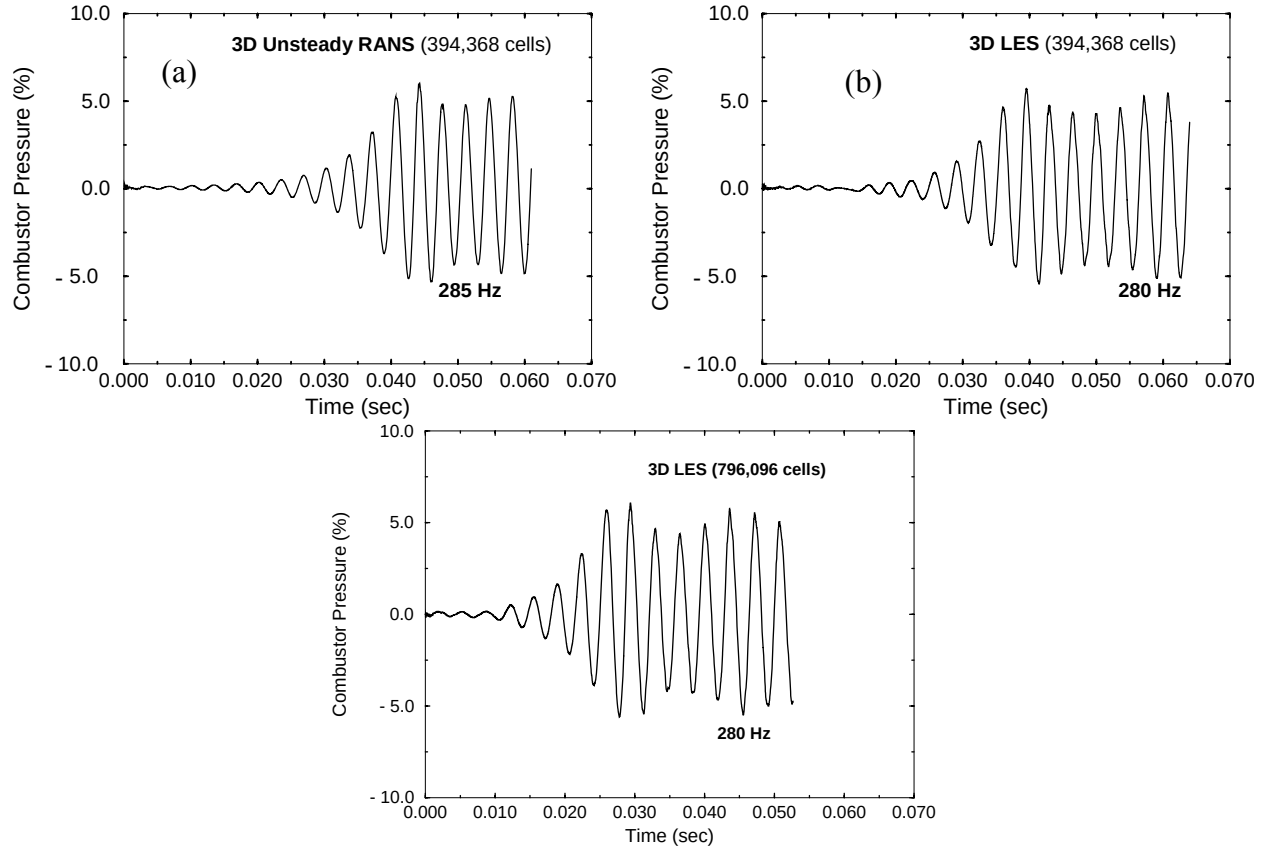

Figure 76. Predicted Combustor Pressure History using 3D Modeling

It was found that the 3D unsteady RANS remained axisymmetric throughout the transient calculation. Figure 77 shows the predicted fuel iso-surface at max pressure using 3D RANS and LES. The LES results show non-axisymmetric and irregular features, whereas the unsteady RANS remains axisymmetric. The maximum shear layer viscosity with LES (394,000 cells) is approximately two orders of magnitude less than that computed with unsteady RANS. Figure 78

shows the LES (394,368 cells) effective viscosity iso-surface (0.0002 kg/m/sec) at the time of maximum pressure. Significant non-axisymmetric and smaller-scale structures are formed throughout the flowfield. These features are not captured with unsteady RANS.

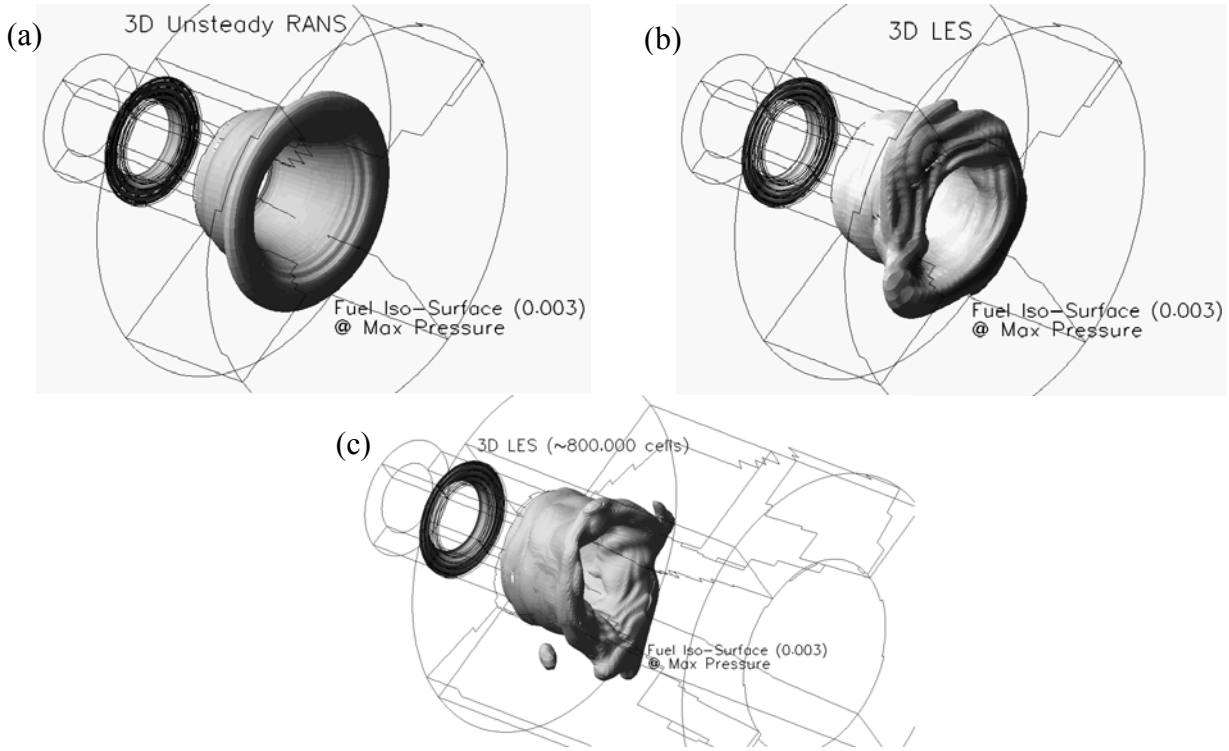

Figure 77. Predicted Fuel Mass Fraction Iso-surface at Maximum Pressure using (a) 3D Unsteady RANS, (b) 3D LES (394,368 cells), and (c) 3D LES (796,096 cells)

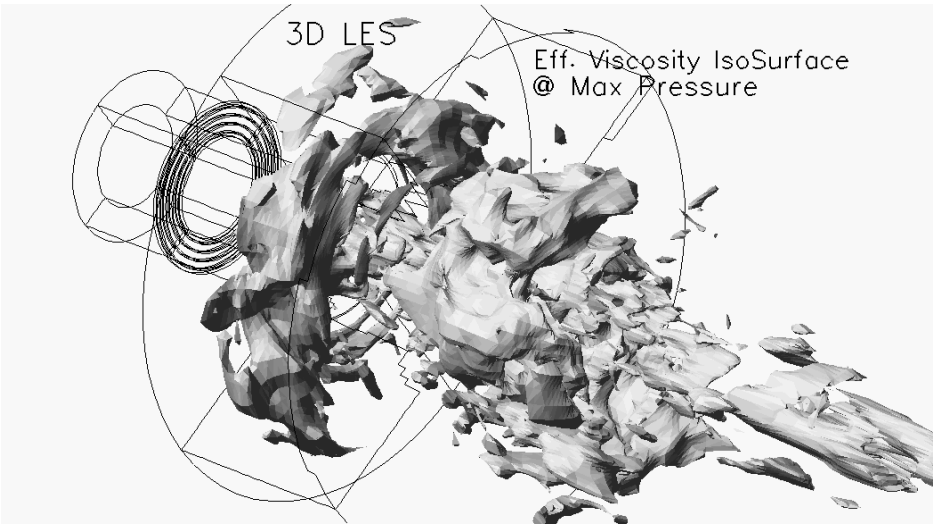

Figure 78. Predicted LES Effective Viscosity Iso-surface at Maximum Pressure

The predicted motion of the reacting flowfield can be observed during the oscillation cycle. Unfortunately, experimental flowfield or flameshape images were not obtained for direct comparison to the predictions. This type of data is expected to be acquired in a current DOE-SimVal experimental program. Figures 79 and 80 show instantaneous axial velocity and heat release snapshots using 2D unsteady RANS and 3D LES (394,000 cells) during the oscillation cycle. Although the snapshots do not coincide exactly in sync during the cycle due to different dump times of the output, they are approximately in sync. These results do show that the global features of the unsteady flow are similar between the two prediction techniques. For example, significant backflow through the neck and lower heat release rates are observed when the combustor pressure is low. The smaller scale features of the flow are captured with the 3D LES computations, but not with unsteady RANS. Small burning pockets of gas become separated from the main flame zone and irregular flow features are allowed to form and decay in the 3D LES predictions. Also, the flow does not stay axisymmetric during the 3D LES calculations as the burning flame zone is allowed to oscillate across or around the centerline.

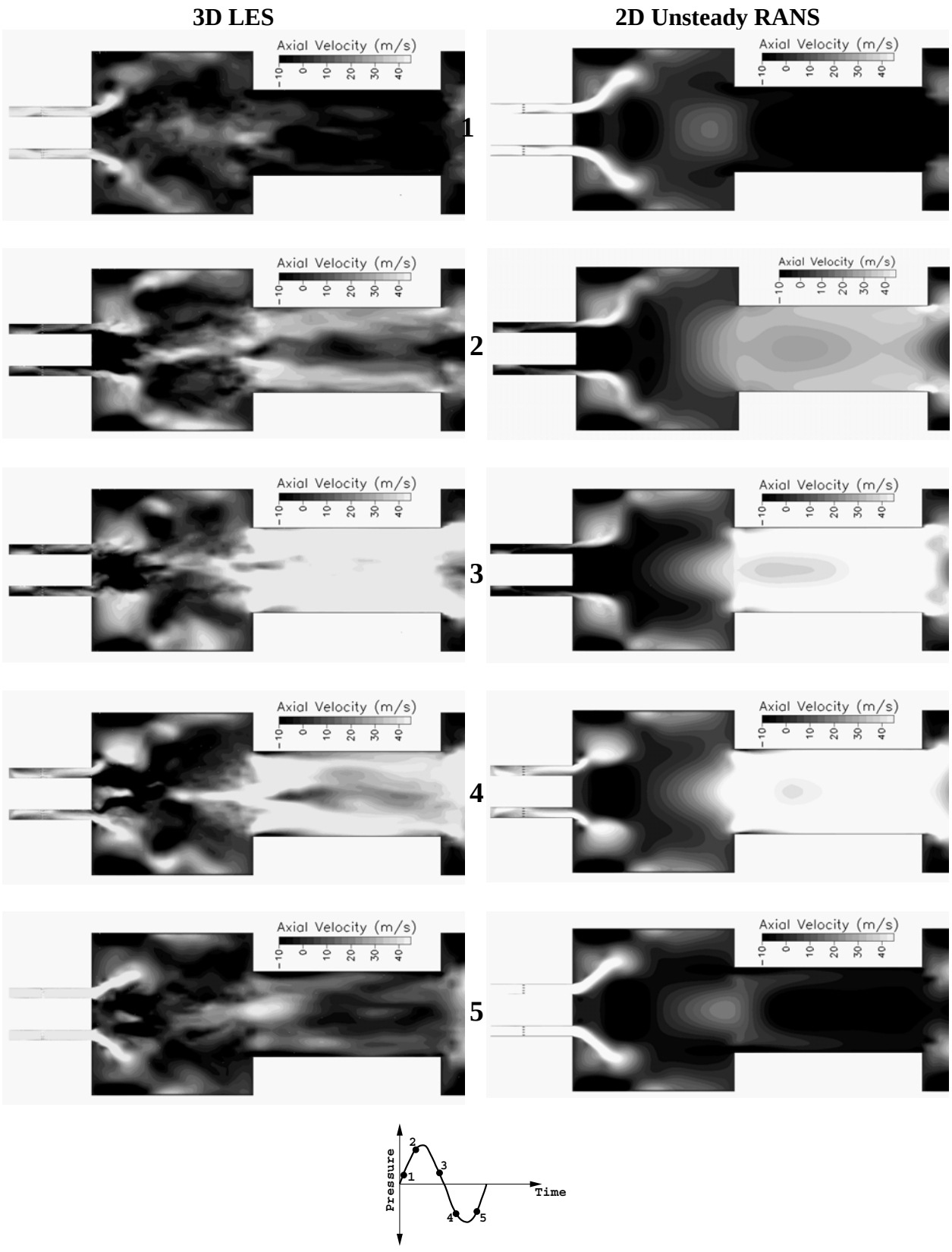

Figure 79. Instantaneous Axial Velocity Contours Using 2D Unsteady RANS and 3D LES

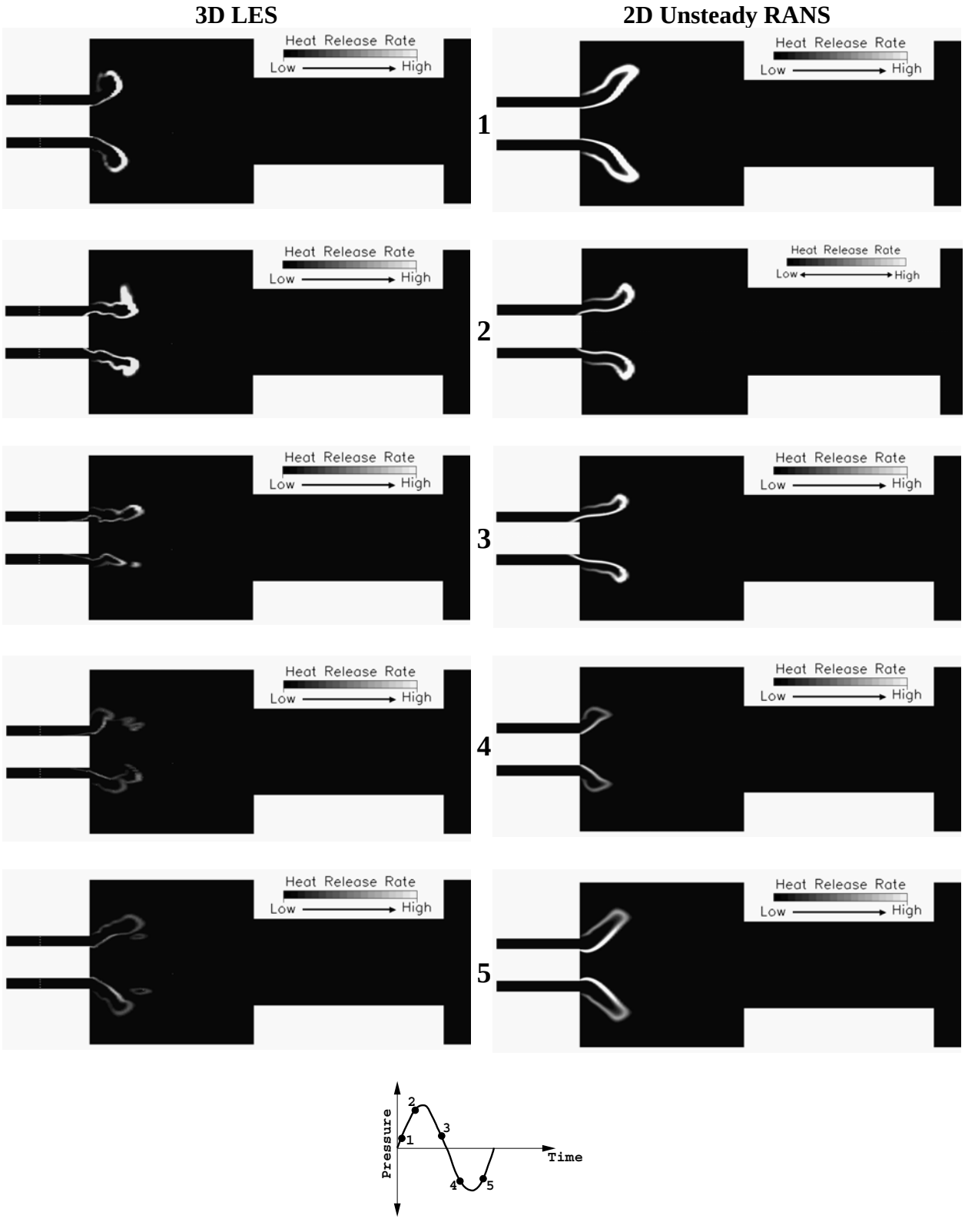

Figure 80. Instantaneous Heat Release Contours Using 2D Unsteady RANS and 3D LES

These 3D LES calculations show that CFD-ACE+ is correctly predicting the oscillation magnitude in the DOE-NETL combustor. The predicted frequency is still too high (280 Hz vs. 225 Hz). The effects of swirler vane wakes and fuel injection through discrete orifices and more detailed chemistry subgrid models may be needed. The swirler/spoke geometry has been obtained from DOE-NETL and has been included in the LES model. These new LES results were reported in the paper by Cannon et al. (2001), where frequencies as low as 229 Hz were predicted.

4.2.5 DOE-HAT Lean Premixed Combustor

The DOE-HAT combustor configuration was modeled and comparisons to experimental CO and NO_x measurements were performed (Cannon, et al., 2003). The DOE-HAT combustor was studied in an experimental program at DOE-NETL in Morgantown, WV, in collaboration with UTRC. Experiments were performed at lean conditions over a range of equivalence ratio, pressure, and moisture level. Also, two different nozzle configurations were studied. For the validation simulations performed here, only the equivalence ratio was varied. The calculations will be performed with dry reactants and with one particular nozzle. The nozzle consists of an axial swirler and fuel spoke downstream of the swirler. The nozzle flow dumps into a cylindrical refractory-lined combustor. A 3-hole water-cooled suction probe is situated downstream in the combustor to provide CO and NO_x measurements.

Steady-state calculations were first performed on a 1/16th sector of the nozzle to predict the fuel flow through the spoke and out into the air stream within the nozzle. Then the predicted exit profiles of velocity, pressure, temperature, turbulence quantities, and equivalence ratio were mapped to a full 3D combustor geometry as an inlet. This boundary condition mapping prevents extremely large grid counts that would be needed to model all 15 swirl vanes and fuel spokes. It was found that the mixing was strong enough in the nozzle to achieve a tangential uniformity before dumping into the combustor. However, there were significant radial gradients at the nozzle exit that could only be predicted with the full swirl vane/spoke geometry.

The swirl vane/fuel spoke geometry is shown in Figure 81. The geometry is rotated and copied to show 3 vanes and 3 spokes. This detailed steady-state modeling of the nozzle required ~1 million cells and was performed on a 14 PC cluster. Domain decomposition was performed normal to the x-direction in such a manner that identical cyclic faces were maintained on each processor. A many-to-one grid interface was utilized within the combustor to enable coarser cells in the downstream section of the combustor. The following flow conditions were modeled in the initial baseline case:

T_{inlet} = 734 K (862°F)
P_{comb} = 200 psia (13.6 atm)
m_{air} = 0.96 kg/sec (2.116 lbm/sec)
PHI = 0.54 (CH4-air); 0.58 (natural gas-air)
Nozzle_ACD = 12.3 cm^2 (0.79 in^2)

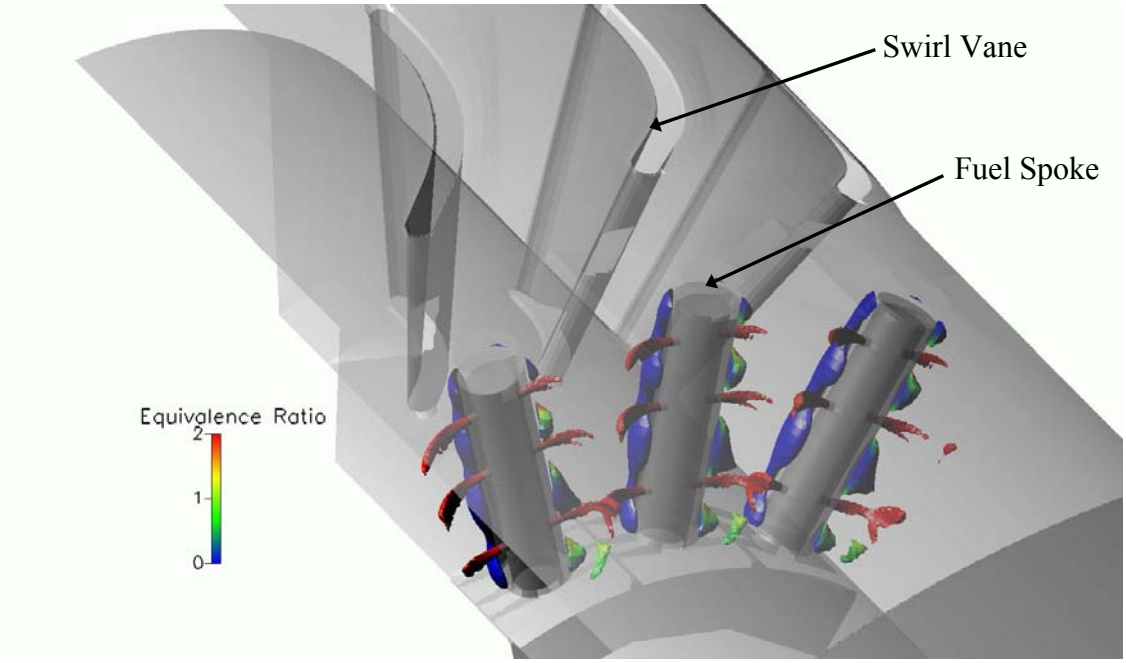

Figure 81. Velocity Magnitude Contour (140 m/s) Colored with PHI for Full Swirler Vane/Fuel Spoke Geometry

Fixed mass flow boundaries for air and methane were assumed upstream of the swirl vane and fuel spoke manifold respectively. Fuel jet velocities near 230 m/s were predicted through the fuel orifices and an ~18% pressure drop was predicted through each fuel orifice. The OD of the fuel nozzle was 2.48" and the ID was 1.38". The combustor diameter was 4.25". CO and NO_x measurements were provided from a 3-hole probe at a 15" location downstream of the fuel nozzle.

The predicted results along a radial-axial plane from the detailed swirl-vane/fuel spoke geometry are shown in Figure 82. These results were obtained from similar conditions to the baseline, except that the equivalence ratio was leaner at a value of 0.5 (natural gas-air). These results show that higher axial and tangential velocities are formed along the OD of the nozzle. This is due to the lower blockage from the swirler and fuel spoke along the nozzle OD. The higher axial velocities on the OD create leaner mixtures on the OD. This lean OD mixture results in a relatively lean region along the combustor OD. The equivalence ratio in the combustor outer recirculation zone is ~0.35. The central recirculation zone equivalence ratio is ~0.6.

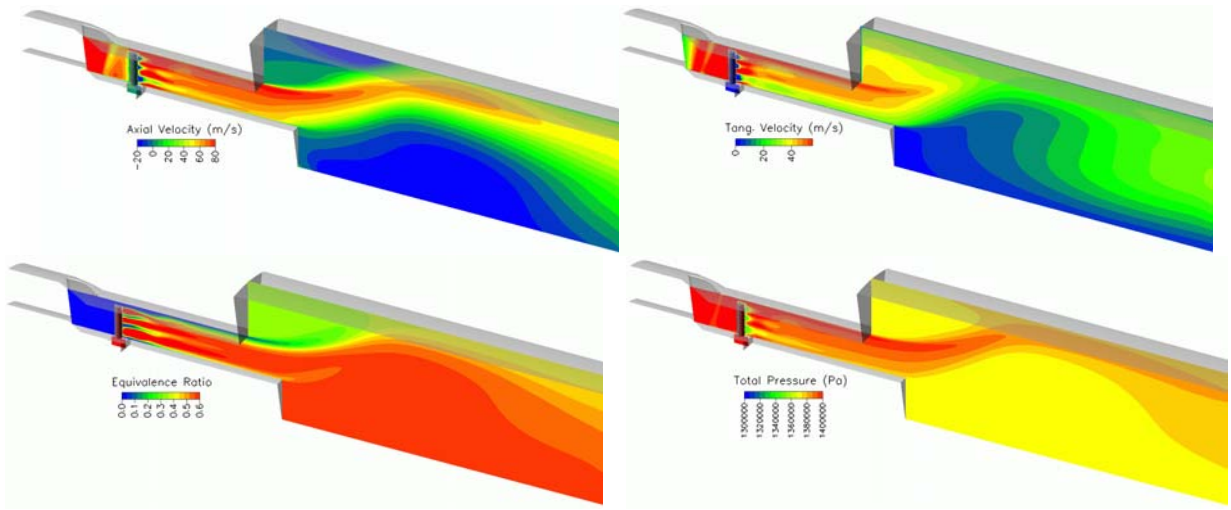

Figure 82. Axial-Radial Planes of Axial and Tangential Velocity, Equivalence Ratio, and Total Pressure

Figure 83 shows the radial-tangential planes of predicted equivalence ratio, total pressure, and axial velocity near the nozzle exit. These results clearly show the tangential uniformity achieved near the nozzle exit. This allowed for a simplified radial profile boundary condition mapping to the full 3D combustor geometry used in the LES calculations.

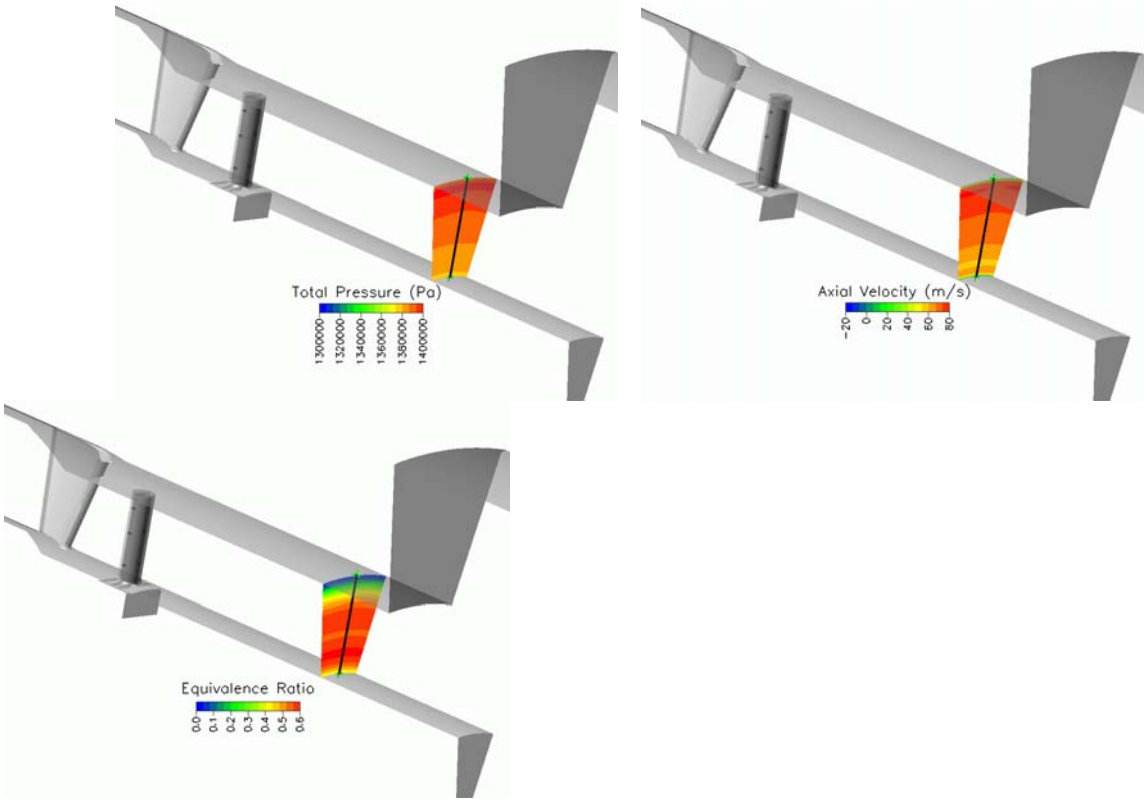

Figure 83. Predicted Radial-Tangential Planes of Axial Velocity, Total Pressure, and Equivalence Ratio ½" Upstream of OD Nozzle Dump Plane

The previously predicted profiles of velocity, equivalence ratio, temperature, pressure, and turbulence kinetic energy were mapped to the full 3D combustor inlet bc. Figure 84 shows the computational domain for the 3D combustor that started ½" upstream of the nozzle OD dump plane and ended 18.5" downstream of the nozzle dump. A fixed mass inlet was applied and a fixed static pressure was applied at the exit. RMS velocity fluctuations of 10 m/s were applied at the inlet. A many-to-one interface was used part-way down the combustor to coarsen the grid in downstream regions. A total of 1.34 million cells were required. The computational domain was decomposed onto 22 processors and calculations were performed on CFDRC's Linux cluster of 1400 and 1670 MHz AMD Athlon processors.

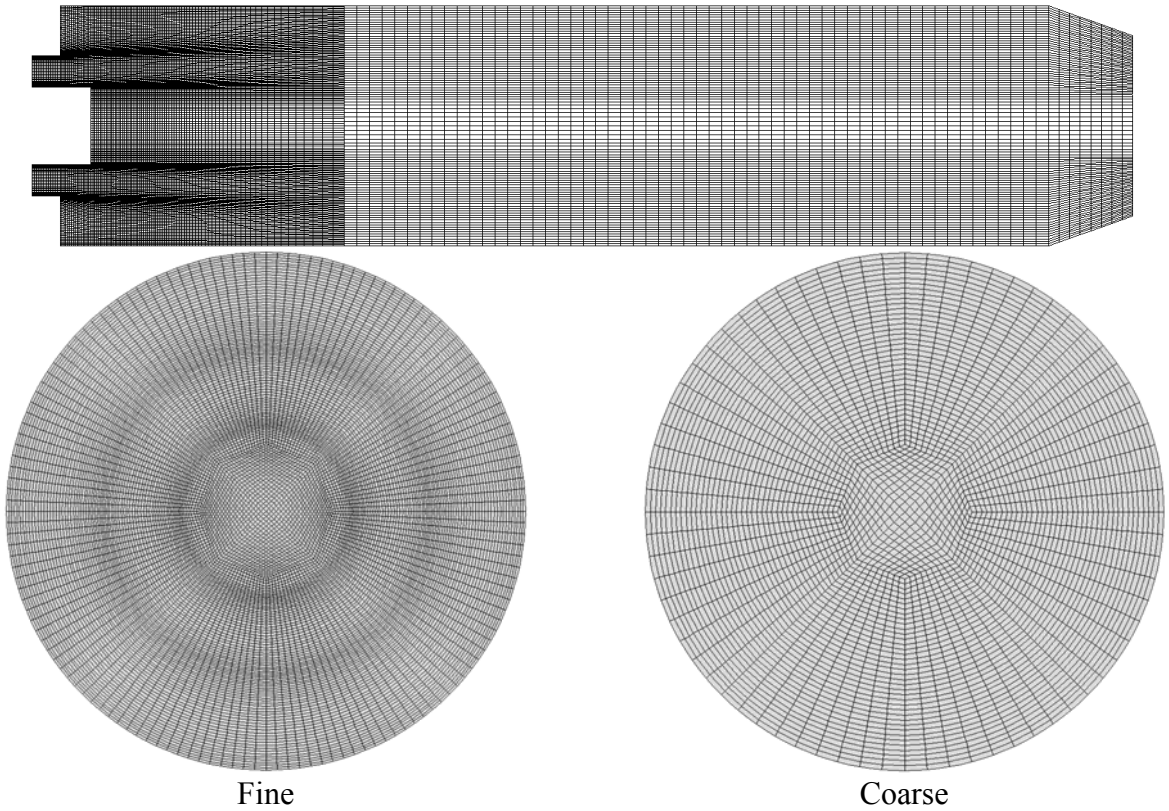

Figure 84. Computational Domain and Grid for 3D LES of the DOE-HAT Combustor

A converged steady-state solution was used as the initial conditions for the LES runs. The LES calculations were performed for 3-4 flows through times at a time step of 7.5E-6 seconds. Although more flow-through times were desired for better statistics, time restrictions limited us to 3-4 flow-through times for this study. Statistics were collected for the last 2-3 flow-through times. The equivalence ratio case of 0.58 was initially modeled. Figure 85 shows the LES instantaneous and mean flowfield variables for this first case. Also included are the RANS predictions. These results show that non-symmetric transient structures are captured with the LES. The temperature contours indicate high-frequency unsteadiness forming in the outer and inner shear layers. The leaner fuel-air mixture from the nozzle OD flow is maintained ¾ of the way down the combustor outer wall. This lean flowfield produces low CO and NO_x emissions near the combustor wall at the 15" downstream location. The core of the flow shows significant CO in the upstream section of the combustor and in the reaction zone shear layers.

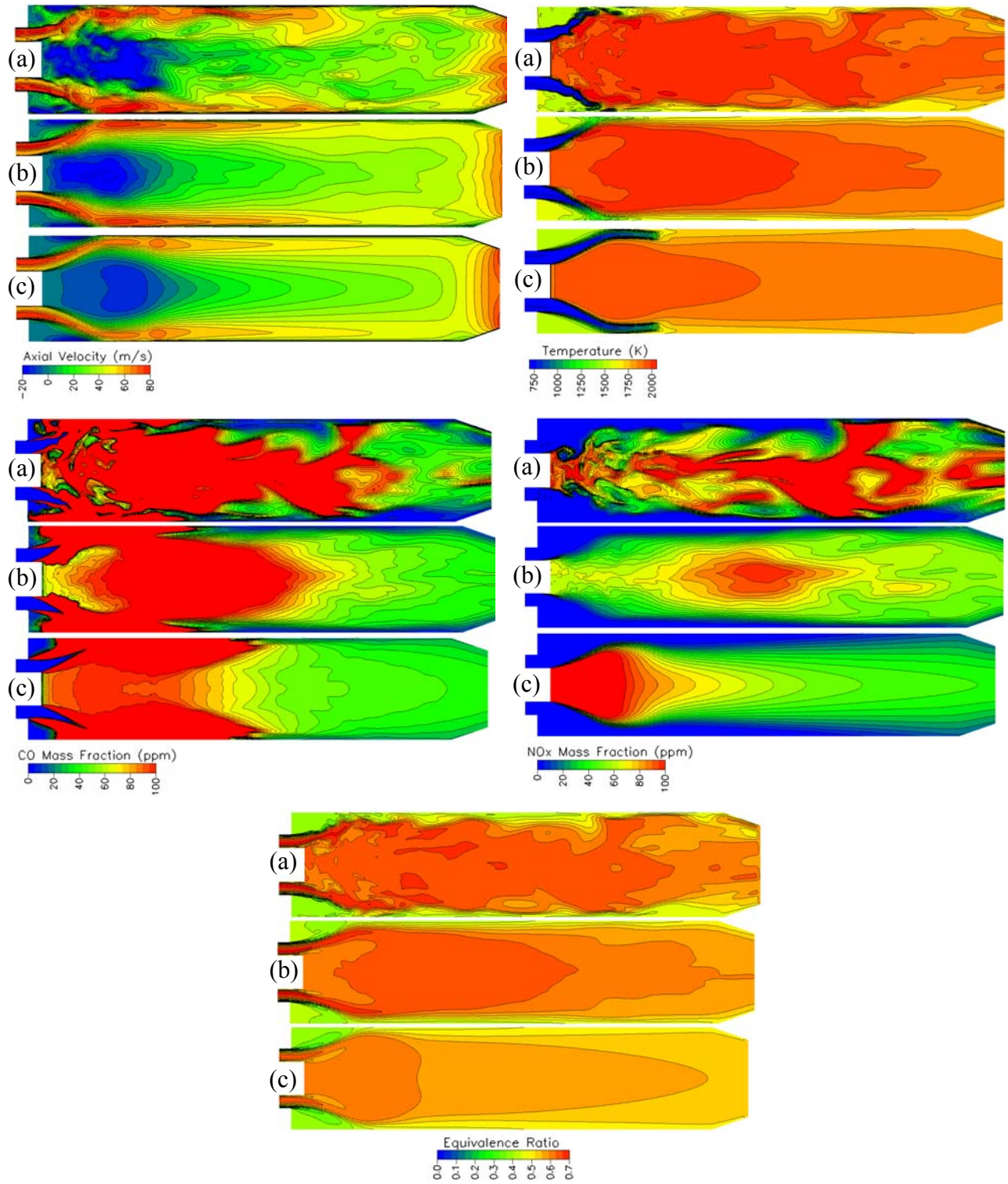

Figure 85. LES and RANS Flowfield Variables for Case 1 (ϕ=0.58); (a) LES Snapshot, (b) LES Mean, and (c) RANS Mean

Overall, the RANS predictions appear to show a longer flame and stronger fuel-air mixing compared to the LES. The NO_x predictions show the largest differences between the RANS and LES. The RANS predictions are approximately 17 ppm lower for NO_x at the backend. The LES predicts a leaner equivalence ratio just downstream of the injector dump plane. This shifts the maximum NO_x location downstream compared to RANS.

The LES predicted pressure, axial velocity, and temperature history and Fourier transforms are shown in Figure 86 for monitor points in the inner and outer shear layer near the fuel nozzle dump plane. The predicted results indicate that strong fluctuations do occur in the shear layers, particularly at the inner shear layer location. A 400 Hz frequency shows up in the pressure signal and this corresponds closely with the ¼ wave acoustic frequency for a closed/open pipe. This oscillation is relatively small at less than 1% of the mean pressure. The outer shear layer axial velocity monitor point indicates a 272 Hz preferred frequency. The temperature monitor point indicates strong temperature fluctuations at the inner shear layer location, though the fluctuations seem to occur at a random rate and not at a particular preferred frequency.

Calculations were also performed at equivalence ratios of 0.50 and 0.42. Figure 87 shows instantaneous snapshots of equivalence ratio, temperature, CO, and NO_x for these leaner cases. It is clear that these cases show the flame to be longer and that cold reactants extend further down the combustor walls compared to the ϕ=0.58 case. The CO emissions are substantially higher along the outer walls for the leanest case (ϕ=0.42). The central core, on the other hand, exhibits less CO for this ϕ=0.42 case compared to the ϕ=0.58 and 0.50 cases. This would be expected since at higher temperatures the CO_2 can dissociate to CO more readily. The near wall fluid is not hot enough for the leanest case to oxidize the CO to CO_2 and thus the high CO at downstream near wall locations.

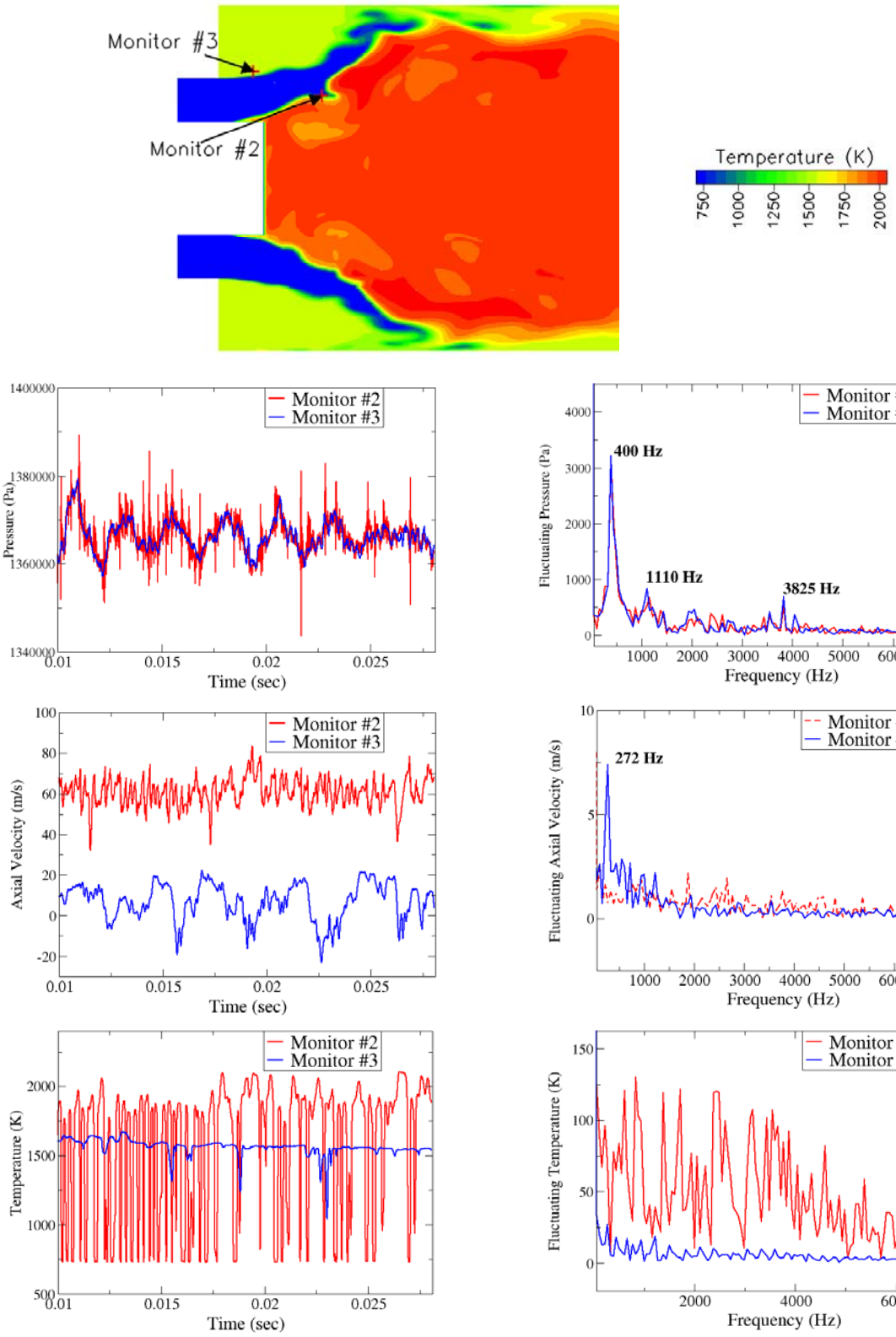

Figure 86. Predicted Pressure, Axial Velocity, and Temperature Time History and Fourier Transforms at Monitor #2 and #3 at Inner and Outer Flame Shear Layer for Case 1 (ϕ=0.58)

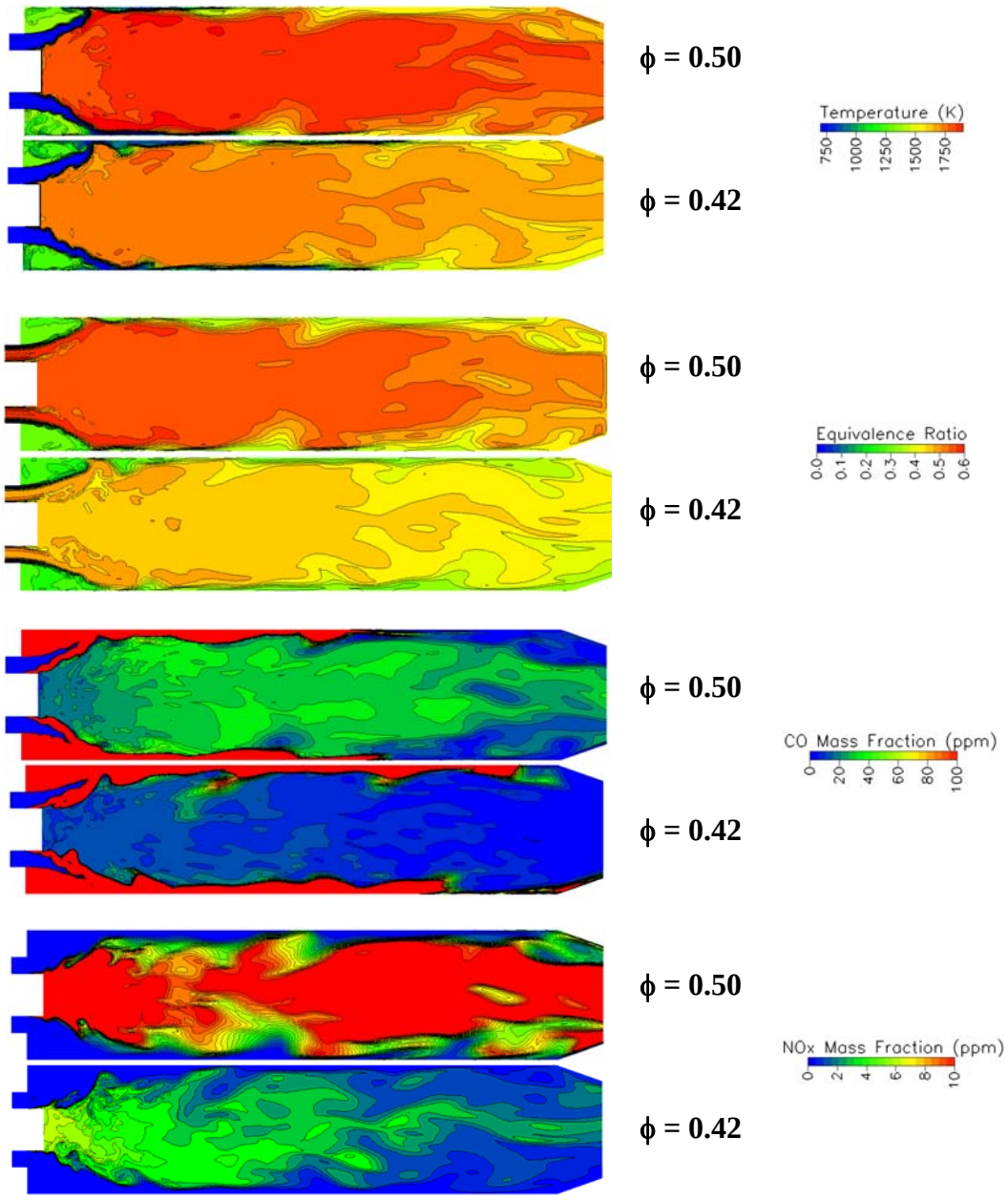

Figure 87. LES Instantaneous Snapshots of Temperature, Equivalence Ratio, CO Emissions, and NO_x Emissions for Cases 2 and 3 (ϕ=0.5 and 0.42)

The NO_x predictions show significantly more emissions for the ϕ=0.50 case (compared to ϕ=0.42 case) as would be expected with the 150 K higher temperatures. The leanest case shows very low NO_x emissions at the combustor exit plane (0-3 ppm). The instantaneous NO_x emissions follow closely the local equivalence ratio and temperature contours. Even in the downstream core regions, variations in equivalence ratio exist, where leaner and richer pockets exhibit lower and higher NO_x levels respectively. The non-linear effect of these unmixed regions will significantly affect the time-averaged NO_x levels.

Comparisons of predicted and measured time-averaged CO and NO_x emissions at a 15" downstream combustor location were made. Table 9 shows the comparison. The measured values were obtained from a 3-hole suction probe with one port located at the combustor centerline and two ports (180° apart) located 1 11/16" away from the centerline. Figure 88 shows the combustor configuration with the 3 port locations that were averaged from the LES and RANS calculations.

Table 9. Comparisons of Measured and Predicted Time-Averaged CO and NO_x Emissions

	Equiv. Ratio	**Experimental**	**LES**	**RANS**
CO (ppm)	0.58	44.3	38.3	38.2
	0.50	9.7	19.9	26.9
	0.42	70.4	41.7	51.5
NO_x (ppm)	0.58	41.5	46.4	29.9
	0.50	8.4	9.3	8.2
	0.42	2.0	0.98	0.44

Figure 88. 3-Hole Suction Probe Measurement Locations

These comparisons show that the LES modeling was quite close to the measurements for the ϕ=0.58 conditions. The CO emissions were overpredicted by a factor of 2 at ϕ=0.50 and were underpredicted by a similar amount at ϕ=0.42. Despite these quantitative discrepancies, the qualitative agreement with the data was good since the initial decrease and then increase in CO with decreasing ϕ was captured. From the flame zone contours it was clear that much of the heat release and CO oxidation was occurring near the combustor walls for the leanest cases. Relatively large grid cells were utilized in this study near the wall and a law of the wall assumption was used for the flow-field wall boundary conditions. A more appropriate wall boundary treatment may be needed to capture the near-wall turbulent mixing effects on CO formation and oxidation. An adiabatic wall boundary condition was used. Small amounts of heat loss could influence the temperature sensitive CO oxidation rates near the wall. Overall RANS predictions of CO were just as good as the LES. Differences were observed between the two predictive methods, as the LES was better at ϕ=0.5 and RANS was better at 0.42.

The NO_x comparisons between the LES and measurements were quite good. The largest discrepancy was at the leanest condition where the predictions were half the measured value (1 vs. 2 ppm). This discrepancy could easily be within the band of the experimental measurement. On the other hand, the NO_x mechanism was limited since it only included thermal NO_x. It is known that the N_2O pathway is an important NO_x pathway at ultra-lean conditions (Steele et al., 1995). It is possible that the inclusion of the N_2O pathway would increase the predicted NO_x emissions at the leanest condition. The RANS predictions of NO_x were not as good at ϕ=0.58 and 0.42, compared to the LES. Slight differences in the mixing were observed between the LES and RANS as shown in Figure 85. These small differences have large impacts on NO_x emissions.

4.2.6 Initial SIMVAL Analysis

Initial CFD calculations were run on the SimVal combustor that was soon to be tested at DOE NETL. The intent of the SIMVAL experiments was to provide experimental data for validating combustion CFD codes, with particular emphasis on understanding combustion instability and variable fuel effects at actual gas turbine combustor conditions. The intial geometry investigated included a choke plate immediately upstream of the swirl vanes and a choked nozzle at the downstream end of a resonant section. Figure 89 shows the baseline geometry.

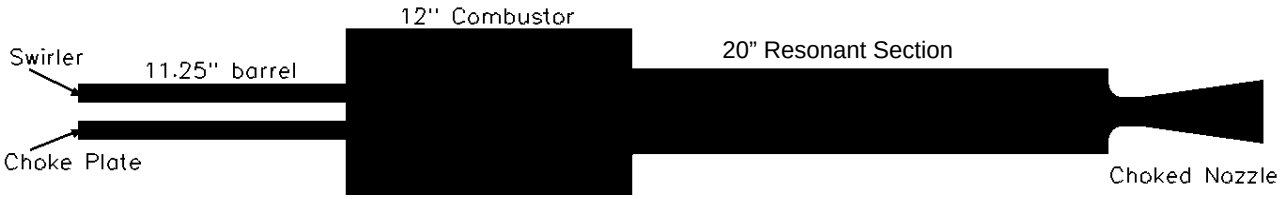

Figure 89. SimVal 2D Axisymmetric Geometry for Baseline Case

Initial transient 2D axisymmetric calculations, including unsteady RANS and LES, were performed at various conditions. These initial simulations provide insight towards instability mechanisms that are driven for the baseline geometry. They also provide further insight on appropriate boundary conditions for LES. Several cases were run with variations in the barrel length, combustor length, equivalence ratio, and turbulence model.

Baseline Case

The baseline case was simulated at the following conditions:

PHI=0.6
V_{noz} = 45 m/s
Swirl Angle = 45°
P = 5.1 atm
T_{in} = 533 K
T_{wall} = 700 K

A fixed mass flow with completely premixed reactants was assumed at the inlet with a constant swirl angle. The fully burned conditions provided a choked flow at the nozzle throat. An

extrapolated boundary condition was used at the supersonic nozzle exit. A total of 12,000 cells was used for unsteady RANS and 65,000 cells for LES. Timesteps of 1E-5 and 3E-6 seconds were used for unsteady RANS and LES respectively. The calculations were performed on the parallel Linux PC cluster using between 6 and 8 processors.

Steady-state predictions for the baseline case are shown in Figure 90. The steady results show the expected swirl stabilized flame with central and outer recirculation zones. The swirling flow attaches to the outer combustor wall before flowing out through the resonant section and into the choked nozzle. Transient predictions were initially performed with unsteady RANS, starting from the steady-state initial conditions. Figure 91 shows the predicted pressure history monitored at the combustor dome face. A dominant frequency of 400 Hz was predicted at an amplitude of ~1.9% of the mean pressure. Harmonics of that frequency were observed at very low amplitudes. The fundamental longitudinal frequency for the hot gas combustor/resonant section is ~510 Hz. The quarter wave frequency for the cold gas barrel is ~406 Hz. A likely driver of instability in this system would be the coupling of these two modes that provides a strong variation in mass flow rate entering the combustor and flamezone. The predicted frequency of the system corresponds to the natural quarter wave frequency of the cold gas barrel. A series of runs were then performed with different lengths of the barrel.

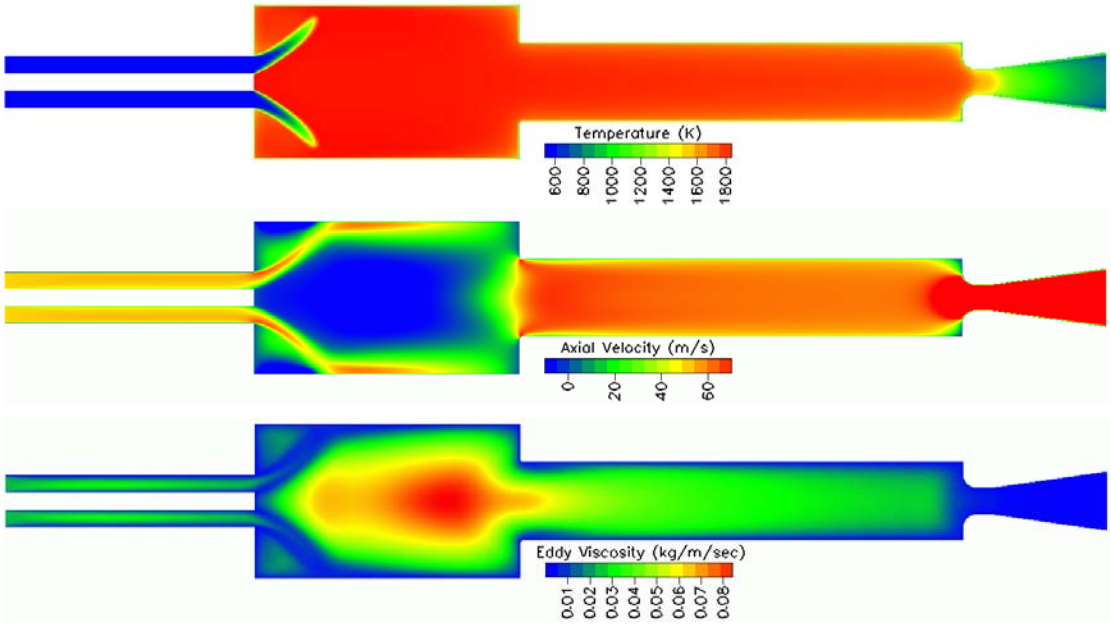

Figure 90. Steady-state Predictions of Temperature, Axial Velocity, and Eddy Viscosity for Baseline SimVal Case

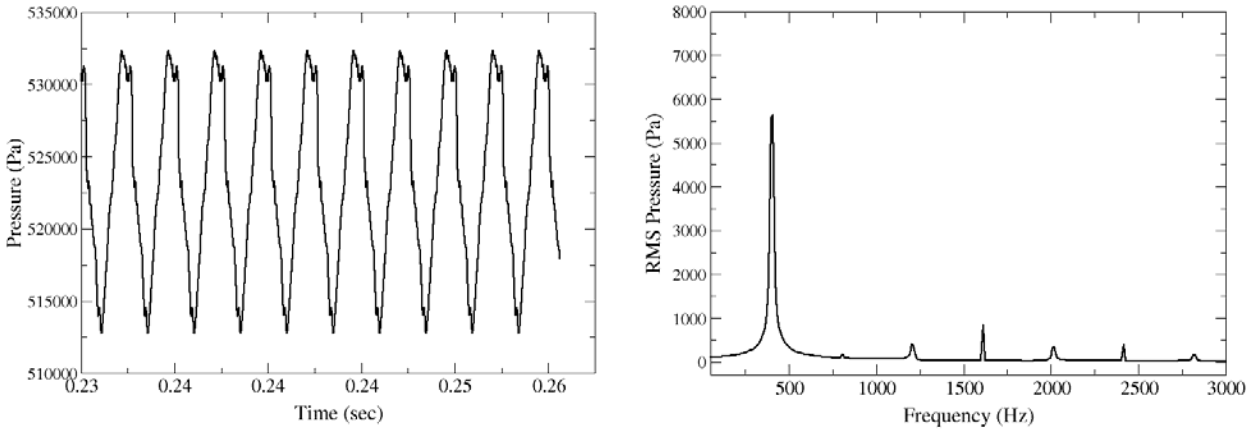

Figure 91. Time History and Fourier Transformed Signal of Predicted Combustor Pressure at Dome Face for Baseline SimVal Case

Unsteady RANS simulations were performed for cases with barrel lengths between 4.75" and 16". Table 10 shows the predicted oscillations from the unsteady RANS calculations with the different barrel lengths. The amplitudes of oscillation observed in these cases are less than has been observed in the past for instabilities driven by equivalence ratio modulation (Richards and Janus, 1997). The largest amplitude oscillation was observed in the baseline case. The smallest amplitude oscillation was observed in the 6.75" barrel case. The 6.75" case also showed two strong frequencies, 1023 and 512 Hz. The higher 1023 frequency exhibited higher peak-to-peak amplitudes. These results indicate that oscillations tend to occur near the fundamental frequency of the combustor/resonant section and its 2nd harmonic. Figure 92 shows the time series and fourier transform of the combustor pressure for Case 2. The occurrence of strong harmonics is observed. The oscillation frequency increases as the barrel length is shortened. A significant jump to the 2nd harmonic (~1020 Hz) occurs at the two shortest barrel lengths.

Table 10. Predicted Oscillations for Varying Barrel Lengths

	Barrel Length	**Oscillation Amplitude**	*Frequency*
Case 1	16.0"	0.8%	405 Hz (weak harmonics)
Baseline	11.25"	1.9%	401 Hz (weak harmonics)
Case 2	8.75"	1.2%	457 Hz (strong harmonics)
Case 3	6.75"	0.6%, 0.3%	1023 Hz, 512 Hz (strong harmonics)
Case 4	4.75"	1.1%	1027 Hz (weak harmonics)

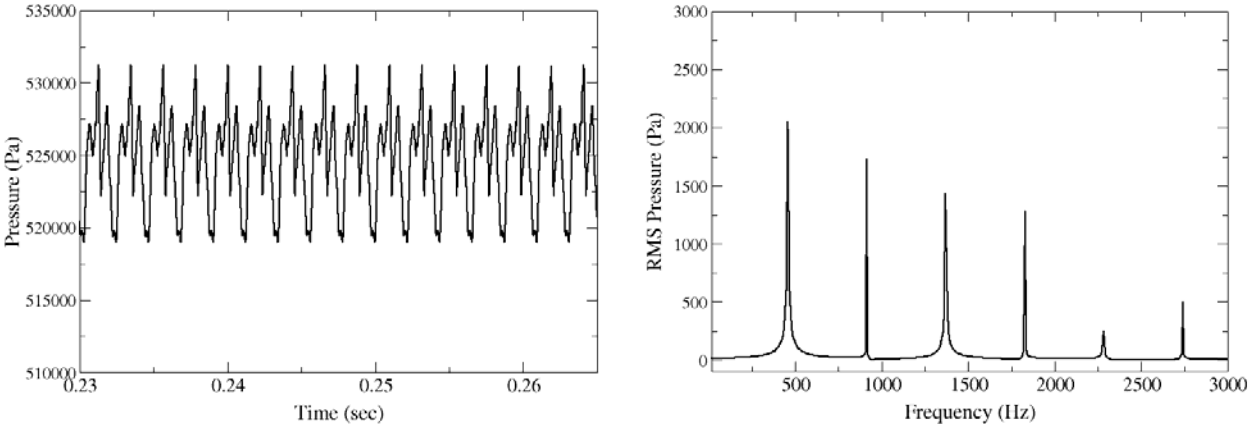

Figure 92. Predicted Time Series and Fourier Transform of Combustor Pressure for Case 2

In addition to trying different barrel lengths, the effect of the resonant section was studied. A case without a combustor neck was tested. This new geometry is shown in Figure 93, where the neckdown is replaced with an extended combustor length. This new straight-pipe combustor case utilized a 16" barrel neck. Figure 94 shows the predicted time series and fourier transform of the combustor pressure. A very high oscillation with an amplitude of 11.5% of the mean pressure and a frequency of 464 Hz was predicted. Higher order harmonics were also observed. The frequency of this oscillation corresponds closely to the longitudinal mode of the combustor. The presence of the original resonant section damps the instability significantly. The original 12" combustor has a longitudinal mode frequency of ~1300 Hz. It is possible that this higher frequency mode helps cancel out some of the lower frequency oscillation, making the system more stable. The original resonant section also provides a small pressure drop in the system as the flow is accelerated. This small pressure drop and the smaller effective combustor volume (or mass) may help avoid the larger pressure oscillations.

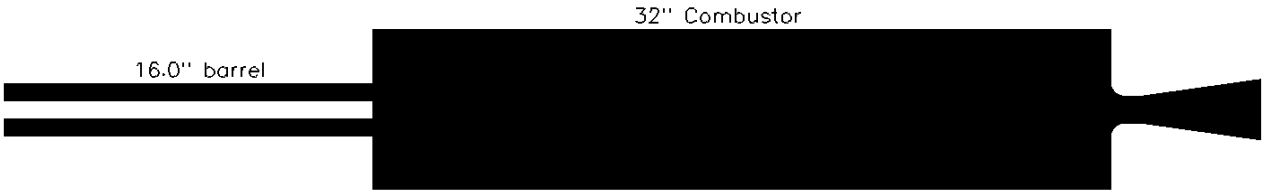

Figure 93. Geometry for Long Pipe Combustor Case

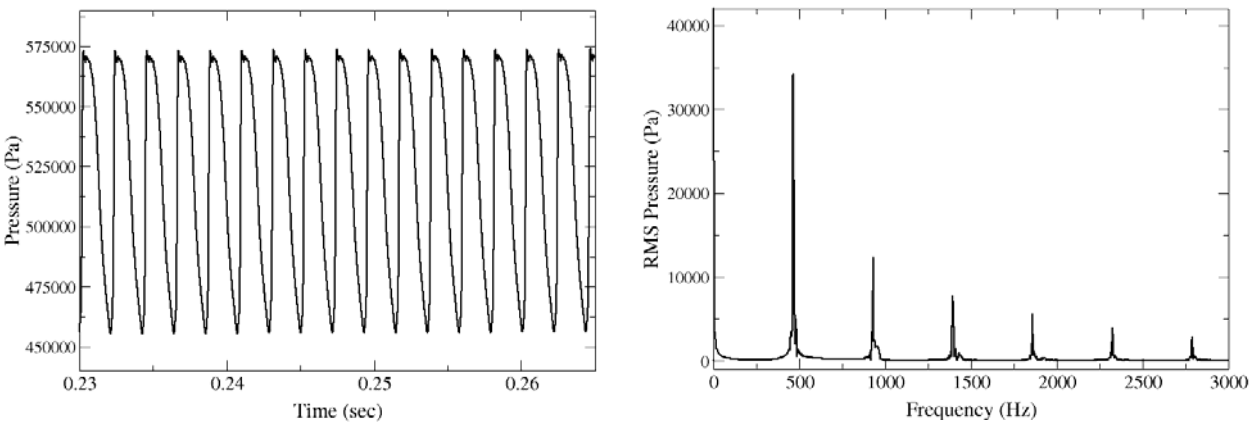

Figure 94. Predicted Time Series and Fourier Transform of Combustor Pressure for Combustor Pipe Case

It is interesting to observe the different flameshapes that are predicted during the oscillation for the large-amplitude instability and the smaller instability. Figures 95 through 98 show predicted instantaneous temperature, axial velocity, heat release, and pressure contours during the cycle (min and max pressure) for the combustor pipe case and Case 4. Significantly more motion occurs during the straight pipe instability. Despite the high amplitude oscillations in the straight pipe case, the flow does not go up inside the barrel at any time during the instability. Previous calculations of the old DOE-NETL case with unchoked barrel flow and equivalence ratio modulation showed significant backflow into the barrel ID during the high pressure portion of the cycle. From the pressure results, it appears that the resonant section adds one or more additional higher frequency modes, so that a single ~500 Hz mode is not as easily excited. The flow changes induced from the resonant section definitely plays a strong role in the potential for developing combustion instability. It seems likely that the barrel length would not have a large impact on the instability for the straight-pipe combustor. These results indicate that the prudent use of neckdown sections creating regions of acceleration and different acoustic modes in the combustor is an effective way of eliminating longitudinal-mode combustion instabilities. One needs to be careful that an effective Helmholtz resonator is not then created for allowing bulk-mode instabilities. The theoretical Helmholtz resonator frequency for Case 4 is ~173 Hz and was not excited at the simulated conditions.

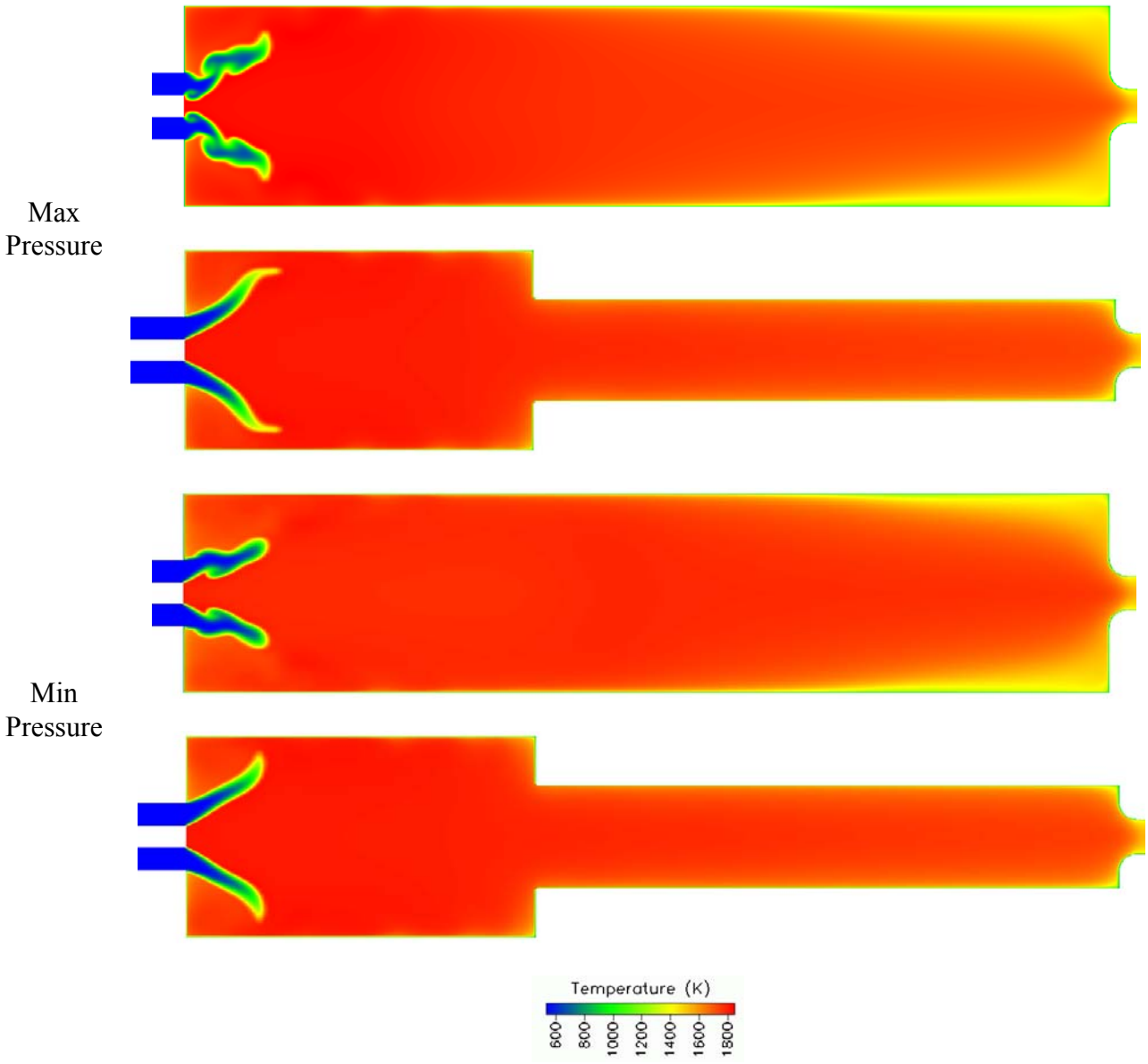

Figure 95. Predicted Instantaneous Temperature Contours at Max and Min Pressure During Instability Cycle for Straight-pipe and Resonant Section Combustor Cases

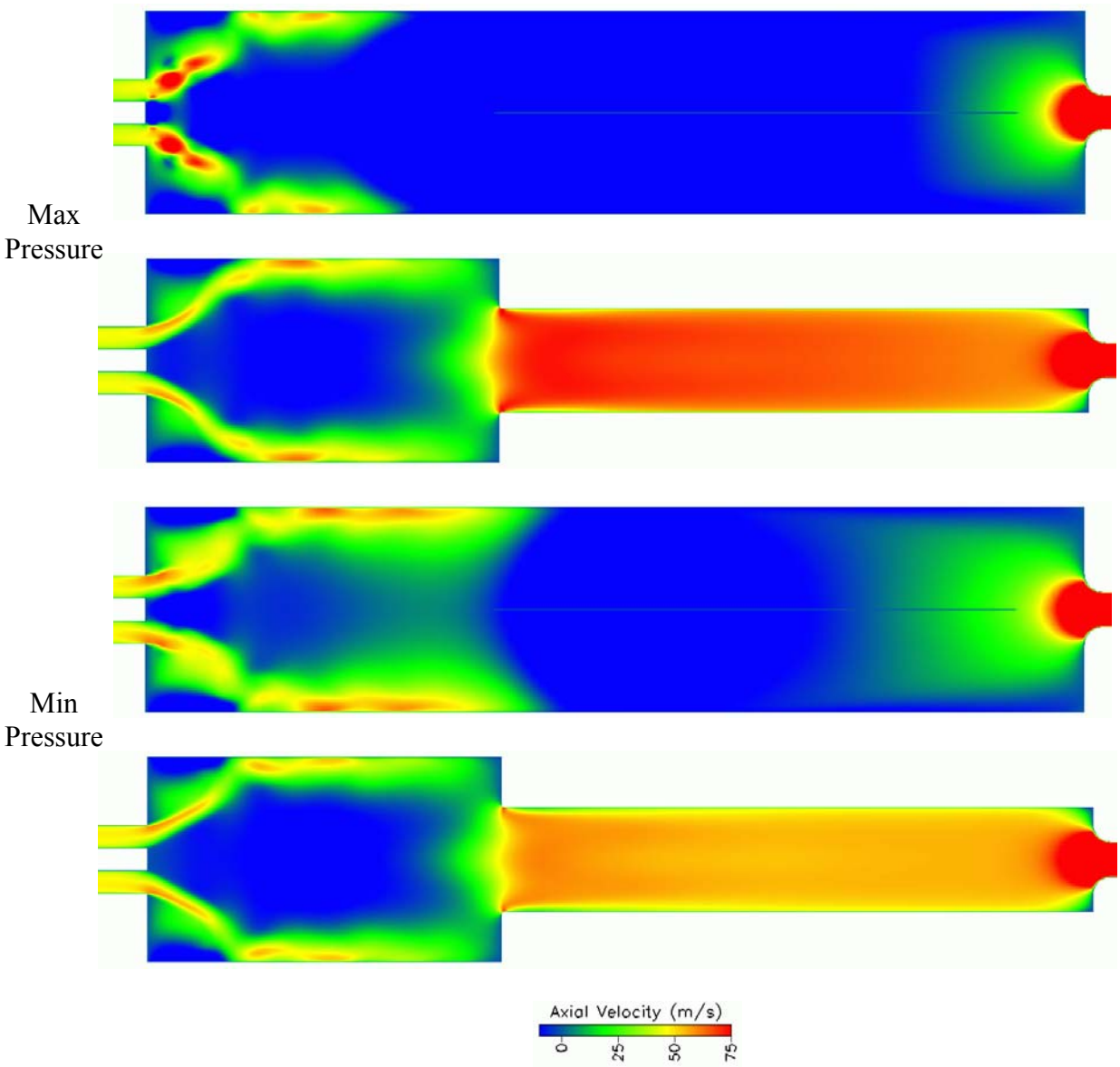

Figure 96. Predicted Instantaneous Axial Velocity Contours at Max and Min Pressure During Instability Cycle for Straight-pipe and Resonant Section Combustor Cases

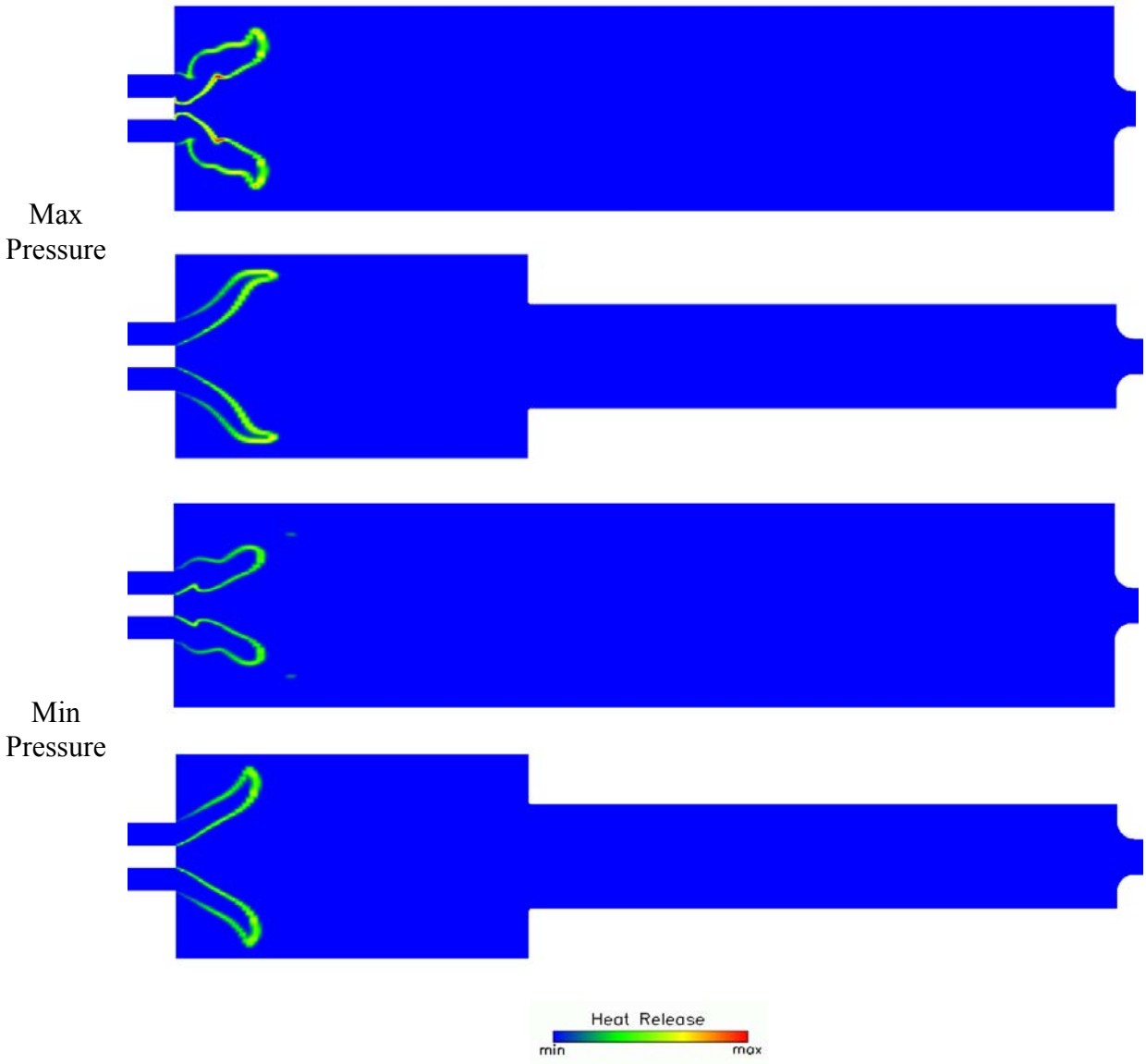

Figure 97. Predicted Instantaneous Heat Release Contours at Max and Min Pressure During Instability Cycle for Straight-pipe and Resonant Section Combustor Cases

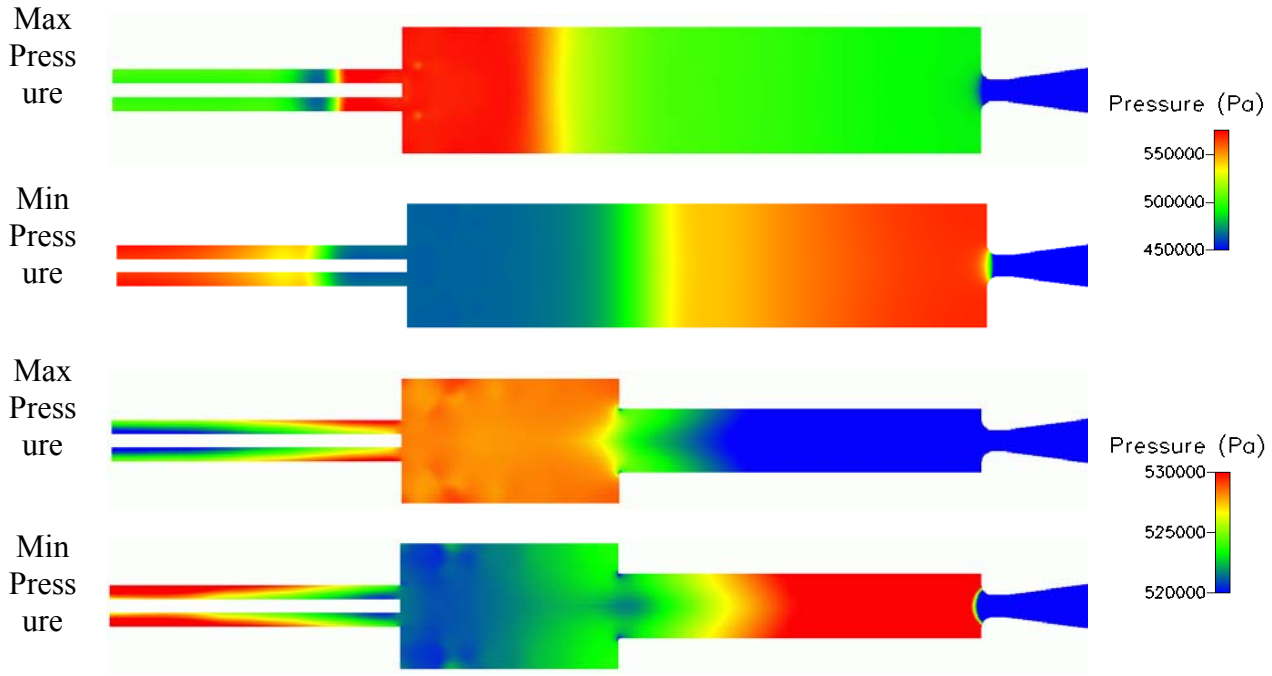

Figure 98. Predicted Instantaneous Pressure Contours at Max and Min Pressure During Instability Cycle for Straight-pipe and Resonant Section Combustor Cases

Several cases were also simulated at different fuel-air equivalence ratios. Table 11 presents the oscillation results for cases with different fuel-air equivalence ratios. All equivalence ratio cases were run with the baseline geometry. The low amplitude oscillations for the leanest case seems to be from spreading the flame out significantly in the axial direction. A spatially distributed heat release zone should always help minimize acoustic/heat release coupling.

Table 11. Predicted Oscillations for Varying Mixture Equivalence Ratio

	Equivalence Ratio	**Oscillation Amplitude**	*Frequency*
Case 5	0.5	0.2%	440 Hz (weak harmonics)
Baseline	0.6	1.9%	401 Hz (weak harmonics)
Case 6	0.7	1.1%	447 Hz (strong 3rd harmonic)
Case 7	0.8	0.9%	468 Hz (strong 3rd harmonic)

Final calculations were performed by utilizing LES models for describing the subgrid turbulence. In order to achieve adequate turbulence levels inside the barrel, high speed jets were introduced at the swirler inlet boundary. Without the turbulent jets in LES mode, significant recirculation along the barrel ID (up to the swirler) occurred. Table 12 shows the results using unsteady RANS and LES with the Smagorinsky and LDKM subgrid turbulence models. These results are

interesting since they show not much effect of turbulence model on the lower frequency oscillation.

Table 12. Predicted Oscillations for Unsteady RANS and LES

	Turbulence Model	**Oscillation Amplitude**	*Frequency*
Case 8	Unsteady RANS	1.8%	397 Hz (weak harmonics)
Case 9	Smagorinsky	1.8%	411 Hz & 1359 Hz
Case 10	LDKM	2.3%	411 Hz & 1341 Hz

Despite the similarities in capturing the low frequency oscillation, the LES cases predicted higher frequency oscillations compared to the unsteady RANS. Figure 99 shows the predicted temperature contours at max and min pressure for the unsteady RANS and LES with LDKM. The LES case predicts smaller structures and pockets of cold reactants that tear away from the main unburned fluid. Also, the LES case allows hot products to recirculate back along the barrel ID during part of the cycle.

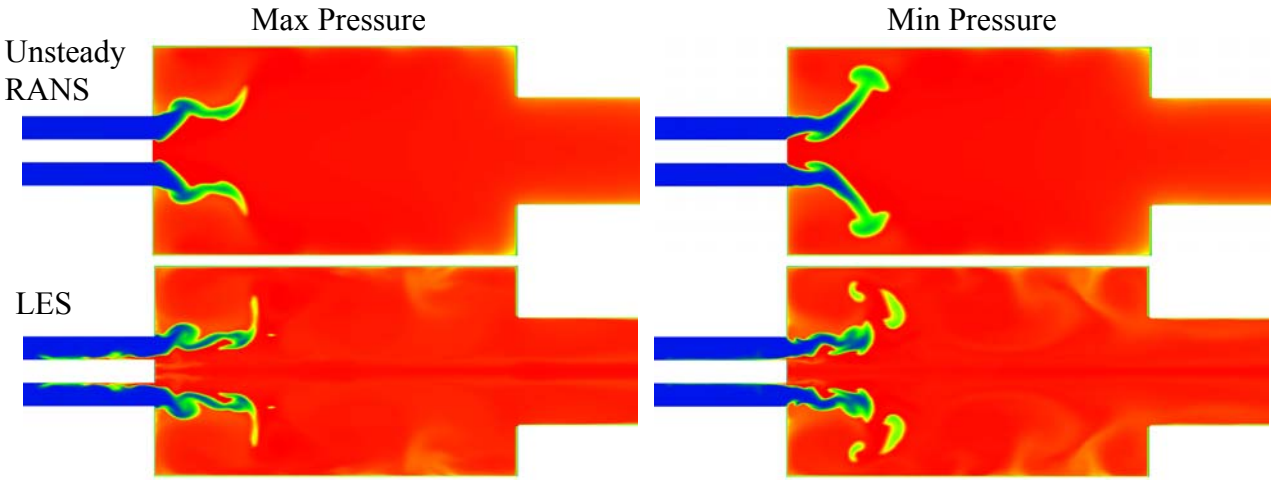

Figure 99. Predicted Instantaneous Temperature Contours at Max and Min Pressure for the Unsteady RANS and LES with LDKM

4.2.7 Second Consortium Meeting

The second meeting of the Combustion LES Consortium was held January 31 – February 1, 2002, at CFD Research Corporation (CFDRC) in Huntsville, Alabama. At the second meeting, 18 organizations were represented. Attendees were: M.S. Anand from Rolls Royce, Jurgen Schumacher from Honeywell, Mel Noble and Alan Kubasco from Solar, Paul Matys from Coen, Alan Sayre from McDermott Technologies, Jeff Lovett from Pratt & Whitney, Erlendur Steinthorsson from Parker Hannifin, Shiva Srinivasan from GE Power Systems, George Kalinovich from Woodward FST, Thanh Tran from Vapor Power, Carol Schnepper from John Zink, Dan Maloney and David Huckaby from DOE-NETL, Balu Sekar from Air Force Research Laboratory, Suresh Menon from Georgia Tech, Prateep Chatterjee from Virginia Tech, Marvin

Rocker from NASA MSFC, Jamey Condevaux from Williams Int., and Steve Cannon, Virgil Adumitroaie, Keith McDaniel, Scott Crocker, Baifang Zuo, and Cliff Smith from CFDRC.

The first part of the meeting consisted of presentations by the CFDRC team describing their progress in implementing advanced models and solution methods into the existing unstructured, compressible CFD-ACE+ code. Highlights of the presentations were:

1. Reduced chemistry models (5-20 species) have been developed for the following fuels: natural gas, propane, hydrogen, syngas, and JP8. These reduced models were developed from full kinetic mechanisms using the CARM code developed by J.Y. Chen of University of California, Berkeley. These models have been implemented into CFD-ACE+ and tested.
2. In Situ Adaptive Tabulation (ISAT) methods, developed by Pope, have been implemented into CFD-ACE+. These methods allow for chemistry source terms to be stored and later read from a table, rather than always performing direct integration. Pope reports computational speedup factors of 10-50 using ISAT compared to direct numerical integration. To date, CFD-ACE+ has only realized speedup factors of four. A number of modifications have been identified that should improve the computational efficiency, including a better method of calculating the mapping gradient matrix and a better table tree structure (P-K instead of the BSP).
3. Suresh Menon reported on the progress made in developing artificial neural nets (ANN). An ANN for 1-step CH4-Air chemistry was trained at two different turbulent flame conditions (F1 and F3) in a 1-D Linear Eddy flame zone code. The ANN was then successfully used to predict a F2 turbulent flame. The ANN approach is being further developed for the more detailed chemical mechanisms.
4. A 64 PC Beowulf cluster was built from scratch, costing about $1000 per PC. The PC cluster performs at the speed of a supercomputer, at a tenth of the cost.
5. Parallelization of the code has been dramatically improved. Tests were performed that show 80% computational efficiency on a Beowulf cluster of 64 PCs when running a 3.5M cell LES case.
6. The Linear Eddy Mixing (LEM) model, developed by Suresh Menon at Georgia Tech, was implemented and tested. LEM models the subgrid turbulence-combustion interaction in LES calculations, and is an essential model to accurately calculate turbulent combustion. The LEM model was shown to agree well with the measurements of a premixed reacting backstep experiment, while other steady-state, unsteady RANS, and LES with laminar chemistry calculations did not.
7. Spray tracking and atomization models have been implemented and tested. Future work includes implementing a multi-component vaporization model to allow the use of the reduced (20 species) JP8 mechanism, and a supercritical vaporization model (being developed by the University of Wisconsin – Madison).

Everyone seemed impressed with the development to date.

After these presentations, Dan Maloney discussed the DOE-NETL SimVal experiment that was scheduled to start in the summer, 2002 and continue running for a number of years. This experiment will provide extensive measurements to be used for code validation of turbulent

reacting flows at realistic gas turbine conditions. The experimental geometry will have hard (choked) acoustic boundaries at both the inlet and exit to establish the full computational domain. Measurements will consist of high response pressure measurements, flame visualization, exit emissions, lean blowout, etc. The experiment is constructed so as to systematically change various parameters that might affect instability and emissions. DOE will make the measurements available to the public, and are hopeful that the measurements will become a benchmark for CFD validation of turbulent reacting flows.

Steve Cannon of CFDRC then presented preliminary predictions of the DOE-NETL SimVal experiment. These predictions were performed using 2D URANS and LES methods, realizing that 3D computations will follow in the future. The baseline case showed a 400-hertz instability. The premix barrel length was shown to have a substantial effect on pressure oscillation amplitude and frequency. The effect of eliminating the downstream resonant section and replacing it with an increased combustor section was also studied. Finally, the effect of equivalence ratio on instability was presented.

Validation Cases

On the second day, the focus shifted to what validation cases should be run by CFDRC during alpha testing. Funding was available to perform four validation cases. Steve Cannon presented a number of potential validation cases, and then the consortium members broke into three work groups to assess the cases and list what cases they desired. The three work groups consisted of: 1) burner/boiler manufacturers, 2) industrial gas turbines, and 3) aero/liquid fuel gas turbines. The burner/boiler manufacturers stated they wanted the following cases: 1) Bluff-body experiment of Vanderbilt, 2) Tecflam experiment, and 3) Weak-swirl experiment from Berkeley. It was assumed that the DOE-NETL SimVal experiment would also be one of the four cases studied. This group also expressed the desire to be able to accurately predict emissions (NO_x, CO, OH), temperature profiles, gaseous radiation, flame instability, and burner-to-burner interaction.

The industrial gas turbine group assigned the following cases to their want list: 1) GE LM6000 case, 2) P&W Dry Hat experiment (tested at DOE), and 3) Solar Taurus 70 case. Once again, the DOE-NETL SimVal case was assumed to be one of the cases that would be studied. It is unsure if the data from the first three cases are in the public domain. Consortium members (Shiva Srinivasan, Dan Maloney, and Mel Noble) were asked to check on the public domain issue. Issues important to this group included vortex shedding from fuel spokes, fuel-air distribution at the end of the fuel injector, premixedness, and heat flux to the liner.

The aero/liquid fuel group did not decide on four cases, but instead listed approximately fourteen cases, ranging from diffuser flows, non-swirling and swirling jets and flames, swirling recirculating flames, premixed combustor, and flames with sound measurements. Other cases they mentioned were a spray data-set from Parker, NASA HOST data, P&W data for combustion instability, and gas-gas co-axial rocket injector data. Unfortunately, this group did not come up with a succinct list.

The recommendations of the work groups were taken into consideration, and a final list of validation cases was selected by CFDRC.

Consortium Funding

The final item discussed at the consortium meeting was how to spend the $150K of consortium money given by consortium members to improve the combustion LES software. Three areas need further development: 1) an improved gaseous radiation model, 2) post-processing software for combustion LES and general combustion analysis, and 3) new atomization models (e.g. airblast atomization). After discussing these tasks, the consortium members who contributed to the consortium funding voted on which tasks they preferred. No consensus was reached. CFDRC decided which tasks to fund, once other funding opportunities have been decided.

4.3 Year Three: Beta Testing By Consortium Members

4.3.1 Third Combustion LES Consortium Meeting

The 3rd Combustion LES Consortium meeting was held at CFDRC in Huntsville, Alabama, from December 3 – 5, 2002. The first day included an overview of technical accomplishments that were achieved during the first two years of the program. Then, results from alpha testing of the software were presented. Following these validation results, the beta testers presented their test cases for future testing of the LES software. Table 13 shows the beta test cases that were selected and the important features of each case.

Table 13. Beta Test Sites and LES Validation Cases

	Case	Details
Coen Company (Paul Matys)	Duct Burner Flame	Predict Lean Blowout - effect of fuel flow - effect of O_2 concentration - compare CFD-ACE+ LES with Fluent and measurements
Virginia Tech (Uri Vandsburger, Prateep Chatterjee)	Swirl-Stabilized Combustor (CH_4-air)	P = 1 atm Swirl Numbers = 0.79, 1.19 ϕ = 0.6, 0.55, 0.5 Compare with Virginia Tech Data
DOE (David Huckaby)	Lean Premixed Combustor (CH_4-air)	Develop user-sub to track ions Compare with DOE-NETL Ionization Probe Data
Rolls-Royce (Sunil James)	Sydney Swirl Burner (CH_4-air)	Compare LES with Sydney Data
University of California, Irvine (Vince McDonnell)	• RQL Combustor (CH_4 and C_3H_8) • Capstone Combustor	Compare LES to temp/species PLIF measurements Investigate pressure effect up to 6 atm
McDermott Technologies (Alan Sayre)	IFRF Burner (Natural Gas)	Compare LES with other codes and IFRF data
Woodward (Kamran Shahroudi)	Woodward Nozzles (Natural Gas)	Investigate secondary fuel/air mixing Compare LES to experiments
Solar Turbines (Mel Noble and Alan Kubasco)	Solar Dual-Fuel Injector (Natural Gas)	Investigate f/a ratio at exit of injector - compare to data - compare with STAR-CD
Parker Hannifin (Erlender Steinthorsson)	• Fuel Injector tested at UCI • Multi-port Injector tested at University of Cincinnati	Compare LES with data and with Fluent

The second day included an overview of the software (CFD-GEOM, CFD-VIEW, and CFD-ACE+). A sample case (turbulent reacting flow over a backstep) was then setup by each trainee. The sample case utilized the LDKM subgrid turbulence model and the Linear Eddy subgrid chemistry model. Proper numerical solution methods and relaxation parameters for combustion LES were also demonstrated. On the final day, each trainee setup the LES case to run in parallel on CFDRC's Linux cluster of PCs. Each trainee decomposed the case onto 4 processors and ran the simulation for several timesteps. Overall, the meeting went well. Each trainee was given a free parallel perpetual license to the beta version of the LES software.

In the end, only six organizations actually ran cases and interacted closely with CFDRC engineers. These organizations were: Coen, Virginia Tech, Rolls-Royce, University of

California, Irvine, McDermott Technologies, and Solar Turbines.

4.3.2 Beta Testing

In this section of the report, a short review of the results will be presented for each organization. Reports written by each organization are included in the Appendix of this final report.

Solar Turbines: Solar Turbines ran a case that simulates fuel-air mixing in an industrial gas turbine premixer. The premixer geometry includes an upstream plenum that feeds a swirler. Fuel is injected through orifices located near the leading edge of the swirl vanes. The premixer annular passage dumps into a combustor geometry. A 36 degree sector was modeled that included 1 swirl vane and fuel injected from just a single orifice (as in the experiment). Cyclic boundary conditions were needed for this configuration.

Solar desired to use a grid from Grid-Pro, another commercial grid generator. A substantial amount of time was spent by CFDRC to modify CFD-ACE+ so that Grid-Pro grids could be run. In the end, we had to generate the grid with CFD-GEOM (CFDRC's grid generation package), and export the grid to Solar. However, Solar could not get CFD-ACE+ to run on their SGI computer system, so CFDRC had to set-up and run the case. The solution files were sent to Solar for post-processing.

Comparisons between measurements of fuel mass fraction and predictions are shown in Figure 86. Both RANS and LES predictions are shown in Figure 100. It can be seen that the LES predictions are in much better agreement with the measurements than the RANS predictions. It should be noted that four periodic slices are included in the prediction results in Figure 100 since the measurements consisted of a four-vane section. Peak concentration levels are well predicted, as well as the radial penetration.

A final report by Solar Turbines is included as Appendix B at the end of this final report.

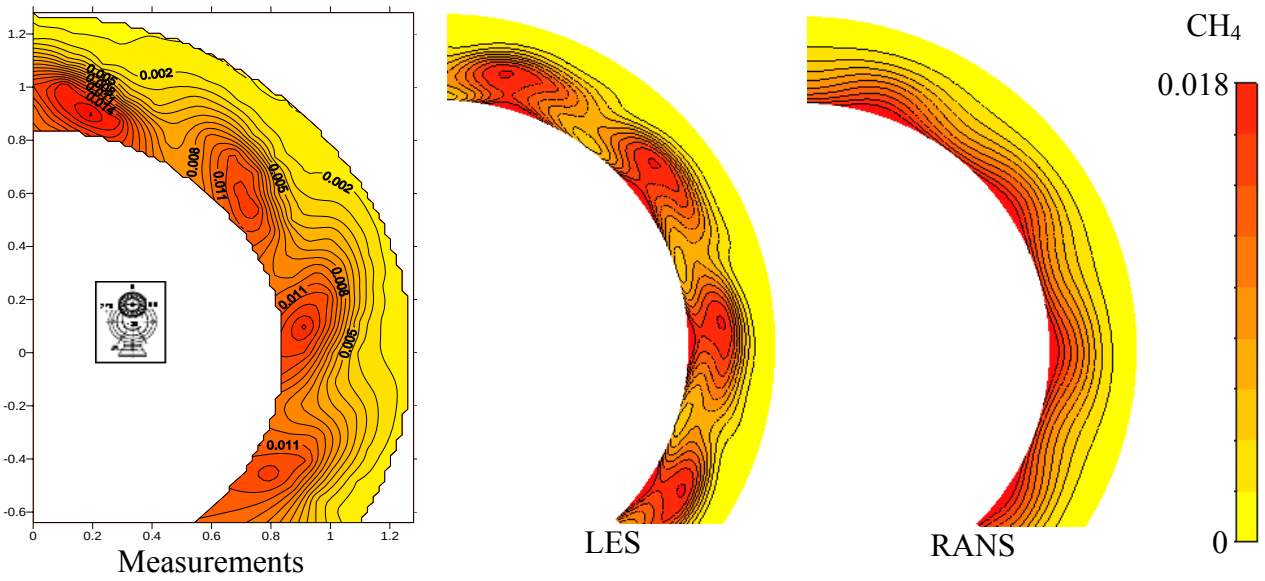

Figure 100. Comparison of Measurements and Predictions at Premixed Exit Plane

Coen: Coen analyzed the combustion behind a duct burner element. Figure 101 presents the case analyzed. The fuel (CH_4) was injected uniformly from the downstream face of the bluffbody. Air enters from the right Figure 101 at 10 m/s and 300K. Unfortunately, no data are available. Coen just compared CFD-ACE+ results with FLUENT results.

Coen used 2D LES analysis, utilizing approximately 10,000 cells. Subgrid models included LDKM for turbulence and assumed pdf (mixture reaction and progress) for turbulence-combustion interaction. The chemistry model employed was a one step-to-equilibrium products kinetics model with rates tuned for methane-air combustion. NO_x was post-processed.

Comparison of CFD-ACE+ and FLUENT predictions are shown in Figure 102. Since only snapshots are presented, it is impossible to assess differences between codes. However, the general flow features appear similar, except the CFD-ACE+ results appear less dissipative (i.e., finer structures are evident near the flameholder for CFD-ACE+). This is probably because the FLUENT predictions used the Smagorinsky model for turbulence, while the CFD-ACE+ predictions used the LDKM model (known to be less dissipative).

Coen commented that the grid generation was difficult to learn/understand because the technique/logic was completely different than FLUENT/Gambit. Other beta testers have stated just the opposite, indicating different users like different gridding techniques. A lot of time was spent in trying to install and use the Linux Operating System, resulting in less time available to assess the code. Coen commented that LES may not be ready for everyday CFD modeling when quick, straightforward answers are needed. However, Coen also stated that LES can (should) be used for selected cases that require accurate prediction of turbulence-combustion interaction.

Coen's final report is included as Appendix C at the end of this final report.

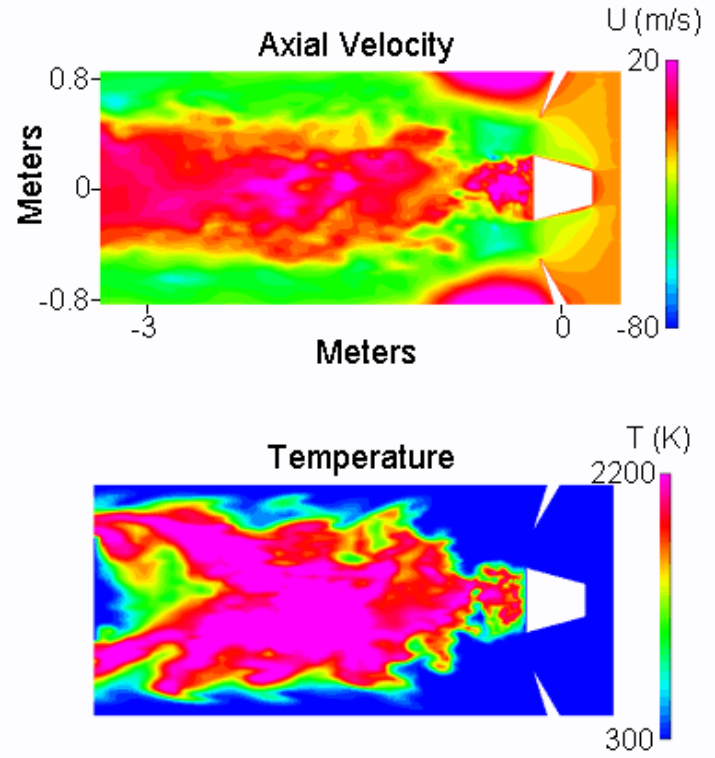

Figure 101. Coen Case: Combustion Behind Duct Burner Element

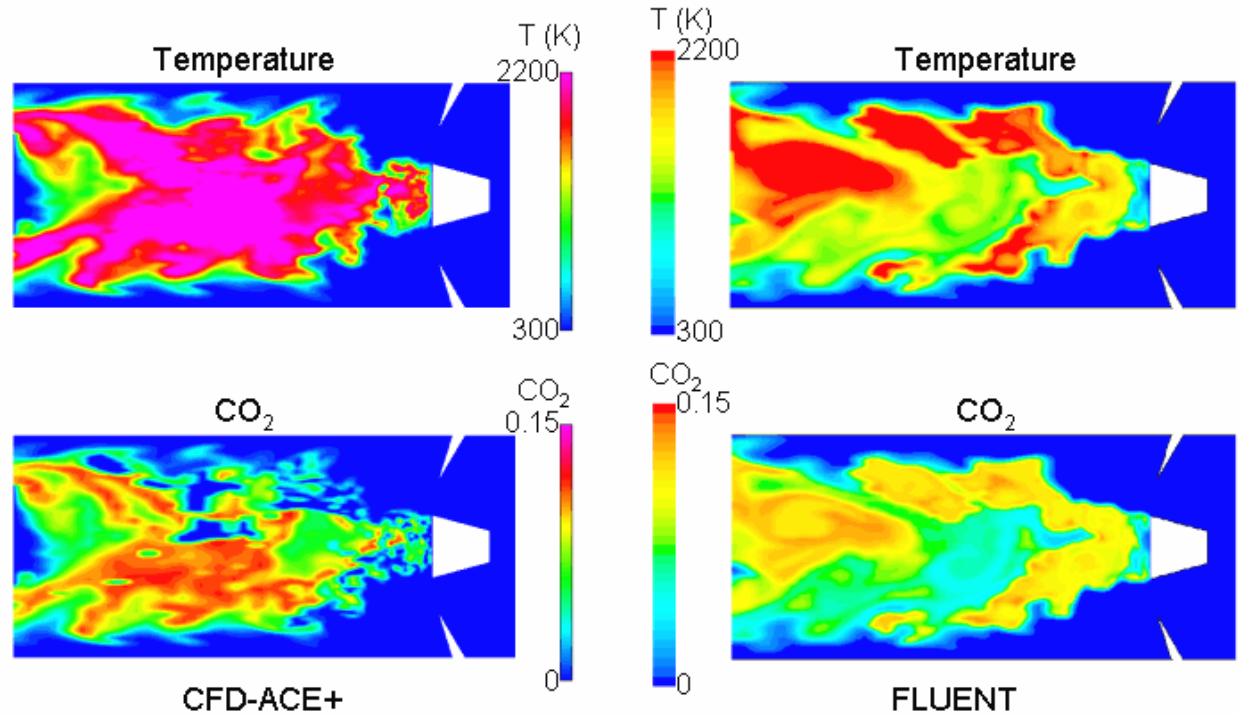

Figure 102. CFD-ACE+ and FLUENT Comparisons; Use of LDKM Results in Less Dissipative Analysis

Rolls-Royce: Rolls Royce experienced a lot of difficulty installing the software on their computer system. This was especially true when Rolls-Royce went from Version 2002 (initial release of CFD-ACE+ at end of 3rd consortium meeting) to Version 2003 (released in Spring 2003). The main reason for the installation/running difficulty was that CFDRC did not support the Rolls-Royce computer system with Version 2003. Rolls-Royce also experienced difficulties when running on the PC cluster at the Pittsburgh Supercomputer Center (PSC), mainly due to downtime for security modifications and other issues. The PC cluster was also very slow (~400 MHertz chip speeds).

The case Rolls-Royce selected for code checkout/validation was the Sydney SMA2 Swirling Methane/Air Flame (see Figure 103). There were numerous issues that caused the case not-to-run/diverge on the PSC PC cluster. One major "bug" that caused significant problems (and took a long time to find) was the naming of the fuel as "FUEL". This caused the restart file to be in error (mixture fraction was set to 0.0), and caused divergence in most cases when restart was invoked. When the 3D LES case was finally running, the flame appeared to be wrong (flame elongated). At this point, it was uncovered that pure methane was specified at the inlet, rather than methane and air at the inlet (user error). In the end, Rolls-Royce was not able to successfully run the case. A final report is included as Appendix E and includes lessons learned and suggested code improvements.

Figure 103. Sydney SMA2 Validation Case

Virginia Tech: Virginia Tech analyzed a premixed turbulent swirl stabilized combustor shown in Figure 104. Their desire is to use combustion LES to calculate the transfer function between u' and q' (for their reduced order models). Virginia Tech performed high fidelity 2D LES calculations using LDKM, Chen's mechanism, and LEM. An example of their calculations is shown in Figure 105. No experimental data were available at the writing of Virginia Tech's final report.

Virginia Tech's final report is included as Appendix D at the end of this final report.

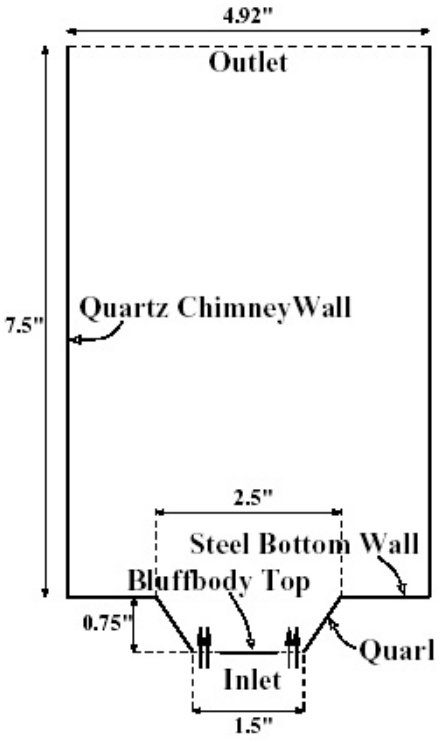

Figure 104. Combustor Being Tested by Virginia Tech

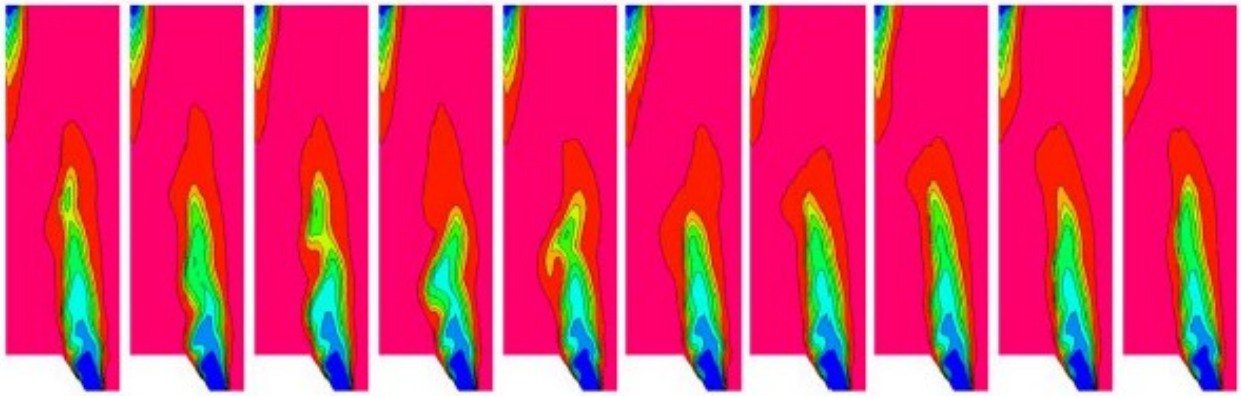

Figure 105. Example of Temperature Snapshots

McDermott Technologies: McDermott ran the 300 kW BERL natural gas case (see Figures 106 and 107). A cold flow 3D LES case was completed, and a hot 3D RANS case was completed. The RANS simulation has gas temperatures that were 300-400K higher than measured. Radiation was then included in the RANS analysis, and temperature agreement was much better. The next step in the analysis process was to run 3D combustion LES analysis but McDermott ran out of time. We did not receive a final report from McDermott Technologies.

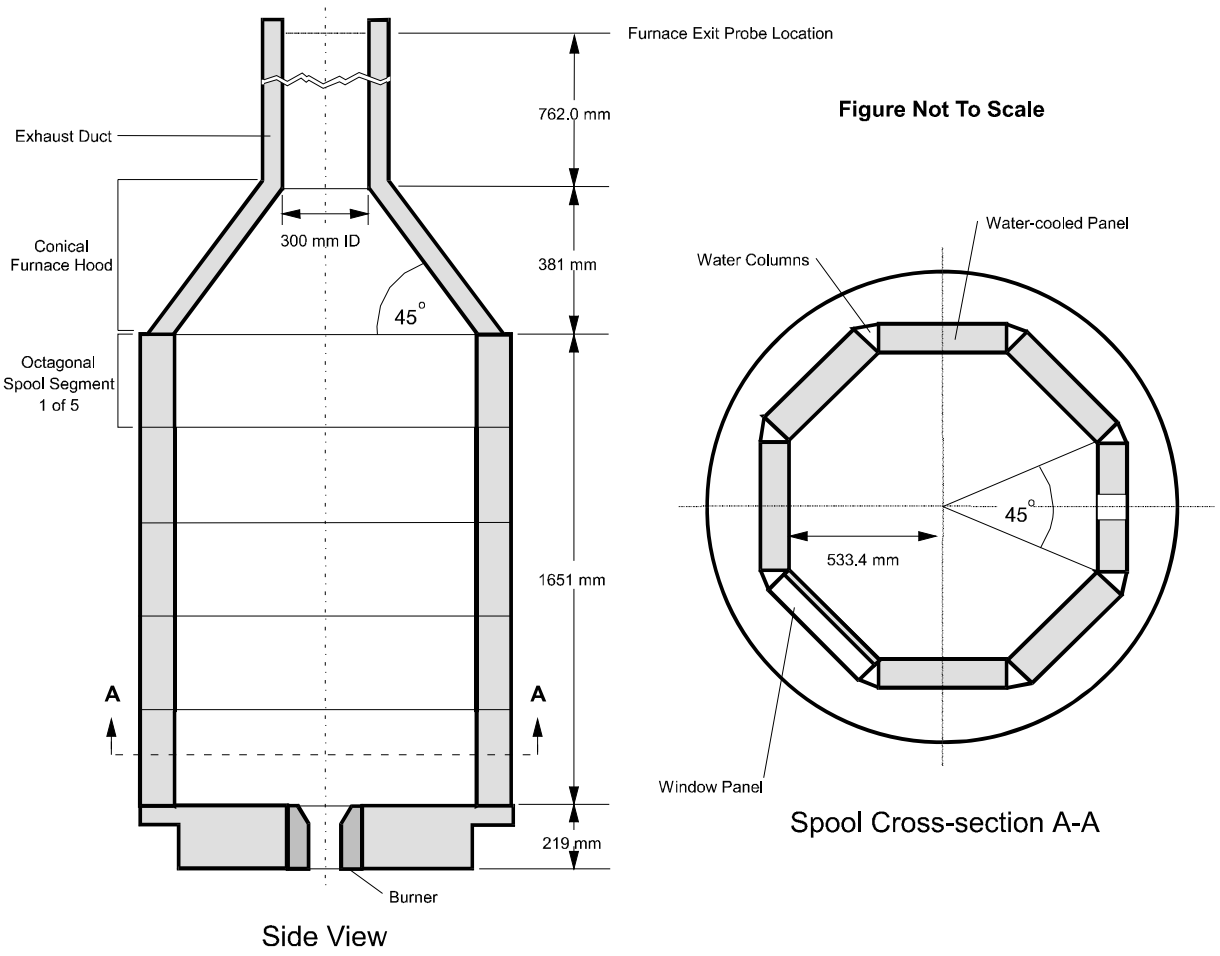

Figure 106. Schematic of BERL Furnace (Forniciari et al., 1994)

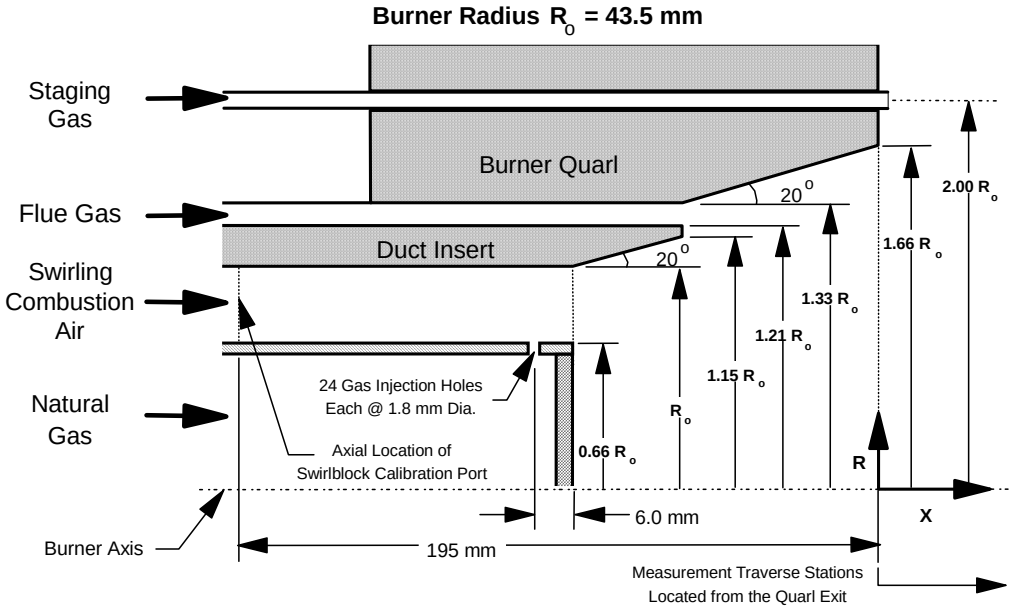

Figure 107. IFRF 300 kW Natural Gas Burner (Forniciari et al., 1994)

University of California, Irvine (UCI): UCI had significant problems/issues installing the software and running parallel simulations. All of these issues were finally resolved; however, little time was left to run meaningful LES simulations. CFDRC received UCI's final report, and it is included as Appendix F of this final report. We expect UCI to continue using our software in the years ahead.

4.3.3 Overall Results of Beta Testing

As we look at the results of beta testing, it is obvious that we underestimated the issues of software installation and parallel running on various computer platforms/operating systems. It took too much time to get the software up and running, leaving almost no time for the real task of running cases and validating the software against experimental data. Still, a significant number of "bugs" were identified and resolved. Table 14 presents a list of problems uncovered during beta testing. In addition, a number of code improvements were identified and suggested for implementation. Overall, the beta testing was very helpful in the software development-process, resulting in an improved software product. It also put the software in the hands of combustion system designers, and promoted the technology transfer of the software.

Table 14. List of Problems Reported by Beta Testers

1. Enthalpy was incorrectly computed using chem1 during startup. (2002-Keith)
2. SGS Kinetic energy computed incorrectly causing divergence. (All)
3. NEWRUN variable incorrectly set, causing startup problems. (2003-Keith)
4. Undefined boundaries internal to decomposed blocks after decomposition corrupts simulation setup. (Rolls-Royce)
5. Segmentation violation in input_ic_chem2. (Rolls-Royce)
6. DTF file locking causes deadlock on NFS mounted systems. (2002+2003-Babcox &Wilcox)
7. Vmix = 0.0. (2003-Keith)
8. Web help not working in release of V2003. (Coen Co, All)
9. Array not allocated; "indexing into array" error. (V2002-VT)
10. V2002 solver dies after specified interval output. (Babcox &Wilcox)
11. Multiple parallel bugs with cyclic boundaries. (V2002+V2003-Solar Turbines)
12. Unsupported Block Topologies for Plot3d in CFD-GEOM. (Solar Turbines)
13. SGI Origin 3000, and Mandrake Linux Cluster incompatible with our software. (Solar Turbines and Coen)
14. 2003 release of software excluded many operating systems previously compatible with 2002 code. (Rolls-Royce)
15. Many systems administered by industrial companies and organizations normally don't use "rsh" because of security reasons and prefer "ssh". (PSC, Virginia Tech, Coen, Babcox&Wilcox)
16. Incompatibility between 2002 and 2003 versions. (All)
17. Displaying of CFD-GUI and CFD-VIEW across the network almost never works because of software and/or hardware graphics. (All)
18. The parallel license wasn't setup correctly limited runs to serial and/or 4 processors initially. (UCI Irvine, Coen, VT, and Solar Turbines)
19. Like the ability to startup a parallel run on remote nodes excluding current login node. (Adrian Spencer, Babcox & Wilcox, VT)
20. Parallel setup difficult for normal users and requires expertise system administration. (All)
21. DTF key number must be repaired from Gridpro DTF output. (Solar Turbines)
22. 2002 Calls Error stop after checking J.Y. Chen reaction mechanisms. (naming convention problem)
23. 2002 and 2003 solver doesn't initialize fuel flow-field properly if "FUEL" is used for the fuel mixture name. (Rolls-Royce)
24. "Array Allocation Error". (Rolls-Royce)
25. Backflow in Outlet causing divergence. (VT)
26. Problems with slm_admin.exe. (UCI, RR)
27. dtf_decompose error for cyclic boundaries. (Solar Turbines, Babcox & Wilcox)

4.3.4 SIMVAL Predictions In Third Year

Additional calculations of the DOE SIMVAL lean premixed combustor were performed in the third year of the project. The SIMVAL combustor will provide experimental data that can be

used to validate combustion CFD codes, with particular emphasis on understanding combustion instability and variable fuel effects at actual gas turbine combustor conditions. Initial experimental data has been taken on May 2003 and released by Dan Maloney at DOE-NETL. CFDRC participated in a panel session at the June 2003 IGTI Gas Turbine Expo in Atlanta. Bob Malecki, of Pratt & Whitney, presented the simulation results and the comparisons to experimental data. The experimental data were not available to CFDRC or the other participants until the panel session. The results from this panel session and subsequent post-dictive calculations will be discussed here.

The baseline geometry of the SimVal combustor includes well-defined acoustic boundaries with a choke plate immediately upstream of the swirl vanes and a choked nozzle at the downstream end of a resonant section. Figure 108 shows the baseline geometry. The baseline operating conditions included:

Air Mass Flow-Rate 0.26 kg/sec
Inlet Air Temperature 600 K (620 F)
Equivalence Ratio 0.47 – 0.7
Pressure ~ 4.5 atm (varied with equivalence ratio)

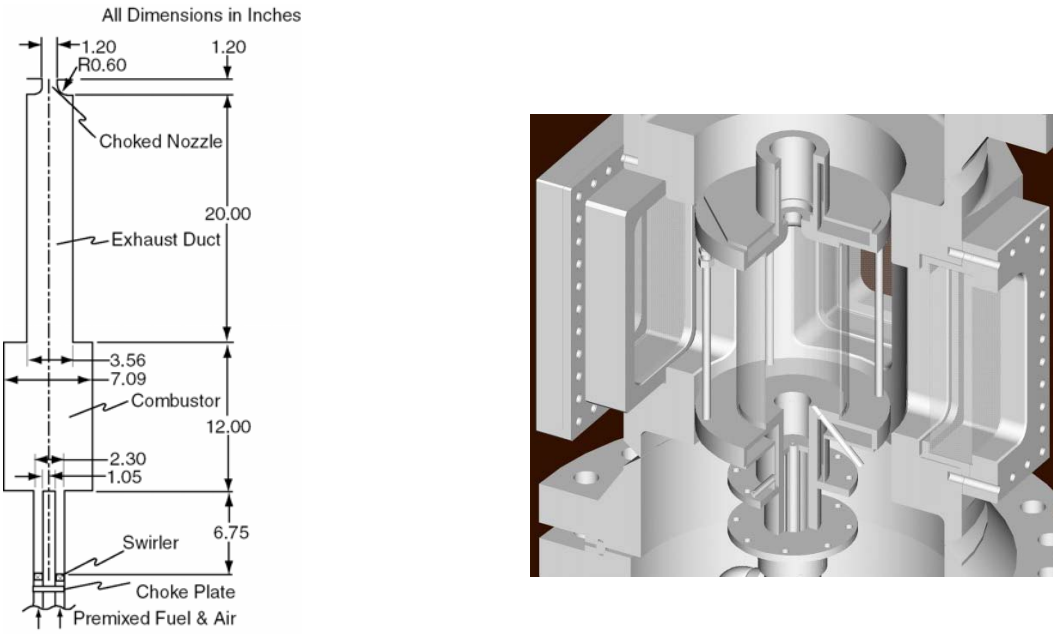

Figure 108. Baseline Geometry for SimVal Combustor

Initial 3D non-reacting calculations of the slot swirler were performed by Bob Malecki of Pratt & Whitney. These full-swirler calculations provided the inlet profiles for the reacting CFD model used by CFDRC. The predicted axial and tangential velocity profiles, as well as the swirl angle in the annular injector region, are shown in Figure 109. It is clear that a recirculation bubble forms just downstream of the swirl vanes. At 2 inches upstream of the combustor dump, the flow is all positive and the swirl angle varies from 55 to 65 degrees. The profiles at the 2 inch location were used in the CFDRC reacting flow models and were applied 7.75 inches upstream of the combustor dump, where the choke plate and swirl vanes are located.

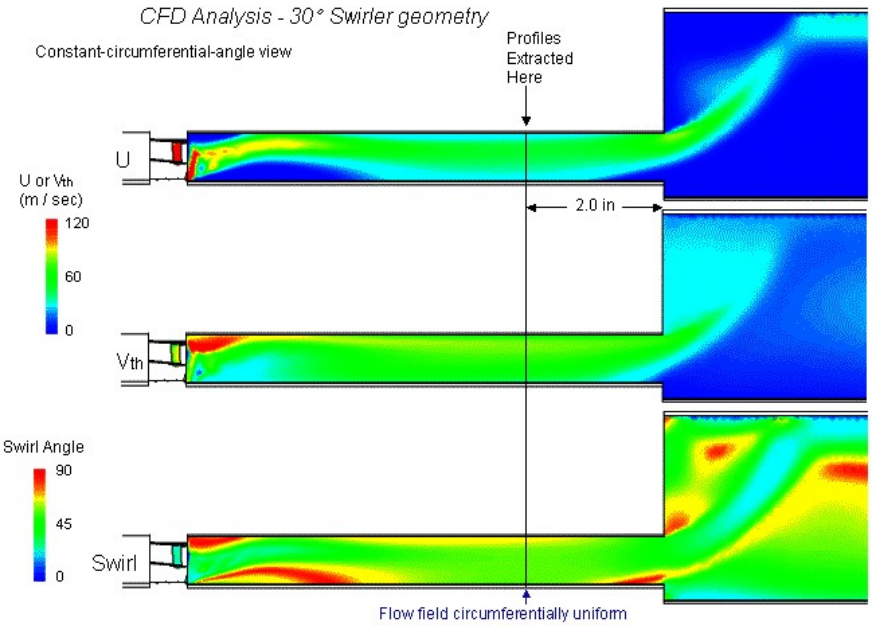

Figure 109. P&W Predicted Non-Reacting Flowfield Through Swirler and Injector Annular Passage

A fixed mass flow with completely premixed reactants was assumed at the inlet with the appropriate profiles on velocity, pressure, and temperature from the P&W simulation. The fully burned conditions provided a choked flow at the exit nozzle throat. An extrapolated boundary condition was used at the supersonic nozzle exit. The 2D axisymmetric geometry used ~15,000 cells and the 3D geometry required ~1,500,000 cells.

Both RANS, unsteady RANS, and LES calculations were performed. Second-order accurate spatial and temporal differencing methods were utilized. The 2-step reaction model assumed finite-rate methane oxidation to CO and then finite-rate CO oxidation to equilibrium products. De-coupled NO_x chemistry that included thermal, nitrous, and prompt mechanisms was included. The 2-dimensional (mixture fraction and reaction progress) assumed PDF method was used to account for turbulence and chemistry interactions. Since the flow was perfectly premixed, mean (or filtered) reaction rates were only affected by fluctuations in the reaction progress. The transport equation for the variance of the reaction progress depends on the turbulent mixing due to subgrid scales for LES. The Ck coefficient for this turbulent mixing term was changed from a value of 2 (for RANS) to a value of 200 for LES. This was needed to produce realistic results. If the standard value of 2 were used, then unrealistically high variances would occur near the burning flame zone and these high variances would in turn reduce the mean reaction rate significantly so that some unburnt fuel would escape the combustor exit. This Ck coefficient could be computed locally using LES filtering techniques and will be implemented in CFD-ACE+.

It was found that wall temperatures in the model were an important boundary condition, since heat loss had a large effect on the emissions in this long residence time (~30 msec) combustor. Initially, hot 1650 K walls were assumed in the air-cooled, quartz lined combustor. Cold 658 K walls were assumed in the dome and water-cooled resonant section. Predicted temperatures for

equivalence ratios of 0.5, 0.6, and 0.7 are shown in Figure 110. The reduction in combustor temperature with downstream distance is apparent due to the heat loss. A difference of 250 K between adiabatic equilibrium and the mean exit temperature was observed. It is interesting to observe the hot product gases in the injector along the ID for the ϕ=0.7 case. The upstream propagation of flame into the injector was quite sensitive to boundary conditions and models.

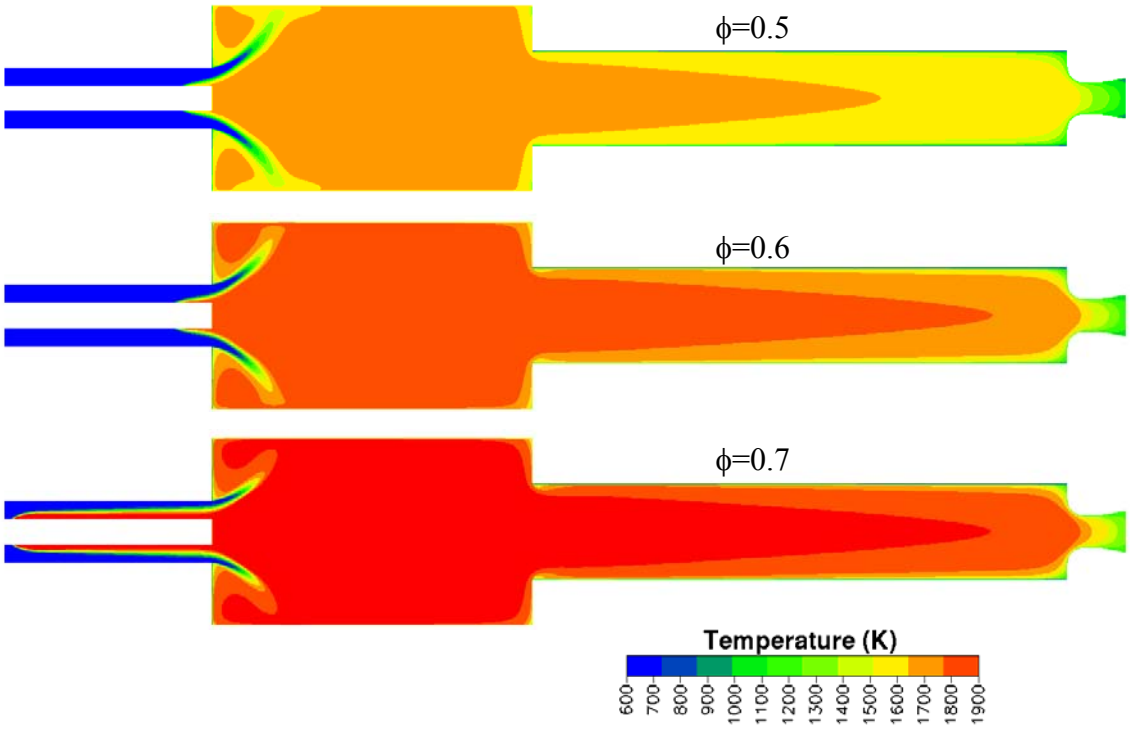

Figure 110. Predicted RANS Temperatures (RNG k-ε) for ϕ = 0.5, 06, and 0.7

If for example, the calculations were performed with the more viscous standard k-e model, rather than the RNG k-e model, then the flame would not penetrate very far up into the injector. Figure 111 shows temperature predictions using the standard k-e model. The experimental evidence seemed to indicate that the flame went upstream only about 0.5-1 inches, not the 6 or 7 inches seen in the RNG k-ε results.

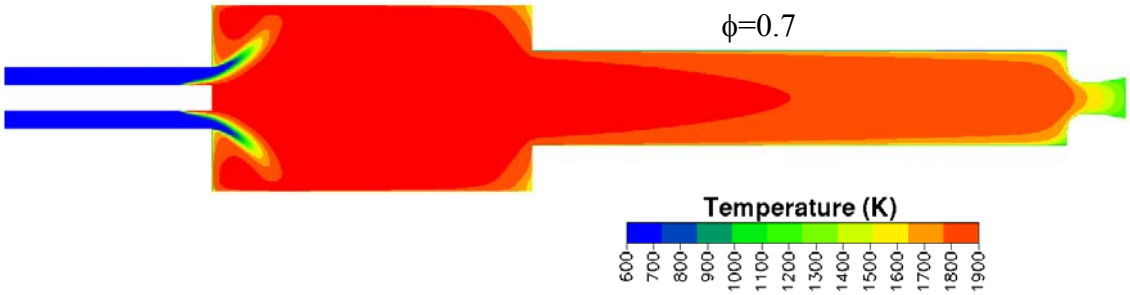

Figure 111. Predicted Steady-state Temperature for Standard k-ε model (ϕ=0.7)

LES calculations were performed for 2D axisymmetric and full 3D geometries. The LES timesteps were 5E-6 seconds and statistics were accumulated over several flow-through times. The sensitivity of the turbulence model was also apparent in LES for predicting the flame propagation (flashback) up inside the injector. Figure 112 shows predicted mean temperatures using different subgrid turbulence models; Localized Dynamic Turbulent Kinetic Energy (LDKM) and Smagorinsky. The LDKM results clearly show the flame propagation up inside the barrel. The use of a finer grid in the injector, with y+ values of ~2, also produced this upstream flame propagation. The more viscous Smagorinsky model did not allow the flame to propagate upstream into the injector. The higher viscosities seem to allow more heat loss at the walls. In addition, the higher viscosities could make the flow have less tendency to separate along the injector ID and/or reduce local flame reaction rates. It is not clear that the wall boundary conditions are being treated correctly for the LDKM model. The consistent treatment of velocities and subgrid kinetic energy at the walls will be studied in more detail.

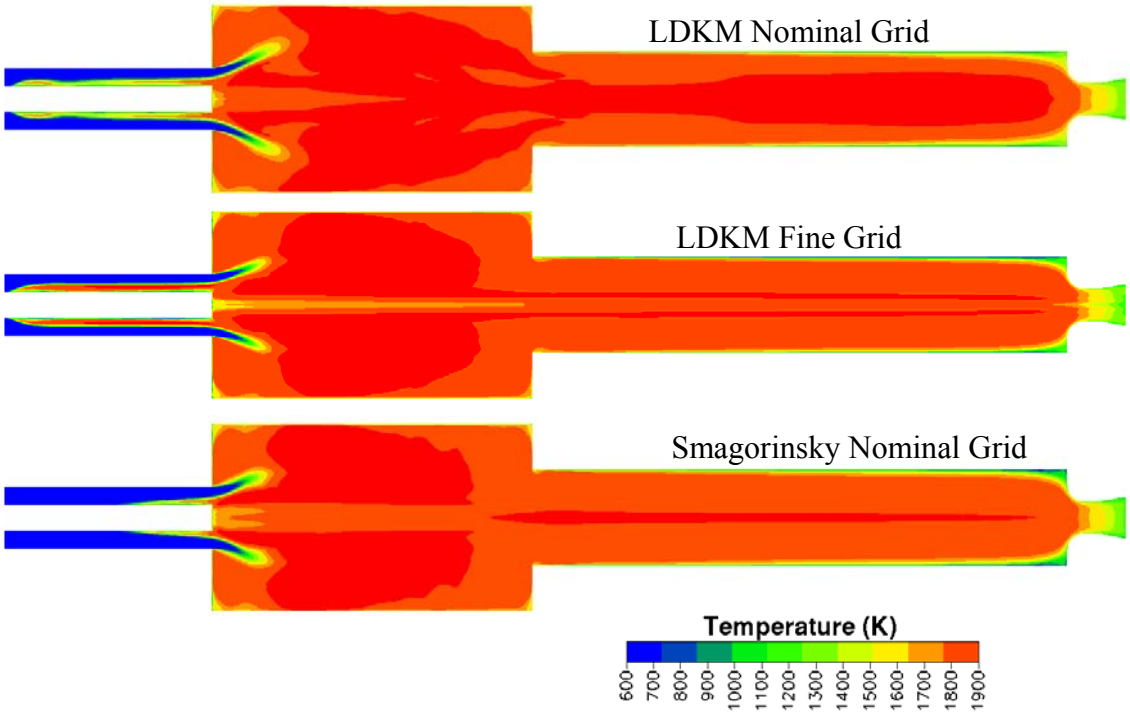

Figure 112. Predicted Temperatures Using LES with Subgrid Turbulence Models of LDKM and Smagorinsky (ϕ=0.65) and With Nominal and Fine Grids (15,000 vs. 30,000 cells)

The NO_x and CO emissions just downstream of the exit nozzle were measured and were compared to the model predictions. Figure 113 shows the predicted NO_x emissions within the flowfield and the area-averaged exit value. Most of the NO_x is formed in the combustor central recirculation zone. The NO_x mixes out in the downstream section of the combustor and remains relatively constant in the resonant section. A ϕ=0.65 case was also simulated since the data only went up to a ϕ of 0.67. A good comparison with data is obtained at the leanest conditions. The model overpredicts the NO_x at ϕ=0.6 and above. This overprediction could be due to the assumed heat loss in the CFD model. To understand the sensitivity of heat loss on the NO_x predictions, the ϕ=0.65 case was run with the cooler combustor wall temperatures that were measured (~1350 K vs. 1650 K). The cooler wall temperatures reduced the NO_x predictions by 30%, giving fairly good agreement with the data (see Figure 114).

The LES cases were run with 1650K wall temperatures. The use of LES with the LDKM model did not substantially change NO_x emissions compared to RANS at ϕ = 0.65 (see Table 15). The Smagorinsky LES results produced lower NO_x than LDKM (see Table 15). This was primarily due to the higher heat loss and reduced flame area for the Smagorinsky case compared to the LDKM case. Figure 115 shows 3D LES results of NO_x rate and vorticity. It can be seen that the NO_x rate increases slightly in regions of high vorticity in the reacting shear layer. The NO_x rate decreases near the combustor walls where significant heat loss occurs.

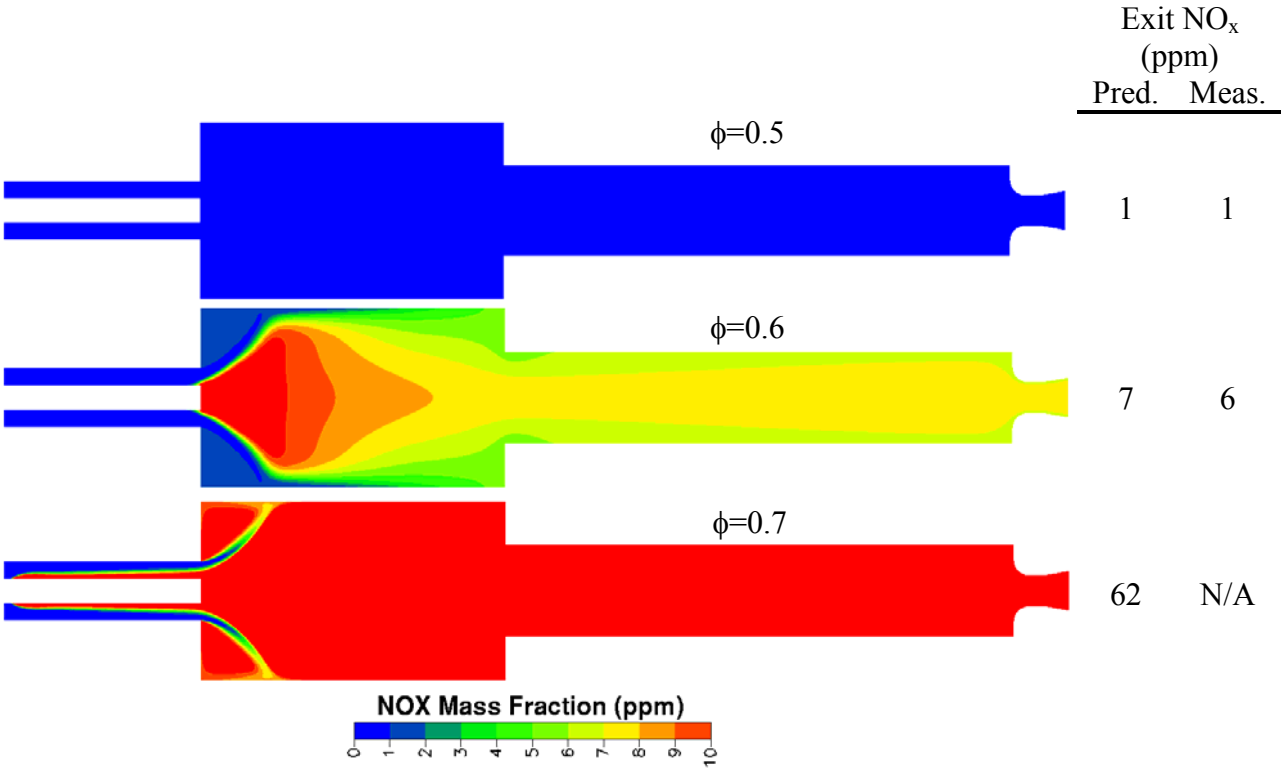

Figure 113. Predictions and Measurements of NO_x Emissions at ϕ=0.5, 0.6, and 0.7 (1650 K Wall Temperatures)

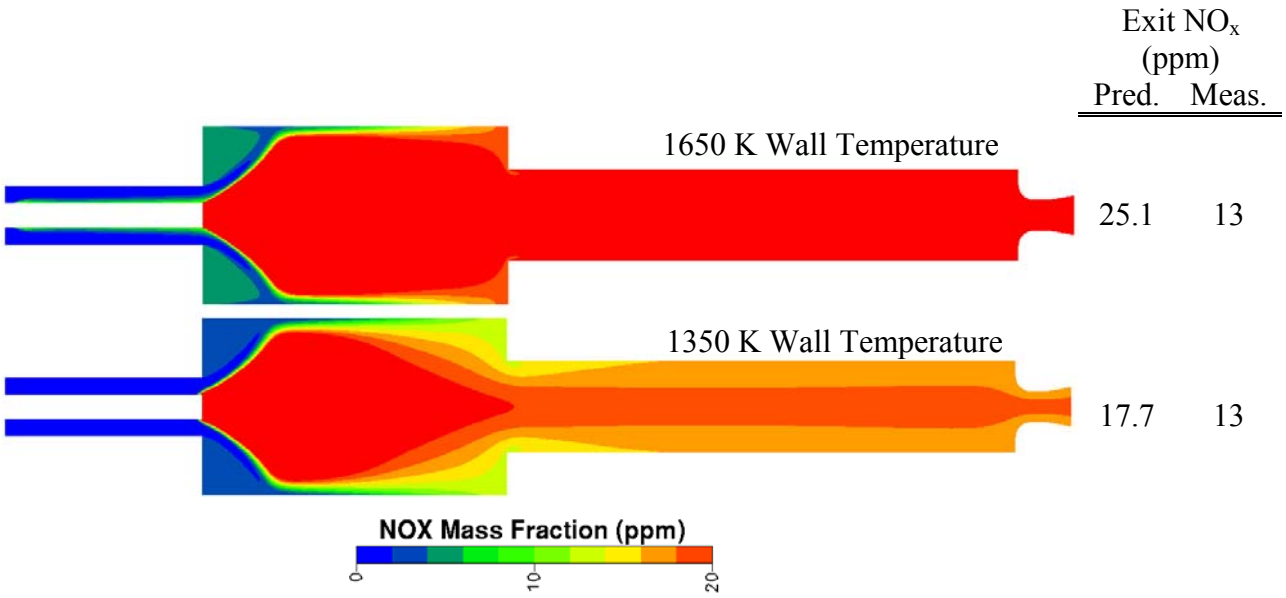

Figure 114. Predictions and Measurements of NO_x Emissions at ϕ=0.65 (1650 vs. 1350 K Combustor Wall Temperatures)

Table 15. Summary of Cases Run

Case #	ϕ	GEOM	TWALL	Wall Grid	TURB	RANS	LES (rms)	NO_x (ppm)	NO_x Data (ppm)	CO (ppm)	CO Data (ppm)	Flash back
1	0.5	2D	1650K	$y^+ > 20$	RNG	√		1	1	2.5	0	N
2	0.6	2D	1650K	$y^+ > 20$	RNG	√		7	6	12	2	N
3	0.7	2D	1650K	$y^+ > 20$	RNG	√		62	~25	41	~10	Y
4	0.65	2D	1650K	$y^+ > 20$	RNG	√		25	13	22	4	N
5	0.65	2D	1350K	$y^+ > 20$	RNG	√		18	13	17	4	N
6	0.7	2D	1650K	$y^+ > 20$	k-ε	√		52	~25	30	~10	N
7	0.65	2D	1650K	$y^+ > 20$	LDKM		(0.2)*	25	13	58	4	Y
8	0.65	2D	1650K	$y^+ \sim 2$	LDKM		(0.9)*	?	13	?	4	Y
9	0.65	2D	1650K	$y^+ > 20$	Smag		(1.2)*	18	13	40	4	N
10	0.7	3D	1650K	$y^+ > 20$	LDKM		(0.4)*	?	~25	?	~10	Y
11	0.6	2D	1650K	$y^+ > 20$	LDKM		?	10	6	30	2	Y

*Dominant frequencies 1200 – 1400 Hertz, function of temperature.

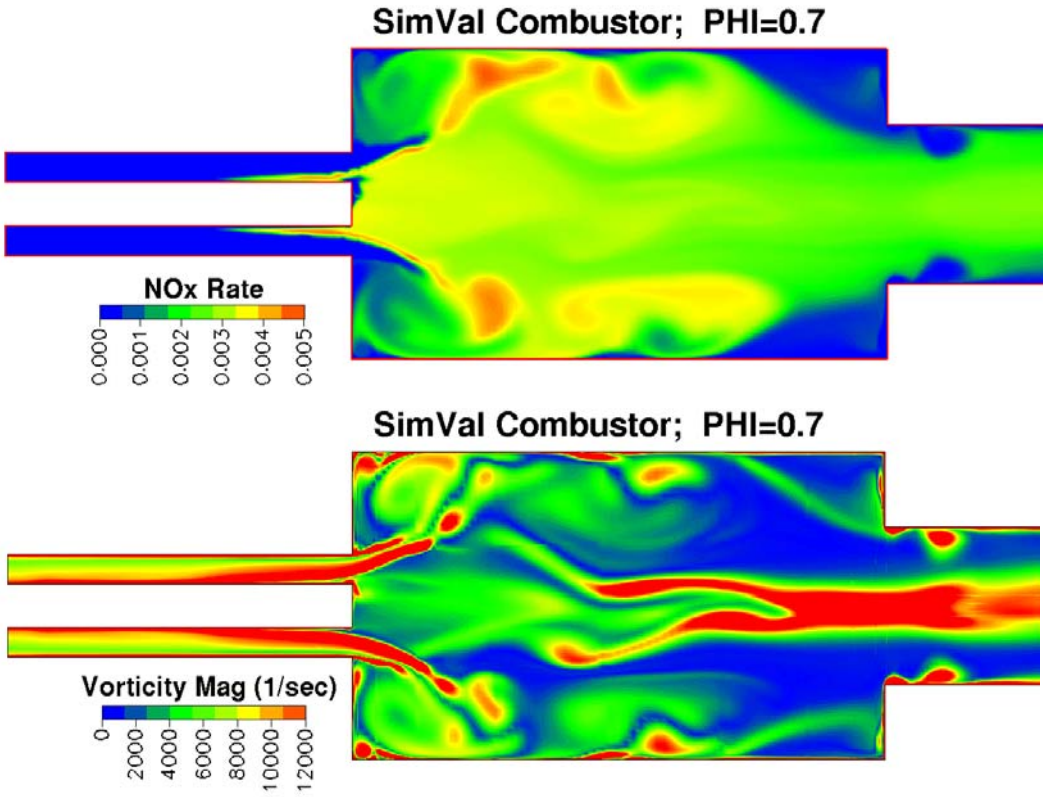

Figure 115. 3D LES Snapshot of Filtered NO_x Source Term and Vorticity Magnitude (ϕ=0.7, LDKM)

CO emissions were also computed and compared to experimental data. These results are shown for RANS in Figure 116. The predicted CO emissions at the combustor exit were very close to equilibrium. The predictions of CO are consistently higher than the measurements. The underpredicted heat loss is one likely reason for the discrepancy. Cases at a ϕ of 0.65 were run with lower combustor wall temperatures and the CO was reduced by 25%, providing better agreement with the data (see Figure 117), but still substantially more than the measurement. It was unclear whether the measurements were in error, or the predictions were in error.

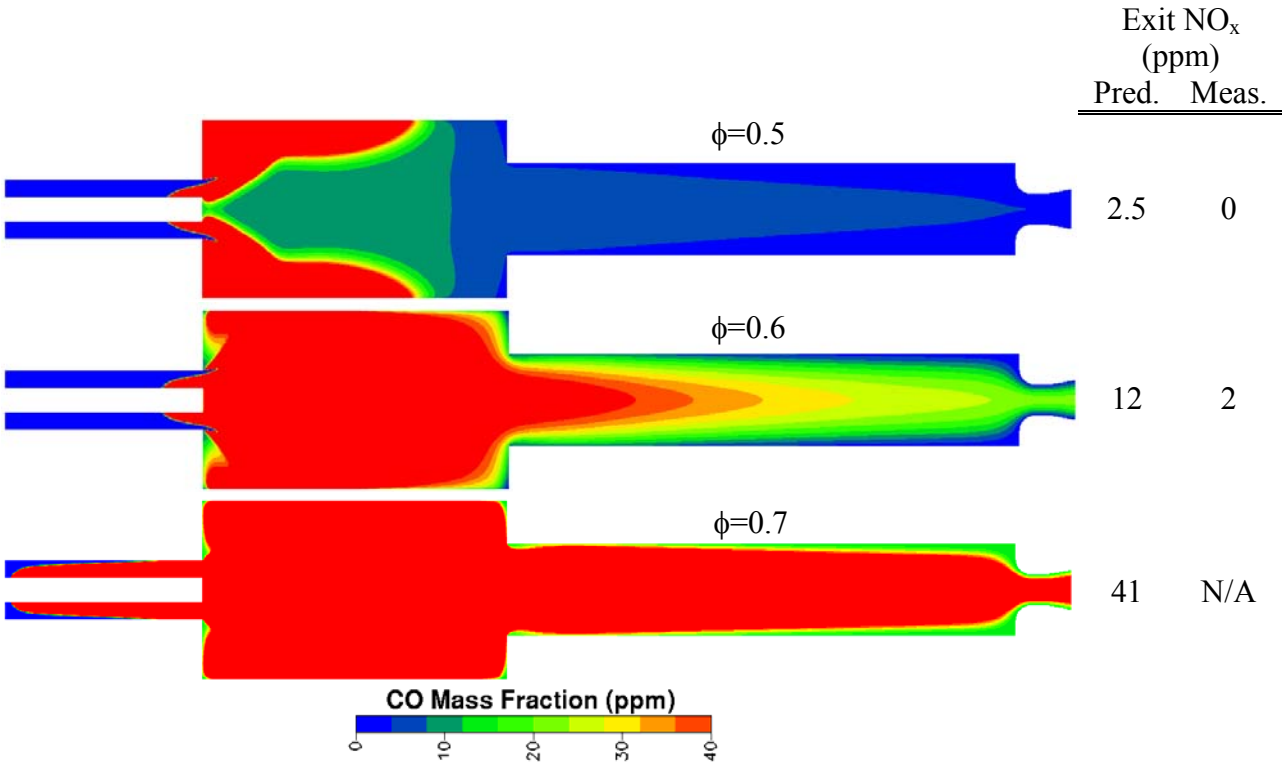

Figure 116. RANS Predictions of CO Emissions (ϕ=0.5, 0.6, and 0.7)

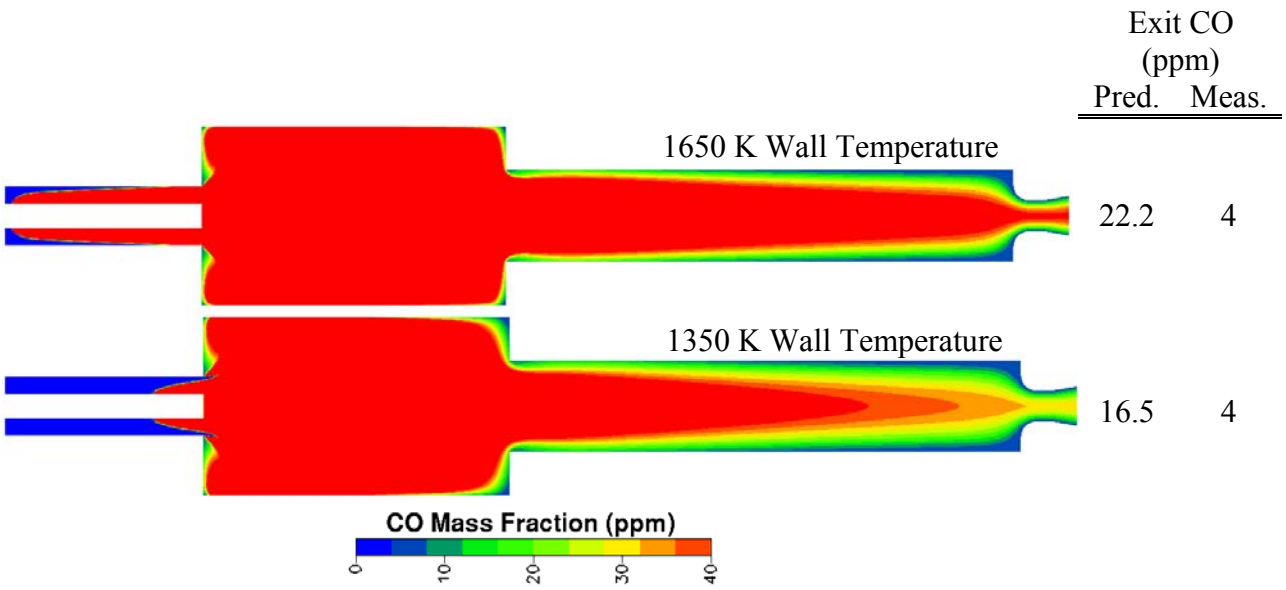

Figure 117. RANS Predictions of CO Emissions (ϕ=0.65 and Twall = 1350 K and 1650 K)

A comparison of measured and predicted dynamic combustor wall pressure was also performed. Figure 118 shows the tabulated results with rms pressure as a function of equivalence ratio. It can be seen that the measured unsteady pressure becomes very large as lean blowout is reached. Also, as the equivalence ratio is varied from 0.59 to 0.61, the combustor becomes very unstable, until finally reaching lower levels of unsteadiness at equivalence ratios higher than 0.67.

The predictions were relatively stable using the LDKM LES model at equivalence ratios of 0.5, 0.6, and 0.7. The 2D LES model did not predict the lean blowout correctly. At ϕ's of 0.6 and 0.7, it is difficult to determine if the model is doing an adequate job or not. Thus, an additional case of ϕ=0.65 was run. Here again, the choice of turbulence model for the LES had an impact on the instability as would be expected. The Smagorinsky model gave the best result, as it predicted rms pressure levels around 1.2 psi. The LDKM produced low levels around 0.2 psi. The LDKM was re-run with a finer grid and rms levels of 0.9 psi were detected. The unsteady RANS results did not produce any measurable level of instability. It is likely that the unsteady RANS is not capable of picking up the high frequencies that are excited in this non-fuel-time-lag system. The excited frequencies were between 1200 and 1400 Hz, depending on combustor temperature. These frequencies correspond to the longitudinal mode of the combustor, and were similar to those frequencies that were measured. Further calculations need to be performed around ϕ=0.6 to determine what is causing the sudden increase and then decrease in combustion instability. It may be that the flame zone shifts closer to the dome as the equivalence ratio is increased to ϕ=0.6, giving high instability levels. Then the flame becomes more distributed along the ID of the injector as the ϕ is further increased above 0.6. This distributed flame in the injector would suppress the coupling of unsteady heat release and acoustics.

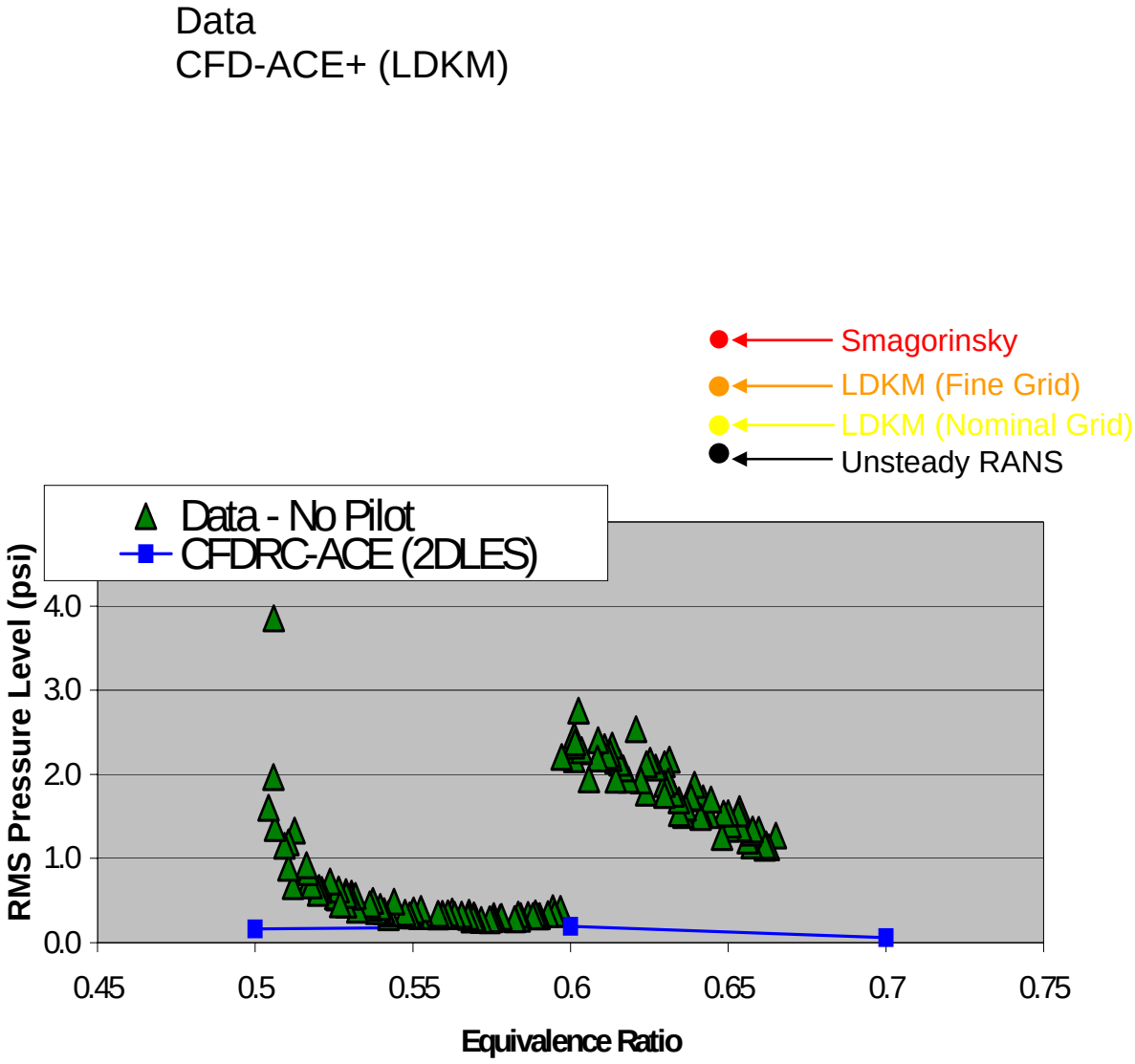

Figure 118. Comparison of Measured and Predicted (2D LES) RMS Pressure Levels in SimVal Combustor

4.4 Year Four: SimVal Analysis

In the fourth year of this project, all of the effort (with limited funding) was focused on performing 3D LES calculations of the SimVal combustor. The first 3D LES calculations were

performed, and the results showed too little heat transfer was predicted in the exhaust duct. This underprediction of heat transfer caused the NOx and CO predictions to be in error compared to the measurements.

In order to better resolve the heat transfer in the exhaust duct, information obtained from a Navy SBIR project was used to modify the near wall grid. Under the Navy Phase I SBIR project, CFDRC studied flow within a heated channel to determine the effects of grid spacing on turbulence and heat transfer. The geometry and grid of the baseline case are shown in Figure 119. The channel was periodic (flow discharging the exit of the domain was input at the inlet of the domain) in both the streamwise and crosswise directions. Walls were located on the top and bottom of the channel. The channel was 3.5 m long, 0.42 m wide, and 0.56 m high. The baseline grid had 100,000 cells, and fully resolved the boundary layers ($y+ < 1$ in first cell). The Reynolds number of this case was 3000 based on channel half height. The top wall was set at a temperature of 400K, and the bottom wall set at a temperature of 300K. DNS data from Debusschere and Rutland (2003) were available for comparison with our LES calculations.

Snapshots of the V-velocity (for reference, the flow velocity was U-velocity) and temperature are shown in Figure 120. The individual eddies are well captured by the LES calculation, in which the Localized Dynamic Kinetic energy Model (LDKM) was used for subgrid turbulence. Comparison of time-averaged axial velocities and temperatures against DNS data are shown in Figure 121 along the channel height. It can be seen that the LES predictions match well with the DNS data. Please note that these calculations fully resolved the boundary layers.

During the course of our study, we uncovered that certain grids, that seemed quite fine, produced purely laminar flows at the same conditions. For instance, if the grid shown in Figure 119 (with a $y+ < 1$) was modified in the x direction only (removing every other grid line), a laminar solution was obtained. To capture the near wall eddies, all near wall grid dimensions (Δx, Δy, and Δz) must be small enough to capture the eddies. This finding means wall cell aspect ratios of 25 or less are required for LES calculations that fully resolve the boundary layer.

Unfortunately, it is unrealistic (in a computational sense) to fully resolve boundary layers in practical LES simulations of more complex geometries (such as the SIMVAL combustor). Instead, LES wall function models are needed, both for velocities and energy, so that grids with $y+ \sim 25$ at the wall can be used. For velocity wall functions, a preliminary version of the Turbulent Boundary Layer Equation (TBLE) outlined by Wang and Moin (2002) was implemented into the LES software, as discussed below.

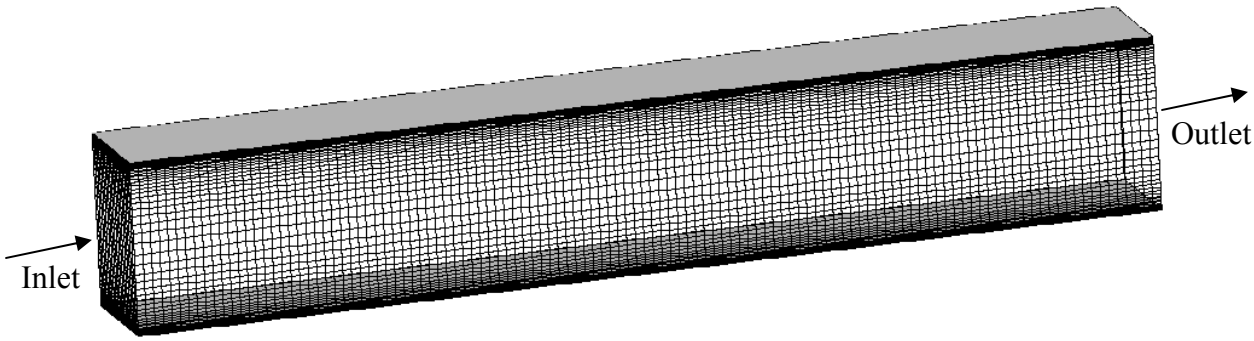

Figure 119. Channel Geometry Showing LES Grid that Fully Resolves Boundary Layers

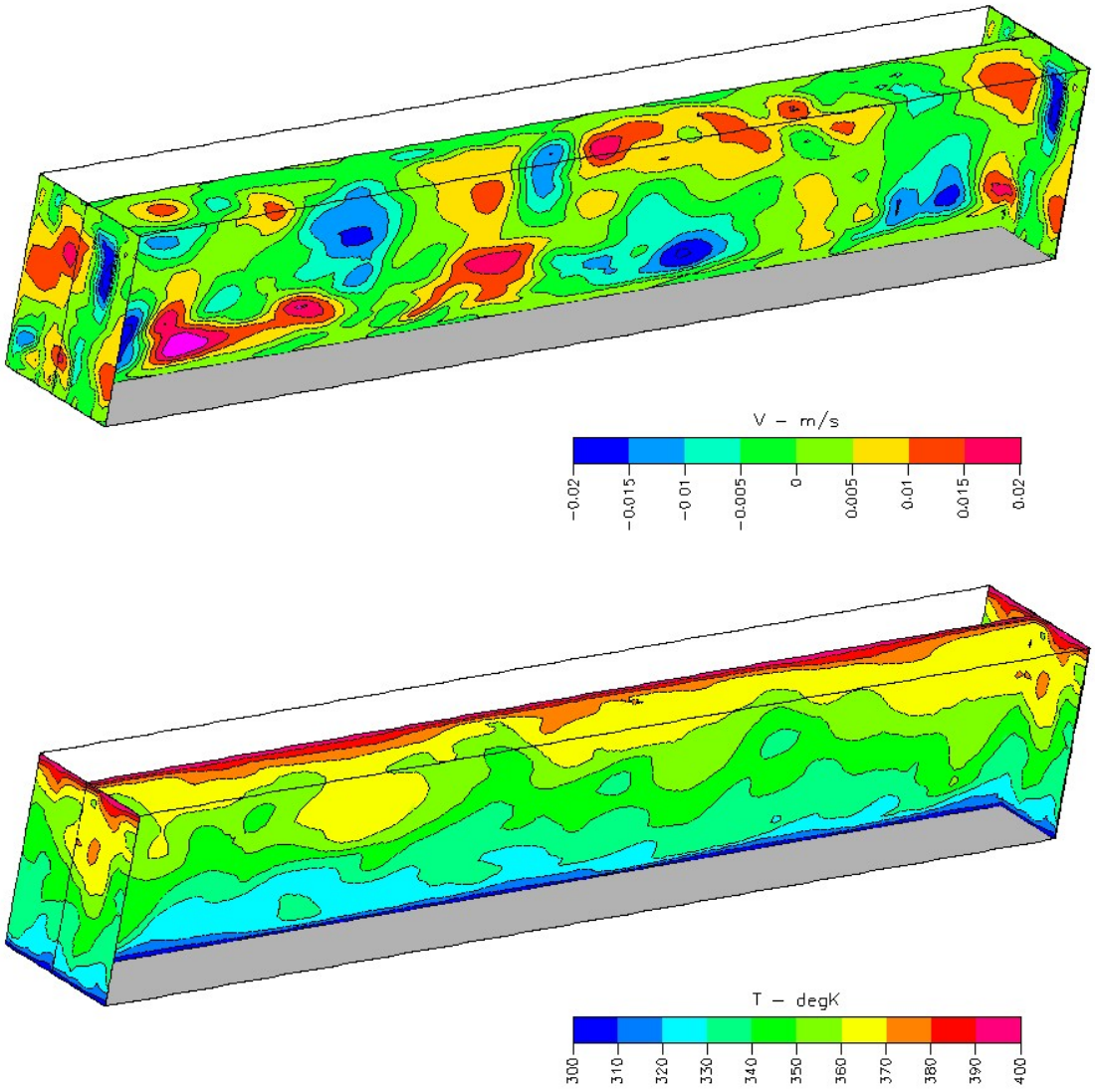

Figure 120. Velocity (Top) and Temperature (Bottom) Snapshot Contours in Thermal Channel Flow Simulation

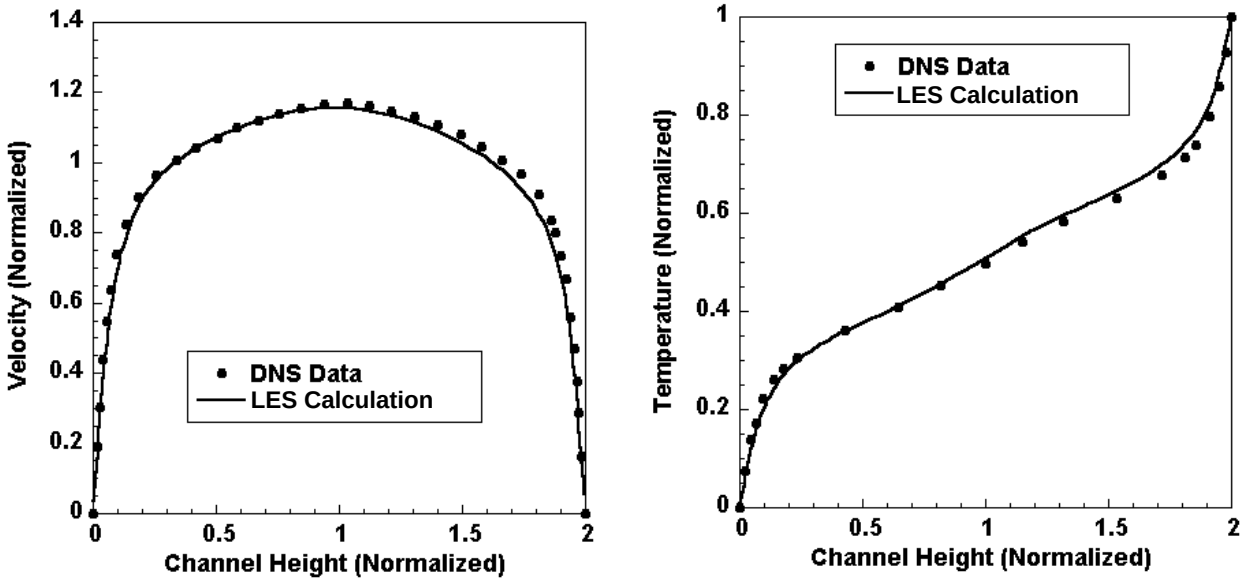

Figure 121. Comparison of Velocity and Temperature Profiles for a LES Calculation (Fully Resolved Boundary Layer) and DNS Data

In the TBLE model, the wall normal velocity is set to zero at the wall and the following equation is solved in the direction of the flow velocity tangential to the wall.

$$\frac{\partial}{\partial x_2}(\nu + \nu_t)\frac{\partial u_i}{\partial x_2} = F_i, \quad F_i = \frac{1}{\rho}\frac{\partial p}{\partial x_i} + \frac{\partial u_i}{\partial t} + \frac{\partial}{\partial x_j}u_i u_j . \tag{33}$$

In Equation 33, the eddy viscosity ν_t can be obtained using one of several mixing-length eddy viscosity models. The following model has been used in the implementation in CFD-ACE+

$$\frac{\nu_t}{\nu} = \kappa y_w^+ \left(1 - e^{-y_w^+/A}\right)^2 . \tag{34}$$

The TBLE equation is solved numerically at each wall cell using a numerical 1-D domain spaced uniformly between the wall the center of the first computational cell. Due to the complexity of solving for and storing the velocity gradients needed to compute the last two terms in Equation 34, a simplified form of the TBLE model is currently being used in CFD-ACE+. The simplified approach drops the time-dependent velocity and velocity gradient terms. The pressure gradient term is still included in the model. Using this assumption, Equation 1 reduces to an ordinary differential equation that can be easily integrated numerically to calculate the wall shear stress. The full TBLE model will be implemented during Phase II of the Navy SBIR Program.

To show the need for improved LES wall functions, additional LES calculations of the thermal channel flow were performed with an y+ of approximately 20. The preliminary TBLE model was used for near-wall velocity, and the highly-inaccurate Reynolds analogy was used for near-wall energy. LES predictions for velocity and temperature across the channel height are compared

with the DNS data in Figure 122. It can be seen that improvements are needed, and will be addressed in Phase II of the Navy SBIR.

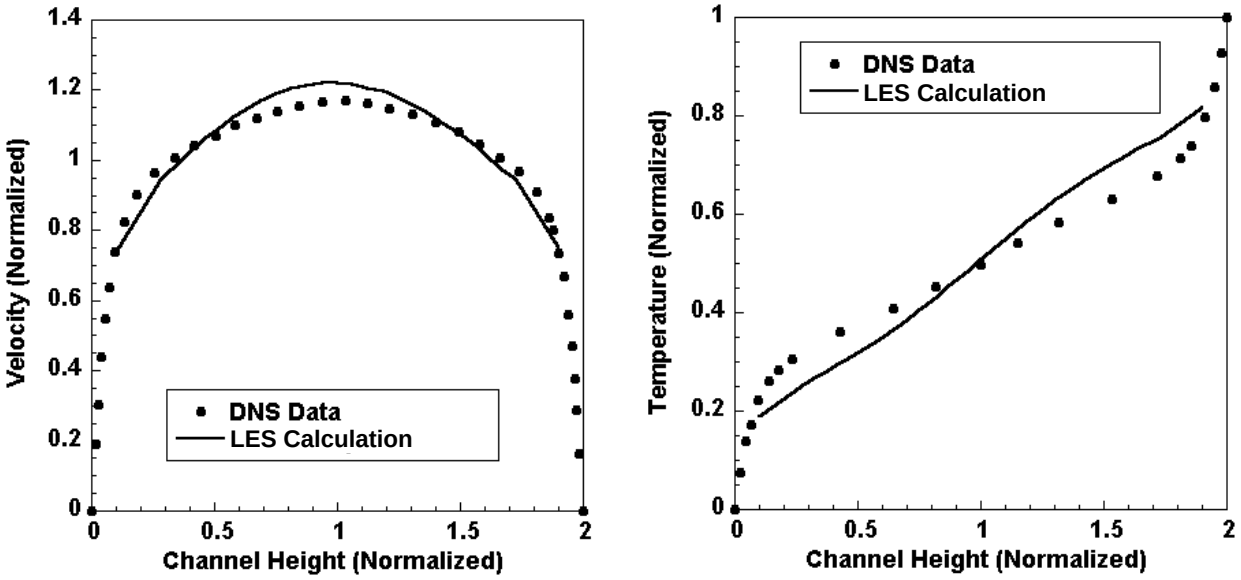

Figure 122. Comparison of Velocity and Temperature Profiles for LES (Wall Function Treatment) Versus DNS Data

The grid of the SIMVAL case was assessed, and it was found that the near wall grid had aspect ratios ($\Delta x/\Delta y$) greater than 25. Thus, although the near wall y grid dimensions produced a y+ of 1, the grid was too coarse in the axial direction, causing the flow to laminarize next to the wall. Rather than making the grid finer in the axial direction (and fully resolving the boundary layer), we made the grid coarser in the radial (y) dimension, thus producing a grid with y+ around 20, and keeping the near wall aspect ratios around 1-2. We used LES wall functions for velocity and energy as described previously (recognizing their inadequacies that will be addressed in the future). Snapshots of temperature of the LES calculation **(see Figures 123 and 124) show the improvement in the predictions now that vortices near the wall are being captured. Note the vortices captured at the entrance to the exhaust duct and extending downstream. For comparison, a temperature snapshot of an earlier calculation is also shown in Figure 123**, and the lack of vortices in the exhaust duct is evident for the earlier calculation.

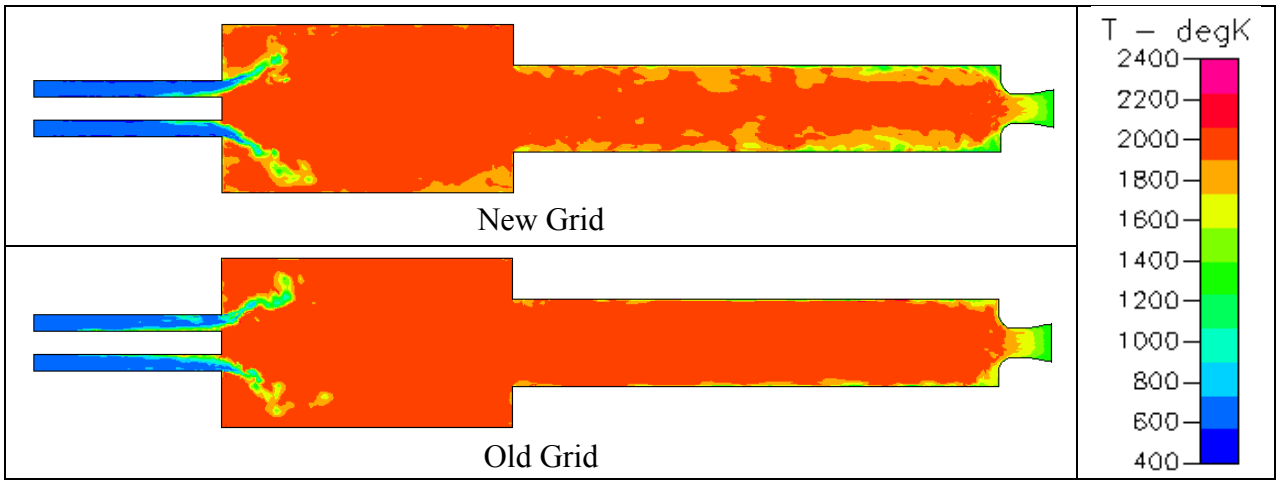

Figure 123. LES Temperature Snapshots

4.4.1 Final 3D LES SIMVAL Calculations

Many preliminary 3D LES cases of the SIMVAL experiment were run. However, only the final cases will be reported here. The final two cases had ϕ's of 0.625 and 0.55, with an inlet temperature of 600°k and a combustor pressure of approximately 75 psia. Most of the analysis will focus of the ϕ of 0.625 case.

Snapshots of u-velocity and temperature are shown in Figure 124 for the ϕ of 0.625 case. The snapshots show small features and flow unsteadiness, including vortices in the shear layers and vortices next to the wall in the exhaust duct. Comparison of time-averaged LES velocity predictions (u-velocity and w-velocity) and RANS velocity predictions are presented in Figure 125. It is evident that the LES-predicted flowfield is dramatically different than the RANS-predicted flowfield. RANS predicts a large, central recirculation zone on the centerline, while LES predicts positive axial velocity on the centerline and an annular recirculation zone. The LES solution also has distinct differences in the exhaust duct, including a lower velocity on the centerline than the RANS solution. The swirl velocity in LES is much higher in the premix passage than the RANS swirl velocity (although both solutions have the same inlet swirl velocity). The swirl velocity in LES is also much higher in the combustor, entering the exhaust duct, and in the exhaust duct.

Figure 126 presents comparison of temperature and NO_x contours for RANS and time-averaged LES. The average temperatures are nearly the same, although the LES calculation shows some flame on the inner diameter of the centerbody (premix passage exit), while the RANS calculation does not. The NO_x comparisons show a dramatic difference between LES and RANS, caused by the difference in residence times. The RANS solution predicts most of the NO_x is formed in the central recirculation zone of the combustor, and little NO_x is formed in the exhaust duct. In contrast, LES predicts little NO_x formed in the combustor, and a substantial amount of NO_x formed in the exhaust duct. Overall, the LES NO_x at the exhaust exit was 9.5 ppm, while the RANS NO_x was 7.0 ppm. Comparison to SIMVAL measurements, presented in Figure 127, shows the LES predictions to be in better agreement with the measurements. These SIMVAL measurements were taken June, 2004.

Predictions of combustion dynamics are shown in Figure 128 for the two equivalence ratio cases. LES predicts a relatively quite flame, and two dominant frequencies: 400 Hertz and 1300 Hertz. The predicted rms pressure levels are lower than the measurements (see Figure 129). Longer run times may be required in the LES calculations.

A number of animations of the ϕ of 0.625 case was performed. The starting frames of these animations are shown in Figures 130, 131, and 132. These animations will be useful in demonstrating and understanding the unsteadiness of the flowfield.

In addition to modeling the SIMVAL experiment, two additional cases were analyzed to help understand the different turbulent, swirling flowfields being predicted by RANS and LES. The experiment of Lilley, 1985, was analyzed. The Lilley geometry was very similar to the DOE SIMVAL geometry, including an annular swirler, a centerbody, a dump combustor, and constriction downstream of the combustor. Figure 133 shows the Lilley experimental setup. The cases selected for analysis had 45 degrees swirlers, a dump ratio (d/D) of 2.0, a combustor length of 2D, and a contraction nozzle with an area ratio of four. Two other swirl cases were experimentally tested: zero degrees and 70 degrees. Artistic impressions of dividing streamlines with and without contraction nozzle are shown in Figure 135 (from Lilley, 1985). It can be seen that the contraction nozzle had a strong effect on the centerline recirculation zone, resulting in an annular recirculation zone and positive axial velocity on the centerline.

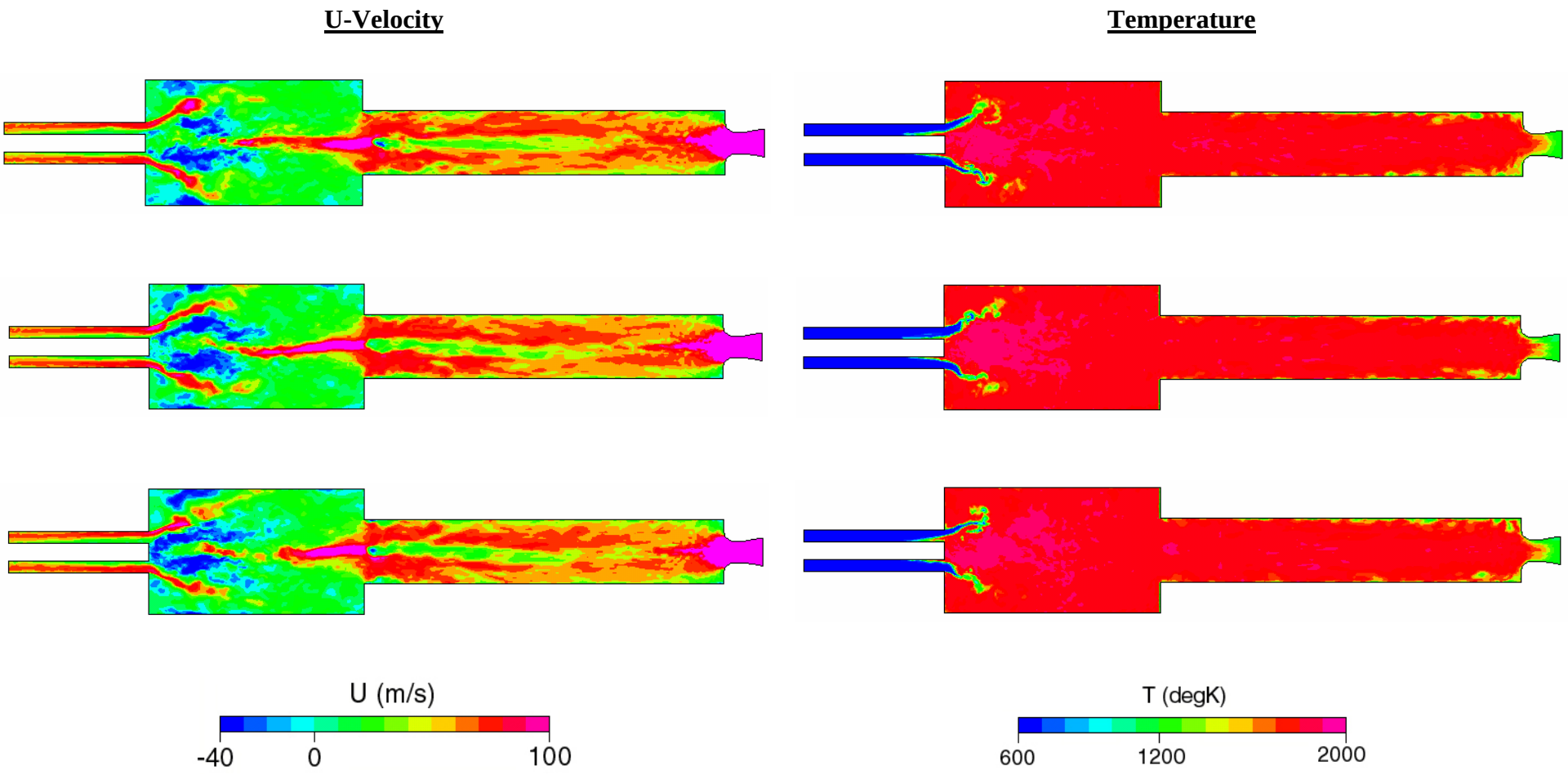

$\phi = 0.625, \quad T_3 = 600\ \text{K}, \quad P_3 \approx 75\ \text{psia}$

Figure 124. Velocity and Temperature Snapshots from Final 3D LES Results

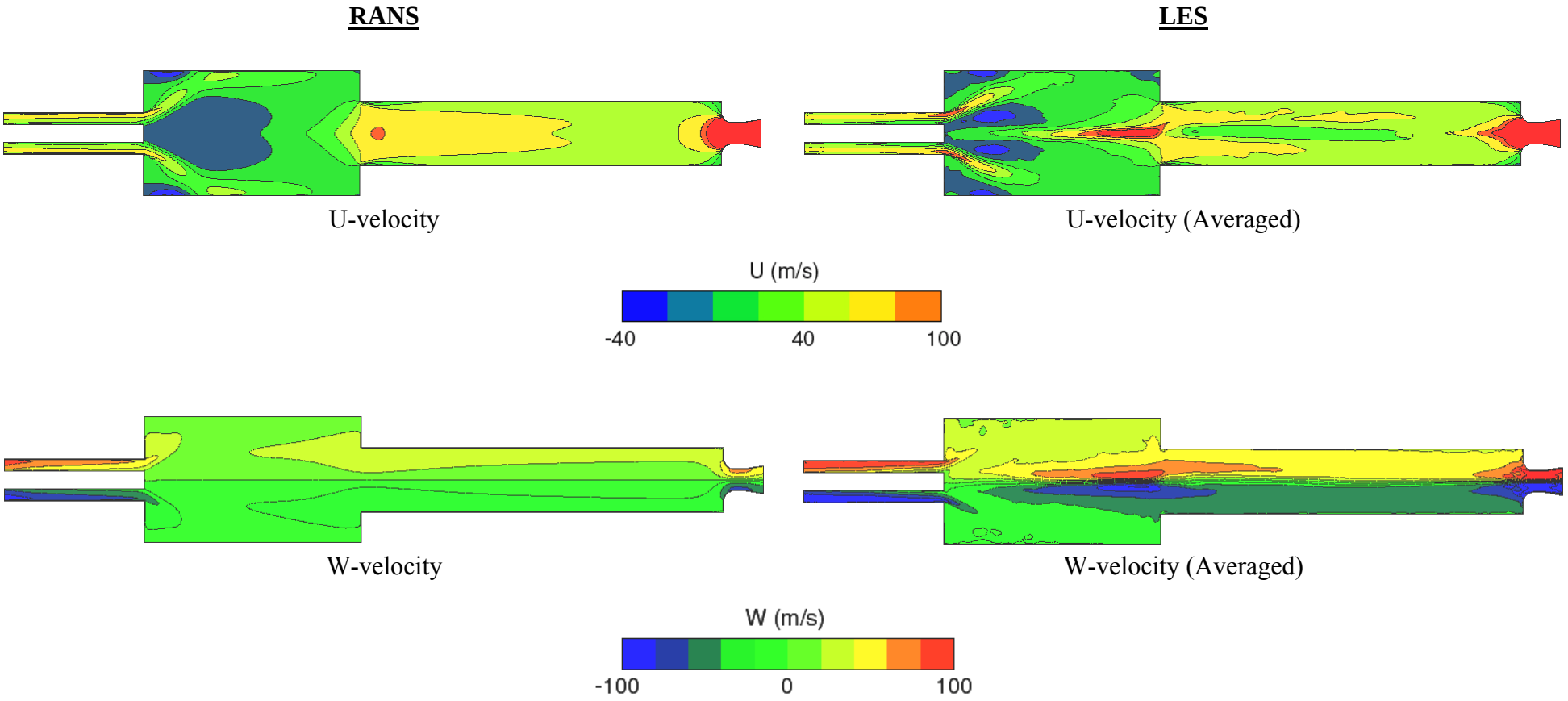

Figure 125. Comparison of Velocity Predictions for RANS and LES

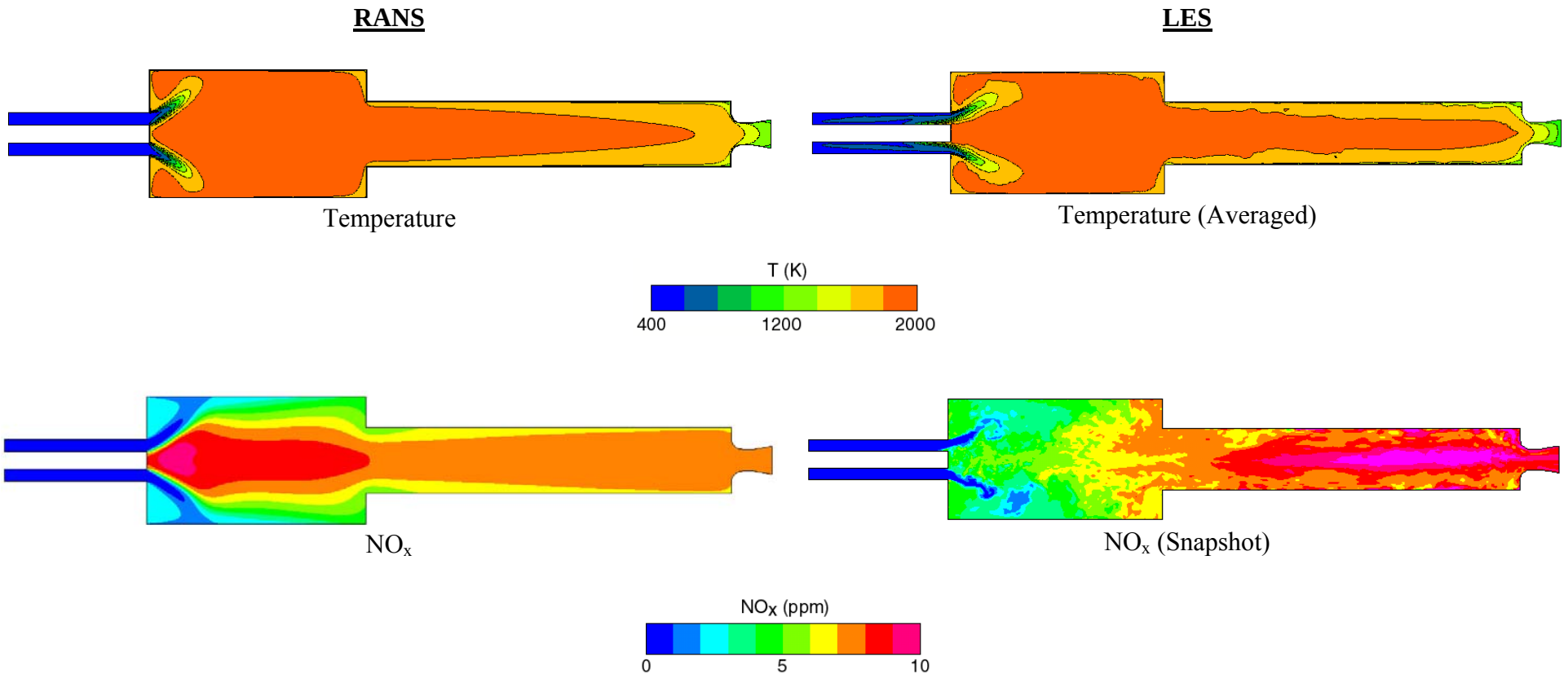

Figure 126. Comparison of Temperature and NO_x Predictions for RANS and LES

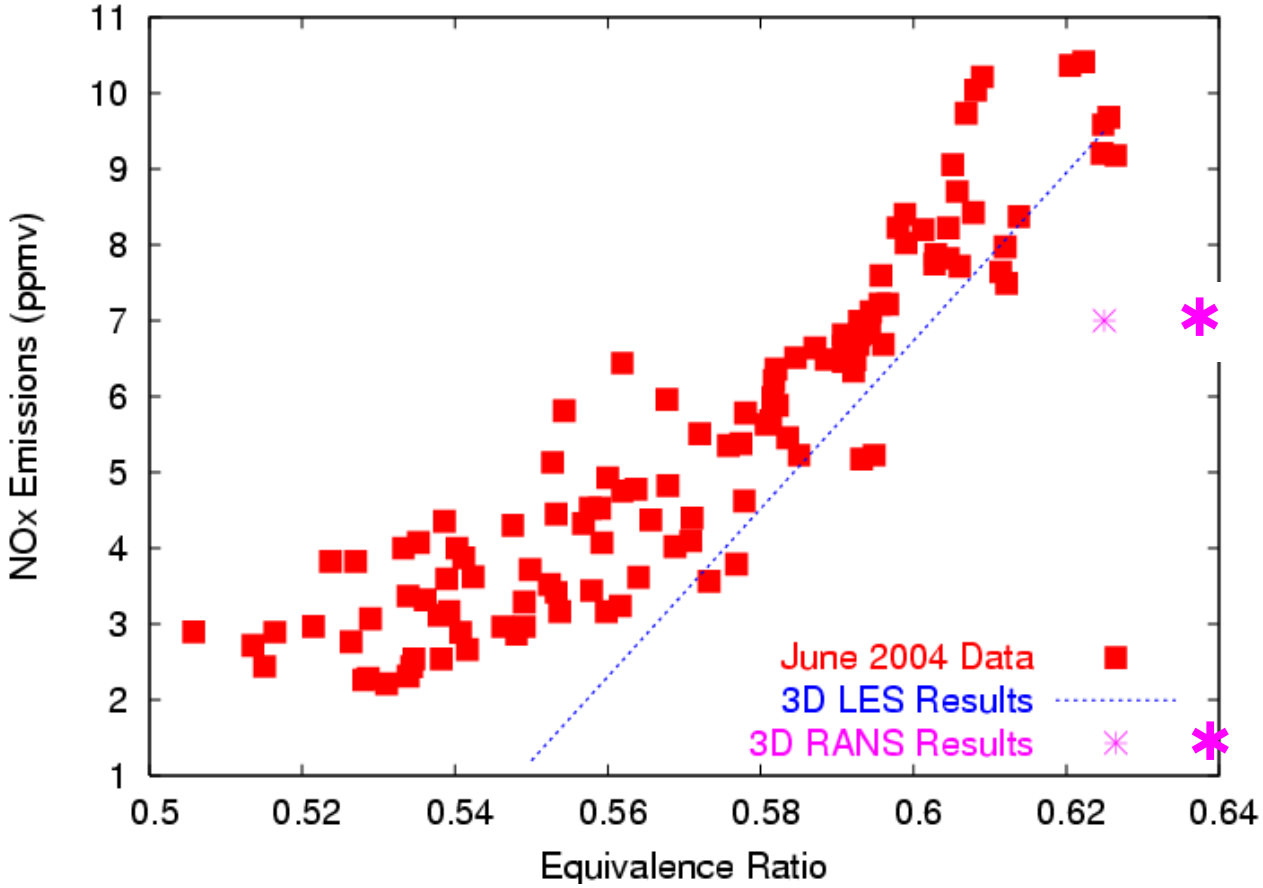

Figure 127. Comparison of NO_x Predictions with SIMVAL Measurements

ϕ = 0.55

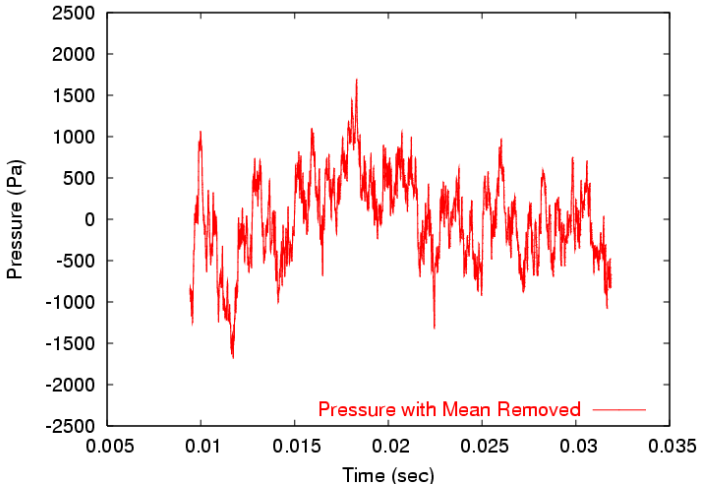

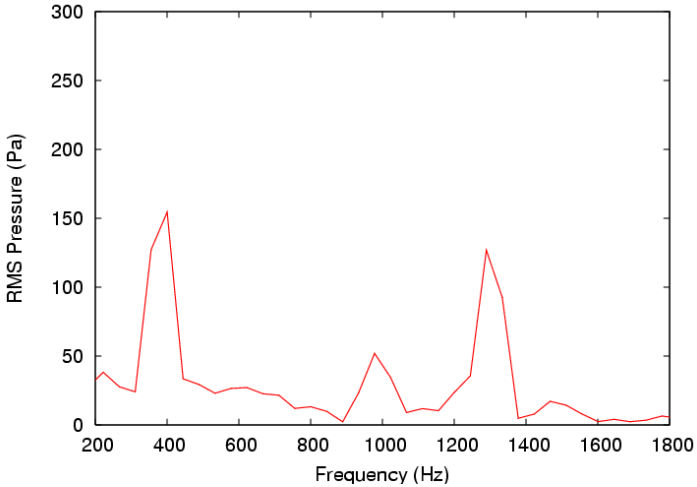

Pressure (Pa) Trace

RMS Pressure (Pa)

ϕ = 0.625

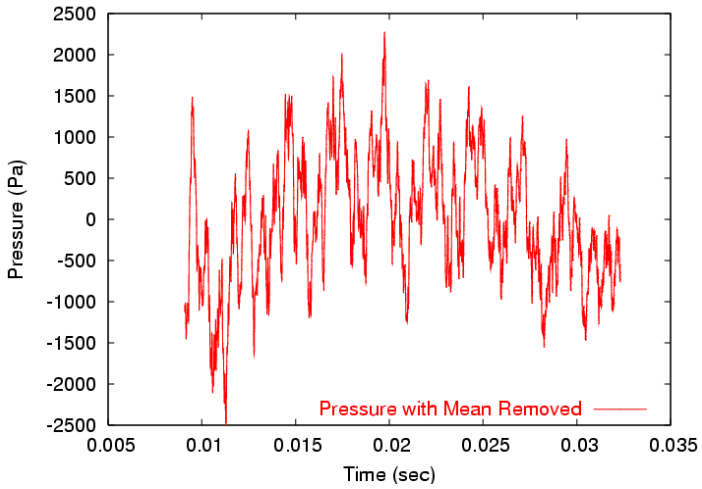

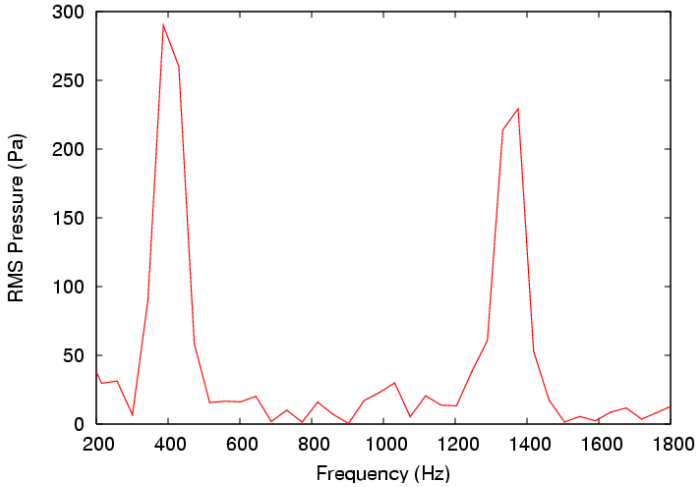

Figure 128. Predicted LES Combustion Dynamics

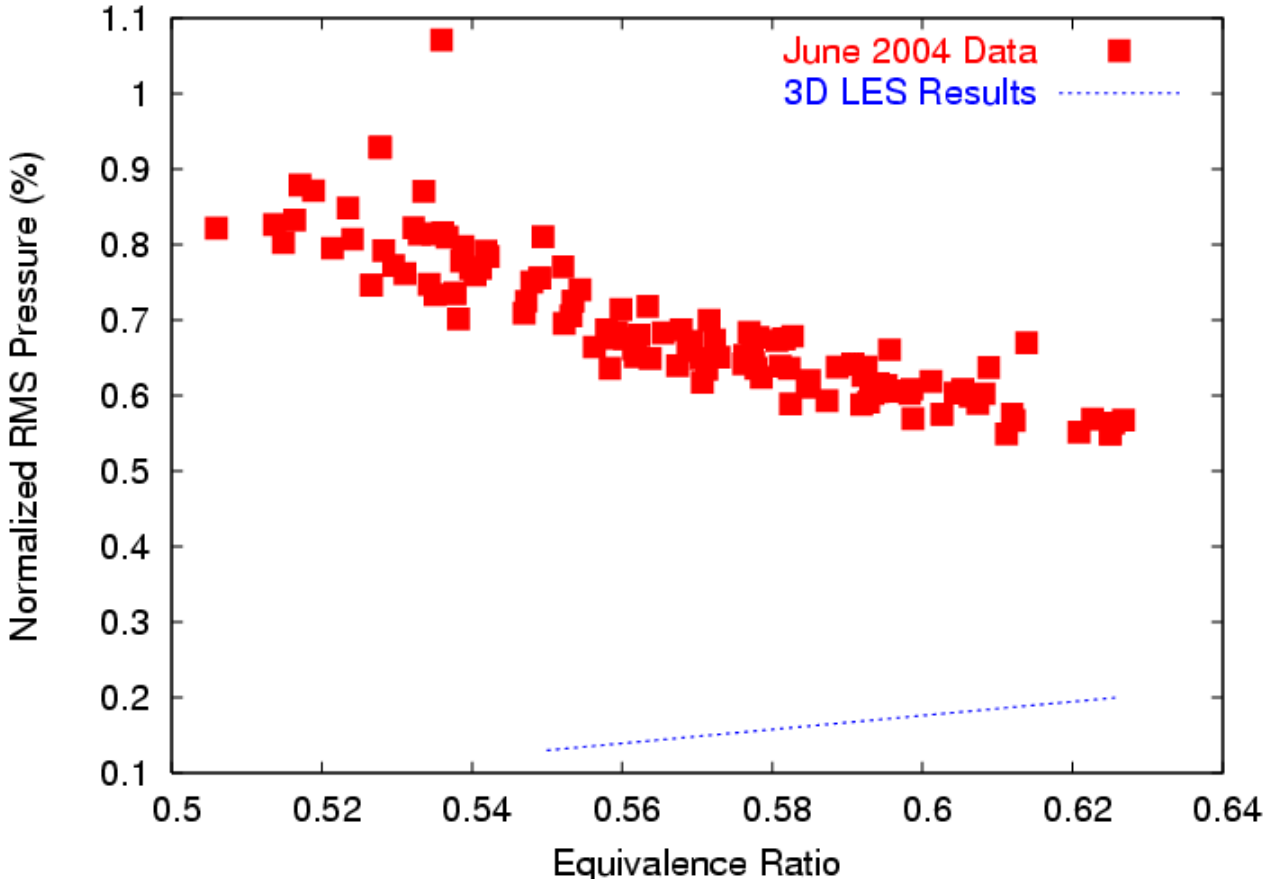

Figure 129. Comparison of Predicted LES Combustion Dynamics with SIMVAL Measurements

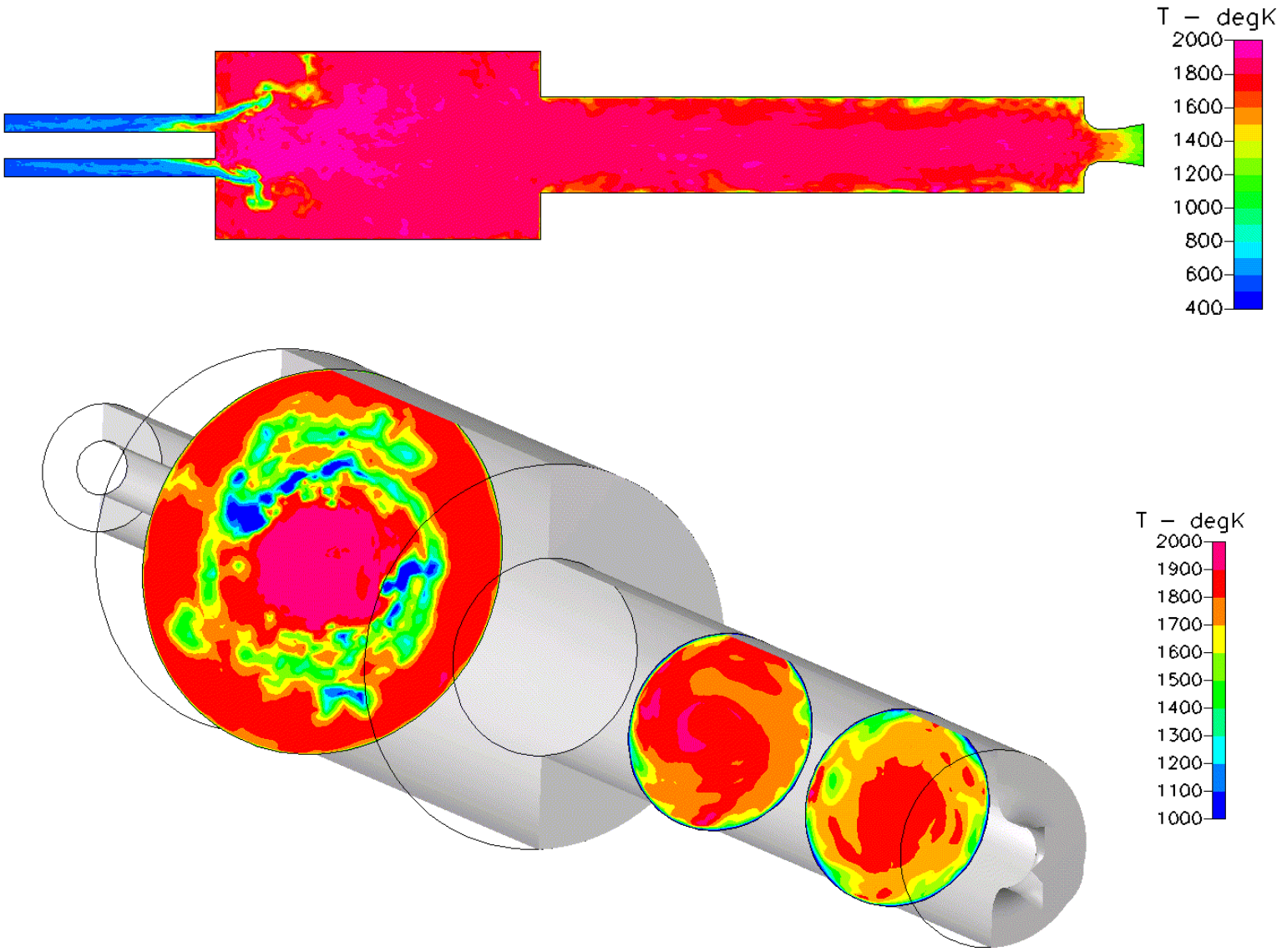

Figure 130. Initial Snapshots of Temperature Animations

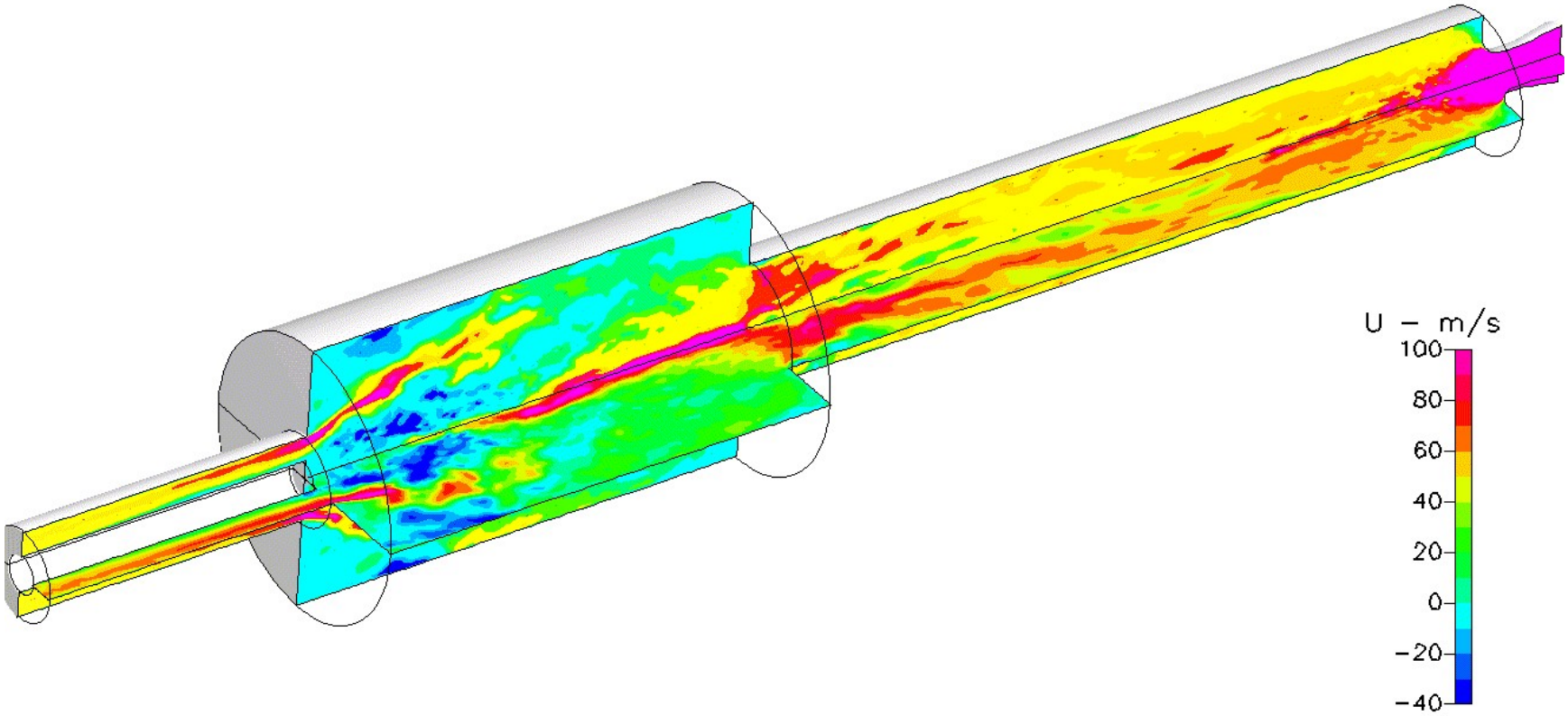

Figure 131. Initial Snapshots of Velocity Animations

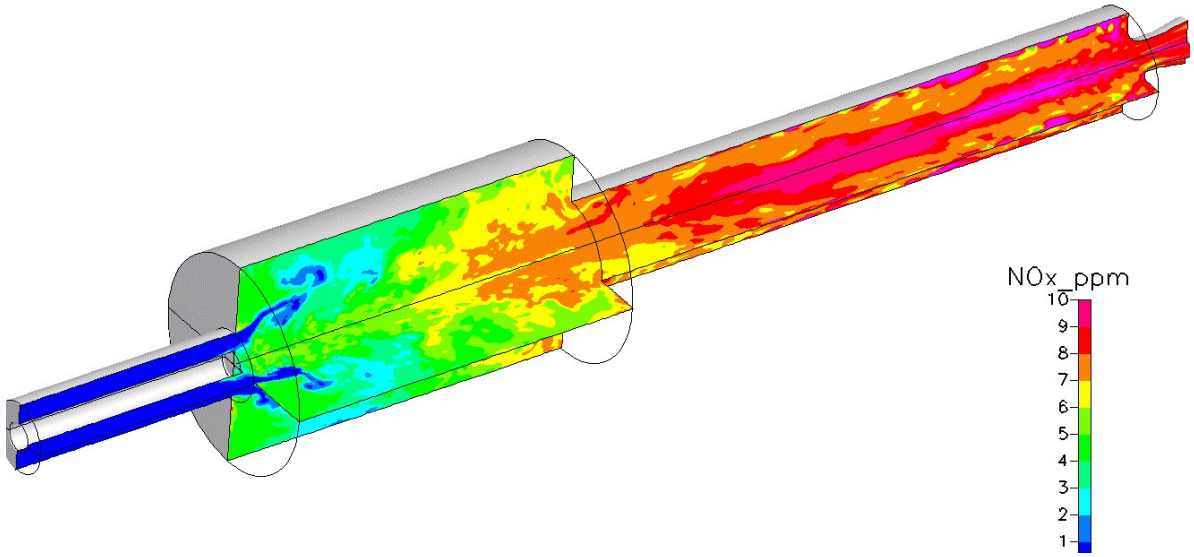

Figure 132. Initial Snapshots of NO_x Animations

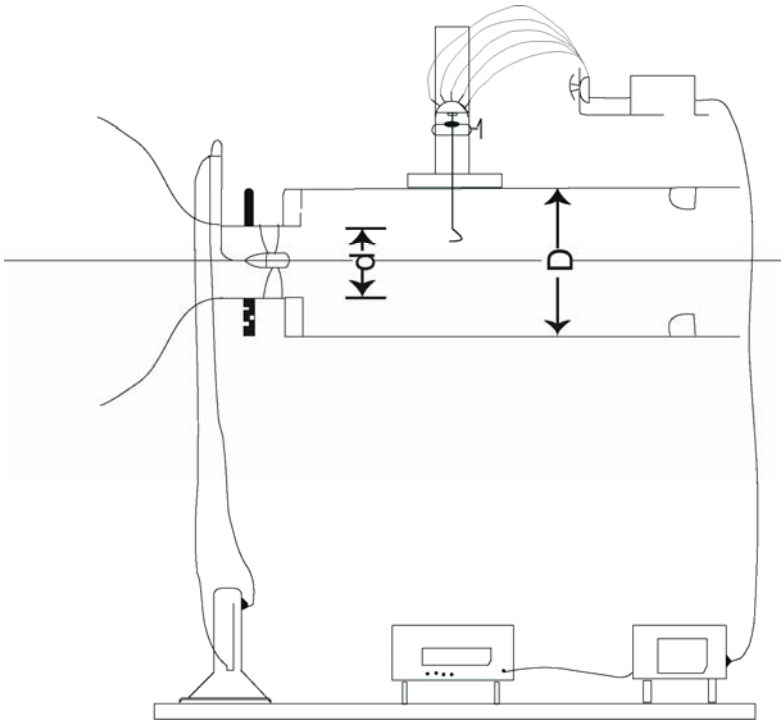

Figure 133. Lilley's Experimental Setup; Flow from Left to Right

The 45 degree swirler cases with and without contraction nozzle were analyzed using RANS and LES. The predictions are shown in Figure 127, and comparisons of measurements and predictions of axial and swirl velocities at different axial locations (X/D=0.0, 0.5, 1.0, and 1.5) are shown in Figure 135. It can be seen that LES captures the annular recirculation zone for the contraction nozzle case, while RANS does not. This is a very important finding, and shows the need of developing LES codes for improved mixing predictions.

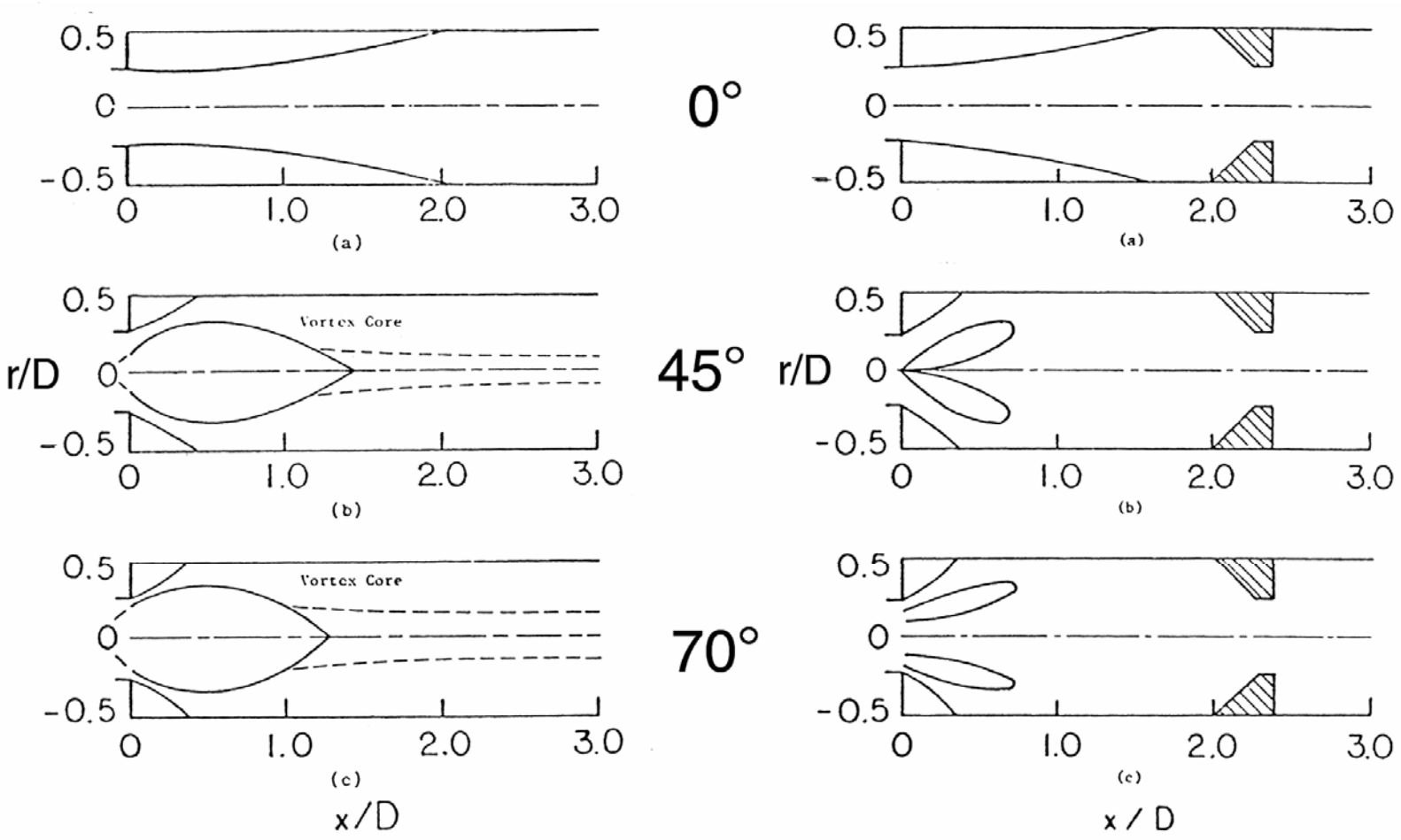

Figure 134. Artistic Impression of Dividing Streamlines from Lilley Experiment

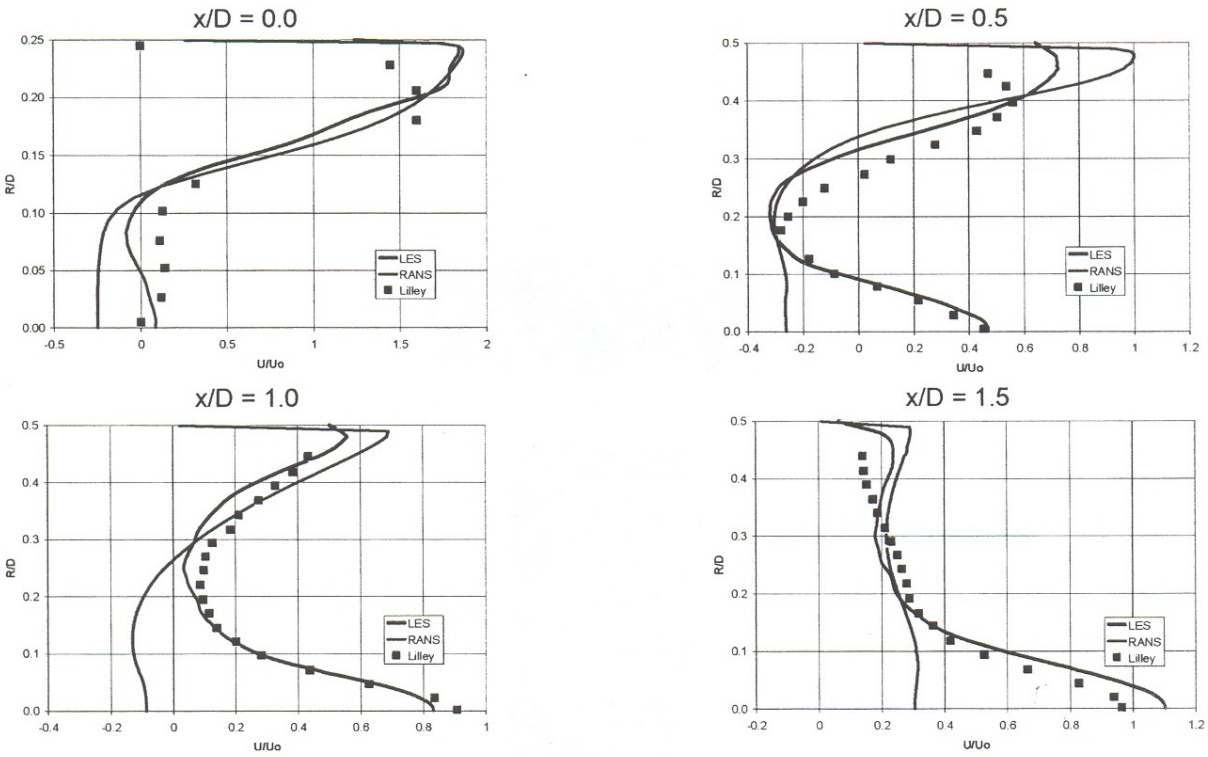

(a) Axial Velocity Comparison

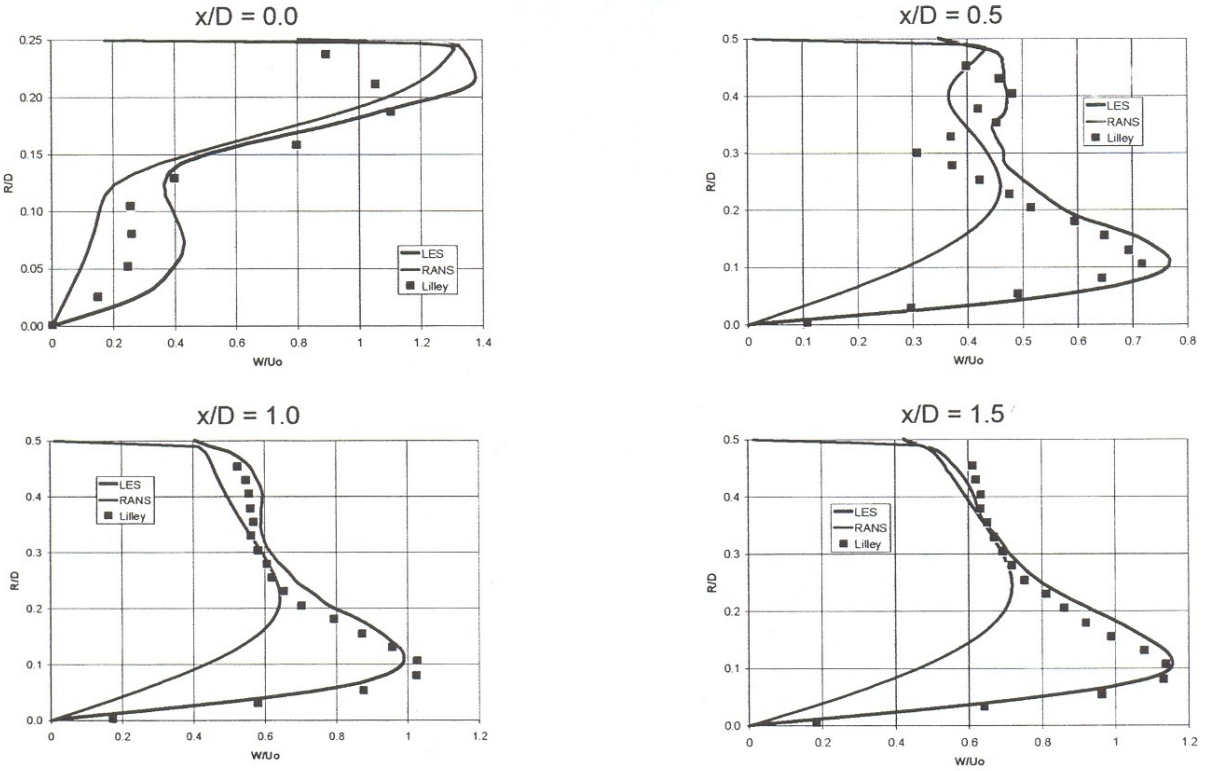

(b) Swirl Velocity Comparison

Figure 135. Comparison of Axial and Swirl Velocities to Lilley's Experiment

5. CONCLUSIONS

This four-year project focused on developing combustion Large Eddy Simulation (LES) software to aid the design of low emissions combustion system for Vision 21 plants. The latest physical subgrid models were incorporated into a commercial LES code, and extensive validation was performed. The time accurate LES methodology was shown to give superior (i.e. more accurate) prediction capability compared to conventional steady Reynolds Averaged Navier Stokes (RANS) codes, mainly due to the improvement in turbulent mixing predictions with LES. LES was also able to predict transient events (e.g. instability, lean blowout, flashback, ignition, etc.) that RANS could not. The improvement in prediction capability with LES comes at a cost: LES calculations take about ten times longer to run than RANS calculations. Code improvements, such as higher order differencing schemes on unstructured meshes and adaptive mesh refinement, need to be implemented that can reduce run times by an order of magnitude. In addition, computer speeds will continue to get faster (i.e. typically chip speeds double every 18 months). Thus, in the next ten years, LES will become viable as a real (i.e. practical) engineering design tool.

Many lessons were learned during the duration of this project. Some may be controversial, but they are still our beliefs at CFDRC.

1. The Linear Eddy Mixing (LEM) model for turbulent chemistry is very accurate, but too expensive. It is our belief that simpler turbulent combustion models are needed. We have proposed a two-variable, multi-step assumed pdf model as alternative, and are developing this model under a Navy Phase II SBIR project.

2. Chemistry using J.Y. Chen's mechanisms are very accurate, but are too expensive even with ISAT. It is our belief that the chemistry can be simulated using 5-10 step mechanisms with Arrhenius rates, tuned to the conditions of interest. We are currently developing a chemical reactor modeling (CRM) tool that automatically calculates global mechanisms using a detailed chemical mechanism as a starting point. Multiple reactor options are available, including perfectly stirred and/or plugged flow reactors, laminar 1D flame profiles, and opposed diffusion flame.

3. Near-wall models (both velocity and thermal) are needed for practical LES calculations (resolution down to the wall is not practical). CFDRC is developing such models in a Navy Phase II SBIR project.

4. Automatic load balancing is a necessary future in LES calculation with massive parallelization. Parallel division based on number of cells per processor result in significant under usage of certain processors because of stiff kinetics and/or spray.

5. Data storage and processing of data is a large issue. The generation of movies tends to be difficult because large files of data must be manipulated.

6. Pre- and post-processing is a large issue as grids continue to get larger. Parallelization and distributed architecture is needed for pre- and post-processing software.

This project also enabled the transfer of the LES technology to combustor designers. This was accomplished through an industrial/university/government combustion LES consortium. Three meetings were held during the course of the project and over 20 combustion organizations attended at least one of the meetings. Six consortium members were trained and tested a beta version of the software in the third year of the project. The beta testing was mainly unsuccessful because 1) there were many computer platform related issues; 2) inexperienced users; and 3) the immaturity of the code. Still, the beta testing helped in the development process of the LES software, and introduced the virtues and pitfalls of LES to the combustion community.

There is still a need to continue developing combustion LES technology. The current version of our LES software (January 2005) is vastly improved compared to the beta version of 2003. The time needed to develop a practical version LES tool was greatly underestimated in this project. Still, great progress was made, and future projects promise to fill many of the modeling gaps uncovered.

6. REFERENCES

Avva, R.K. and Sundaram, S. (1998), "Large Eddy Simulation of Incompressible Flows Using a Finite Volume Approach," AIAA-98-0539.

Bardina, J., Ferziger, J.H., Reynolds, W.C., (1980), "Improved Subgrid Model for Large-Eddy Simulation," AIAA Paper 80-1357.

Bilger, R. W. (1993), "Conditional moment closure for turbulent reacting flows," Phys. Fluids A., 5, 436-444.

Blasco, J.A., Fueyo, N., Dopazo, C., and Ballester, J. (1998), "Modeling the Temporal Evolution of a Reduced Combustion Chemical System With an Artificial Neural Network," Combustion and Flame, 113:38-52.

Bowman, C.T., Hanson, R.K., Davidson, D.F., Gardner, W.C., Lissianski, V., Smith, G.P., Golden, D.M., Frenklach, M., Goldenberg, M., (1996), http://www.me.berkeley.edu/gri_mech/.

Bushe, K. & Steiner, H. (1999), "Conditional moment closure for large eddy simulation of non-premixed turbulent reacting flows," Phys. Fluids., 11, 1896-1906 .

Brodkey, R. S., (1981), "Fundamentals of Turbulent Motion," Chem. Eng. Comm. 8, 1-23.

R.W. (1997), "Comprehensive Model for Lean Premixed Combustion in Industrial Gas Turbines-Part I. Validation," Western States Section/The Combustion Institute, Livermore, California, April 14-15.

Cannon, S.M., Zuo, B.F., and Smith, C.E., (2003), "LES Prediction of Combustor Emissions from a Practical Industrial Fuel Injector," GT-2003-38200, Proceedings of ASME Turbo Expo 2003, Atlanta, GA, June 16-19.

Cannon, S.M., McDaniel, K.S., and Smith, C.E., (2001), "Sensitivity Analysis of Combustion Dynamics Using Time-Accurate CFD Modeling," AIAA-2001-3971, 37th AIAA/ASME/SAE/ASEE Joint Propulsion Meeting & Exhibit, Salt Lake City, UT.

Cannon, S.M, Adumitroaie, V., Smith, C.E. and Sekar, B., (2001), "3D LES Modeling of Combustion Dynamics in Lean Premixed Combustors," To be presented at the *ASME Turbo Expo 2001*, New Orleans, LA, June 4-7.

Cannon, S.M., Smith, C.E., and Lovett, J., (2000), "LES Modeling of Combustion Dynamics in a Liquid-Fueled Flametube Combustor," AIAA-2000-3126, presented at the 36th AIAA/ASME/SAE/ASEE Joint Propulsion Conference and Exhibit, Huntsville, AL.

Cannon, S.M., Brewster, B.S., and Smoot, L.D. (1999), "PDF Modeling of Lean Premixed Combustion Using In-Situ Tabulated Chemistry," *Combustion and Flame,* vol. 119, pp. 233-252.

Cannon, S.M., Brewster, B.S., and Smoot, L.D. (1998), "Stochastic Modeling of CO and NO in Premixed Methane Combustion," *Combustion and Flame*, vol. 113, ppp. 135-146.

Cannon, S.M., (1997), "Modeling of Lean Premixed Gaseous Turbulent Combustion," Dissertation Brigham Young University.

Cannon, S.M., Brewster, B.S., Smoot, L.D., Murray, R. and Hedman, P.O. (1997), "Comprehensive Model for Lean Premixed Combustion in Industrial Gas Turbines - Part I. Validation," WSS/CI- 97S-041, Spring 1997 Meeting of the Western States Section/The Combustion Institute, Livermore, CA.

Ciofalo, M., (1994), "Large-Eddy Simulation: A Critical Survey of Models and Applications," Adv. in Heat Transfer, vol. 25, 321-419.

Chen, J.-Y. (1997), "Development of Reduced Mechanisms for Numerical Modeling of Turbulent Combustion," Workshop on Numerical Aspects of Reduction in Chemical Kinetics, CERMICS-ENPC Cite Descartes - Champus sur Marne, France, September, 2.

Chen, J.-Y. (1988), "A General Procedure for Constructing Reduced Reaction Mechanisms with Given Independent Relations," Combustion Science and Technology, Vol. 57, pp. 89-94.

Christo, F.C., Masri, A.R., Nebot, E.M., and Pope, S.B. (1996), "An Integrated PDF/Neural Network Approach for Simulating Turbulent Reacting Systems," 26th Symposium (International) on Combustion/The Combustion Institute, pp. 43-48.

Collins, M.W. and Voke, P.R., (1983), "The Application of Large Eddy Simulation to Engineering Problems," Heat Technol. (Bologna), 1(1), pp. 36-55.

Colucci, P. J., Givi, P. and Drummond, J. P., (1998), "Large Eddy Simulation of Reacting Turbulent Flows," http:// science.nas.nasa.gov/cgi-bin/onramp/TechSums/9596Ext/Show, 7118.

Colucci, P. J., Jaberi, F. A., Givi, P. & Pope, S. B. (1998), "Filtered density functions for large eddy simulation of turbulent reacting flows," Phys. Fluids., 10, 499-515.

Cook, A. W. & Riley, J. J. (1994), "A subgrid model for equilibrium chemistryin turbulent flows," Phys. Fluids., 6, 2868-2870.

Correa, S.M. (1993), "Turbulence-Chemistry Interactions in the Intermediate Regime of Premixed Combustion," *Combustion and Flame*, vol. 93, pp. 469-486.

Correa, S. M., (1992), "A Review of NOx Formation under Gas-Turbine Combustion Conditions," Comb. Sci. and Tech., 87, 329-362.

David, E.., (1993), "Modélisation des Ecoulements Compressibles et Hypersoniques: une Approche Instationnaire", PhD Thesis, Natl. Polytech. Inst., Grenoble.

Debusschere, B. and Rutland, C.J., (2003), "Turbulent Scalar Transport Mechanisms in Plane Channel and Couette Flows," *International Journal of Heat and Mass Transfer*, Vol. 47, pp. 1771-1781

Dopazo, C., (1994), "Recent Developments in PDF Methods," pages 375--47, In Libby and Williams.

Frankel, S.H., Adumitroaie, V., Madnia, C.K., and Givi, P., (1993), "Large Eddy Simulations of Turbulent Reacting Flows by Assumed PDF Methods," In Ragab, S. A. and Piomelli, U., editors, Engineering Applications of Large Eddy Simulations, ASME, Number 162, pp. 81-101.

Frankel, S. H., McMurtry, P. A., and Givi, P. (1995), "Linear Eddy Modeling of Reactant Conversion and Selectivity in Turbulent Flows," AICHE Journal, Vol. 41, pp. 258-266.

Germano, M., Piomelli, U., Moin, P., and Cabot W., (1991), "A Dynamic Subgrid-Scale Eddy Viscosity Model," Phys. Fluids 3, pp. 1760-1765.

Ghosal, S. and Moin, P., (1995), "The Basic Equations for the Large Eddy Simulation of Turbulent Flows in Complex Geometry," J. Comp. Phys., 118, 24--37.

Givi, P., (1994), "Spectral and Random Vortex Methods in Turbulent Reacting Flow," In Libby and Williams, Chapter 8, pp. 475-572.

Glassman, I., (1987), Combustion, Academic Press: London.

Hamer, A.J. and Roby, R.J. (1997), "CFD Modeling of a Gas Turbine Combustor Using Reduced Chemical Kinetic Mechanisms," AIAA 97-3242, 33rd AIAA/ASME/SAE/ASEE Joint Propulsion Conference & Exhibit, Seattle, WA, July. 6-9, 1997.

Jiang, Y., Fricker, D.M., and Coirier, W.J (1999), "Parallelization of a Fully Implicit Unstructured Pressure-based Flow Solver Using MPI," (AIAA-99-3274).

Jones, W. P., (1994), “Turbulence modelling and numerical solution methods for variable density and combusting flows,” In Libby and Williams, chapter 6, pages 309--374.
Kerstein, A. R. (1988), "A Linear-Eddy Model of Turbulent Scalar Transport and Mixing," Combustion Science and Technology, Vol. 60, p. 391.
Kerstein, A. R. (1991), "Linear Eddy Modeling of Turbulent Transport: 6. Microstructure of Diffusive Scalar Mixing Fields," Journal of Fluid Mechanics, Vol. 231, p. 361.
Kim, W. and Menon, S., (1997), "Application of the Localized Dynamic Subgrid-Scale Model to Turbulent Wall-Bounded Flows", AIAA paper 97-0210.
Klimenko, A. Yu. (1990), "Multicomponent diffusion of various admixtures in tur bulent flows," Fluid Dynamics., 25, 327-334.
Leonard, A. D., (1995), “An Adaptive Probability Density Function Method for Turbulent Supersonic Combustion Simulations,” CFDRC Report: 4425/1.
Lesieur, M. and Metais, O., (1996), “New Trends in Large-Eddy Simulations of Turbulence,” Annu. Rev. Fluid Mech., 28, pp. 45-82.
Lesieur, M., (1998), “Turbulence in Fluids,” Kluwer Academic Publishers, Dordrecht, The Netherlands.
Libby, P.A. and Williams, F.A., (1994), “Turbulent Reacting Flows,” Academic Press, London, UK.
Lilley, D.G., (1985), “Swirling Flows in Typical Combustor Geometries,” AIAA-85-0184, AIAA 23rd Aerospace Sciences Meeting, Reno, NV.
Lilly, D.K., (1992), “A Proposed Modification of the Germano Subgrid-Scale Closure Method,” Phys. Fluids 4, pp. 633-634.
Lilly, D.K., (1976), “The Representation of Small-Scale Turbulence in Numerical Simulation Experiments,” In Proceedings of IBM Scientific Computing Symposium Environmental Sciences, pp. 195-210, IBM Form No. 320-1951.
Lumley, J.L., editor, (1990), “Whither Turbulence? Turbulence at the Crossroads,” Lecture Notes in Physics, Vol. 357, Springer-Verlag, New York, NY.
Madnia, C. K. and Givi, P., (1993), “Direct Numerical Simulation and Large Edddy Simulation of Reacting Homogeneous Turbulence,” In Galperin and Orszag, chapter 15, pp. 315--346.
Mallampalli, H.P., Fletcher, T.H. and Chen, J.-Y., (1997), "Evaluation of CH4/NOx Reduced Mechanisms Used for Modeling Lean Premixed Turbulent Combustion of Natural Gas," submitted to *Combustion and Flame*.
Maloney, D., (2001), Personal Communication, DOE-NETL.
McMillan, O. J. and Ferziger, J. H., (1980), “Tests of New Subgrid Scale Models in Strained Turbulence,” AIAA Paper, 80-1339.
Menon, S. (1999),”Computational and Modeling Constraints for LES of Turbulent Combustion”, 35th JANNAF Combustion Airbreathing Propulsion Meeting, Cocoa Beach FL, 18-21 Oct 1999.
Montgomery, C.J., Cremer, M.A., Heap, M.P., Chen, J.-Y., Westbrook, C.K., and Maurice, L.Q. (1999), “Reduced Chemical Kinetic Mechanisms for Hydrocarbon Fuels,” AIAA 99-2220, Los Angeles, CA.
Oran, E. S. and Boris, J. P., (1981), “Detailed Modeling of Combustion Systems,” Prog. Energy Combust. Sci. 7, 1--72.
Peters, N., (1991), “Reducing mechanisms”, In Smooke, chapter 3, pages 48--67.

Peters, N. (1997), "Four lectures on turbulent combustion," ERCOFTAG Summer School, Institut fur Technische Mechanik, RTWH Aachen, Germany.

Pitz, R.W. and Daily, J.W., (1983), "Combustion in a Turbulent Mixing Layer Formed at a Rearward-Facing Step," AIAA J. 21 pp.1565-1570.

Pope, S.B., (1999), "A Perspective on Turbulence Modeling," Modeling Complex Turbulent Flows, M.D. Salas ed., Netherlands: Kluwer Academic Publishers, pp. 53-67.

Pope, S.B. (1997), "Computationally efficient implementation of combustion chemistry using in situ adaptive tabulation," Combustion Theory and Modeling, Vol. 1, pp. 41-63.

Pope, S. B. (1985), "PDF methods for turbulent reactive flows," Prog. Energy Comb. Sci., 11, 119-192.

Prasad, K., and Koseff, R., (1989), "Reynolds Number and End-wall Effects on a Lid-driven Cavity Flow", Phys. Fluids A, Vol. 1, No. 2, February 1989.

Richards, G.A. and Janus, M.C., (1997), "Characterization of Oscillations During Premix Gas Turbine Combustion," Presented at the *International Gas Turbine and Aeroengine Congress and Exhibition*, ASME Paper 97-GT-244, Orlando, FL, June 2-5.

Rogallo, R.S. and Moin, P., (1984), "Numerical Simulation of Turbulent Flow," *Ann. Rev. Fluid Mech.*, vol. 16, pp. 99-137.

Salvetti M. V., and Banerjee S., (1995), "A Priori Tests of a New Dynamic Subgrid-Scale Model for Finite-Difference Large-Eddy Simulations," Phys. Fluids 7, (11), pp. 2831-2847.

Schumann, U., (1989), "Large Eddy Simulation of Turbulent Diffusion with Chemical Reactions in the Convective Boundary Layer," *Atmospheric Environment,* vol. 23, no. 8, pp. 1713-1726.

Schumann, U., (1975), "Subgrid Scale Model for Finite Difference Simulations of Turbulent Flows in Plane Channels and Annuli," J. Comp. Phys., 18, pp. 376-404.

Smith, C.E. and Cannon, S.M. (1999), "CFD Assessment of Passive and Active Control Strategies for Lean, Premixed Combustors," 37th AIAA Aerospace Sciences Meeting and Exhibit, AIAA-99-0714, Reno, NV.

Smith, C.E., Leonard, A.D., (1997), "CFD Modeling of Combustion Instability in Premixed Axisymmetric Combustors," International Gas Turbine & Aeroengine Congress & Exhibition, Orlando, FL.

Smith, N. S. A. (1994), "Development of Conditional Moment Closure Method for Modelling Turbulent Combustion", PhD thesis, Department of Mechanical & Mechatronic Engineering, University of Sydney, Sydney, Australia.

Smooke, M. D., editor, (1991), "Reduced Kinetic Mechanisms and Asymptotic Approximations for Methane-Air Flames," vol. 384, Lecture Notes in Physics, Springer-Verlag, Berlin.

Spalding, D. B., (1977), "Development of the eddy-break-up model of turbulent combustion," In Proceedings of 16th Symp. (Int.) on Combustion, page 1657, The Combustion Institute, Pittsburgh, PA.

Steele, R.C., Cowell, L.H., Cannon, S.M., and Smith, C.E. (1999), "Passive Control of Combustion Instability in Lean Premixed Combustors," International Gas Turbine & Aeroengine Congress and Exposition, Indianapolis, Indiana.

Toor, H. L., (1962), "Mass transfer in dilute turbulent and nonturbulent systems with rapid irreversible reactions and equal diffusivities," AIChE J. 8, 70--78.

Vreman, B., Geurts, B. and Kuerten, H., (1995), "A Priori Tests of Large-Eddy Simulation of the Compressible Plane Mixing Layer," J. of Eng. Math., 29, 299-327.

Wang, M. and Moin, P., (2002), “Dynamic Wall Modeling for Large-Eddy Simulation of Complex Turbulent Flows,” Physics of Fluids, Vol. 14, pp. 2043-2051.

Weller, H.G., Tabor, G., Gosman, A.D., and Fureby, C., (1998), “Application of a Flame-Wrinkling LES Combustion Model to a Turbulent Mixing Layer,” 27th Combustion Symposium.

Westbrook, C.K. and Dryer, F.L., (1981), "Simplified Reaction Mechanisms for the Oxidation of Hydrocarbon Fuels in Flames," *Combustion Science and Technology*, vol. 27, pp. 31-43.

Westenberg, A.A. (1971), "Kinetics of NO and CO in Lean, Premixed Hydrocarbon-Air Flames," *Combustion Science and Technology*, vol. 4, pp. 59-64.

APPENDIX A — WORK SCHEDULE

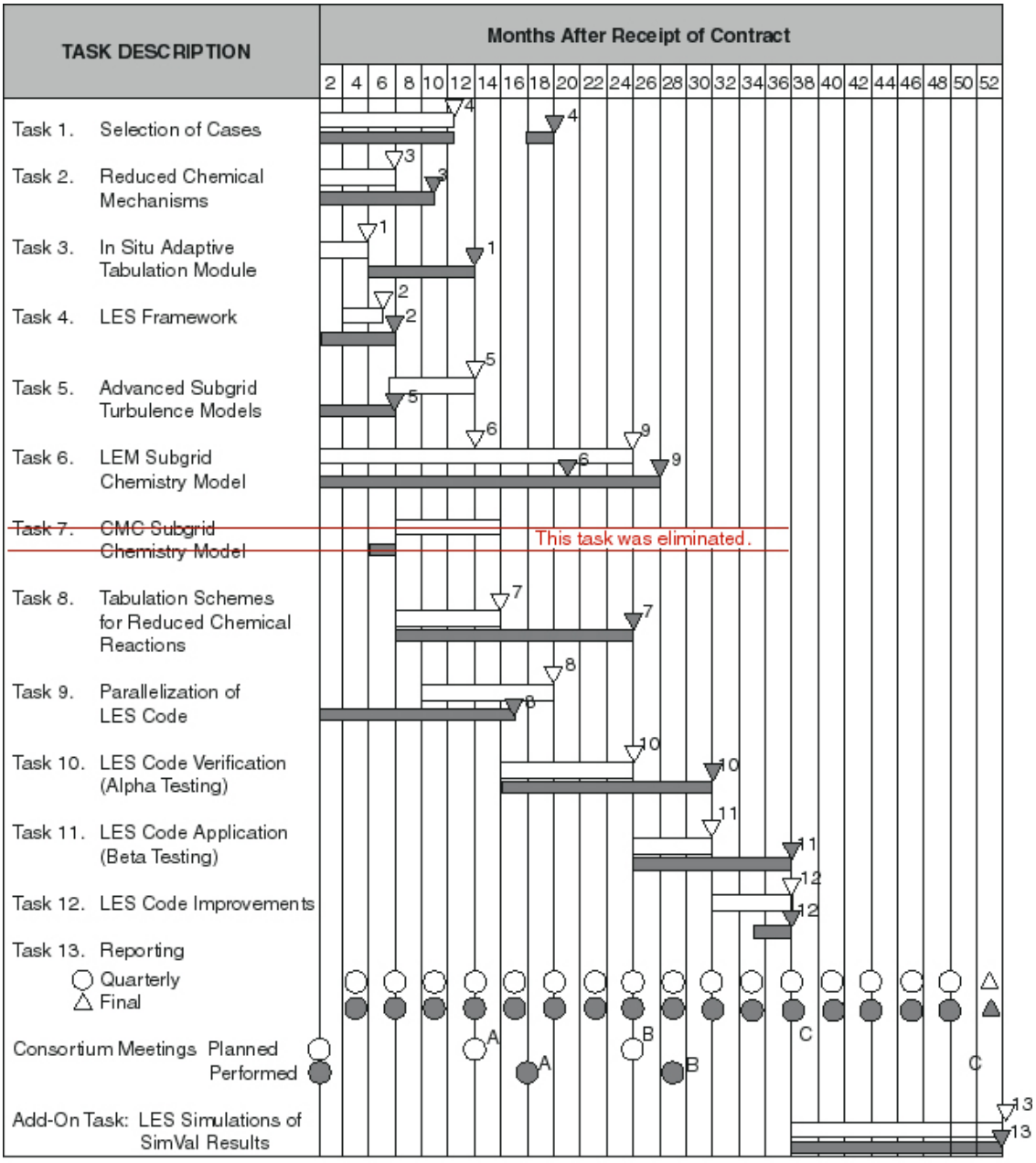

Key Milestones

1 Complete In-Situ Adaptive Tabulation Module
2 Complete LES Framework Modification to CFD-ACE+
3 Complete Reduced Mechanisms
4 Complete Selection of Cases
5 Complete Implementation of Turbulence Models
6 Complete Implementation of Initial Version of LEM Model
7 Complete Tabulation Schemes
8 Complete Parallelization of LES Code
9 Complete Implementation of LEM Model
10 Complete Alpha Testing of LES Code
11 Complete Beta Testing of LES Code
12 Final Release of LES Code
13 Complete SimVal Comparisons

Performance Targets

A Alpha Release of LES Code
B Beta Release of LES Code
C Final Commercial Release of LES Code

Planned
Performed

APPENDIX B

Solar Turbines' Final Report

Solar® Turbines
A Caterpillar Company

An Evaluation of CFDRC's

LES Software For Design Of Combustion Systems
(Beta Version)

By
Alan J. Kubasco
Solar Turbines Incorporated

1.0 INTRODUCTION

CFDRC is working to develop revolutionary Large Eddy Simulation (LES) CFD combustion simulation software to reduce development costs and time associated with industrial combustor development. The program focus is directed toward low emissions industrial combustors burning gaseous fuels. This work is funded under a DOE / Vision 21 contract.

A twenty-member consortium consisting of government, academic, and industrial organizations was formed to guide and direct software development. Selected industrial partners would act as beta testers to validate/compare predicted results against experimental data and to provide feedback to CFDRC for further software improvement.

This new software is being developed using Large Eddy Simulation (LES), which is better able to model the transient nature of gaseous-fueled turbulent combustion. Solar Turbines is particularly interested in the capabilities of this new software because it has the potential to accurately predict fuel-air mixing profiles. This is particularly important in the design of low emissions fuel injectors.

2.0 SOFTWARE EVALUATION/EXPERIENCE WITH SOFTWARE

Solar selected a Mars injector for which UC Irvine had previously acquired extensive velocity and fuel-air mixture fraction data for which to evaluate the LES software. The first step in this process was to generate the fluid

mesh. Solar used the mesh generation software GridPro by Program Development Corp. of White Plains, NY. The CFD mesh of the Mars injector was completed in mid-February, 2003 and ready for incorporation into the LES software.

The next 3 months or so were spent trying to convert the GridPro mesh into the dtf format required by CFD-ACE -- we were unsuccessful. The conversion problem was complicated by the fact that the mesh was periodic. We will continue to work with the software developers from GridPro and CFDRC to solve this problem.

In order that Solar acquire some experience in using the LES software, the decision was made to have CFDRC mesh a model of a thick vane injector with a single fuel injection port in each vane for which Solar had fuel-air mixture data. CFDRC would setup the model in the LES mode, initiate the run, and then transfer the files to Solar for the completion of the run. Unfortunately, because of set-up and system incompatibility problems Solar has been unsuccessful in getting the LES software to run on our SGI system. We will continue to work with CFDRC and Program Development Corp. to solve both the grid conversion problem and the software installation issues.

CFDRC ran this model on a sixteen-node Linux cluster to 8000 sweeps. The data was sent to Solar for comparison to experimental data and will be discussed in a subsequent section.

Although we were not able to run the software, numerous exchanges between Solar and CFDRC called attention to a few shortcomings in the LES software. They are:

Boundary Selection: The boundary selection process seems to involve using the screen cursor to individually pick the boundary areas. This can be a tedious task on a complex geometry.

A competitor's software uses a screen cursor selected 'seed' vertex on one of the surface cells of the boundary to initiate the boundary surface selection. The selection process automatically continues until an edge is encountered. This is a very useful feature when working with intricate geometries that are not easily displayed in their entirety on the screen.

Model Decomposition: Although we have not had experience in setting up and decomposing a large model it is my impression that stopping a job and decomposing the model to run on a different number of nodes is not a simple process. In my experience with other CFD software this is a rather easy task, taking at most about five minutes for a large model.

Exporting Data To Third Party Post-Processors: The capability to export the data directly to a FieldView format for post-processing would be a significant benefit.

3.0 Experimental Setup

The experimental data used for model comparison was obtained at the exit plane of a ten-vane gaseous fuel injector. A photograph of a similar rig setup is shown below.

The photograph shows the exit end of the injector with the fuel/air sampling rake in place. The sampling rake is comprised of a series of individual gas sampling tubes. The setup used to obtain the data to compare to the LES results used a six-probe rake system traversed over a 120-degree sector.

Each of the ten-swirler vanes used in the injector has six 0.052-inch diameter fuel injection ports located on the leading edge – three on the pressure side and three on the suction side. For this experiment five of the ports were blocked out using a metal foil tape leaving only one fuel injection port on the pressure side of the vane. The figure below shows the swirler and the location of the fuel port.

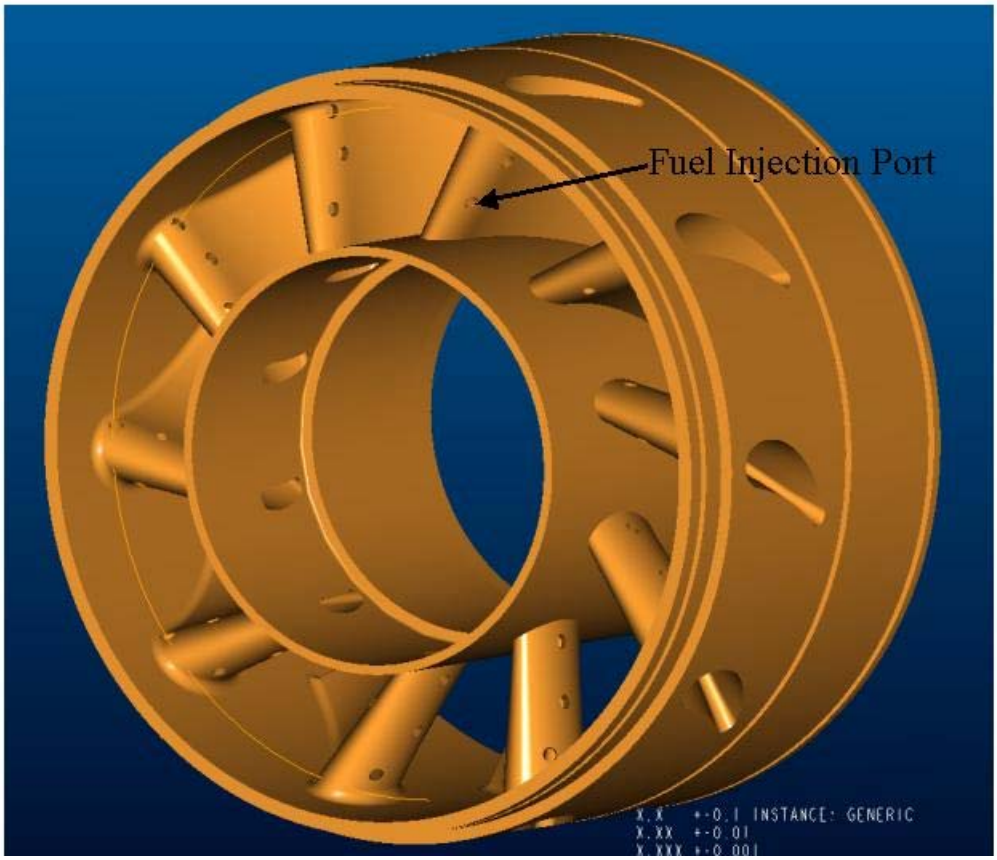

4.0 COMPARISON OF LES MODEL RESULTS TO EXPERIMENTAL DATA

Fuel-air mixture data from the experimental rig is shown in the contour plot below. The measurements indicate that mixing is more intense in the inner

half of the annulus. One can still discern the pressure of the individual vanes and the single fuel injection ports in each vane. The counter-clockwise rotation of the flow and the rotation of the fuel concentrated zone can also be seen in the contour pattern.

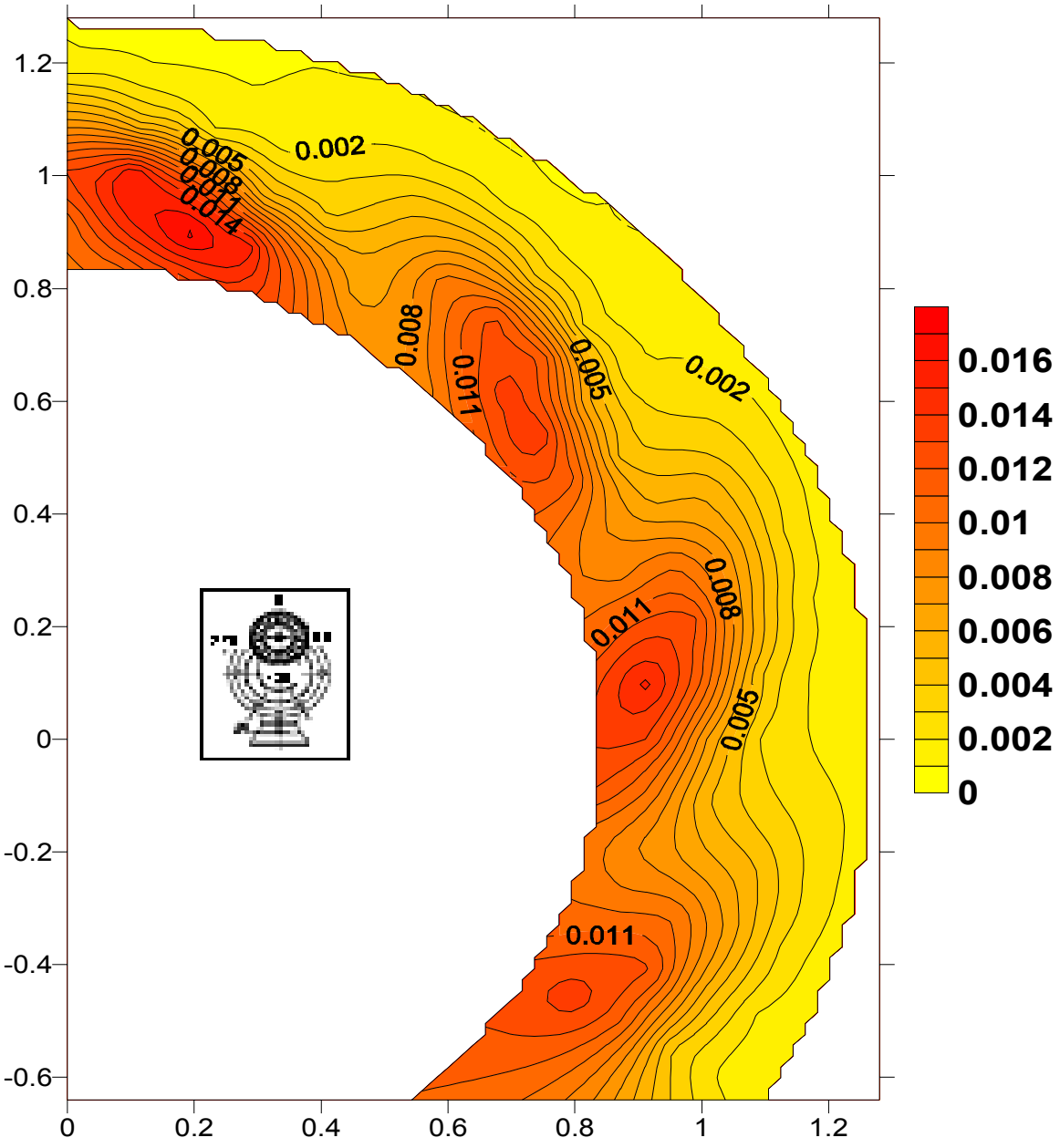

FUEL-AIR MIXTURE DATA FROM EXPERIMENTAL RIG

(Fuel Mass Fraction – View Aft Looking Forward)

The LES model used the same boundary conditions as run in the experimental rig. They are as follows:

Solar® Turbines
A Caterpillar Company

Air Flow Rate = 0.3 lbm/sec
Air Temp = 540 R
Air Inlet Pressure = 15 psia
Fuel Flowrate = 0.002 lbm/sec
Fuel Temp = 540 R
Fuel Pressure ~15 psia

The LES prediction of fuel mass fraction at a plane corresponding to the fuel-air sampling rake is shown below. LES predicts a much higher concentration of fuel in air at the swirler hub.

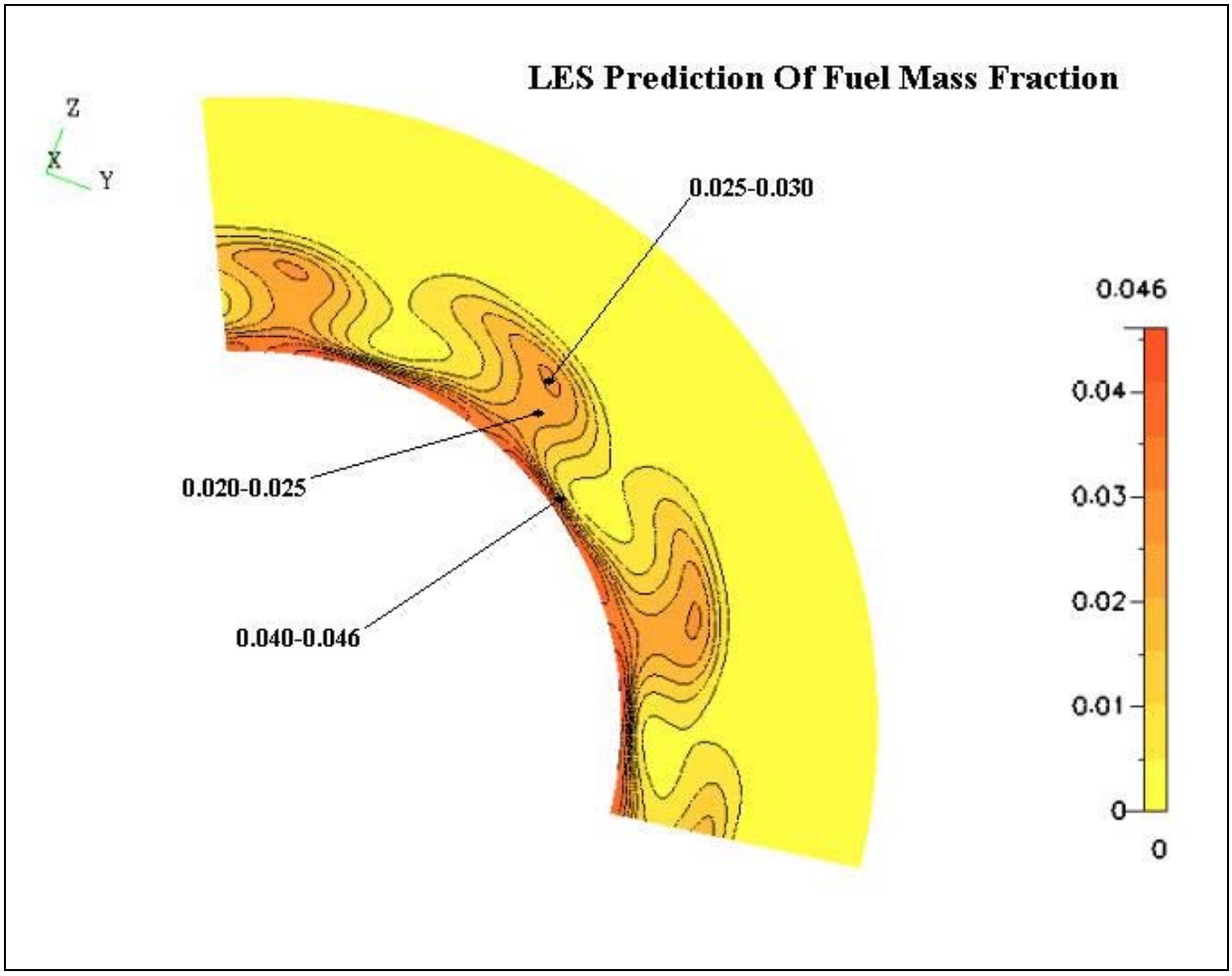

LES FUEL-AIR MIXTURE PREDICTION
(Mass Fraction Fuel – View Aft Looking Forward)

The pressure of the ten vanes - each with a single fuel injection port- are very evident. LES correctly predicts the counter-clockwise swirl component and the shearing action tending to mix and spread the fuel concentrated in the lobes.

Obviously, there is a difference between the LES prediction and the experimental data. This difference can be due to a number of factors associated with both the LES model and the experimental.

Possible Experimental Inaccuracies:

1) Metal foil tape was used to cover five of the six fuel ports on the vane leading edge. This tape is acting to some degree as a turbulence generator. How much additional mixing this is causing is unknown.
2) Six fuel-air sampling tubes were used with the inner and outer most tubes 0.045 inches from the walls. Therefore, the flow adjacent to the wall is not being sampled.
3) No attempt was made to sample the fuel-air mixture isokinetically.
4) The uniformity of the airflow into the swirler is an unknown.

Possible LES Modeling Inaccuracies:

1) Mesh density may not have been sufficient enough to resolve the finer details.
2) Uniform air velocity profile at the inlet may not replicate actual experimental conditions.
3) The fuel velocity profile may not reflect actual experimental conditions.

5.0 SUMMARY

The LES software predicts only the very general trend of the fuel-air mixing profile as measured experimentally. The high concentration of fuel in air predicted in the layer adjacent to the hub is unexpected and counterintuitive. Further investigation is needed to determine what in the LES software is causing this to occur.

APPENDIX C

Coen's Final Report

LES STUDY OF
COMBUSTION IN DUCT BURNER

REPORT

Submitted To:
CFD Research Corporation
Huntsville, AL 35805

Prepared By:
Paul Matys
Coen Company, Inc.
Woodland, CA 95776
pmatys@coen.com

August, 2003

TABLE OF CONTENTS

LIST OF FIGURES

LIST OF TABLES

1. INTRODUCTION

The objective of this study was to predict unsteady gas flow and combustion behind a duct burner element using Large Eddy Simulation (LES). A commercial CFD code from CFD Research Corporation was evaluated. The results were compared with results from another commercial CFD package Fluent, and qualitatively with available measurements. The geometry of the duct burner was simplified to a bluff body with 2 baffles (see Figures 1), and was represented by 2D computational domain with about 10,000 computational cells. The air enters the duct at 10m/s and 300K. The fuel is released from the downstream face of the bluff-body at 0.5m/s and 300K. A summary of input data is shown in Table 1.

The CFDRC solver includes transport equations for mass, momentum, energy and species. The localized dynamic subgrid kinetic energy model (LDKM) was used to model turbulence. Combustion was modeled with PDF method and one step prescribed reaction. CO concentration was predicted by CO chemistry model, and thermal NOx was calculated by the decoupled NOx-model. For comparison, Fluent commercial code was used with very similar, however, understandably not identical physical models. For LES modeling Smagorinsky-Lily model was selected and for combustion PDF-model and equilibrium was used.

Table 1 Summary of inputs

Air inlet velocity	10m/s (33ft/s)
Air temperature	300K (80F)
CH4 inlet vel.	0.5m/s (1.6ft/s), 300K
CH4 temperature	300K (80F)

2. SUMMARY OF RESULTS

The results of the computer simulation are presented on a number of figures that show velocity field as contours of velocity magnitude and velocity components, gas temperature and species concentration.

Figures 1-10 show the results from CFDRC simulation. Velocity field downstream of the bluff body is characterized by a number of small flow structures as shown on Figure 1 and 2. The gas temperature is presented on Figure 3, there are number of high temperature zones resulting from combustion with the maximum gas temperature reaching slightly above 2200K. The concentration of species is shown on Figures 4-9. Methane quickly reacts into CO and hydrogen compounds. The mixing between oxygen and combustible gases in the bluff body wake seems to be limiting the overall fuel combustion rate. The flow field is fractionated into a number of recirculation zones of different scale.

The results from Fluent simulation are shown on Figures 11-20. The results are similar to CFDRC-results in qualitative sense. The gas temperature and concentration of species are roughly in the same range of values. There is, however, noticeable difference in the turbulent viscosity plots (Figures 9 and 19) with Fluent values being about 3 times smaller than those predicted by CFDRC software.

3. COMMENTS

- The initial difficulties at the early stage of the project were related to learning how to use CFDRC software. It was necessary to start with simpler cases and slowly progress to more complex cases that involved unsteady LES and eventually combustion. By far the most difficult and time consuming part of the case setup was to create geometry grid. The "GEOM" module of the software was found to be difficult to learn or understand as it is using technique/logic completely different from other commercial grid generation software (e.g. Fluent/Gambit).
- The parallel running of the software required the purchase of the necessary hardware and installation of Linux OS. Before this project the Linux OS has not been used on the company PC's, and there was very limited experience with this operating system at the administrative level. There were severe prolonged problems with the incompatibilities between the hardware and Linux version necessary to run CFDRC software. Red Hat OS could not be installed due to missing hardware support, and Mandrake Linux OS was not supported by CFDRC, and was giving warning and error messages. Substantial amount of time was devoted to troubleshoot this problem with some CFDRC help. In the end the newer version of Red Hat provided full hardware support. The other problems with parallel running on the Linux cluster was related to the administrative level of cluster software configuration. The permission between different cluster nodes were not working properly for a long time. In the end the parallel running capability on the Linux cluster was achieved, however, in the hindsight the time spent on the hardware software setup and initial troubleshooting was disproportionate as compared with the overall time assigned to this project.
- Initial Linux OS was selected for running and post processing of the results. However, eventually the case setup/pre processing and post processing was moved to Windows-PC due to insufficient support on Linux for other auxiliary software (word processing, graphics manipulation etc). The Linux OS system still seems to be reasonable choice for running the cases, specially due to easy

control from Windows-PC (e.g., using VNC, Exceed) and easy file transfer between Windows-PC and Linux-PC using Samba software.

- The newer version of CFDRC software suite V2003 is much improved in terms of help resources and user-friendliness, however, the difficult operation of GEOM module still seems to be the biggest stumbling block preventing from fast, efficient usage of the CFDRC-software.
- The test case for the LES combustion represents simplified geometry of the duct burner. In simplification the geometry consists of bluff body with baffles. The geometry can be treated as 2D. This assumption substantially reduces CPU-time required to run a case, on the other hand the 3D-effects of unsteady LES simulation are lost. In the future the results from 2D vs. fully 3D case will be compared and evaluated. At the present time, 2D case seems to be a good choice for the test case because it allows for quick running and troubleshooting of the cases, and quick learning of the fine tuning necessary to run unsteady LES-combustion cases.
- The initial results from CFDRC runs were suffering from unreasonably low combustion temperature. After some improvement in the grid and adjustments in the discretization schemes and under-relaxation factors, i.e., fine tuning of the model, the predicted temperature and flow pattern/structure were more reasonable.
- The initial runs with Fluent went smoothly, as there was previous experience with running unsteady LES-combustion with this software. The gas temperature was at reasonable level, and large structures (eddies) could be observed downstream of the bluff body. After comparing initial results from Fluent and CFDRC, it was concluded that large flow structures predicted by Fluent were not acceptable. The fine tuning of the Fluent model with the help of the Fluent-Support resulted in the quite dramatic change in the flow field with much smaller flow structures downstream of the bluff body, and good qualitative resemblance to the results obtained with the CFDRC software. This experience highlights the pitfalls of LES simulation which requires extensive testing and very careful selection of physical sub-models, discretization schemes, under-relaxation factors, time step and grid size.

- The experimental validation of unsteady LES combustion is very difficult, and at this stage for this project is limited only to qualitative comparison with the flow field observed in the test yard for similar geometries, and values of CO downstream of the flame. The prediction of CO by CFDRC or Fluent software varied widely between different combustion models. The final results from simulations were still almost by order of magnitude different from experimentally observed values for similar flow and combustion situation.
- At the present time, the unsteady LES combustion modeling seems to be in the early stage, both in terms of physical models and validation. More time is necessary to learn how to use the models and how to interpret the results. The LES simulations may not be ready yet to be used for everyday CFD modeling when quick and straightforward answers are expected from CFD modeling. However, even now, LES can be used for selected cases, where traditional modeling fails to give full and accurate prediction of the flow-combustion interaction. Even at this early stage of the software development the results from LES simulation provide valuable insight into the flow field and combustion process.

4. FIGURES

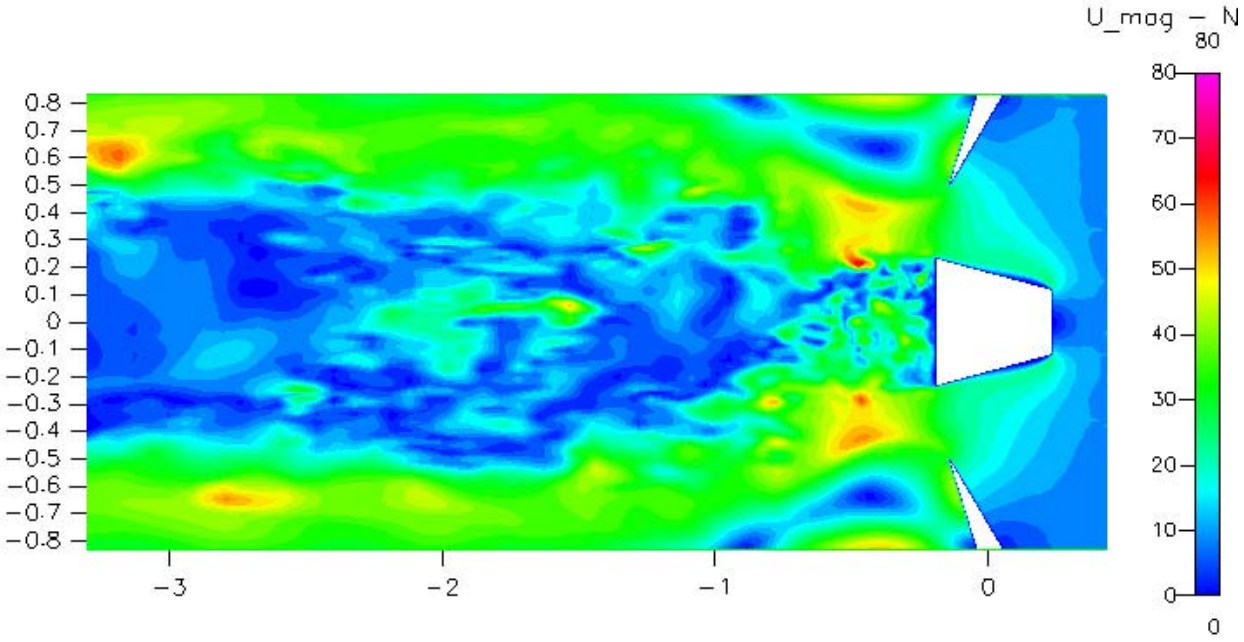

Figure 1 Velocity Magnitude (m/s)

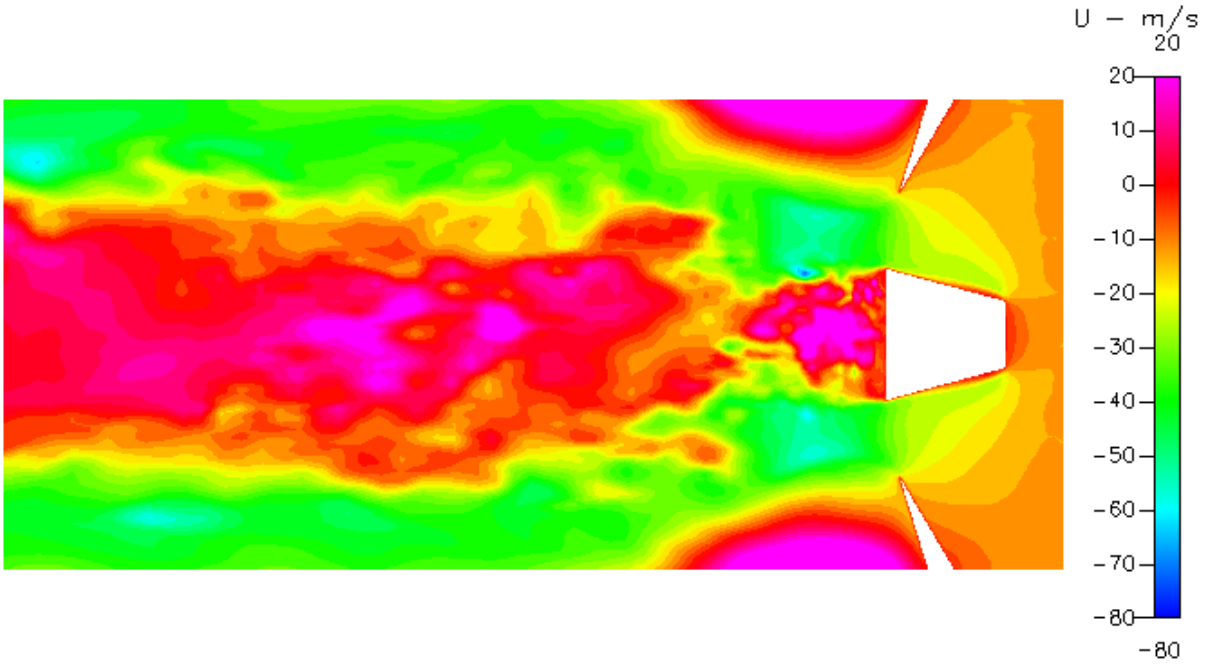

Figure 2 U-velocity component

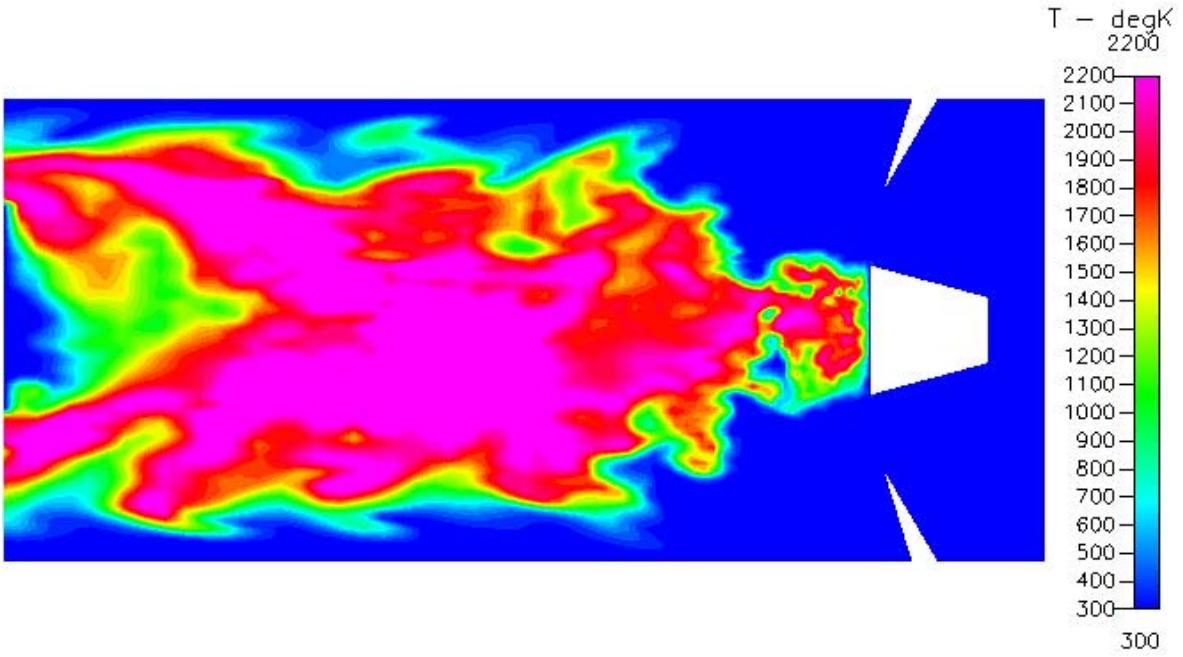

Figure 3 Gas temperature

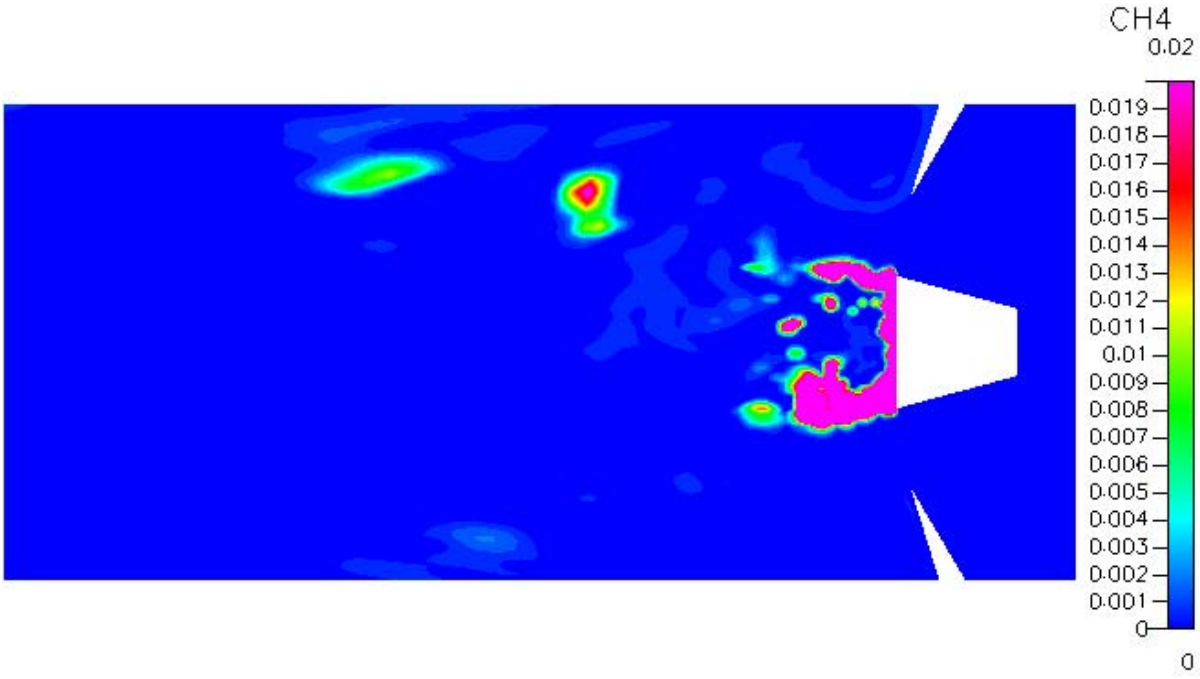

Figure 4 Mass fraction of methane

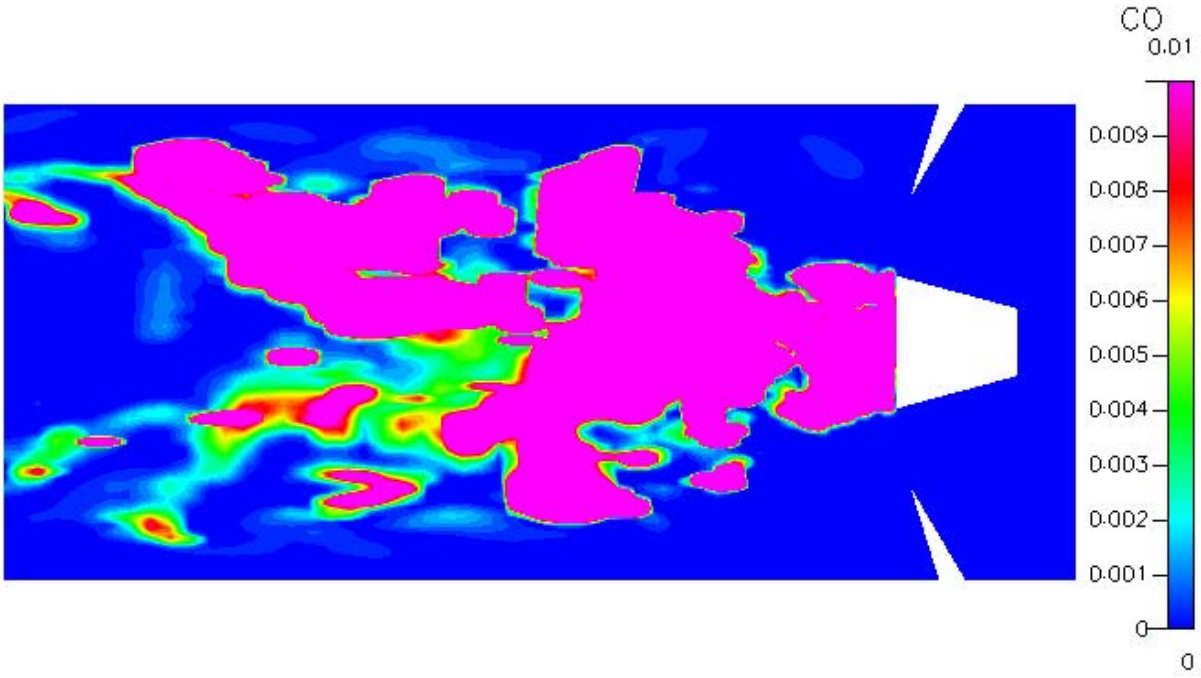

Figure 5 Mass fraction of CO

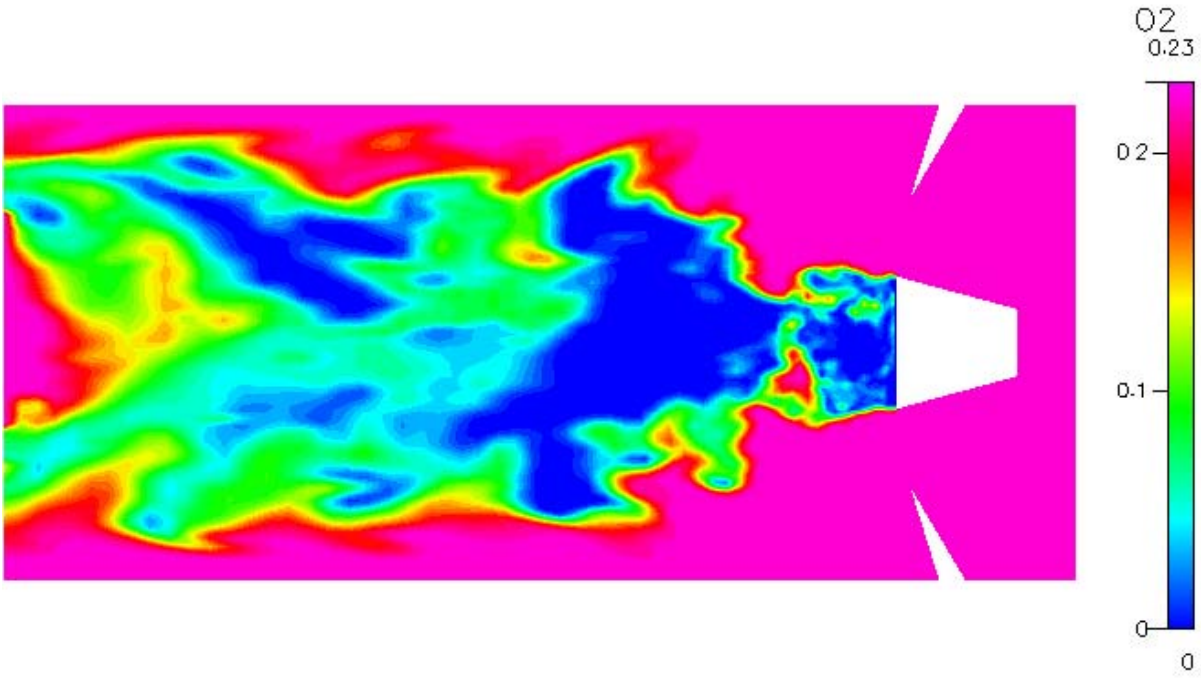

Figure 6 Mass fraction of oxygen

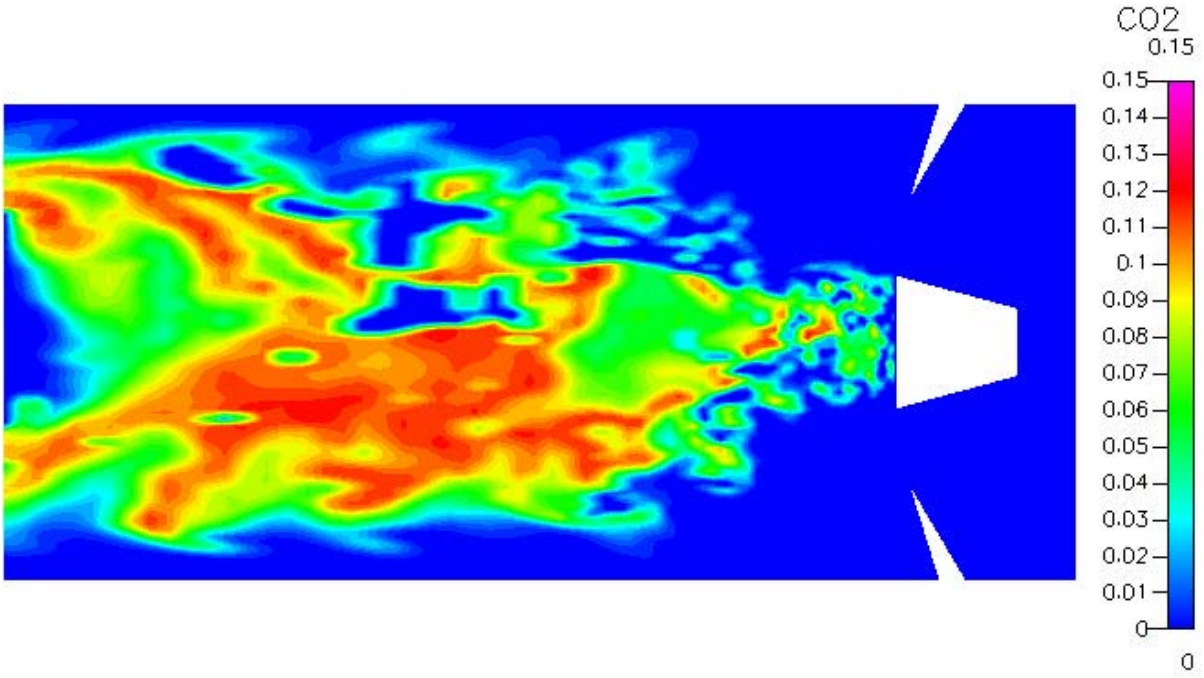

Figure 7 Mass fraction of CO2

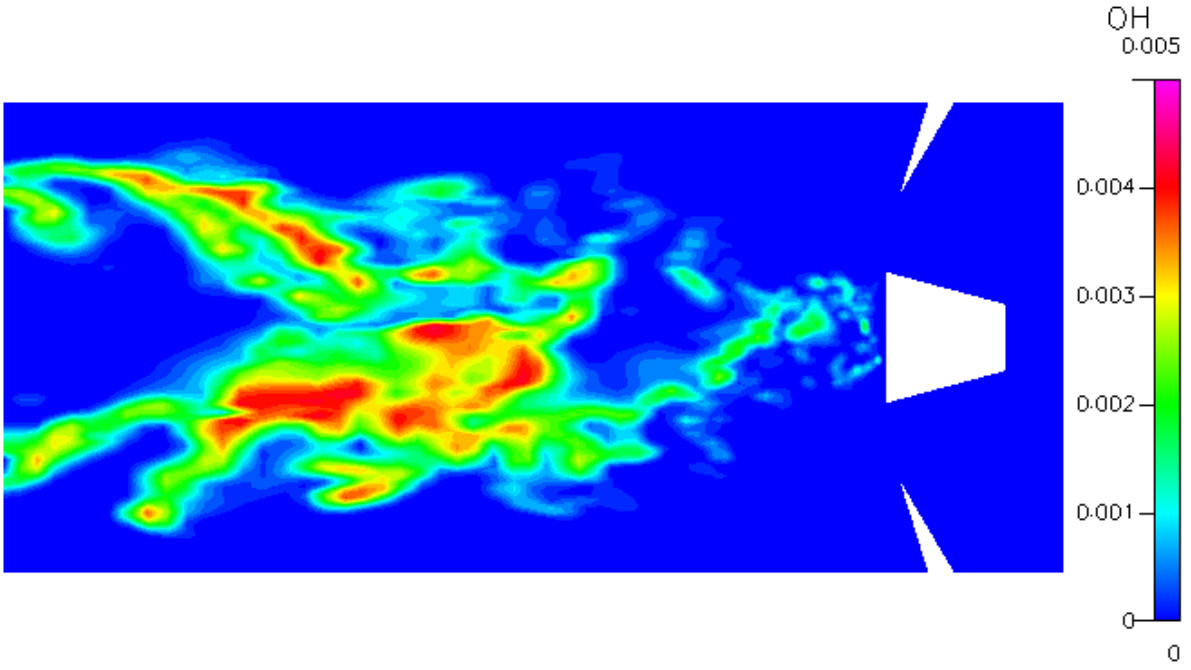

Figure 8 Mass fraction of OH

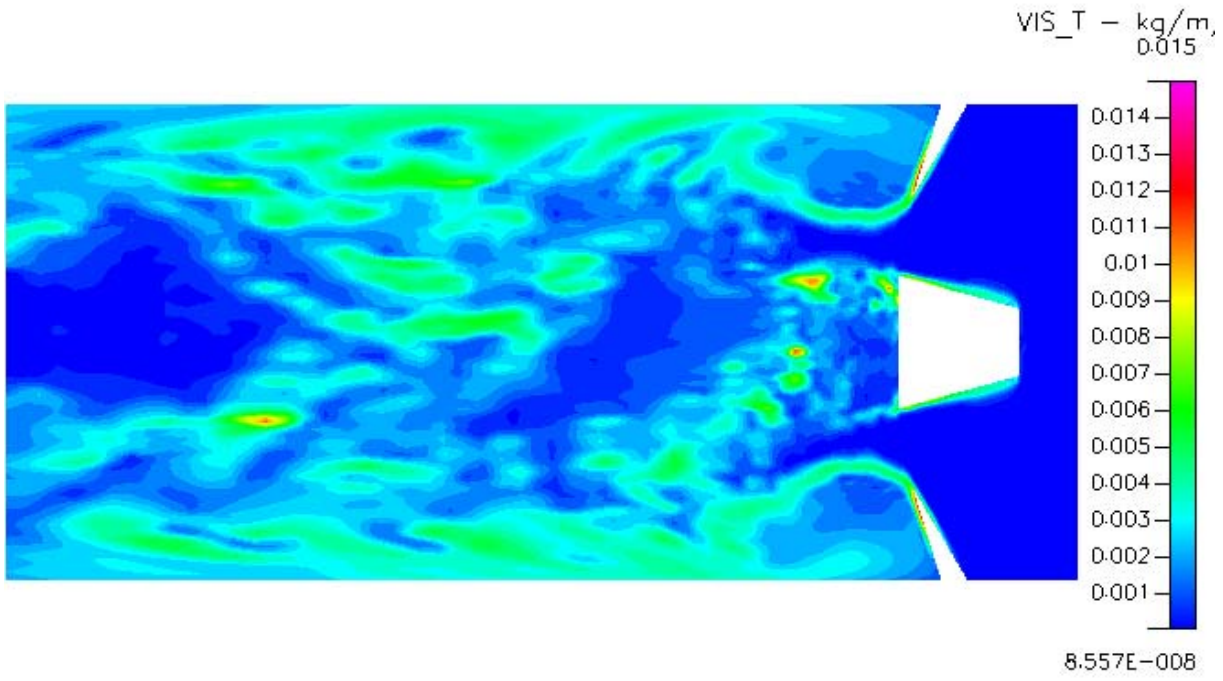

Figure 9 Turbulent viscosity

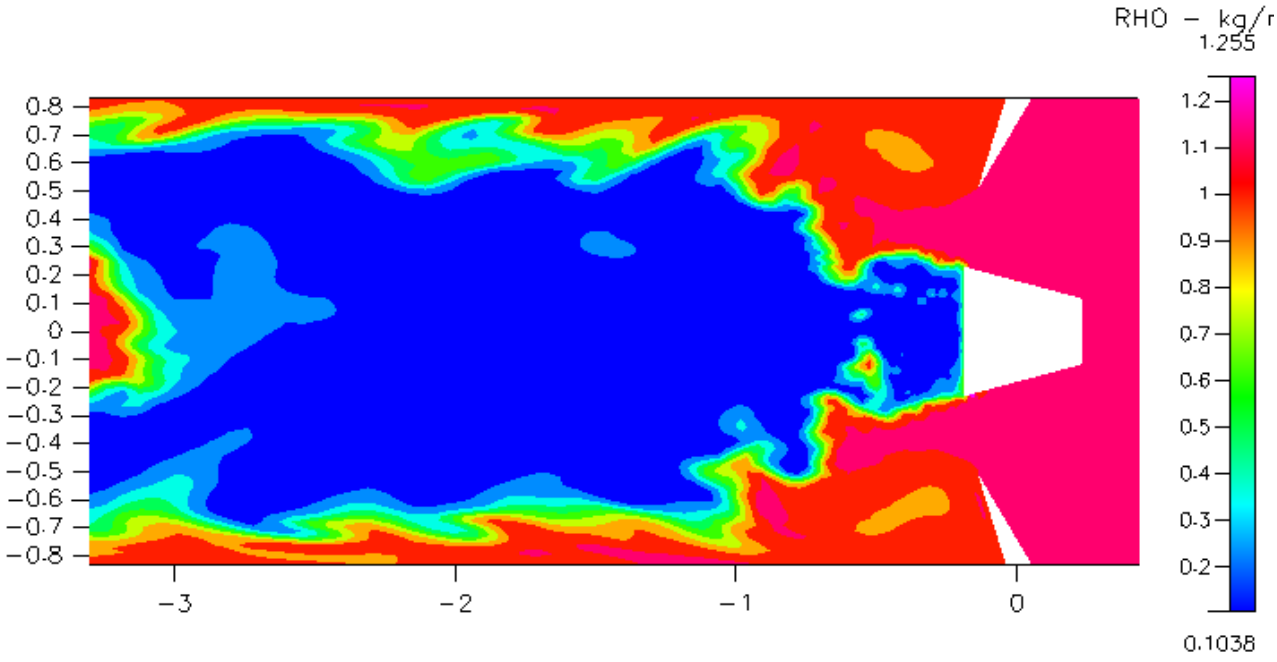

Figure 10 Gas mixture density

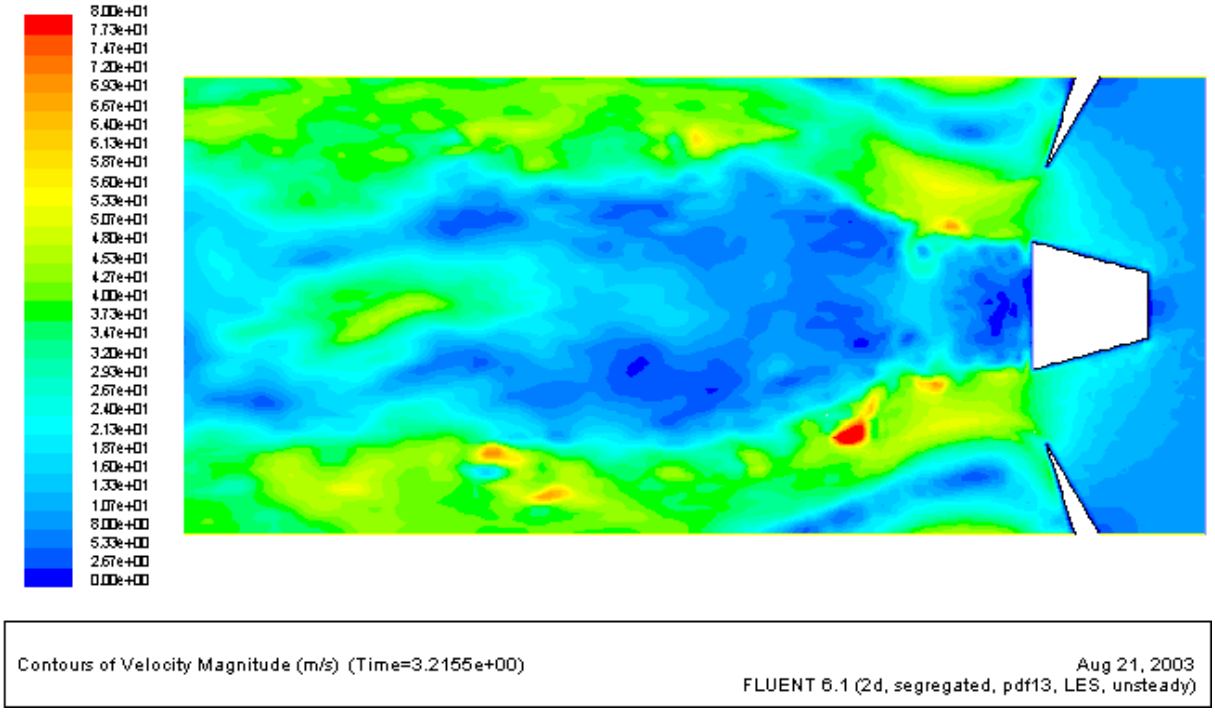

Figure 11 Velocity Magnitude (m/s) - Fluent

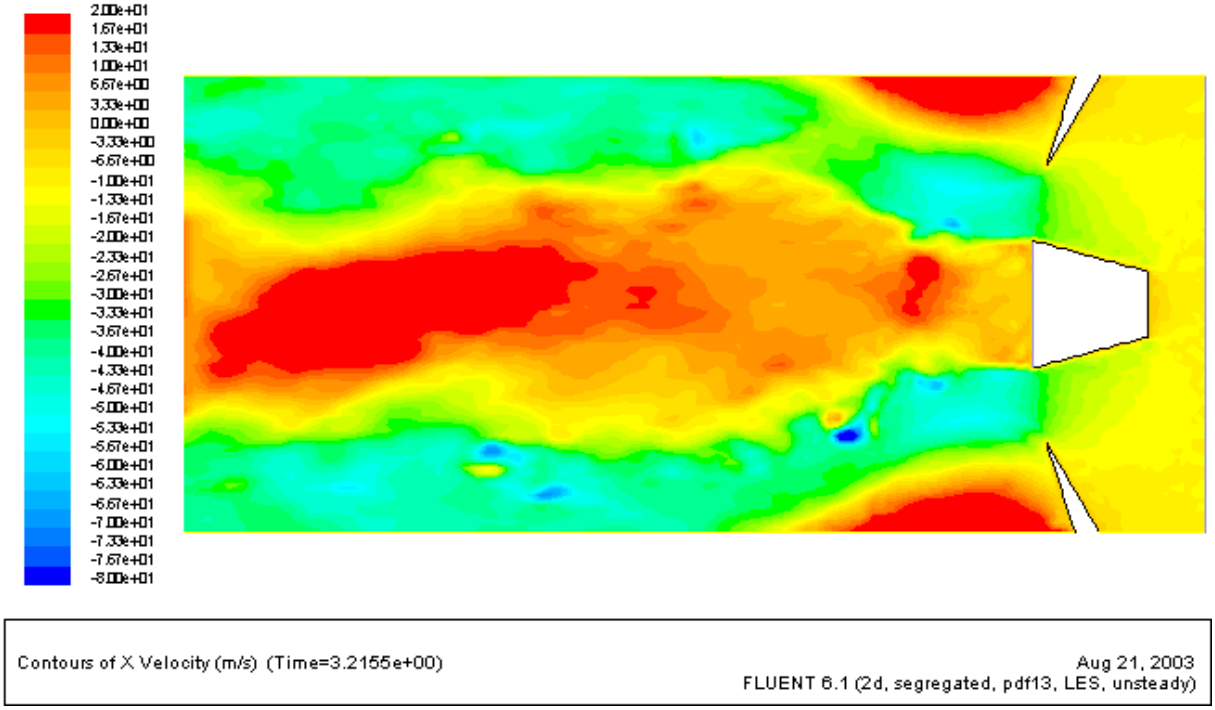

Figure 12 U-velocity component - Fluent

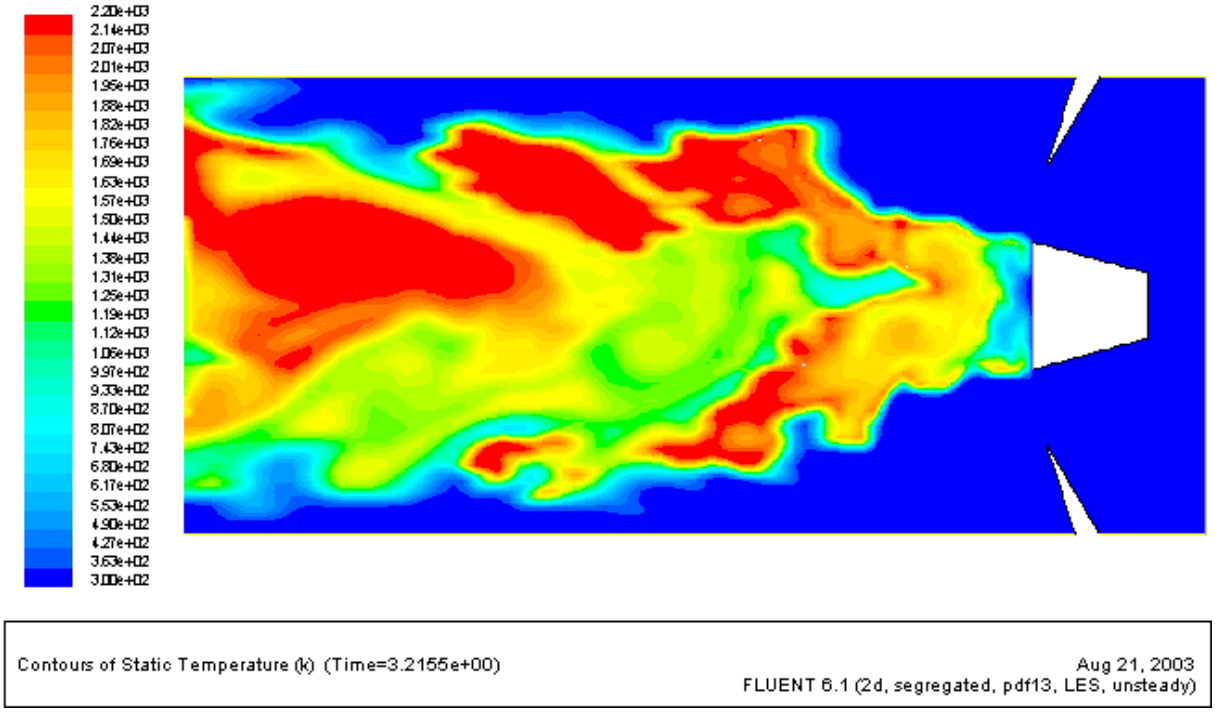

Figure 13 Gas temperature - Fluent

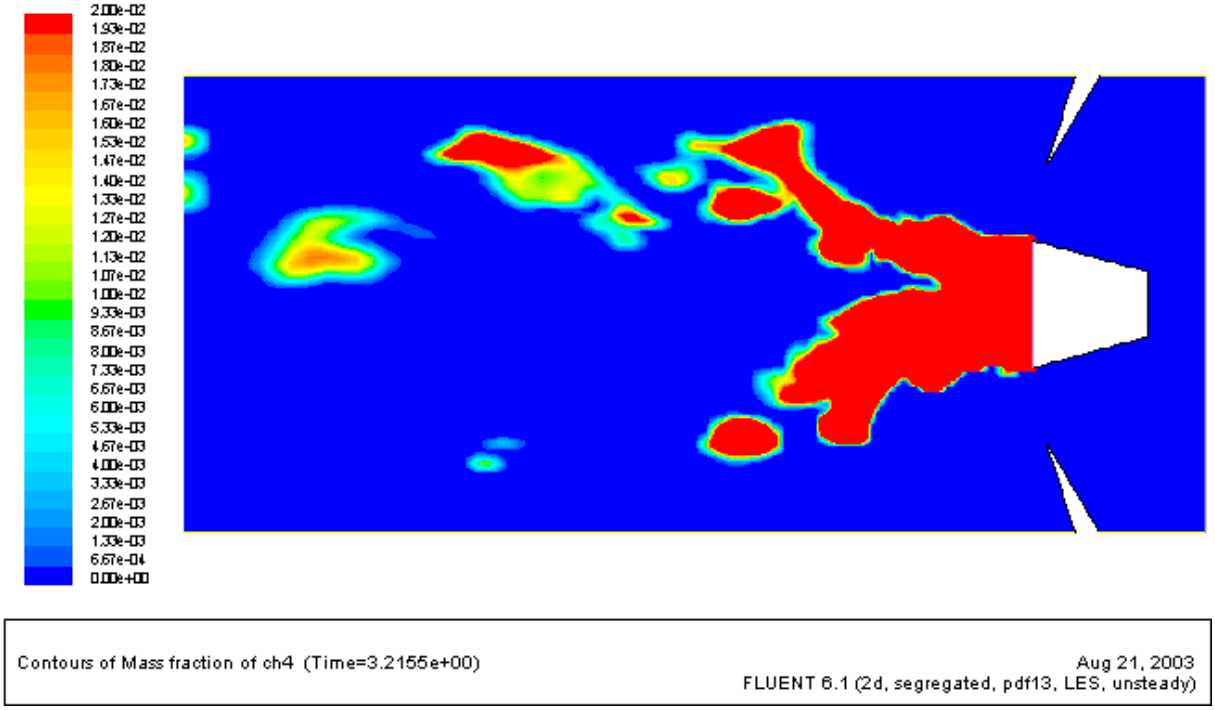

Figure 14 Mass fraction of methane - Fluent

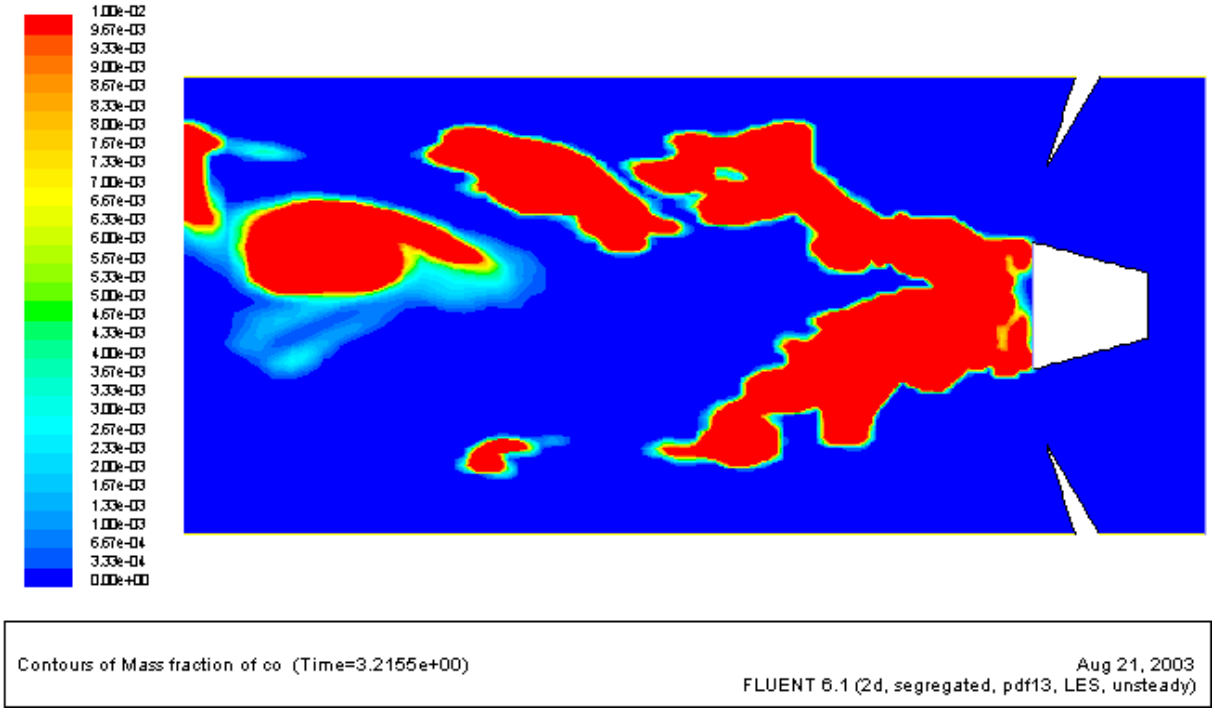

Figure 15 Mass fraction of CO - Fluent

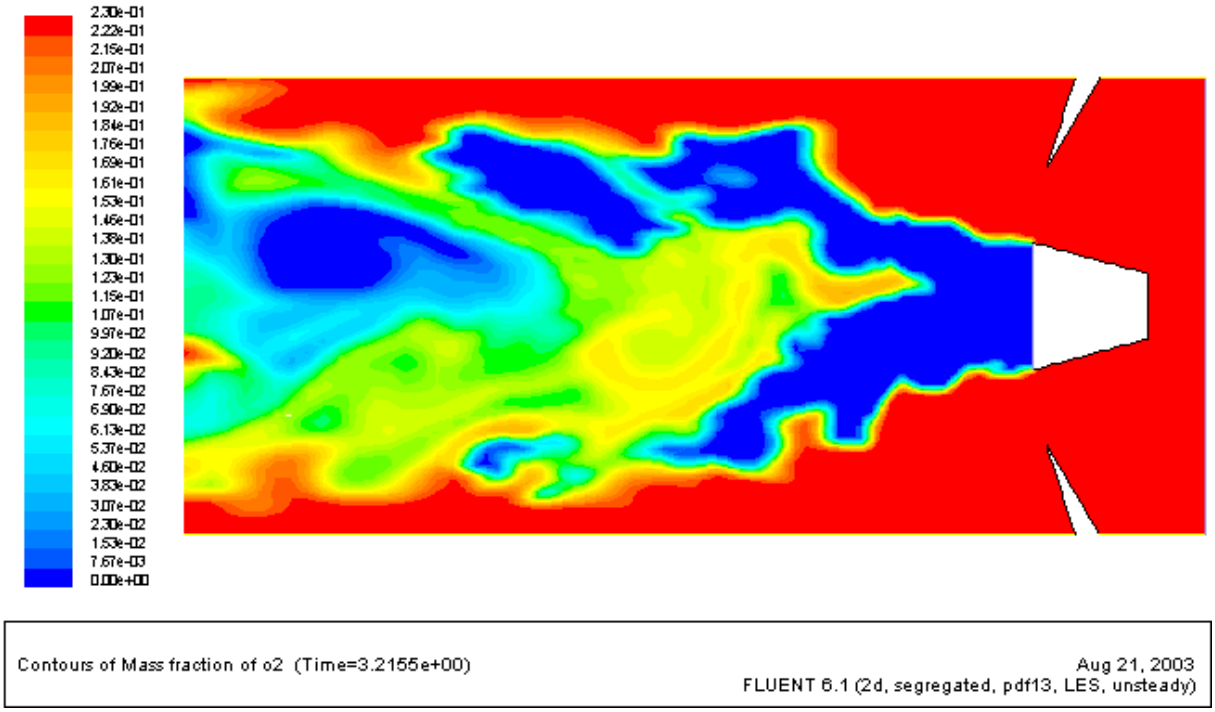

Figure 16 Mass fraction of oxygen - Fluent

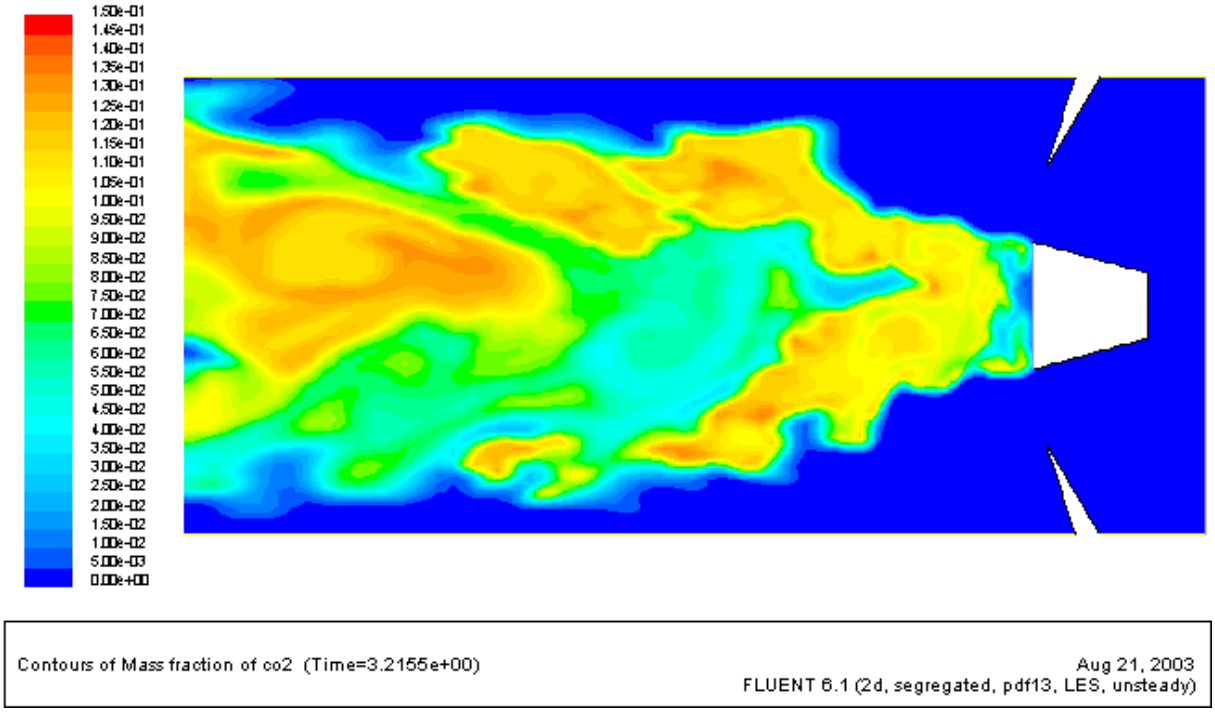

Figure 17 Mass fraction of CO2 - Fluent

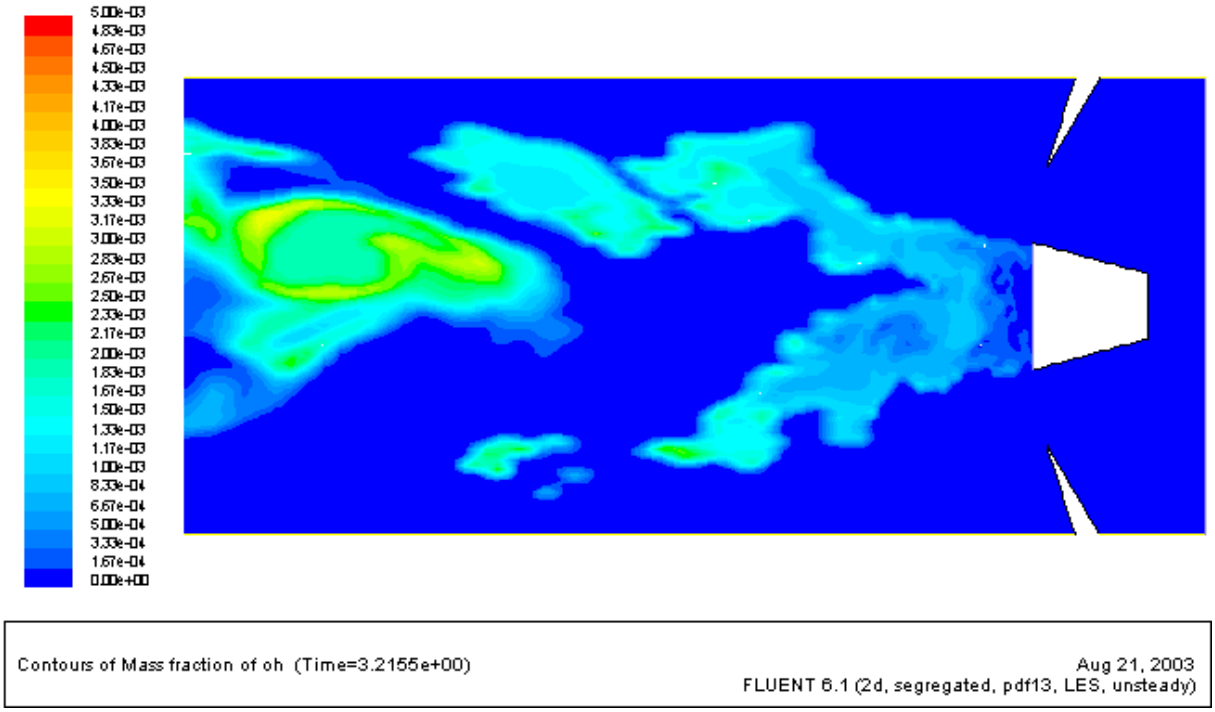

Figure 18 Mass fraction of OH - Fluent

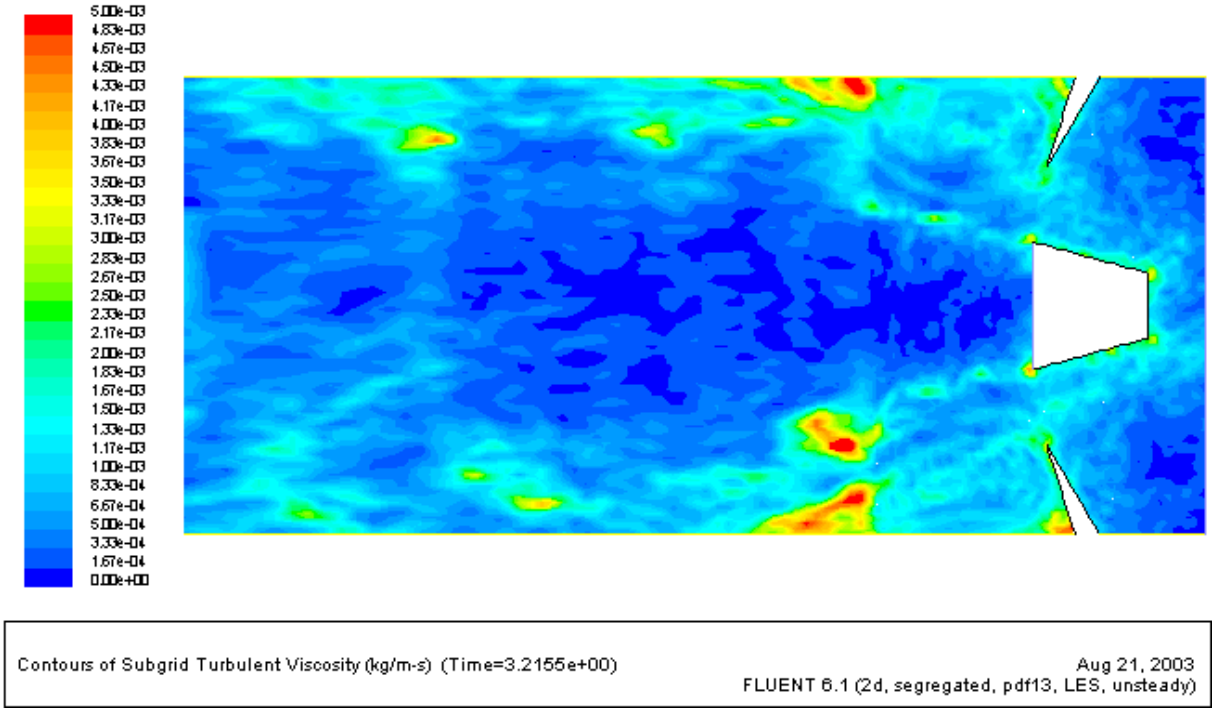

Figure 19 Turbulent viscosity - Fluent

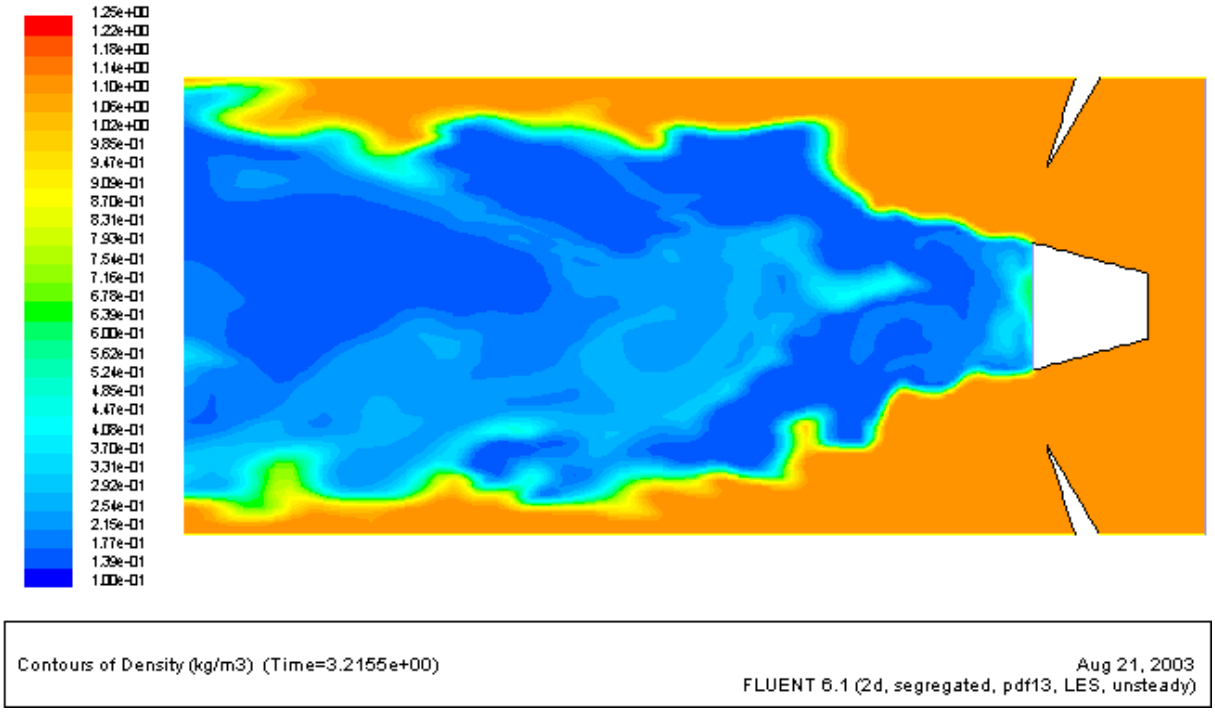

Figure 20 Gas mixture density - Fluent

APPENDIX D

Virginia Tech's Final Report

Simulation of Reacting Flows in a Premixed Turbulent Swirl Stabilized Combustor for Determination of Flame Dynamics

A Validation Study of the CFDRC LES Combustion Code

Progress Report Submitted to:

Dr. Steven M. Cannon
CFD Research Corporation
215 Wynn Drive
Huntsville, AL 35805

by:

Prateep Chatterjee – Research Scientist
Uri Vandsburger – Supervisor
Department of Mechanical Engineering, Virginia Tech
Blacksburg, VA 24061

September 5, 2003

Executive Summary

A CFD study of unsteady reacting flow process inside a combustor geometry has been performed to investigate the effects of acoustics on the unsteady heat release rate of a premixed gaseous flame. The motivation for undertaking the study is the problem of combustion instabilities which result from acoustic waves in the combustor perturbing heat release from the flame by generating fluctuations in flame surface area. These combustion instabilities are detrimental to the operation of gas turbine systems and must be controlled. Combustion control algorthims implement empirical or reduced order model based transfer functions between various variables, including the transfer function between unsteady velocity (u') and the unsteady heat release rate (q'). The objective of this study has been to calculate this transfer function. The transfer function calculated will in turn help in the development of reduced order models that will lead to elimination of combustion instabilities.

The CFDRC LES beta code has been used for calculation of the transfer function. Only part of the actual experimental combustor geometry (at Virginia Tech) has been used for the simulation to reduce the computation cost. Steady state inlet boundary conditions have been generated using experimental data and an unsteady component of velocity has been imposed at the inlet boundary. The resulting reacting flow field has been investigated and different unsteady phenomena have been seen to be occurring. Flame front instabilities have been seen to occur and data has been collected for subsequent investigations of the transfer function between u' and q'.

This document is only a progress report, since much work remains to be done. Among the issues to be addressed will be improving the accuracy of the imposed acoustic boundary conditions and the investigation of various unsteady phenomena observed in the present computations by conducting experiments and changing inflow conditions. Further validation of the LES code will be performed by collecting useful experimental data.

1 Introduction

Reduction of pollutant formation in gas turbines has been an important issue for gas turbine constructors. Lean premixed prevaporized (LPP) combustors are one of the choices, amongst several different methodologies being developed to match international emission standards. LPP combustors have reduced NOx production but are susceptible to combustion instabilities [1]. Acoustic waves in the combustor perturb heat release by generating fluctuations in flame surface [2] and/or mixture fraction. If this unsteady heat release couples with acoustics, some eigenfrequencies of the combustor may be encouraged depending on the phase lag between acoustic waves and unsteady combustion. Understanding and preventing the resulting resonances are important issues in the development of LPP combustors.

Linear acoustics may be used to analyze and model combustion-acoustic interactions. These models are used to predict self-sustained frequencies in gas turbine combustors [3]. In these models, the flame is viewed as an acoustic device which generates an unsteady heat release depending on local acoustics. These simple interaction models usually comprise of a frequency dependent transfer function, relating heat release fluctuations with pressure and/or velocity fluctuations. The transfer functions (frequency response function – FRF) are not only dependent on frequency, but also depend on the combustor geometry, operation mode of the combustor and on the interaction of vortices with the flame front. It is possible to derive the FRFs using analytical calculations for simple combustor configurations, but the use of analytical models to obtain transfer functions for complex combustion systems have met with very limited success [4].

There is a need to develop reduced order models with the help of FRFs that describe the dynamic response of swirl stabilized flames to perturbations in the velocity and mixture fraction of the incoming reactants. These models are expected to be simple and yet, exhibit all the dominant dynamic characteristics of the combustion process.

Since a large number of physical variables are involved in the combustion process occurring in complex swirl stabilized combustors, simple systems (burner stabilized laminar flat flames) were initially studied here at Virginia Tech [5]. Having understood the dynamics of laminar flat flames and developed methodologies to build reduced order flame dynamic models, an experimental setup was designed and fabricated to study the dynamics of turbulent swirling flames at VACCG (Virginia Active Combustion Control Group) laboratory at Virginia Tech. The technique developed at VACCG to measure the open loop transfer function of laminar flat flame dynamics will be used for developing the transfer function for the flame dynamics (within the linear range) of swirl stabilized turbulent flames.

The experimental setup used to study the dynamics of turbulent swirl stabilized flames is schematically shown in Figure 1. The system consists of mass flow meters, an air-fuel mixing system, the flow control system, a turbulent variable swirl combustor, the dynamic velocity measurement system, the dynamic OH* measurement system, and the data acquisition system. The fuel flow measured using an array of mass flow meters is fed into a premixer that thoroughly premixes the fuel and air prior to the injection of the premixed charge into the combustor. Microphones were used to obtain dynamic velocity signal, while the OH* chemiluminescence captured by viewing the entire flame from the side was taken as the measure of the dynamic heat release rate. Controlled acoustic perturbations were imparted to the flow using a speaker. The dynamic signals were analyzed using the Hewlett Packard frequency analyzer, while the flow parameters were recorded using a data acquisition system.

The flame in the turbulent variable swirl combustor is stabilized by the presence of the central recirculation zone (CRZ) and the outer re-circulation zone (ORZ), as shown in Figure 2. The CRZ and the ORZ re-circulate the products of combustion back to the inlet of the combustor, thereby enabling the transfer of energy from the hot products of combustion to the incoming reactants. This fluid-dynamic feature of swirl stabilized flames that creates a continuous ignition source, eliminates the

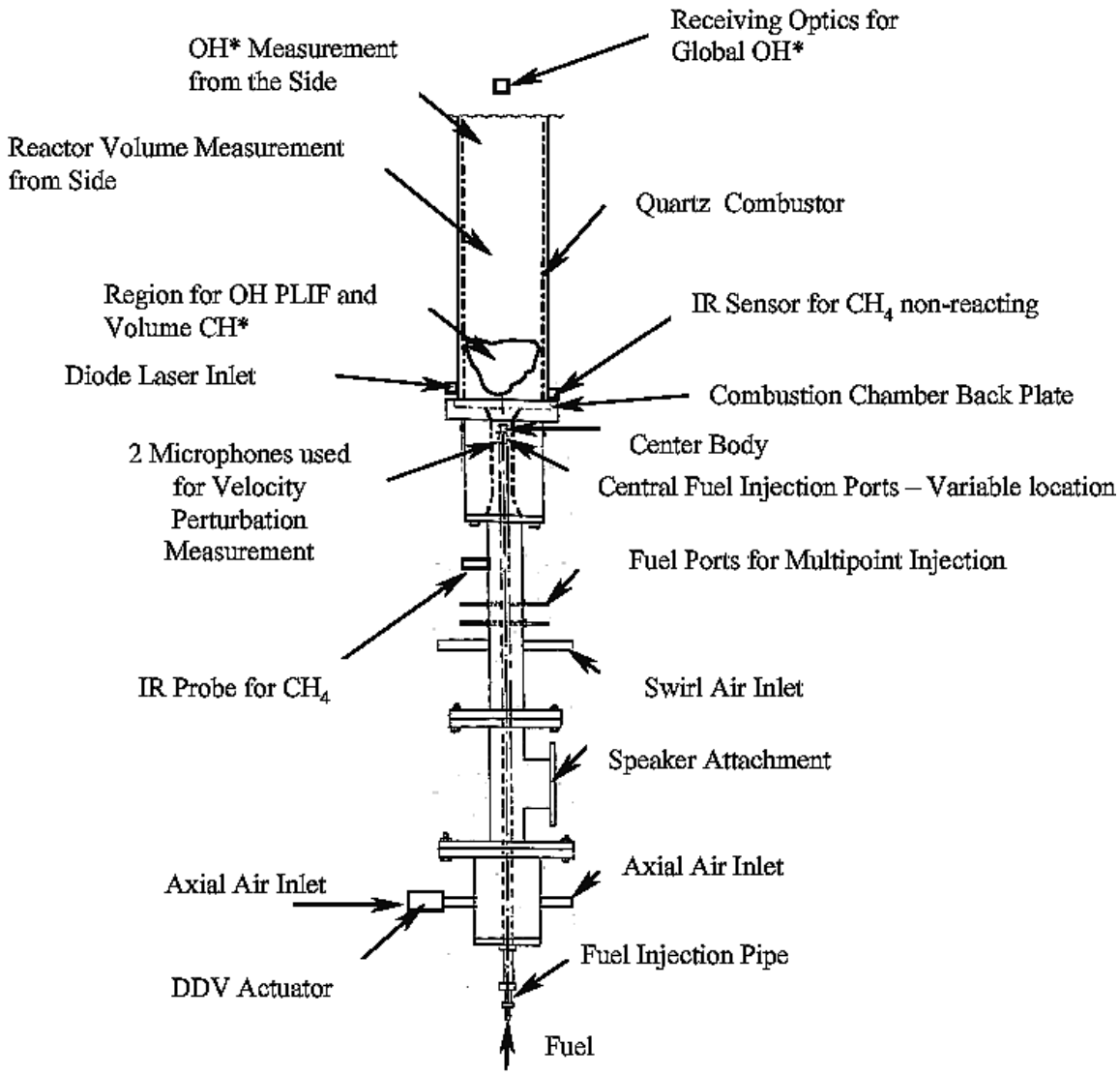

Figure 1: Schematic of the experimental setup

need for an external energy re-circulator as was required for laminar flat flames. By altering the flow field and hence, the strength of the re-circulating zones, the flame could be forced to reside in either of the re-circulating zones or on the shear layer between the re-circulating zones. Such a variation in the flow field could be achieved by changing the swirl number and hence, the swirl strength of the flow entering the combustion chamber.

The variable swirl turbulent combustor was designed with a maximum pressure rating of 150 psig, a maximum thermal rating of $400\,kW$ and is capable of accommodating $200\,SCFM$ of total flow. It has a variable swirl generation arrangement that generates a maximum swirl number[1] (S_g), of 1.86.

Although OH* chemiluminescence is presently considered as the most accurate measure of the dynamic heat release rate, q', its signal generates only qualitative results. The systems level analysis of the combustion process, however requires a quantitative result for q'. Thus, there is an urgent need to characterize the OH* signal and acquire capabilities to extract quantitative values of the dynamic heat release rate from the OH* signal. A study aimed at achieving the above goals would involve experiments on simple laminar combustors and physics based modeling or CFD analysis of the combustor. The comparison between the experimental and the computational results would then provide the calibration of the OH* signal.

The objective of this study is to perform a CFD analysis of the experimental combustor, in particular calculate the transfer function between u' and q' for the "flame dynamics" part of the closed loop dynamic system (shown in Figure 3). In this study,

[1]Swirl number is defined usually in the following form: $S = \frac{\int_{R_i}^{R_o} \rho u_z u_\theta 2\pi r^2 dr}{\int_{R_i}^{R_o} \rho\left(u_z^2 - u_\theta^2/2\right) 2\pi R_o r dr}$ (refer Ribeiro et. al [6]), but in the experiments conducted at VACCG the swirl number calculated is the geometrical swirl number, defined as: $S_g = \frac{R_o \pi r_e}{A_t} \frac{(Tangential\ flow\ rate)^2}{(Total\ flow\ rate)^2}$, where R_o is the radius of the inlet of the quarl, r_e is the radius on which the tangential inlets are attached with respect to the center of the combustor and A_t is the total area of the tangential inlets.

the effect on q' because of equivalence ratio fluctuations, Φ', has not been included. In the experimental combustor, Φ' is not present because the air and fuel are perfectly premixed.

Using the transfer function computed from the CFD results, a qualitative estimation of heat release can be obtained by comparing the CFD data with the experimental OH* qualitative data. Another objective of the study is to use CFD to explain near field acoustic effects on the heat release rate. These near field acoustic effects are at least two dimensional in nature (axi-symmetric) and are responsible for the excessive increase in the OH* chemiluminescence. They need to be accounted for in the systems level description of the combustion process, so as to accurately predict the occurrence of thermo-acoustic instabilities.

2 CFD Model

Computational studies of premixed combustion processes are often restricted by the limitations of the Reynolds average simulation (RANS) models [7] and the turbulent combustion models used to represent the mean flame and its effects on the flowfield. The concept of large eddy simulation (LES) thus provides a more natural approach to analyzing unsteady turbulent reacting flows. LES has the potential to provide quantitative data about flame response [8]. According to Kaufmann et al. [9], LES will provide reliable information for flame transfer functions in gas turbines only if all of the following requirements are matched:

1. Full 3-D compressible Navier-Stokes equations must be solved using structured/unstructured grids for complex combustor geometries,
2. Numerical methods with small dissipation/dispersion should be used,
3. LES models for flow dynamics in complex wall bounded flows are required,

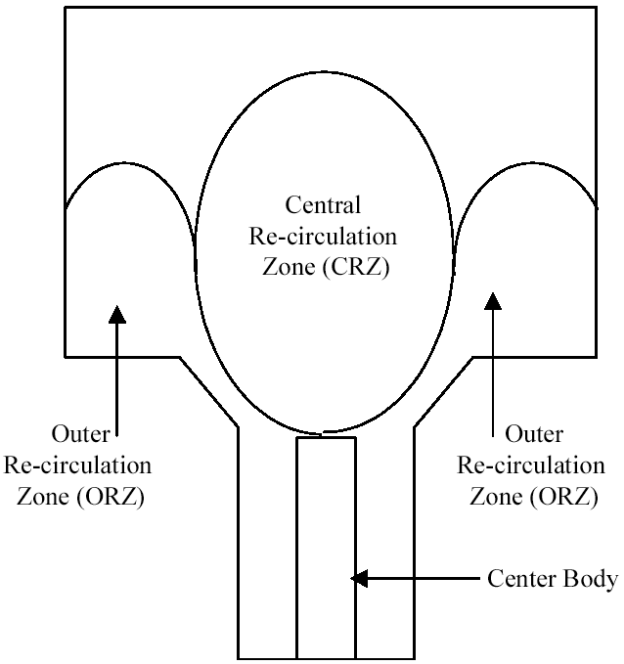

Figure 2: Recirculation zones in the combustion chamber

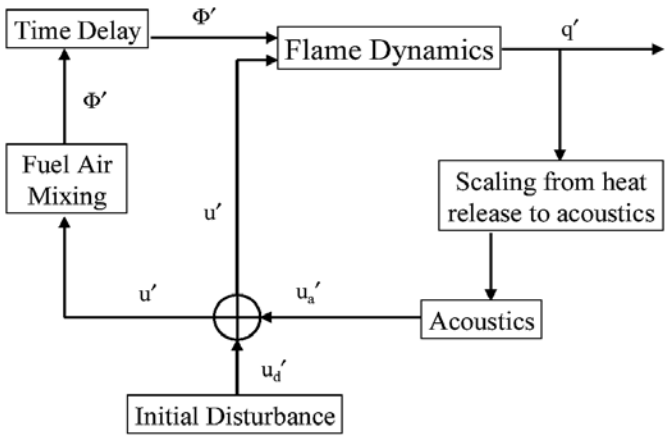

Figure 3: System level description of the thermoacoustic combustion process

4. LES turbulence/chemistry interaction model must be valid for premixed flames,

5. Unsteady boundary conditions must be modified to inject controlled acoustic perturbations and force the flow without creating spurious modes.

Out of the five requirements listed above, Fluent [10] is able to satisfy the first requirement and to some degree the fifth requirement. Although dynamic subgrid scale LES models are available in Fluent, the lack of turbulence/chemistry interaction models prevents the use of the Fluent LES code in simulating unsteady reacting flows. Therefore, as an alternative to using the Fluent commercial code (which has been the code of choice for VACCG in past several years), the CFDRC LES beta code is being used to calculate the transfer function between u' and q' for reacting flow in the VACCG experimental combustor geometry.

The CFDRC LES code satisfies almost all the requirements cited above. Apart from matching the second requirement, which needs the implementation of third-order accurate finite element Taylor–Galerkin-type of schemes [11] or Chimera grid methods with overlapping domain interfaces, the CFDRC LES code is capable of producing flame transfer functions which will be accurate. Problems related to the first requirement are not important in this study because the experimental combustion chamber has a simple shape. As will be illustrated in the boundary conditions subsection, the last requirement is met to a high degree of accuracy, if not perfectly matched.

2.1 Computational Domain

The experimental setup internal geometry is shown in Figure 4. A long length upstream of the combustor in the setup was selected to eliminate any freestream turbulence. There are four distinct sections can be observed in the schematic: the axial air flow section (at the bottom), the straight section with the swirler, the convergent-divergent section and the combustor (dump) on top. Out of these four sections, the

combustor is the only section of interest for the CFD study. Therefore, only the top part of the experimental setup has been included in the CFD simulation. The LES computational domain is shown in Figure 5. The computational domain comprises of an annular inlet, a circular bluffbody which is aligned with the inlet plane, the diverging section (quarl), the bottom steel wall of the combustor, the quartz cylindrical wall and the outlet. The bluffbody diameter is $0.75''$ which is half the diameter of the inlet plane ($1.5''$). The inlet to the dump has a diameter of $2.5''$ and the outlet of the dump has a diameter of $4.92''$. The height of the combustor is $7.5''$ and this height has been selected so that the eigenmodes of the combustor do not get excited. Therefore, there are no self-sustained frequencies in the combustor. By eliminating self-sustaining frequencies and imposing velocity perturbations at the inlet (known as forcing), a transfer function between u' and the unsteady heat release rate q' can now be obtained.

2.2 Boundary Conditions

Eigenfrequencies strongly depend on the choice of acoustic boundary conditions. The resonant modes of a combustor depend on the acoustic boundary conditions at the inlet and outlet. The method used for inlet forcing should not affect these modes. The real combustor geometry (shown in Figure 4) has been simplified to perform an LES computation (inside the geometry shown in Figure 5) and inlet forcing is applied to the artificial computational inlet. The inlet forcing is a result of imposing an unsteady velocity which will make the computational inlet to act as a velocity node ($u' = 0$ at the velocity node) for waves reflected from the combustion chamber (the dump) to the inlet. The existence of this velocity node in the simulations (this velocity node is not present in the actual combustor) may perturb the results. While imposing velocity oscillations at the computational inlet, it has been assumed that because of the high acoustic impedence present at the flame location, any wave reflected from the outlet

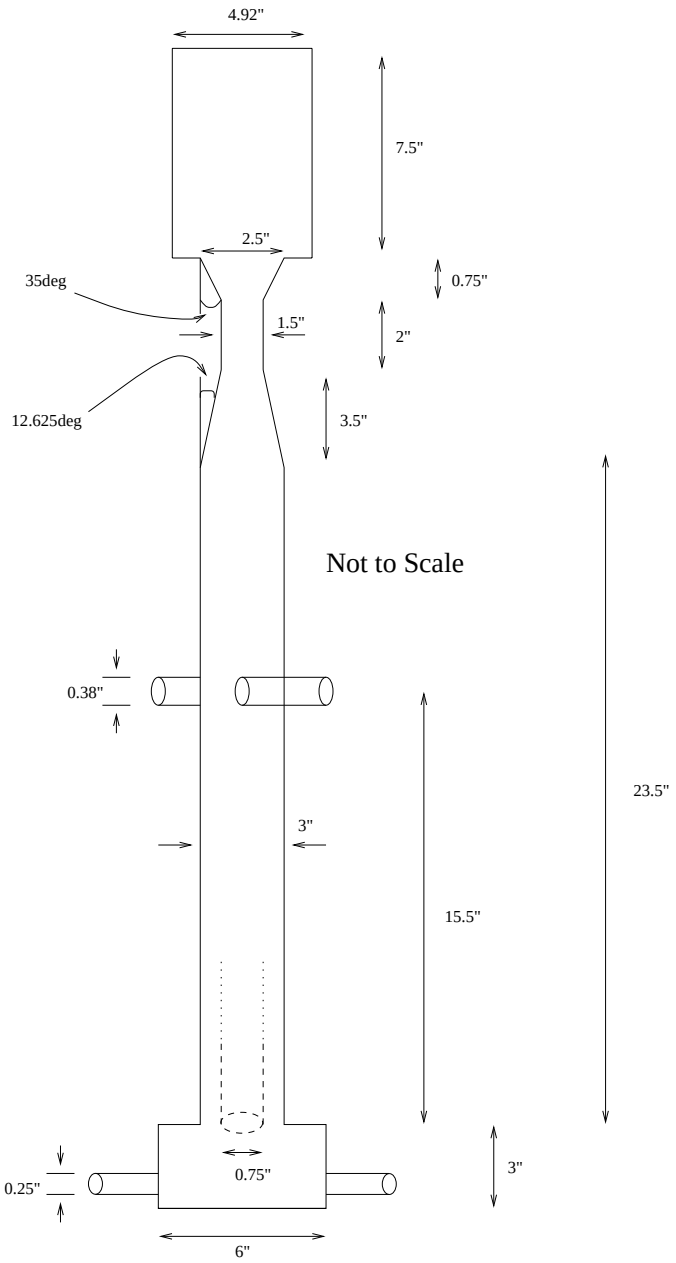

Figure 4: Actual internal geometry of the experimental rig (the centerbody is shown with the dashed line)

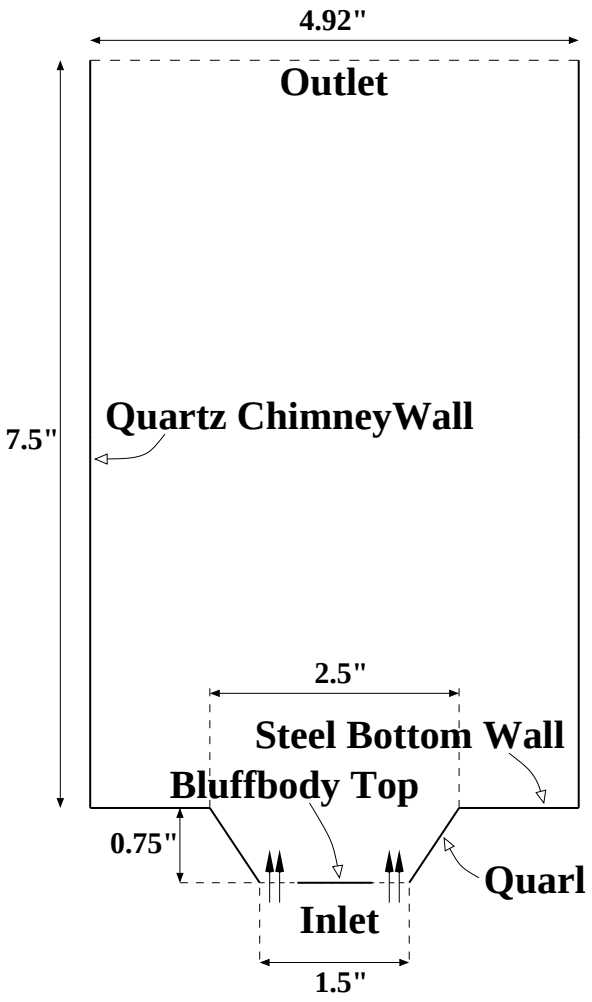

Figure 5: LES computational domain

(which is a reflecting boundary with $p' = 0$) will be dampned by the flame front, in effect eliminating any outgoing waves at the computational inlet. Kaufmann et al. [9] have shown that unless outgoing waves at the computational inlet are eliminated from the forcing, accurate transfer functions can not be obtained. Since a large acoustic impedence is present at the flame front, we are assuming there are no outgoing waves present at the computational inlet.

The LES computation has been performed for an adiabatic case, which means all walls of the computational domain (including the bluffbody top) have been assumed to be insulated. The outlet is at atmospheric pressure (pressure node $\Rightarrow p' = 0$) and at the inlet a combination of mean and fluctuating velocities have been imposed. Since the computational inlet is way downstream of the swirler section of the actual geometry, mean flow velocity profiles at the computational inlet can not be assumed without knowledge of the mean flowfield in the actual combustor geometry. Therefore, hot-wire anemometry has been used to measure mean flow axial, radial and tangential velocities at the computational inlet plane location inside the experimental setup. Mean velocity profiles for a total flow rate of $20\,SCFM$ and a geometric swirl number, S_G of 1.19 were recorded and are shown in Figures 6, 7 and 8.

Since the CFDRC code did not have an option for specifying a subgrid scale turbulent kinetic energy profile at the inlet, a mean value of $0.1\,m^2/s^2$ obtained from the subgrid scale turbulent kinetic energy profile (shown in Figure 9) was specified. This assumption is not very accurate and most probably affects the shape of flame making it less compact. Also, instead of using the axial inlet velocity profile, a mean value of $7\,m/s$ was specified. Sum of twenty sine waves with frequencies ranging between $25\,Hz$ and $750\,Hz$ have been included in the fluctuating velocity component. The following equation shows time dependent axial velocity specification at the computational inlet:

$$u = \bar{u} + u' = \bar{u}\left\{1 + 0.1\left[\sin(2\pi f_1\, t) + \sin(2\pi f_2\, t) + \cdots + \sin(2\pi f_{20}\, t)\right]\right\} \qquad (1)$$

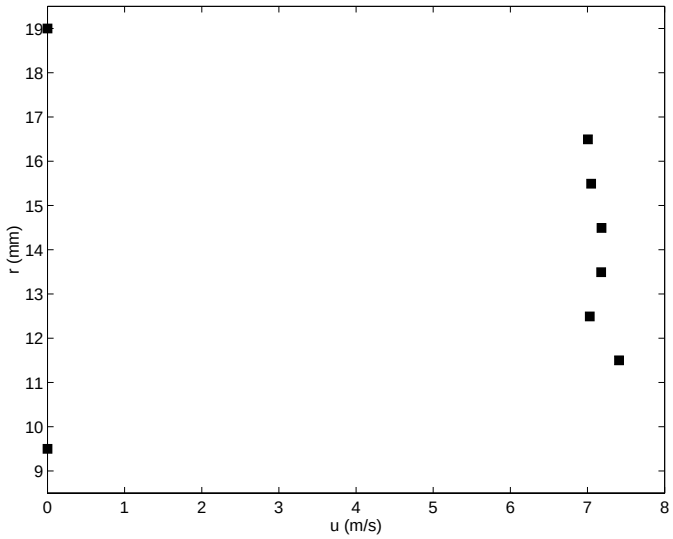

Figure 6: u velocity profile at the computational inlet

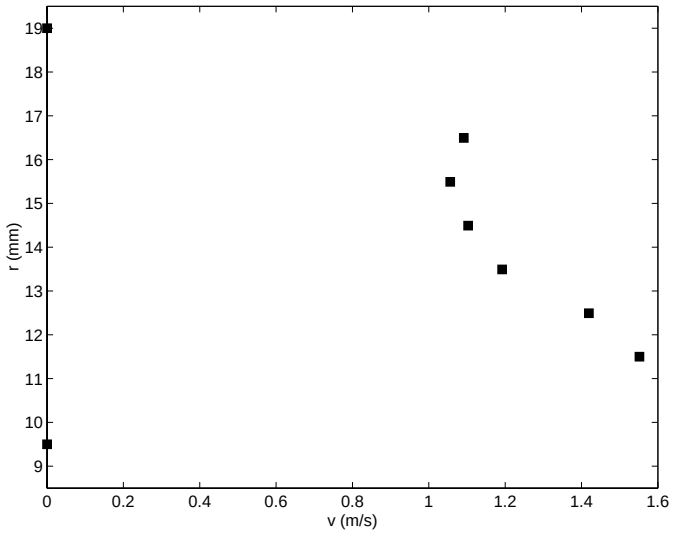

Figure 7: v velocity profile at the computational inlet

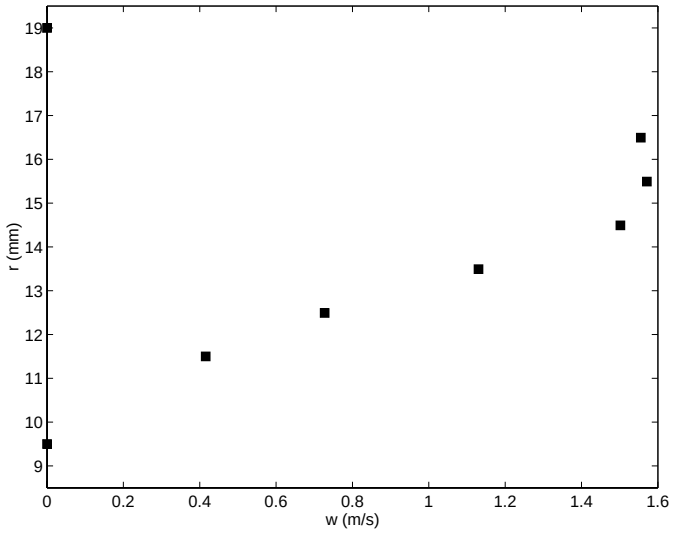

Figure 8: w velocity profile at the computational inlet

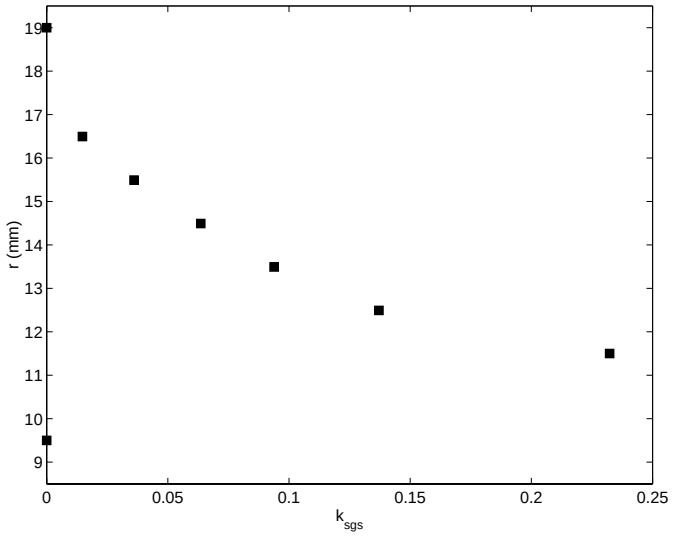

Figure 9: k_{sgs} profile at the computational inlet computed using u, v and w values

The fluctuating component (u') has been set to be 10% of the mean velocity ($\bar{u}$) and the frequencies f_1 to f_{20} lie between values of $25\,Hz$ and $750\,Hz$. A premixed methane-air mixture of equivalence ratio, $\Phi = 0.75$ has been also imposed at the inlet. There are no flucutations in equivalence ratio present in the computations.

2.3 Modeling Parameters

The LES computations have been done on a 2-D axi-symmetric grid, so as to reduce computation time. Full 3-D computations were planned originally, but have not yet been performed because of lack of computational resources. The 2-D axi-symmetric computations can be justified because the flame structure observed in the experimental setup is axi-symmetric. While performing the computations on the 2-D axi-symmetric domain, it was brought to our notice that during the alpha testing phase, 2-D axi-symmetric results showed inaccuracies. The problem was attributed to the lack of artificial viscosity in the LES code and velocity calculations near the axis were found to be inaccurate. We did not observe any such anomalies in our results and therefore, this approach was not abandoned in favor of 2-D/3-D computations.

2.3.1 Flowfield Modeling

The axi-symmetric solver was used with a time step size of $1 \times 10^{-4}\,s$ and the Crank-Nicolson 2nd order accurate time integration scheme was applied. The time step size was chosen based on the Kolmogorov time-scale $(\nu/\epsilon)^{1/2}$. The Kolmogorov time scale was estimated by running a steady state RANS case using a single-step chemistry model. From the RANS results, the R grid factor was also calculated and was found to be less than 1 for almost all of the computational domain, except at the inlet section where small patches of higher values of the grid factor were observed to occur. These patches (with $R \leq O(10)$) were seen to occur randomly over the quarl inlet section of

the domain, however running the RANS solver for several thousand iterations resulted in fewer occurrence of the patches.

In the flow modeling panels of the code, the swirl option was chosen and the reference pressure was kept at $101,325\,N/m^2$. Six iterations per time step with a convergence criteria of 10^{-4} kept the computation time per time step very low (of the order of $12\,s$ on a dual Athlon $2\,GHz$ machine with $2\,GB$ RAM). The 2nd order limiter spatial discretization scheme was used for velocity, turbulence, enthalpy and species whereas central differencing was used for density spatial discretization. A blending factor of 0.1 was used for each of the discretization schemes. The AMG solver has been used for each of the variables. Density was modeled as an ideal-gas, viscosity using the mixture Sutherland's law, specific heat using the mixture JANNAF method, thermal conductivity by specifying the Prandtl number to be 0.707 and mass diffusion modeled by specifying the Schmidt number to be 0.7. The localized dynamic kinetic energy model (LDKM) was used to model the sugrid scale stresses. This model was preferred over the Smagorinsky model because even though LDKM is equally computationally expensive, it provides better estimation of the subgrid stresses as compared to the Smagorinsky model.

The solution was initialized by assuming air-fuel mixture to be present in the quarl section and air to be present in the downstream dump section. High temperature was patched in the immediate downstream of the quarl section for ignition.

2.3.2 Chemistry Modeling

Although curve fit mechanisms are known to produce good estimations of the laminar flame speed, for dynamic modeling of the flame (especially while finding the flame response function, FRF) they are not able to capture the flame dynamics accurately. Therefore, reduced reaction models which have been tuned for modeling premixed flames need to be used. The 19 species 15 reactions methane-air model by J. Y.

Chen which is built into the CFDRC code, has been chosen to model chemistry in the CFD analysis. This model, apart from being tested in other validation cases for premixed flame modeling, also includes radicals and minor species like OH and $HCHO$, which are useful in making an estimate of the heat release rate from the combustion process and are particularly useful for validation against experimentally obtained PLIF results.

The turbulence-chemistry interaction modeling is one of the most important aspects for modeling acoustic-flame interactions. Therefore, the subgrid linear eddy model (LEM) has been chosen based on a literature survey which proved LEM's capability of modeling turbulence-chemistry interactions in unsteady reacting flows. It was known prior to the beginning of the beta testing that LEM will prove to be computationally expensive, but the decision of opting for 2-D axi-symmetric modeling eased some of the computational restriction associated with the model. Also, since there were no benchmarks available in literature for the mixture fraction/PDF method in unsteady acoustic-flame interaction modeling, LEM seemed to be the only option left (there is considerable amount of literature available for "dynamically thickened flame model" and the BML model applications in modeling acoustic-flame interactions though).

3 Results and Discussion

The results section has been divided up into two subsections. In the first section, the reacting flowfield structure has been discussed and time averaged contour plots of velocities, temperature and species have been shown. The second subsection showcases the response of the flame to the imposed unsteady velocity perturbations. All results included in this section are for a flow rate of $20\,SCFM$, geometric swirl number (S_g) of 1.19 and $\Phi = 0.75$.

3.1 Reacting Flowfield Structure

Real time data obtained from the LES code was analyzed to obtain time-averaged profiles of velocities, temperature and species mass fractions. Time averaging was carried out for $2\,s$ of data (with a sampling rate of 10,000) for the flow variables. Time averaged velocities and temperature contours are shown in Figure 10. From the figure, it can be noted that the overall structure of the flame has been captured, including the inner and outer recirculation zones (as can be seen in the u velocity contours plot). As expected, the temperature at the inner recirculation zone is high compared to the outer recirculation zone. This high temperature recirculating fluid in the inner recirculation zone is responsible for the constant ignition of the fresh incoming air-fuel mixture. It should be noted that the time averaged v velocity shows an irregular contour pattern inside the quarl, indicating an unsteady process happening at that location. The swirl component of velocity (w) shows a decay from the inlet to the mid-combustor region. Swirl is the highest inside the quarl.

Figure 11 shows the contours of time averaged CH_4, O_2, CO_2 and H_2O mass fractions. The CH_4 mass fraction contours indicate that all the fuel is burnt just downstream of the combustor inlet plane. The actual swirl number (S) is approximately 0.27 and therefore the flame shows less compactness compared to higher swirl number flows. The contours of O_2, CO_2 and H_2O indicate some recirculation at the outlet plane. The recirculation observed in the data has not been validated against experimental observations.

An unsteady phenomena has been observed to occur in the combustion process. Figures 12, 13, 14 and 15 indicate the presence of vortex shedding inside the quarl section. Each of the figures include 10 plots of instantaneous contours of u, v, w velocities and temperature. Each plot corresponds to $\pi/5$ angle for one cycle of the vortex shedding (time difference between each plot is $4 \times 10^{-3}\,s$). By performing a spectral analysis, the vortex shedding frequency was estimated to be approximately $255\,Hz$. The vor-

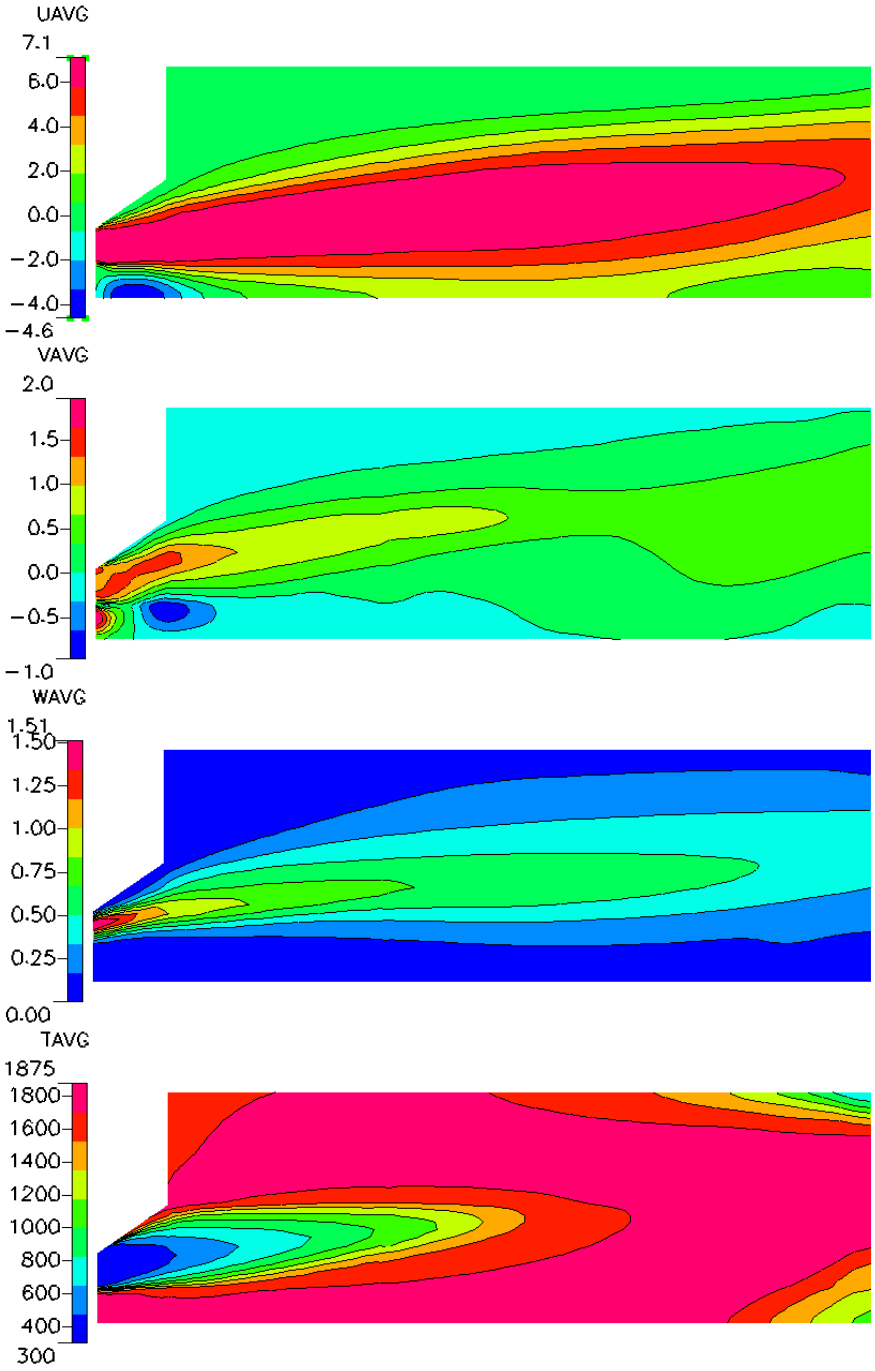

Figure 10: Contours of time averaged u, v, $w\,(m/s)$ and temperature (K)

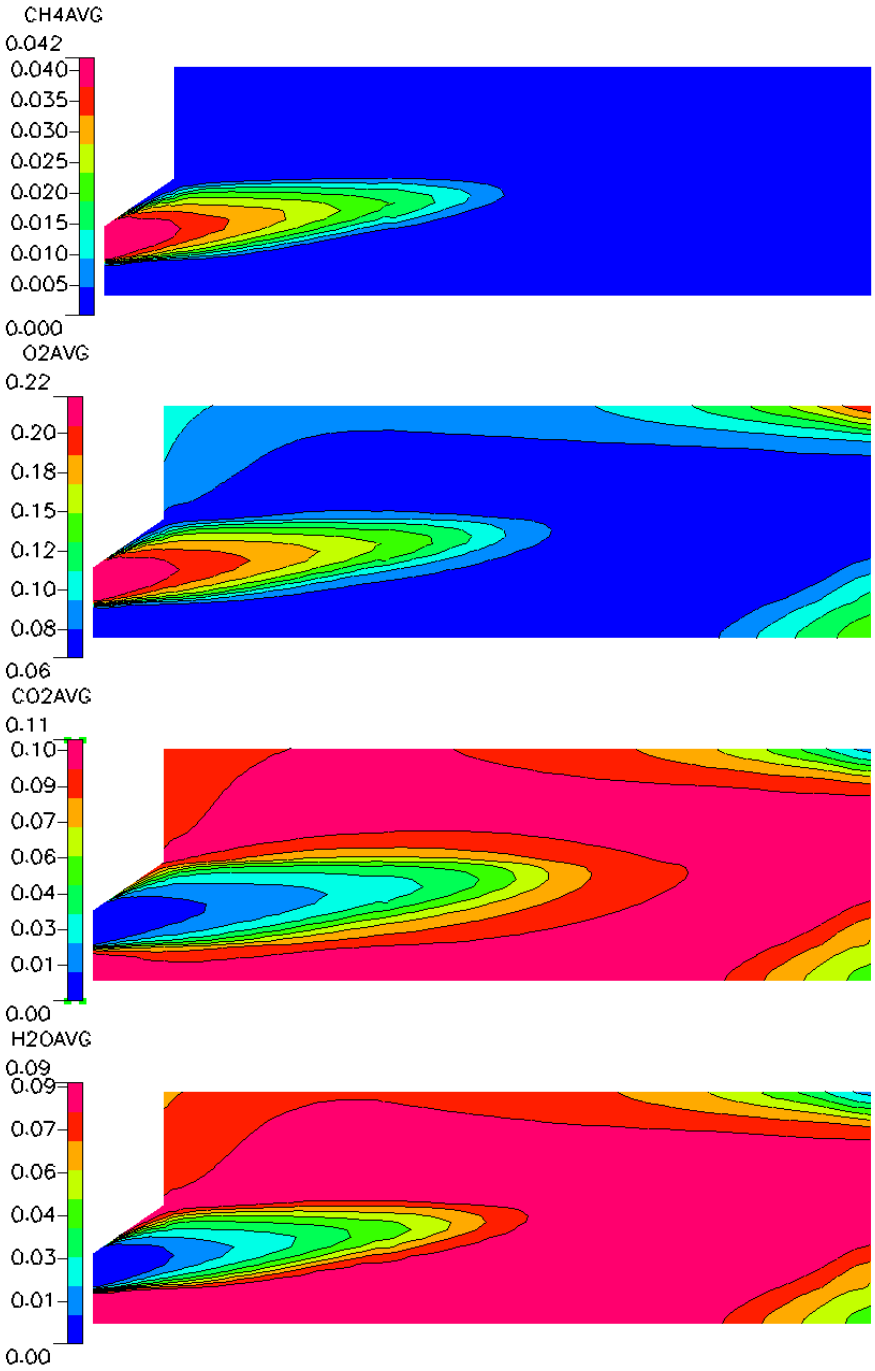

Figure 11: Contours of time averaged mass fractions of CH_4, O_2, CO_2 and H_2O

tex shedding phenomena is clearly visible in Figure 13 which shows the contours of v velocity. The swirl velocity also indicates the presence of vortex shedding, although the radial velocity is a much more clear indicator. The temperature contours in Figure 15 show that the flame shape itself is changing as the vortex passes through the flame every $4 \times 10^{-3}\, s$. This vortex shedding phenomena was not observed in the experimental studies, although the flame surface exhibited a $275\, Hz$ azimuthal mode as seen in phase-locked CCD camera images of the flame. Basically, three alternate explanations can be given to explain this phenomena:

Acoustic waves: Both the inlet and outlet are acoustically reflecting boundaries and therefore, the unsteady phenomena which seems to be vortex shedding can actually be a wave which is getting reflected at each boundary and is creating an unsteady response from the flame while passing through it.

Vortex-flame interaction: The vortex shedding is observed to happen at the quarl walls, which is an indicator of a shear layer instability. This kind of instability is seen to occur in diffusers. In the experimental setup, the vortex shedding was not seen to occur, whereas the CFD results show the $255\, Hz$ phenomena. A possible reason for this anomaly can be attributed to the inaccurate k_{sgs} profile specification at the inlet as well as inaccuracies in the inlet boundary condition velocity profiles. The hot-wire data collection at the narrow $9.5''$ inlet plane annular duct only yielded 6 or 7 points and velocity data for these few points were then used to create the profiles. Slight inaccuracies in specifying the velocity profiles and the turbulence inlet conditions can lead to such shear layer instabilities to occur.

Flame response to azimuthal acoustic wave: Phase locked images of a $275\, Hz$ flame flapping phenomena were recorded using a CCD camera. The flame was excited by a $275\, Hz$ acoustic wave and CCD camera images were taken by phase-locking the camera with the acoustic-driver unit. While taking phase

locked images for a $100\,Hz$ excitation frequency, this "flapping" phenomena was not seen to occur. It is possible that the $275\,Hz$ frequency was always present independent of the frequency of excitation. Phase locking at $100\,Hz$ effectively eliminates any higher frequency content from the images, which means that any higher frequency content (in this case the $275\,Hz$ frequency) was not observed for the $100\,Hz$ excitation case.

A final explanation of the $255\,Hz$ phenomena observed in the CFD results can only be given after closely investigating each of the three possibilities listed above.

3.2 Excited Flame Response

Once a frozen flowfield was achieved, flow forcing at the computational inlet was imposed. Figure 16 shows the time trace of unsteady inlet mass flow rate. As can be seen from the figure, multiple frequency content in the signal are present. Since we are studying linear response of the flame to incoming mass flow rate oscillations, we can safely impose a complex mass flow signal at the inlet (our mass flow rate signal contains 20 discrete frequencies). The power spectral density (PSD) plot of the mass flow oscillations at the inlet can be seen in Figure 17. Each of the twenty frequencies are visible in the power spectrum and each one of them has the same PSD magnitude.

The imposed mass flow rate oscillations result in an unsteady response from the flame. The unsteady temperature measured at different locations in the computational domain show different levels of excitation that results from the imposed mass flow rate oscillations. Figure 18 shows the PSD of temperature at six different locations inside the combustor. The outer recirculation zone temperature does not show frequency content beyond $100\,Hz$. Since the outer recirculation zone acts like a dampner for high frequencies, the PSD does indicate a correct trend. The inner recirculation zone and the mid-combustor 1/2 diameter measurement points lie in a straight line.

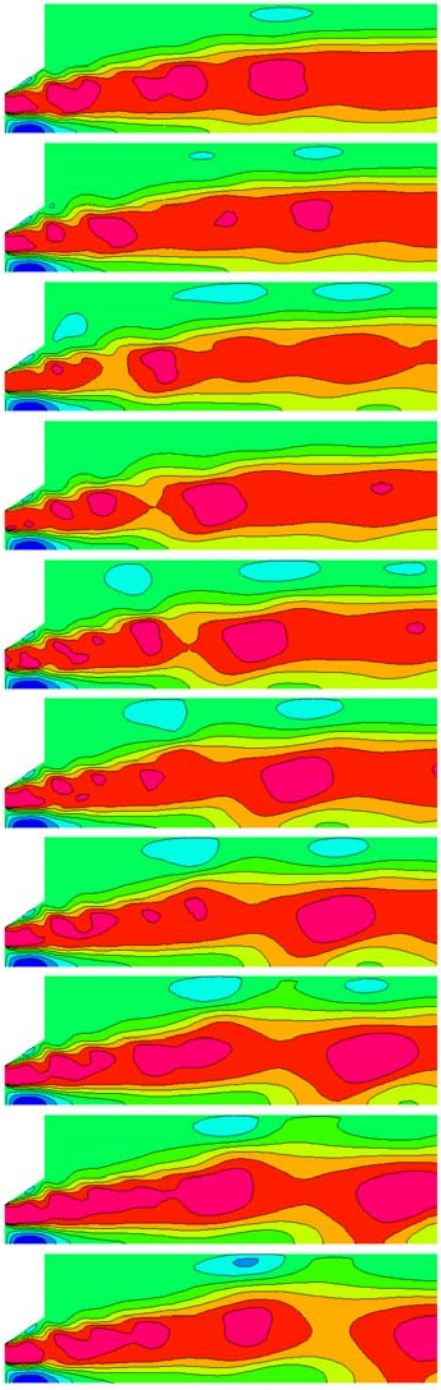

Figure 12: u velocity contours for one cycle of vortex shedding ($255\,Hz$). Each contour plot corresponds to $\pi/5$ radians increment

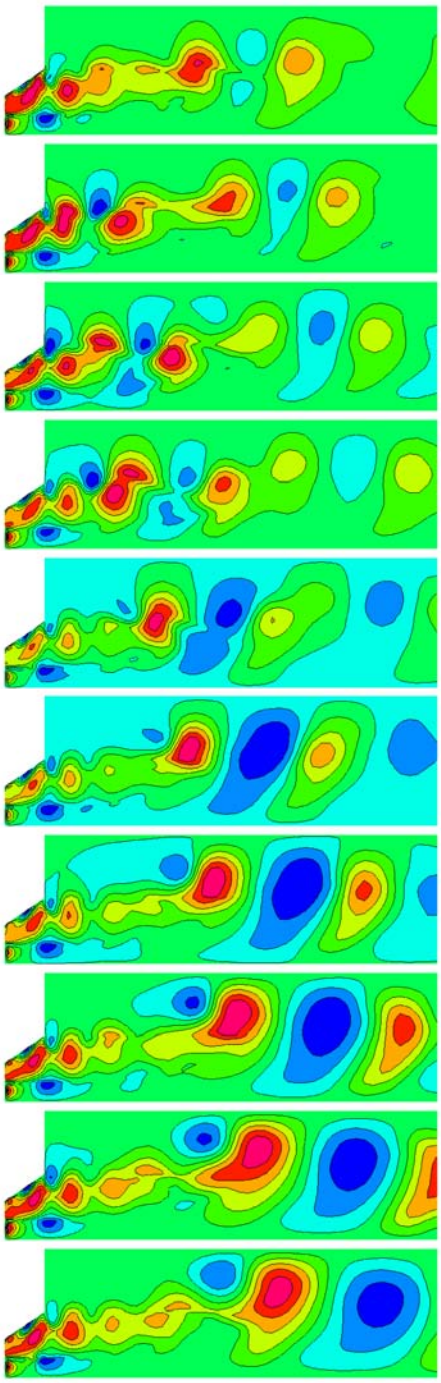

Figure 13: v velocity contours for one cycle of vortex shedding ($255\,Hz$). Each contour plot corresponds to $\pi/5$ radians increment

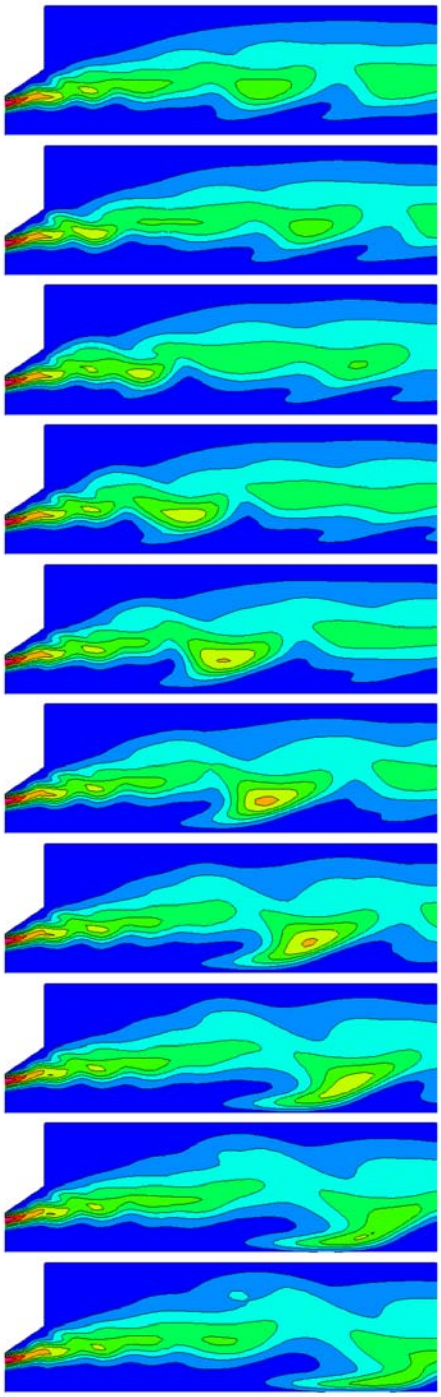

Figure 14: w velocity contours for one cycle of vortex shedding ($255\,Hz$). Each contour plot corresponds to $\pi/5$ radians increment

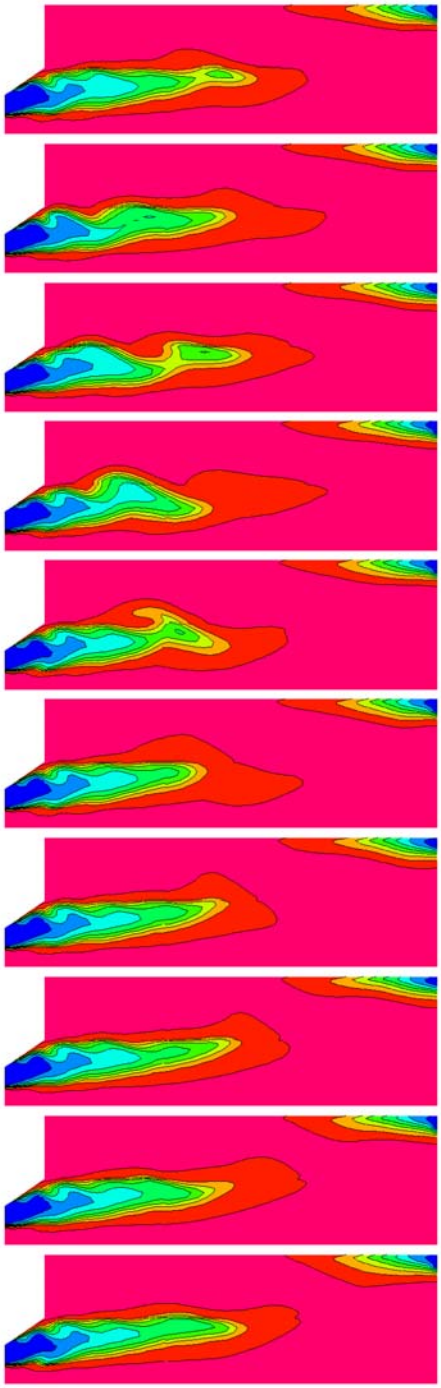

Figure 15: Temperature contours for one cycle of vortex shedding ($255\,Hz$). Each contour plot corresponds to $\pi/5$ radians increment

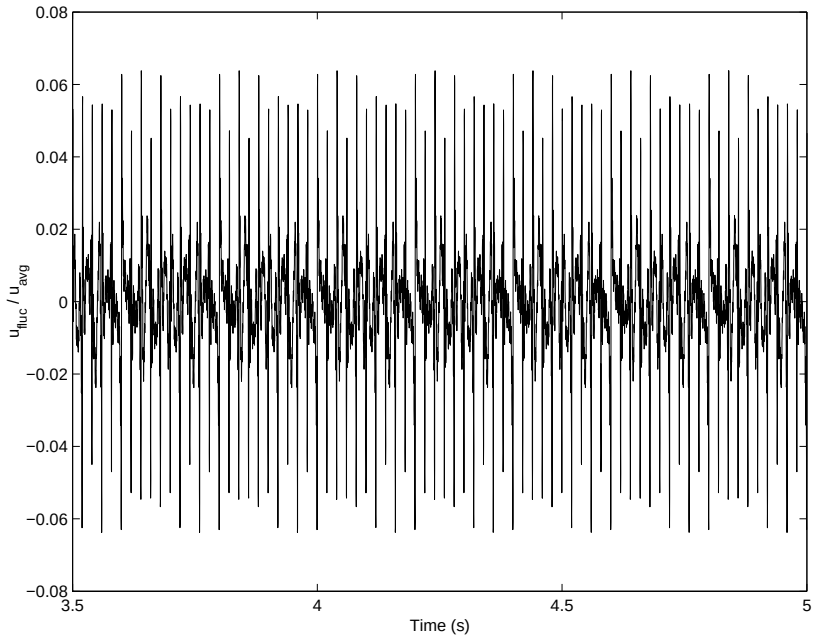

Figure 16: Time trace of inlet normalized mass flow fluctuations

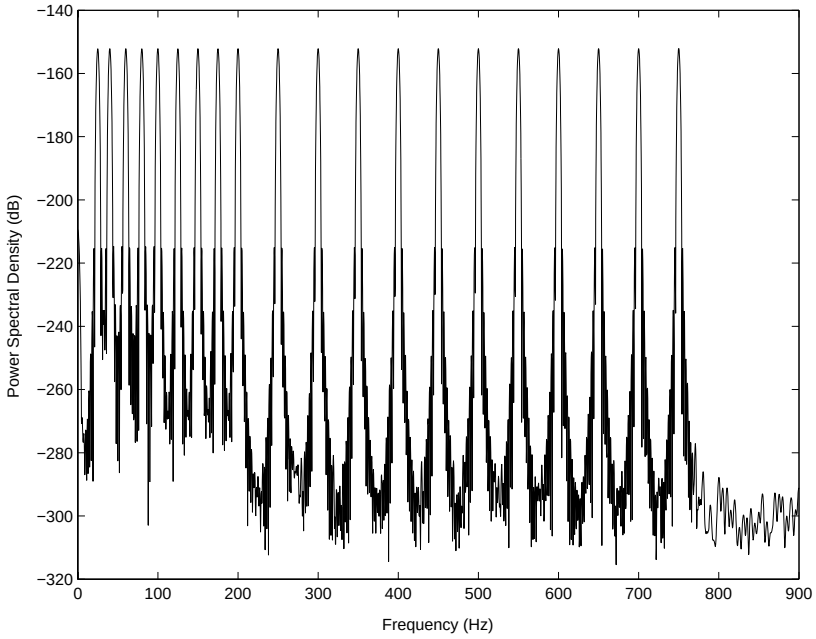

Figure 17: Power spectral density of fluctuating component of inlet mass flow rate

Therefore, it is not surprising to similar levels of PSD for each curve. Sharp peaks can be seen for the inner recirculation zone curve. These peaks are not present in the mid-combustor 1/2 diameter location because the frequencies get damped as we move downstream from the inner recirculation zone. The quarl location and the combustor inlet location both show distinct peaks for each of the frequencies of excitation. The $255\,Hz$ peak is also clearly visible for the two curves. This peak is not visible in the mid-combustor 1/4 diameter location because of of the downstream measurement location.

The main objective of this study has been the investigation of unsteady flame response due to an imposed upstream velocity perturbation. The frequency response function (FRF) or the transfer function needs to be obtained between unsteady heat release rate and unsteady velocity. This exercise has not been completed as yet because of the unexplained phenomena observed in the results. As a first estimate of the FRF, resulting temperature oscillations has been taken as the output and the inlet mass flow rate oscillations has been considered to be the input. The FRF magnitude is shown in Figure 19. The magnitude prediction is seen to follow a trend and a $40\,dB$ drop between $25\,Hz$ and $750\,Hz$ can be observed. The phase relationship between u' and T' has not been predicted correctly by the CFD model. All efforts are presently being directed toward understanding the unsteady heat release phenomena and correct phase predictions between u' and q' needs to be obtained.

4 Ongoing and Future Work

The reported data is part of an ongoing investigation at VACCG in applying CFD to create transfer functions which are to be used in reduced order modeling of the unsteady combustion phenomena. Therefore, investigation into various phenomena influencing the unsteady flame response is being continued. Presently, data is being

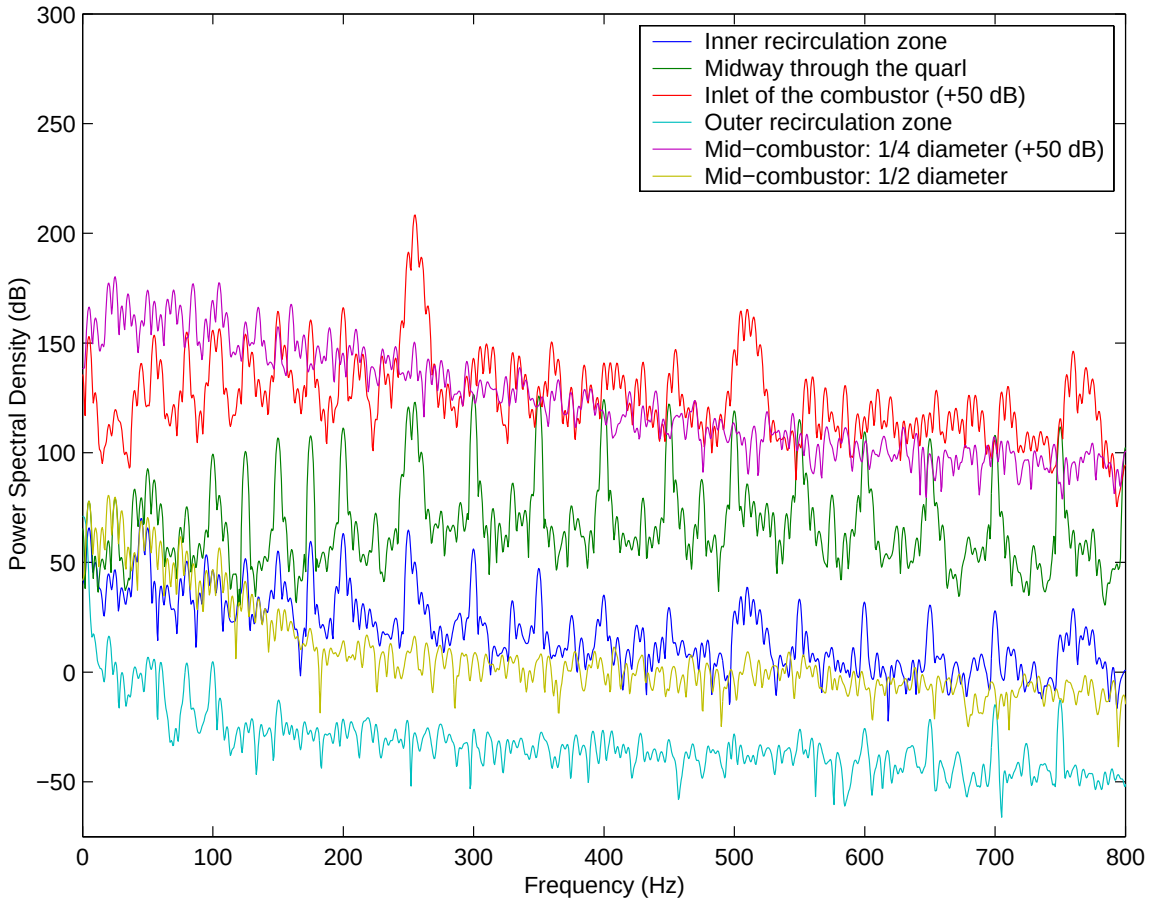

Figure 18: Power spectral density of fluctuating component of temperature at different locations inside the computational domain. The mid-combustor location (1/2 diameter) is 3.75″ downstream of the inlet plane of the combustor and lies on the centerline, whereas the corresponding mid-combustor (1/4 diameter) location is radially at a distance of 1.23″ from the centerline

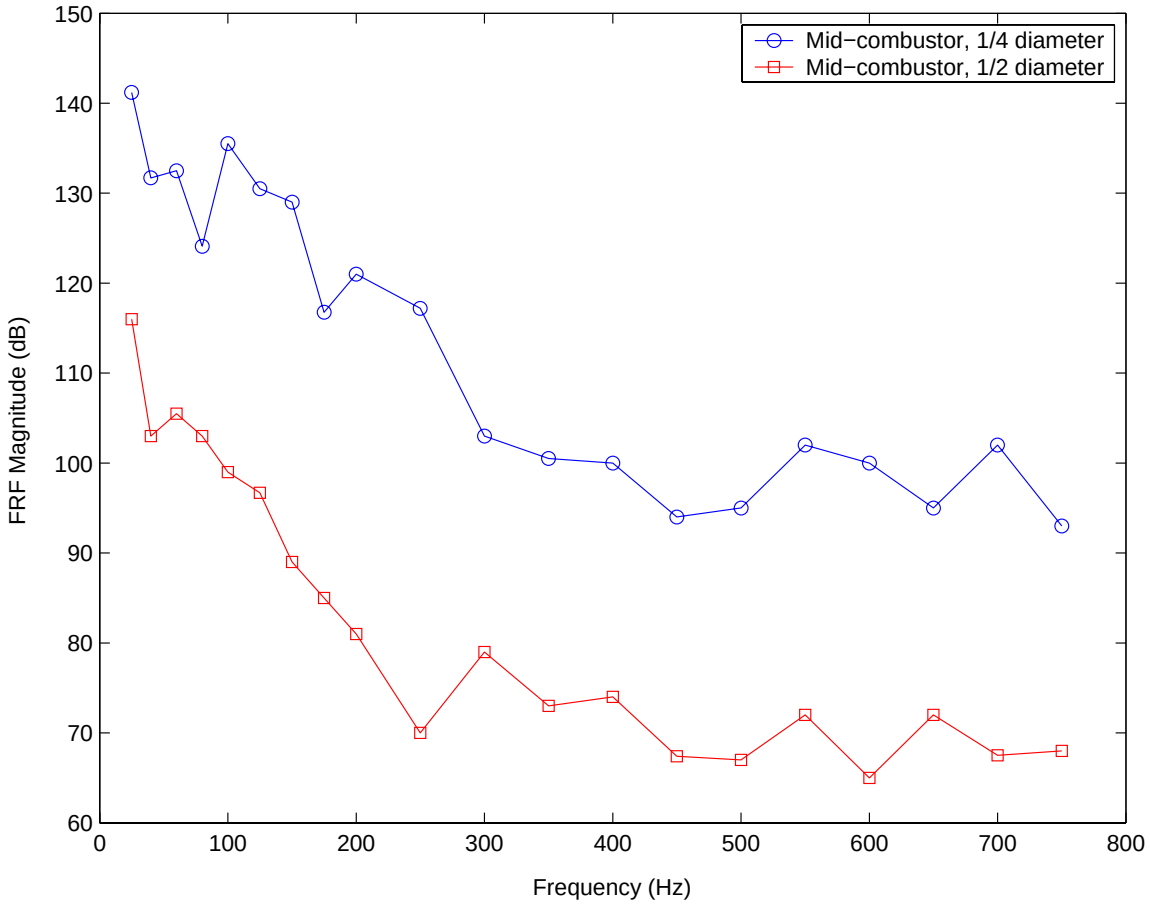

Figure 19: FRF between u' and T': magnitude shown for two locations. The mid-combustor locations were selected because these two locations are downstream of the flame and are not affected by the near-field effects such as the $255\,Hz$ phenomena

collected for the swirl combustor using the CFDRC LES code and FRF between area integrated heat release rate and velocity perturbation will be calculated subsequently.

The following issues will be addressed in the coming months:

1. Non-reflecting inlet boundary condition will be implemented. This implementation may lead us to produce accurate FRFs (particularly the phase information between u' and q'.

2. Comparisons between unsteady temperature measurements inside the experimental combustor and predicted values from the CFD results will be undertaken (experimental studies currently ongoing).

3. Investigation into the $255\,Hz$ phenomena is of high priority. Changes in the inlet boundary condition (including increasing the swirl number) will be undertaken.

4. A change in diffuser angle and the resulting effect on the vortex-shedding phenomena inside the quarl will be investigated.

5. The inlet boundary location and the effect of the downstream conditions on the inlet boundary condition will be investigated.

References

[1] G. J. Bloxsidge, A. P. Dowling, and P. J. Langhorne. Reheat buzz: An acoustically coupled combustion instability. part 2. theory. *Journal of Fluid Mechanics*, 193:445–473, 1988.

[2] A. P. Dowling. Nonlinear self-excited oscillations of a ducted flame. *Journal of Fluid Mechanics*, 346:271–290, 1997.

[3] K. McManus, T. Poinsot, and S. Candel. A review of active control of combustion instabilities. *Progress in Energy and Combustion Science*, 19:1–29, 1993.

[4] M. Fleifil, A. M. Annaswamy, Z. Ghoniem, and A. F. Ghoniem. Response of a laminar premixed flame to flow oscillations: A kinematic model and thermoacoustic instability result. *Combustion and Flame*, 106:487–510, 1996.

[5] P. Chatterjee. Computational fluid dynamics studies of premixed laminar and turbulent combustion dynamics. PhD Dissertation Proposal, 2002.

[6] M. M. Ribeiro and J. H. Whitelaw. Coaxial jets with and without swirl. *Journal of Fluid Mechanics*, 96:769–795, 1980.

[7] C. G. Speziale. *Simulation and Modeling of Turbulent Flows*, chapter Modeling of Turbulent Transport Equations. Oxford University Press, New York, 1996.

[8] T. Poinsot and D. Veynante. *Theoretical and Numerical Combustion*. RT Edwards, Philadelphia, 2001 edition, 2001.

[9] A. Kaufmann, F. Nicoud, and T. Poinsot. Flow forcing techniques for numerical simulation of combustion instabilities. *Combustion and Flame*, 131:371–385, 2002.

[10] Fluent Inc. *Lebanon, NH*.

[11] T. Schonfeld and M. Rudgyard. Steady and unsteady flow simulations using the hybrid flow solver AVBP. *AIAA Journal*, 37(11):1378–1385, 1999.

APPENDIX E

Rolls Royce Final Report

Executive Summary

Rolls-Royce is part of the Industry Consortium that CFD Research Corporation (CFDRC) put together for their program with the Department of Energy (DOE) under their Vision 21 initiative. The objective of the program is to develop a combustor flow analysis software, based on Large Eddy Simulation (LES) methodology to analyze combustion instabilities. The role of Rolls-Royce has been to advise and provide feedback on the development activities through annual meetings hosted by CFDRC, as well as to beta-test and provide feedback on the LES software in the third (and final) year of the program.

This report summarizes the beta-testing of the CFD-ACEU code developed by CFDRC, with the application of the code for LES of swirling flames. Two flow configurations were considered, SMA2: Methane/Air fuel issuing into swirling air, and SMH1: Methane/Hydrogen fuel issuing into swirling air. The burner itself is located in an air co-flow. Since detailed velocity and scalar measurements are available, the two configurations have been studied extensively using Reynolds Averaged Navier-Stokes Simulations (RANS), summarized in proceedings of the bi-annual Turbulent Non-premixed Flame (TNF) workshop. However, the number of reported LES studies of SMA2 and SMH1 has been limited. The two flow configurations, although geometrically simple, are challenging test cases for LES.

This report presents a detailed overview of the steps involved in simulating the two flames. The study showed that CFD-ACEU was able to successfully anchor the flame in SMA2. However, LES showed a different flame structure as compared to RANS. Simulations of SMH1 did not show a stable flame. LES calculations of a gas turbine combustor were also intended. However, due to lack of time, this could not be performed. In light of the results obtained in the present work, further validations of the predictive capability of the LES methodology implemented in CFD-ACE have to be undertaken. Nevertheless, the code is simple to use and quite user friendly for setting up new cases.

Table of Contents

List of Illustrations

1. Introduction

Rolls-Royce is part of an industry consortium set up by CFD Research Corporation (CFDRC), with support from the Department of Energy under its Vision 21 initiative, to review the development of a large eddy simulation (LES) code. The main tasks of consortium members are to review and provide feedback on the progress of the LES development effort and to beta-test the developed code. This report summarizes the beta-testing effort to evaluate CFDRC's LES code, CFD-ACEU, for simulation of turbulent reacting flows.

LES is uniquely suited for predicting turbulent reacting flows since it is well known that turbulent mixing is better predicted by LES than Reynolds Averaged Navier Stokes Simulations (RANS). Accurate prediction of turbulent mixing is critical for high fidelity simulations of reacting fields. This report presents an overview on application of the CFD-ACEU code for LES of swirling flames. Two flow configurations are considered, SMA2: Methane/Air fuel issuing into swirling air, and SMH1: Methane/Hydrogen fuel issuing into swirling air. The burner itself is located in an air co-flow. Since detailed velocity and scalar measurements are available (www.ca.sandia.gov/TNF), the two configurations have been studied extensively using Reynolds Averaged Navier-Stokes Simulations (RANS), summarized in proceedings of the bi-annual Turbulent Non-premixed Flame (TNF) workshop [www.ca.sandia.gov/TNF]. However, the number of reported LES studies of SMA2 and SMH1 has been limited. The two flow configurations, although geometrically simple, are challenging test cases for LES. Also, these cases present a unique opportunity to test the advanced linear-eddy model (LEM) in CFD-ACEU. This report presents simulations of the two swirl burners using CFD-ACEU. It was intended to also include the simulation of a gas turbine combustor as part of the beta-testing depending on time. However, due to lack of time, this could not be attempted.

2. Geometry Modeling

Burner Geometry

The burner, shown in Figure 1, consists of a solid ceramic-faced cylinder measuring 50 mm in diameter that houses the fuel jet and acts as a bluff body for the swirling flow issuing from the narrow annulus that surrounds it. The annular tube is hollow and 60 mm in diameter. It is fed by three jets injecting flow tangentially. The two nested cylinders are mounted in a 130-mm box with air flowing through it more slowly than from the jet and swirling annulus. This box is identified as a co-flow.

Computational Domain and Boundary Conditions

For simplicity and speed, the computational spatial domain begins at the exit plane of burner and ends 600 mm downstream, simplifying the combustor's geometry to boundary conditions at the inlet plane. The inlets among these boundary conditions (jet, swirler and co-flow) were approximated as uniform in space even though profiles were available for them from experimental measurements. The version of the code at Rolls-Royce does not have the feature to specify profiles. The central bluff body is ceramic and its temperature was roughly measured in the experiments. As its specific heat is high and conductivity is low, this face was approximated by an isothermal wall set near the published temperature.

The flow solution was carried out on a structured multiblock grid decomposed into 20 processor domains in the x-direction (Figure 2). The grid for the system is shown in Figure 3 through Figure 5. It is a structured concentric H-grid of 90 x 90 x 80 cells with points distributed by feature as shown in Table 1 and illustrated in Figure 4. The points are distributed uniformly in the *x*-direction. The Rolls-Royce in-house grid generator CHILI (Concentric H-grids by Interpolating Liner Interiors) generated the grid, which holds concentric rings of H-topology at the burner face (Figure 4) and linearly relaxes them to a uniform orthogonal H-grid at the burner exit (Figures 3 & 5). The commercial GRIDGEN software was used to decompose the grid into 13 blocks as needed for ease in applying uniform boundary conditions.

CFD-GUI was the software environment for applying boundary conditions, initial conditions and specifying solution methods and numerical parameters. All solution data including grids, boundary and initial conditions, properties and reactions, solver numerical settings and problem parameters are stored along with solution data in a large comprehensive file in CFDRC's Data Transfer Format (DTF). A command-line utility was used to decompose the multiblock domain further into 20 processor zones as seen in Figure 2. The parallel decomposition is along the i-coordinate and places 32400 cells in each processor zone.

The inflow boundary conditions, listed in Table 2, are uniform approximations to experimentally measured profiles. Note that in SMH1, the fuel is a mixture of methane and hydrogen and in SMA2; the fuel is a mixture of methane and air. Also the swirl number (defined here as the ratio of tangential annular velocity to axial annular velocity) is lower in SMH1.

3. Burner SMA2

The fuel in SMA2 is a mixture of natural gas and air; hence a one-step methane-air reaction mechanism was used to model the chemical reaction. The reaction mechanism and the corresponding rate parameters are listed in Table 3. The steps involved in simulating this burner are:

1. Running a RANS calculation first with low-reaction rates and with an ignition source until a flame is established.

2. Running a RANS calculation again using the solution in 1 above as a restart, removing the ignition source and reverting the rates to the actual values.

3. Using the solution from the run in step 2 as a restart for an LES simulation.

All calculations were performed using a two-variable presumed PDF model. A beta PDF was used for the mixture fraction, while a tridelta PDF was used for the reaction progress variable.

Figure 6 presents temperature field from the transverse mid-plane of the computational domain from step 2 above. The turbulent model used in the RANS calculation is the RNG k-e model. Note the asymmetry in the temperature field indicating unsteadiness of the flowfield in the simulation. This simulation was then used for performing LES. LES was performed using the localized dynamic model with constant coefficients. The time-step used in the simulation was 1E-05 s. At each time-step the solver performs 10 iterations to converge the residual values. Figure 7 presents the temperature field after 900 time-steps. Note that the flowfield has not fully developed yet. However, the flame appears to be anchored at the base of the burner. The formation of large-scale structures is also visible. Figure 9, presents the temperature field after 4700 time-steps. Note that the flame structure is significantly different than that in the RANS simulation (Figure 6). Exact cause of the differences is under investigation. It should be mentioned that the simulation is still in progress.

4. Burner SMH1

Burner SMH1 involves a fuel that is a mixture of methane and hydrogen. Hence, a one-step chemistry mechanism in conjunction with the presumed PDF model cannot be used for the simulation of this burner. Instead, the method that is recommended is to use a reduced chemistry (5-step, 9 species) mechanism in conjunction with laminar chemistry or linear-eddy turbulent combustion model (LEM). The laminar chemistry method uses the least amount of time as compared to LEM and therefore was the method adopted for the present simulations.

The procedure to perform a reacting LES simulation of this configuration was as follows.

1. Perform a non-reacting RANS simulation with the full 9 species.

2. Using 1 above, perform an unsteady RANS with reaction mechanisms all turned on.

3. Using 2 above, perform an unsteady RANS, but with the bluff body temperature increased to 3000 K, which acts as an ignition source.

4. Once reaction has established in 3 above, remove the ignition source and perform an unsteady reacting RANS.

5. Use restart file from 4 above to launch an LES run.

The simulation in step 3 did not show any reaction despite the presence of ignition source. Even, when the temperature of the bluff body was increased to 10000 K, no reaction was observed. Thus, a successful LES for this case could not be performed. Further investigation of the chemistry mechanism/laminar chemistry model is necessary to determine why this case did not show a flame.

Figure 9 presents a close-up plot of the velocity vector field from the unsteady RANS run. The recirculation zone over the bluff body and swirler is easily seen as well as the strong inlet fuel jet. Secondary recirculation in the shear layer between the jet and the inflow of the main recirculation zone is also visible. The jet carries high momentum and is not penetrated or broken up by the swirler and the bluff body's wake.

Figure 10 presents a close-up of the contours of species mass fraction. Classical diffusion jet structure prevails and is not substantially affected by the surrounding swirl and recirculation zones.

The transport of enthalpy from the hot bluff body was observed to be problematic. A steady RANS run with the bluff body temperature of 10000 K showed very slow transport of enthalpy into the flow domain. At convergence, which is achieved by 600 iterations, most primitive variables showed residual values around 1.0E-5. However, enthalpy residual was only 1.0E-1.

5. Code Use and User Feedback

Several issues were encountered during the course of this work. These are summarized below.

1. One of the main problems encountered was the difficulty in performing a reacting RANS calculation directly without lowering the reaction rates and/or performing non-reacting runs first.

2. For SMH1, several attempts were made to establish a flame in the simulation, without any success.

3. Presently, the only subgrid model recommended is the presumed PDF model, which, however cannot be used for SMH1.

4. Another issue was naming convention for mixture fraction. When the mixture was given the name 'fuel', the code did not yield correct results.

5. It has been observed from RANS simulations that the transport of enthalpy from the hot bluff body into the flowfield is rather slow. At convergence, the residual values for enthalpy are significantly higher than those for other primitive variables.

6. Specifying reference pressure instead of absolute pressures at all boundaries caused the code to diverge. This issue needs to be addressed.

7. When loading a multiblock domain, it was noticed that CFD-GUI would (sometimes) attach wall boundary condition to interblock faces.

8. Significant differences are seen in the RANS and LES flame structures in SMA2. LES show significantly higher temperatures near the far end of the computation domain.

9. Problems with coding of the reduced mechanism in the software were encountered and later fixed. License expired issues on the intel cluster were encountered periodically.

10. The CFD-GUI is quite user friendly and can be easily used to set up a simulation. CFD-VIEW was also found to be adequate in visualizing simulation results.

11. The DTF utility was found to be quite handy in splitting domains and quickly changing key parameters in the simulation.

5. Conclusions and Future Steps

This work presents an overview on application of the CFD-ACEU code for large eddy simulations (LES) of swirling flames. This work was performed by Rolls-Royce as a member of the industry consortium set up by CFDRC in support of their development of an LES code. Two flow configurations were considered, SMA2: Methane/Air fuel issuing into swirling air, and SMH1: Methane/Hydrogen fuel issuing into swirling air. The burner itself is located in an air co-flow. The two flow configurations, although geometrically simple, are challenging test cases for LES. This report presents a detailed overview of the steps involved in simulating the two flames. The study showed that CFD-ACEU was able to successfully anchor the flame in SMA2. However, significant differences were observed between RANS and LES simulations. Simulations of SMH1 did not show a stable flame. Even by providing a high temperature at the bluff body face, the flame was not established. In light of the results obtained in the present work, further validations of the predictive capability of the LES methodology implemented in CFD-ACE needs to be undertaken. Nevertheless, the code is simple to use and quite user friendly for setting up new cases.

Block Number	Feature at Block Inlet	Number of I Points	Number of J Points	Number of K Points	Cells on Burner Face	Number of Cells
1	Co-Flow	81	21	91	1800	144 000
2	Co-Flow	81	57	18	952	76 160
3	Co-Flow	81	15	91	1260	100 800
4	Swirler Annulus	81	6	57	280	22 400
5	Co-Flow	81	57	18	952	76 160
6	Swirler Annulus	81	47	6	230	18 400
7	Swirler Annulus	81	6	57	280	22 400
8	Bluff Body	81	47	21	920	73 600
9	Swirler Annulus	81	47	6	230	18 400
10	Bluff Body	81	21	7	120	9600
11	Bluff Body	81	47	21	920	73 600
12	Fuel Jet	81	7	7	36	2880
13	Bluff Body	81	21	7	120	9600
Swirler Faces	Fuel Jet Faces	Bluff Body Faces	Co-Flow Faces			
1020	36	2080	4964		Total Cells	648 000

Table 1. Grid and Feature Summary

Case	CH_4 Mass Fraction	Air Mass Fraction	H_2 Mass Fraction	Bulk Jet Velocity (m/s)	Bulk Swirler Axial Velocity (m/s)	Bulk Co-Flow Velocity (m/s)	Inlet Temp (K)	Swirl Number
SMH 1	0.8884	0.0	0.1116	140.8	42.8	20.0	293.0	0.32
SMA 2	0.216	0.784	0.0000	66.0	16.26	20.0	293.0	1.59
Case				Bulk Jet Turbulence KE (m^2/s^2)	Bulk Swirler Turbulence KE (m^2/s^2)	Bulk Co-Flow KE (m^2/s^2)		
SMH 1				6.00	3.00	1.69		
SMA 2				18.00	15.78	1.95		
Case				Jet Turb Dissipation Mixing Length (m)	Swirler Dissipation Mixing Length (m)	Co-Flow Dissipation Mixing Length (m)		
SMH 1				0.00036	0.00600	0.00600		
SMA 2				0.00036	0.00600	0.00600		

Table 2. Swirl Burner Inflow Conditions

1-step global reaction mechanism for methane CH4 + 2O2 -> CO2 + 2H2O + 0H + 0O + 0OH + 0H2 + 0CO					
A_p	p	n	E_a/R	Concentration Exponents	
2.05E+13	-0.2	0	30 000	0.2	1.3

Table 3. One-step Methane Mechanism for SMA2 Simulation

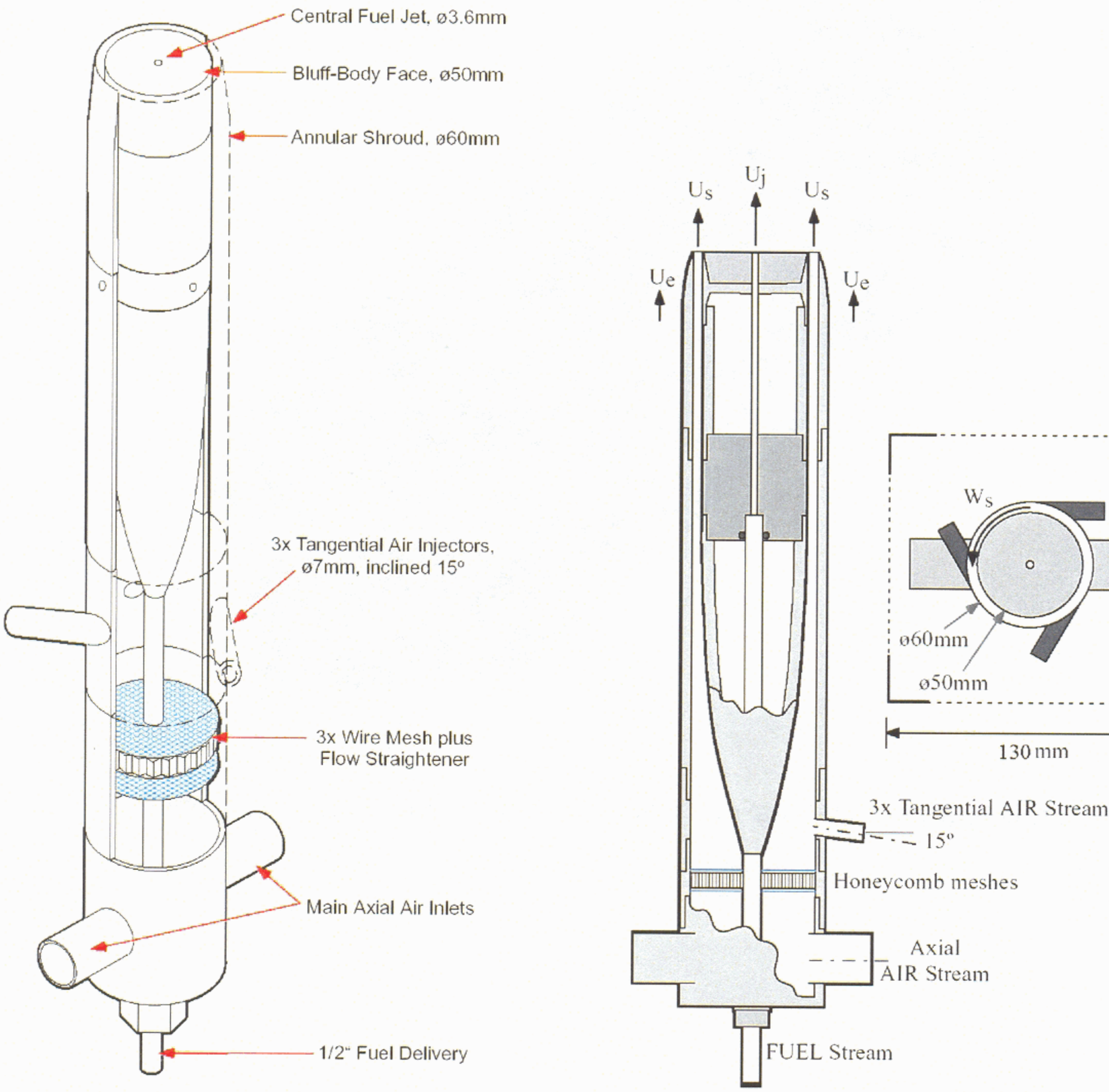

Figure 1. Sandia/Sydney TNF-6 Swirl Burner

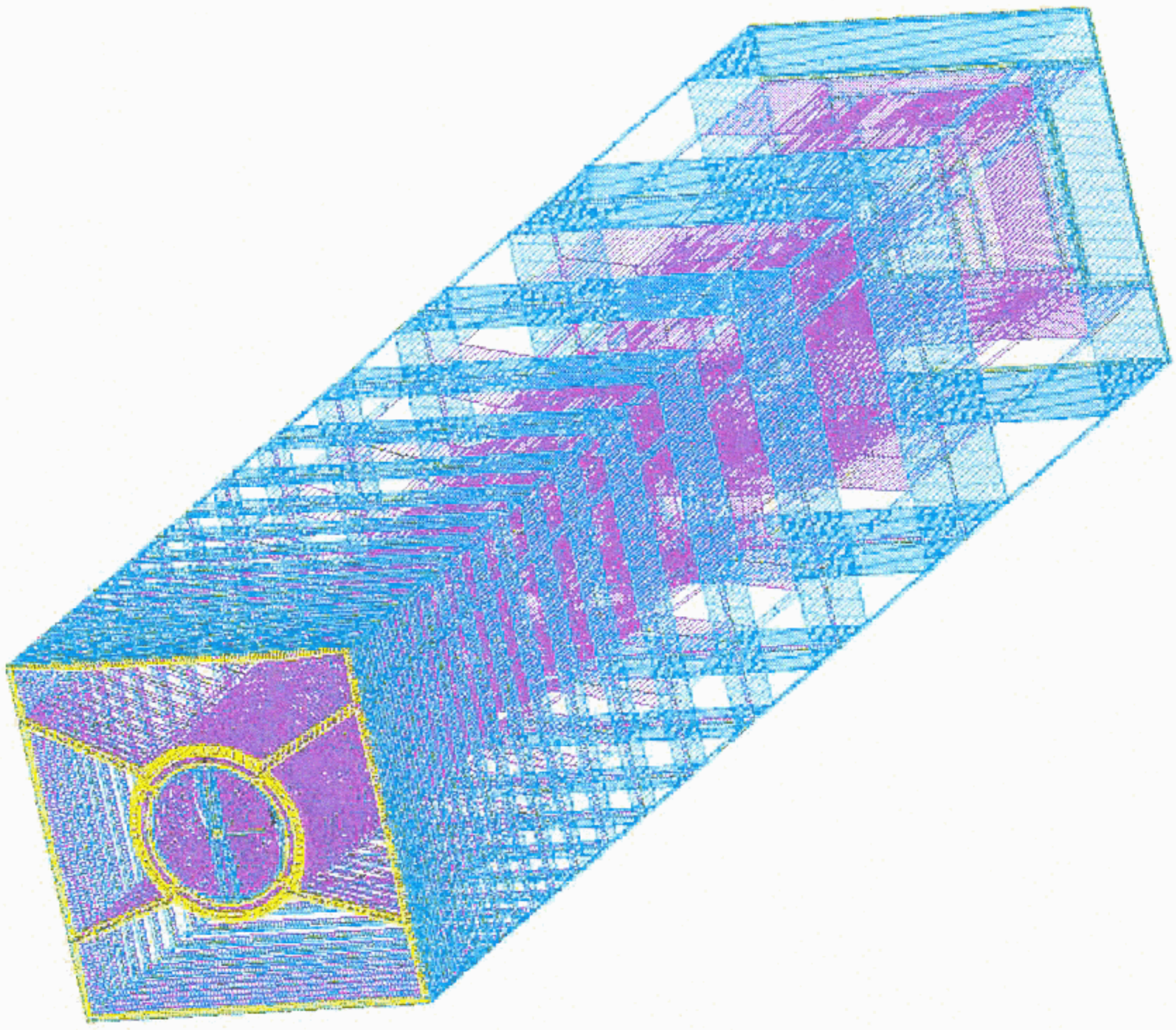

Figure 2.Computational Domain Showing Parallel Decomposition.

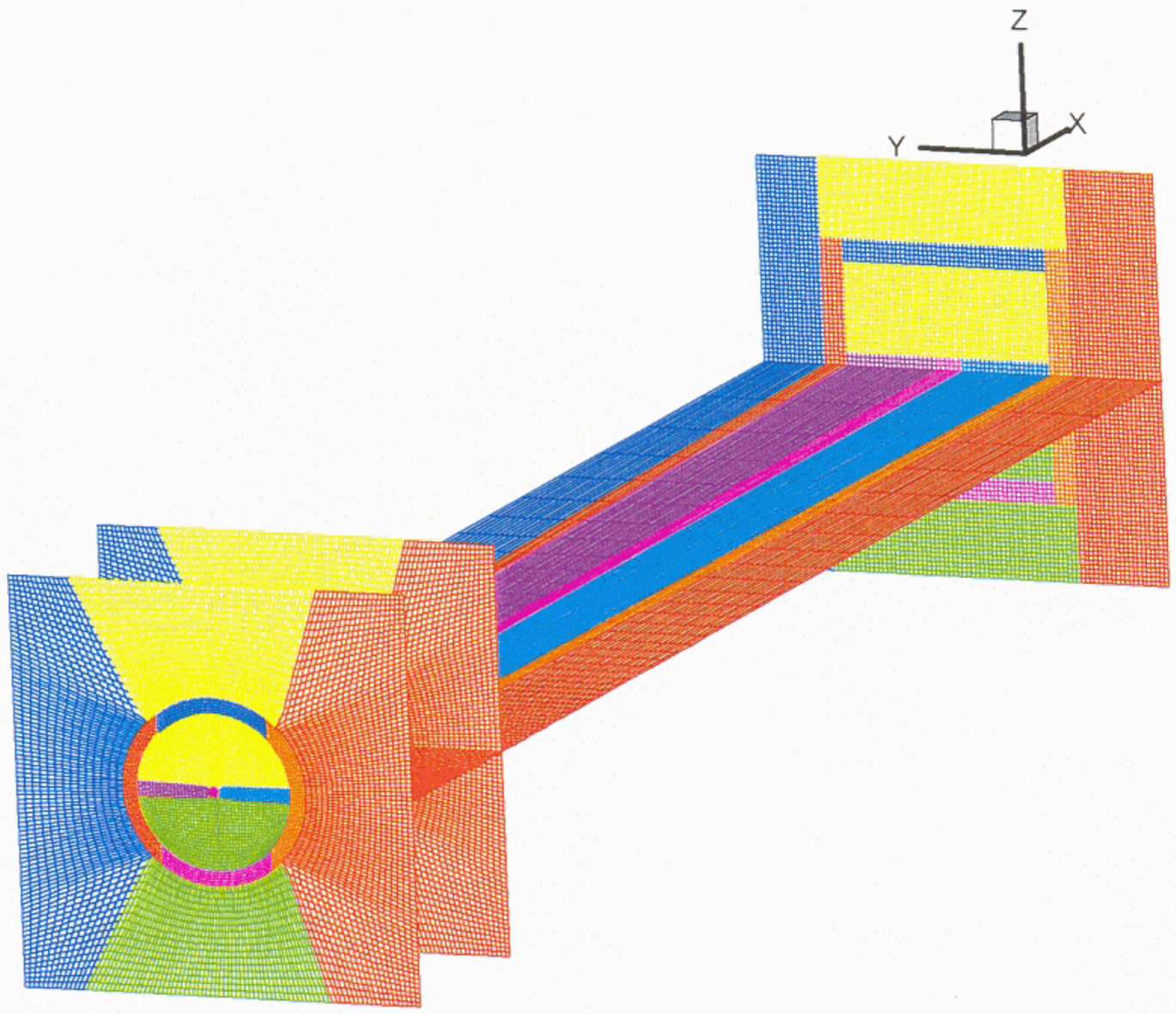

Figure 3. Computational Grid

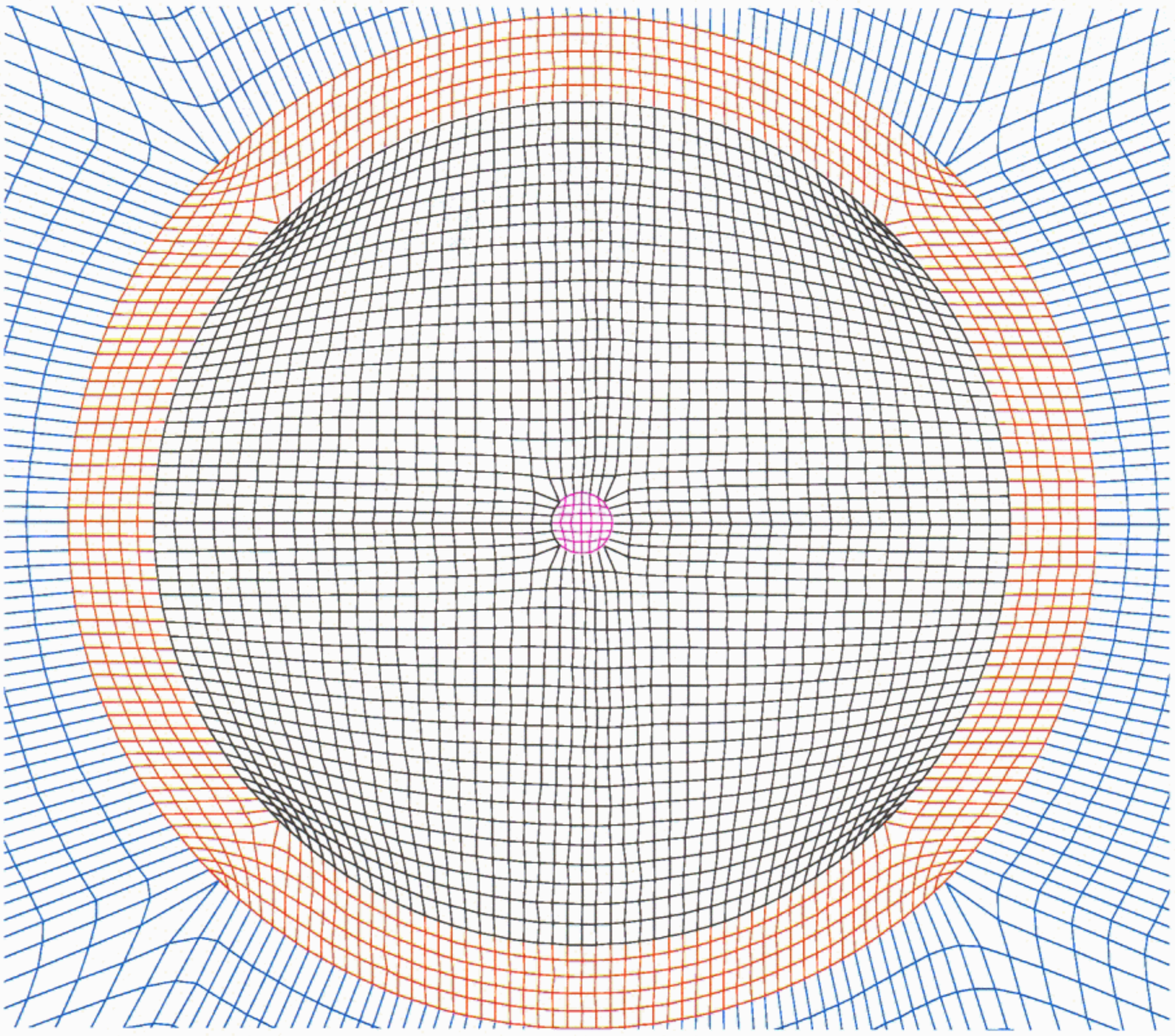

Figure 4. Details of Grid at Burner Face.

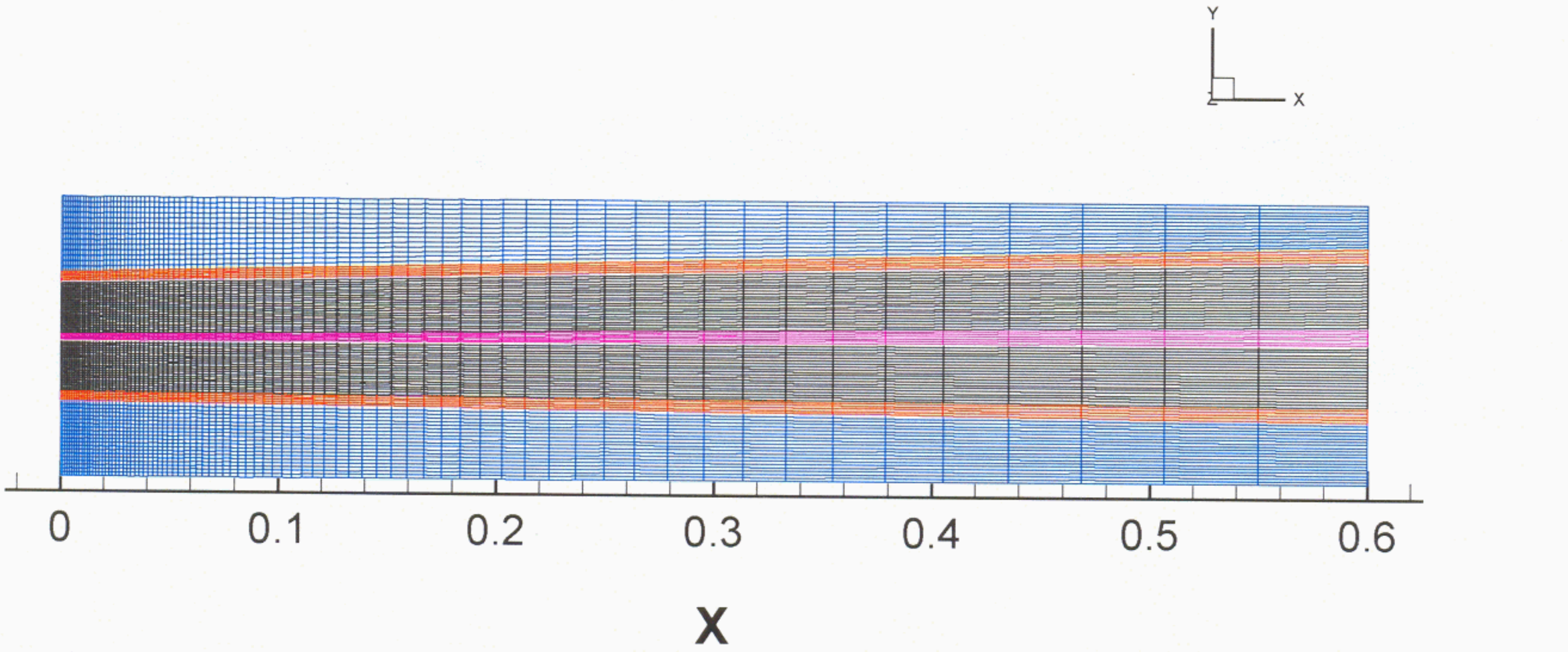

Figure 5. Longitudinal Midplane of the Grid

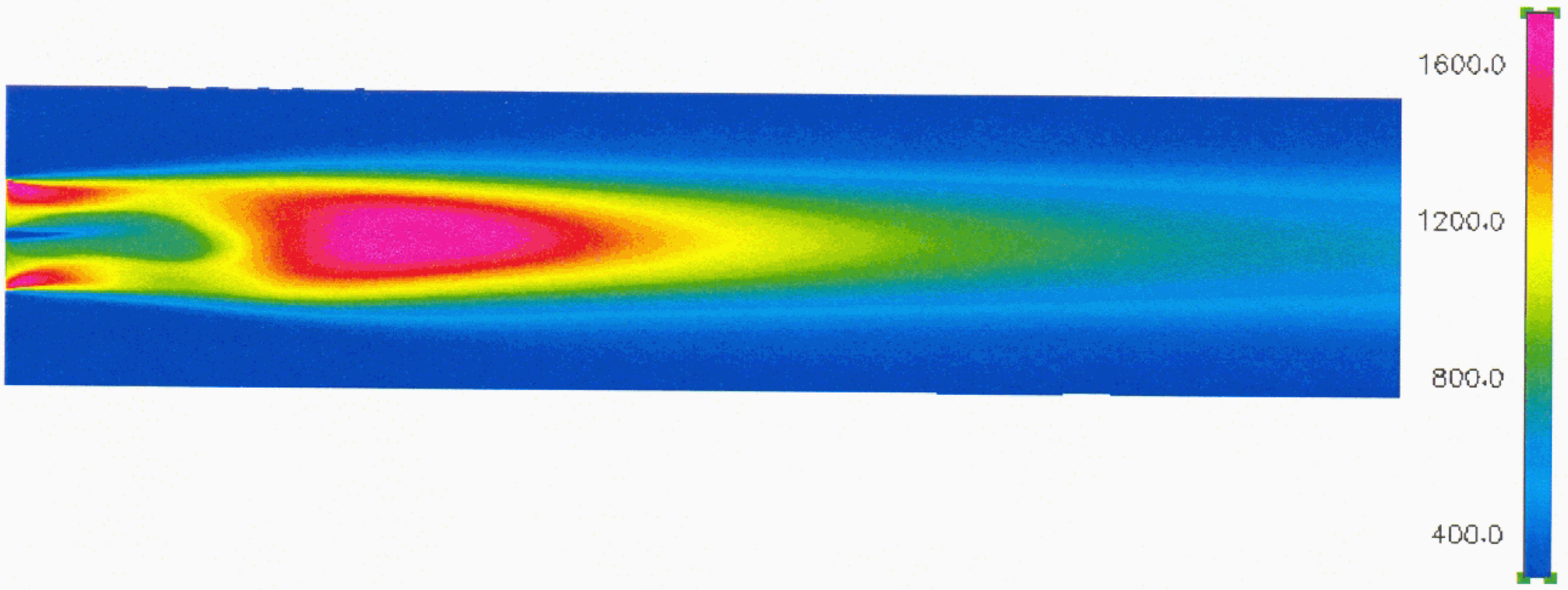

Figure 6. Temperature field (in K) from RANS simulation of SMA2.

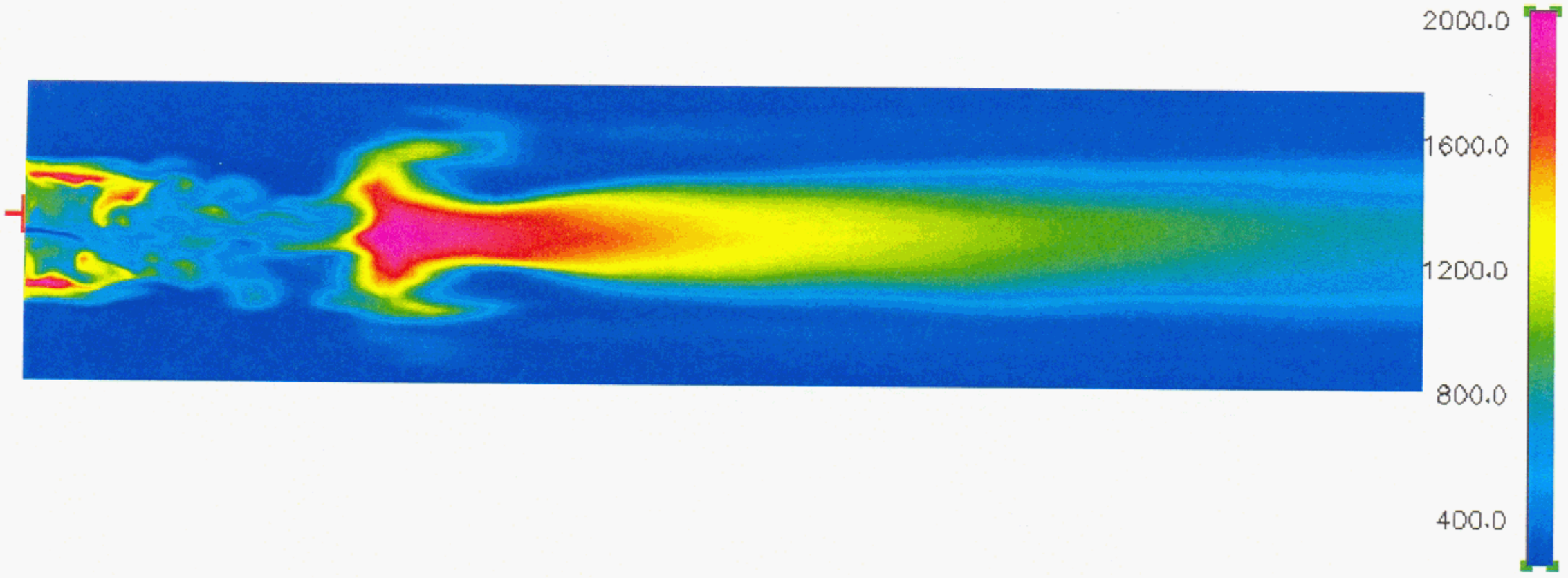

Figure 7. Temperature field from large eddy simulation of SMA2 burner after 900 timesteps.

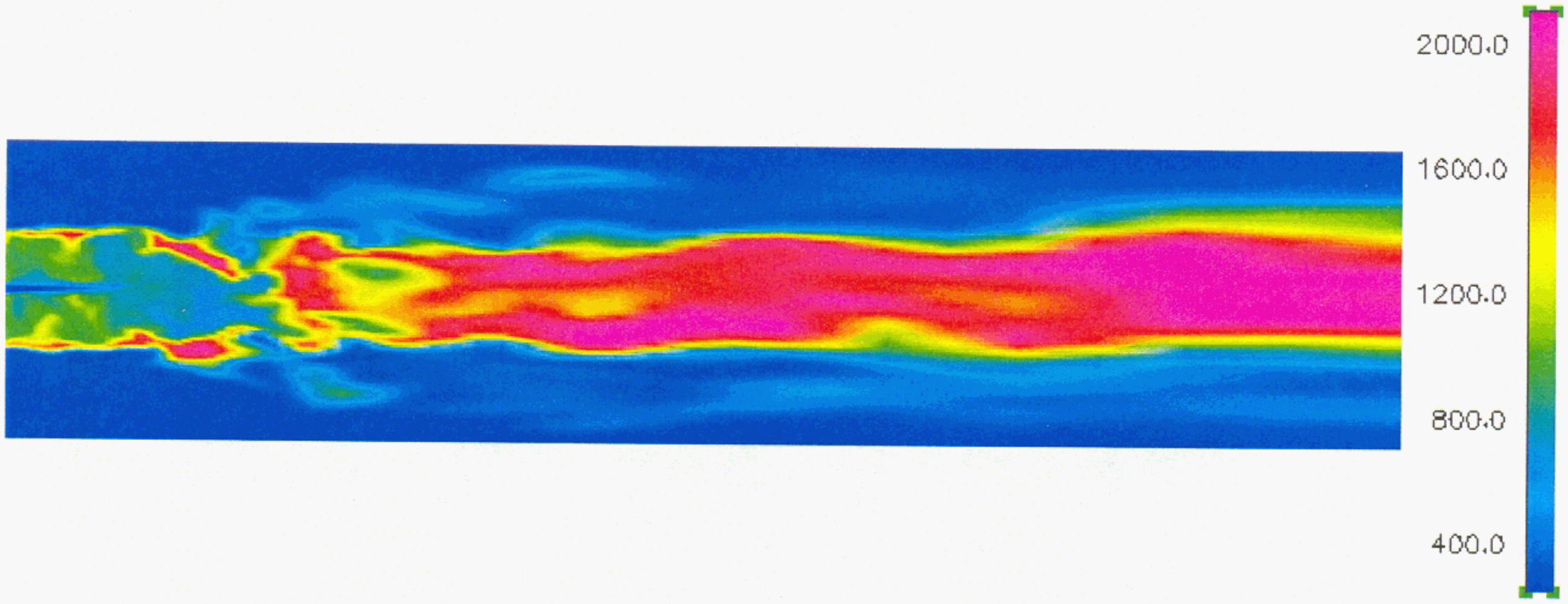

Figure 8. Temperature field from large eddy simulation of SMA2 burner after 4700 time-steps.

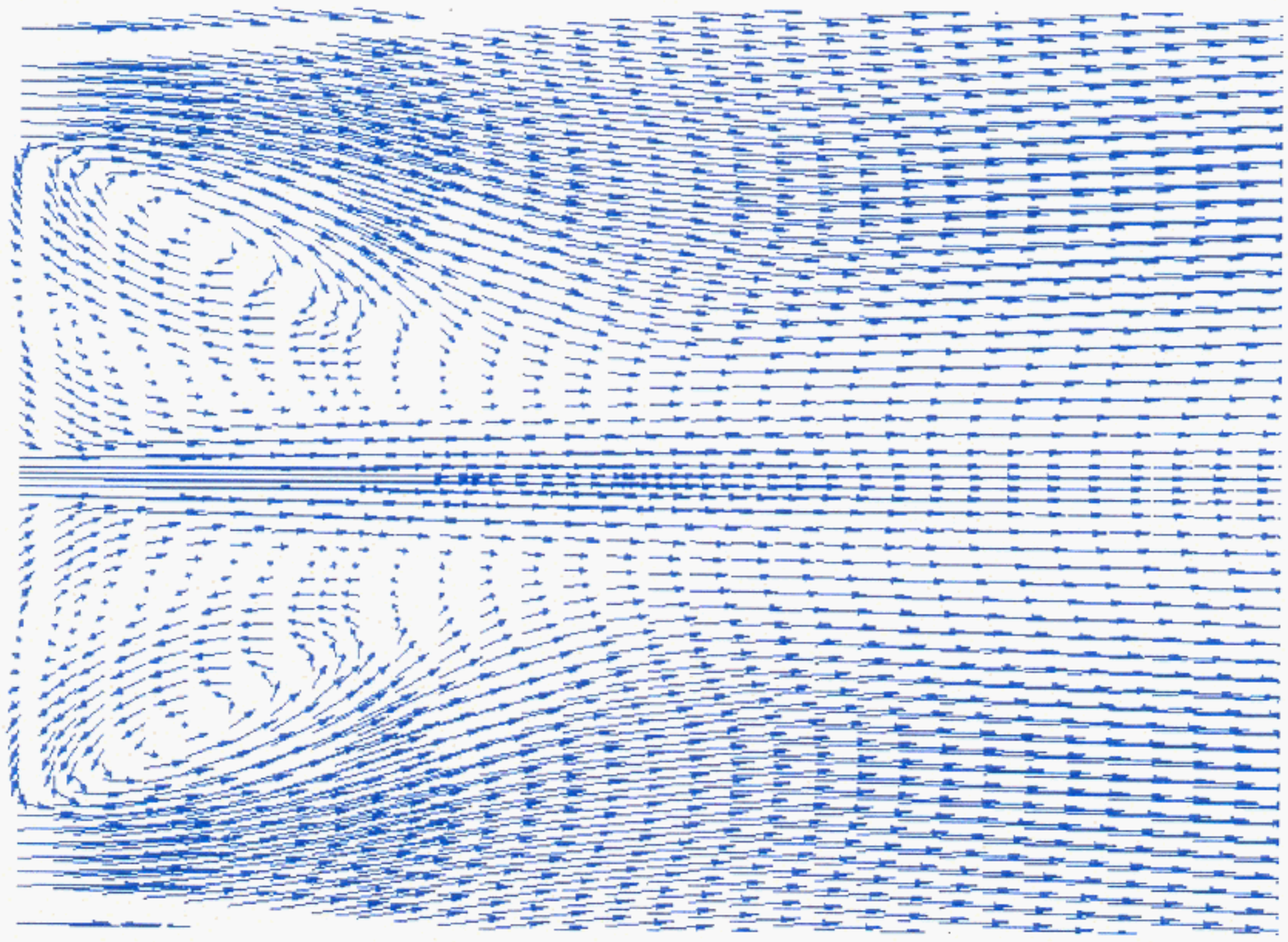

Figure 9. Nonreacting Unsteady RANS Velocity Vectors at Transverse Midplane IN SMH1.

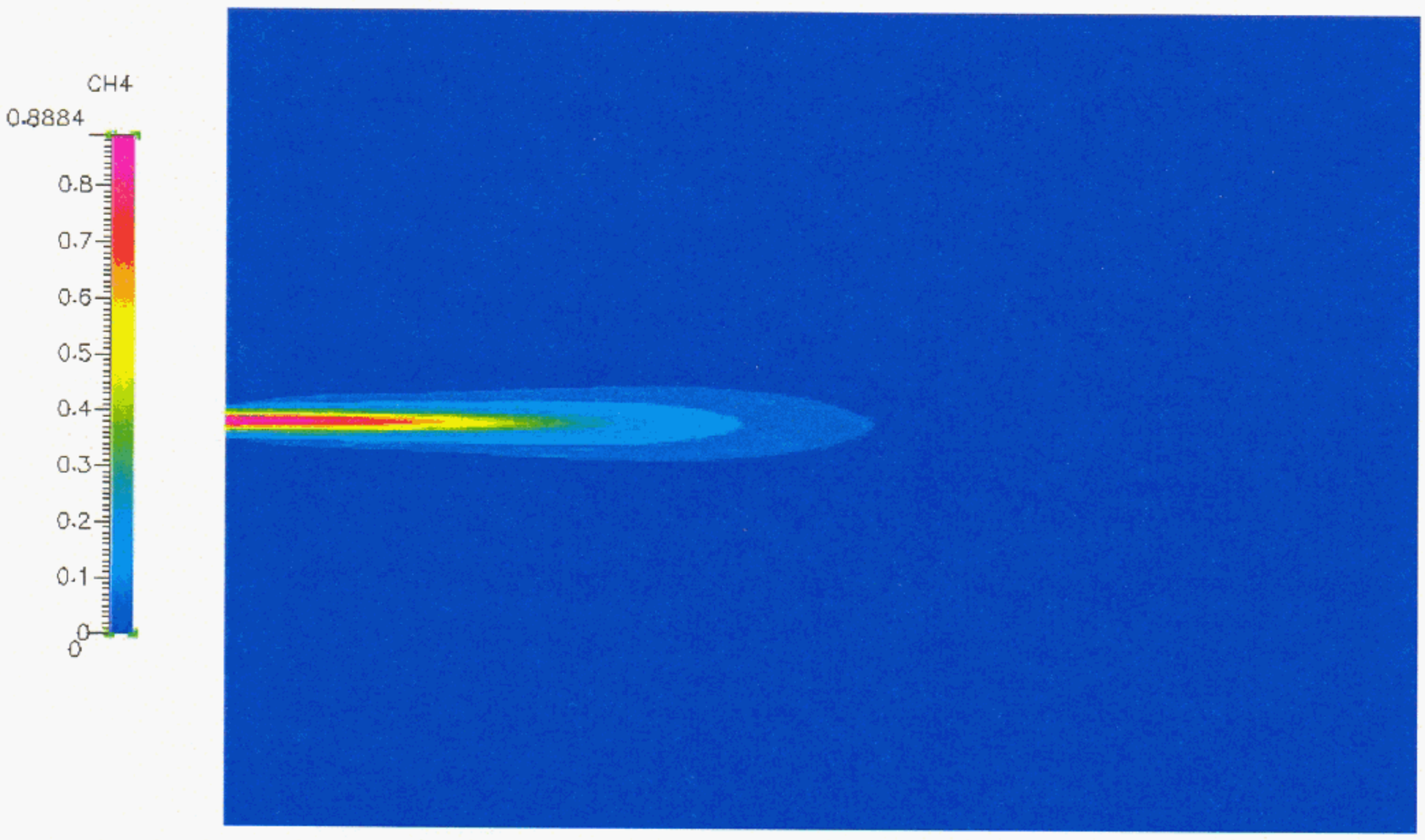

Figure 10. Nonreacting Unsteady RANS Methane Mass Fraction at Transverse Midplane in SMH1.

APPENDIX F

University of California, Irvine (UCI) Final Report

Technical Brief

Implementation and Application of Large Eddy Simulation of an Axisymmetric Confined Flowfield In the Presence of a Bluff Body

Q.Wang, T. Yoshimura, V. Jermakian, and V.G. McDonell

University of California
Irvine, CA 92697-3550
www.ucicl.uci.edu

UCI ARTR 2003-12

15 July 2003

Contents

List of Figures

List of Tables

Executive Summary

This technical brief documents the implementation and application of a Large Eddy Simulation package provided to the UCI Combustion Laboratory (UCICL) by CFD Research Corporation (CFDRC). The software was obtained in early January 2003 and installed on the MPC (Medium Performance Computing) Beowulf Cluster located in University of California, Irvine. This cluster consists of 16 full-time nodes (32 CPUs) and approximately 150 part-time PC lab nodes. More information on this Beowulf Cluster can be obtained at http://mpc.uci.edu/. The test case identified for application of the LES software involved an axisymmetric, confined flow interacting with a bluff body. This test case is associated with a project examining the interaction of jets with a rich product stream at elevated temperature and pressure. The specific test section considered in the present effort is that associated with the rich product generation system. As part of the development of the rich burn section, better understanding of the flowfield generated by the section was desired.

In parallel with the LES simulations, experimental methods were also applied. In the present study, digital particle image velocimetry (DPIV) was utilized. The DPIV system provided instantaneous flowfield maps that could be compared directly the LES simulations. The flowfield was not “driven” by external means. As a result, the ability to specifically “synchronize” time variant behavior between the simulations and measurements was not possible. However, general trends in terms of the instantaneous and time averaged behavior were compared.

The installation process involved more time than anticipated, especially the implementation of parallel operation. Some of the reasons for the additional time included licensing installation troubleshooting and software interaction with Portable Batch System. In addition, challenges were realized due to the manner in which the parallel system use was managed. Specifically, limited use and scheduling of the parallel resources led to automated job termination prior to satisfactory convergence, which caused significant inefficiency in running the case. Attempts to overcome these handicaps were partially successful, but won’t be fully realized until the future.

The results indicate that reasonable agreement between RANS and measurements was achieved. The comparison of time averaged LES solutions and time averaged DPIV results indicates similar agreement, but the total time available for the LES solution was insufficient to make detailed conclusion. The direct quantitative comparison of instantaneous behavior is difficult in the present case, because of limited total solution time for the LES and because the flowfield was not regularly periodic in time, but the general trends in terms of global flow field motion documented by DPIV were reflected in the LES results.

1 Introduction

In December of 2002, UC Irvine was provided with a beta version of the CFDRC Large Eddy Simulation code V2002.2.24 and asked to evaluate the utility and performance of the software by applying it to a problem of interest.

2 Problem Statement

The device selected to apply the LES software to is shown in Figure 1. The development of the rich-burn portion of a Rich-burn, quick-mix, lean-burn combustor is of direct interest. The pre-mixed section leads into the rich-burn section with a bluff-body flame holder. The bluff body is designed to create a re-circulation zone that can confine the primary reaction zone aerodynamically. The bluff body is also designed to prevent flashback by creating a pressure drop, which in turn develops flow speeds exceeding any flame speed. The flame holding section is the basis for the modeling and the experiment documented in this brief. Additional details regarding the geometry of the test device are provided below.

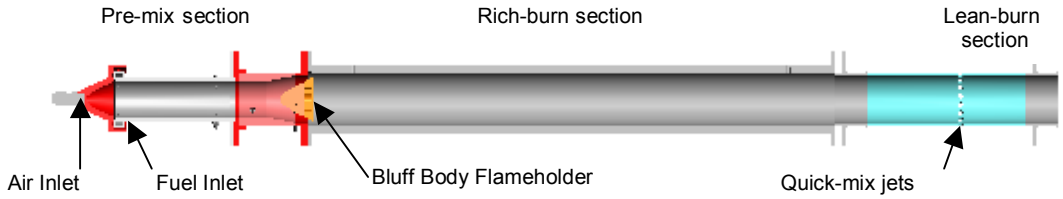

Figure 1. Rich Burn Quick Mix Lean Burn Combustion System.

3 Validation Approach

The approach selected for validation of the LES simulation involved measurements obtained using planar measurements and visualization. Because the LES simulation provides time resolved information about the full flowfield, diagnostics were selected to provide comparable information. Specifically, digital particle image velocimetry (DPIV) was utilized to provide instantaneous planar velocity measurements.

Several experimental conditions were selected for measurement and simulation. These cases were run in parallel and ultimately compared both qualitatitively and quantitatively.

4 Experimental and Numerical Systems

4.1 Test Stand

An existing atmospheric pressure test stand was utilized for the study. The bluff body and fuel pre-mixing sections were mounted on to the test stand in an upfired orientation. The rest of the combustor was replaced with a quartz liner of 3.15" with a length of 12" in order to provide optical access for DPIV measurements. In addition to the quartz liner, optical flats were installed on the laser sheet entry and exit portions of the liner to minimize reflections and to improve the quality of the images. A photograph of the overall experimental setup is shown in Figure 2.

The air mass flow rate was metered with a critical flow orifice (0.18" dia.) and established by monitoring the pressure upstream of the orifice. The critical flow orifice flow rate vs. upstream pressure was established by means of a NIST traceable laminar flow element (Meriam LFE). The pressure drop across the bluff body was monitored using a water manometer.

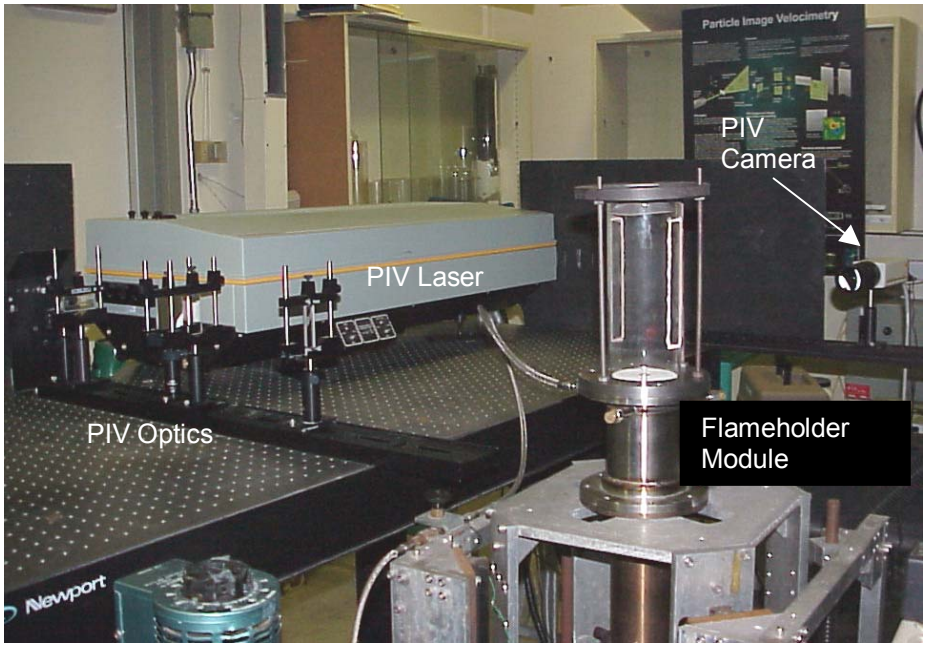

Figure 2. Experimental Facility.

Additional details of the test section setup are illustrated in Figure 3.

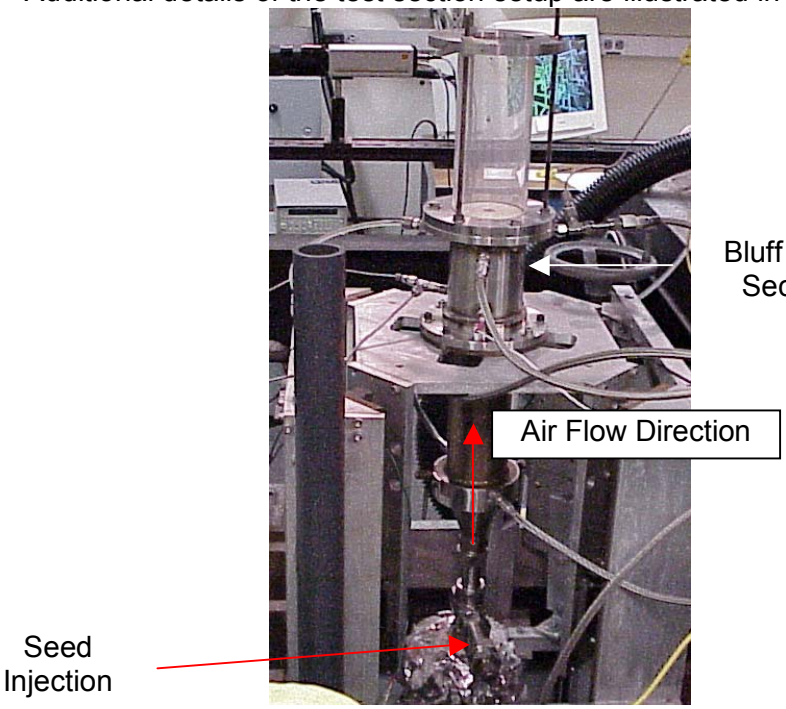

Figure 3. Details of Test Section.

4.2 Test Hardware Geometry and Operating Conditions

The test hardware only receives non-preheated air and flows from the seeding system. The air is injected with a 1" tube that is connected to the air supply. The seed flows are injected through a ½" "T" fitting. The details of the seeding system are described in Section 4.4. An expansion section increases the area of the air and seeder flow by transitioning from a 1" tube to a 3.15" tube. After the expansion section a Vortab® inline flow conditioner is used to provide a uniform concentration and velocity before the bluff body inlet plane. The bluff body section is consists of a 45^0 cone with a 2.99" diameter at the throat. The bluff body creates the re-circulation zone desired for flame holding in a combustor. The strength of the re-circulation zone depends on the air mass flow rate and associated pressure drop across the bluff body. The stagnation point in the re-circulation was assumed to be 3" from the face of the bluff body. The 8" quartz section was an adequate length for testing purposes and prevented ambient air from entering the flow path. The details of the test hardware geometry are shown in Figure 4. Note that the apparent opening in the bluffbody shown in Figure 4 (utilized for the ignitor assembly) was actually filled with a solid tube so that no air flow could enter this passage.

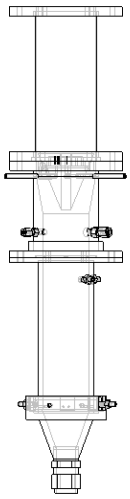

Figure 4. CAD Drawing of the test hardware setup for LES and DPIV.

The CFD geometry and grid are based on the simplified geometry illustrated in Figure 5. The bluff body geometry and the flow area are the most critical regions for the non-reacting flowfield. Preliminary CFD cases were run during the design process of the bluff body in order to establish a suitable pressure drop and recirculation zone for the flows of interest to the project.

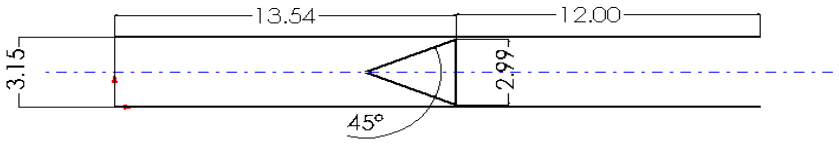

Figure 5. Details of geometry utilized for CFD setup, dimensions are in inches.

The operating condition for the DPIV experiment is summarized in Table 1 and was utilized as the inlet conditions for the CFD simulations.

Table 1. Summary of Operating Conditions.

Orifice Pressure (Pa)	Air Flow Rate (kg/s)	Pressure Drop (Pa)	Temperature (K)
153,063	0.01386	600	300

4.3 CFD Model Information

4.3.1 Grid

The grid developed for the case features and ~1.0 Million cell structured grid, as shown in Figure 6. This grid is a 3D asymmetric grid and was refined several times until the best convergence was achieved.

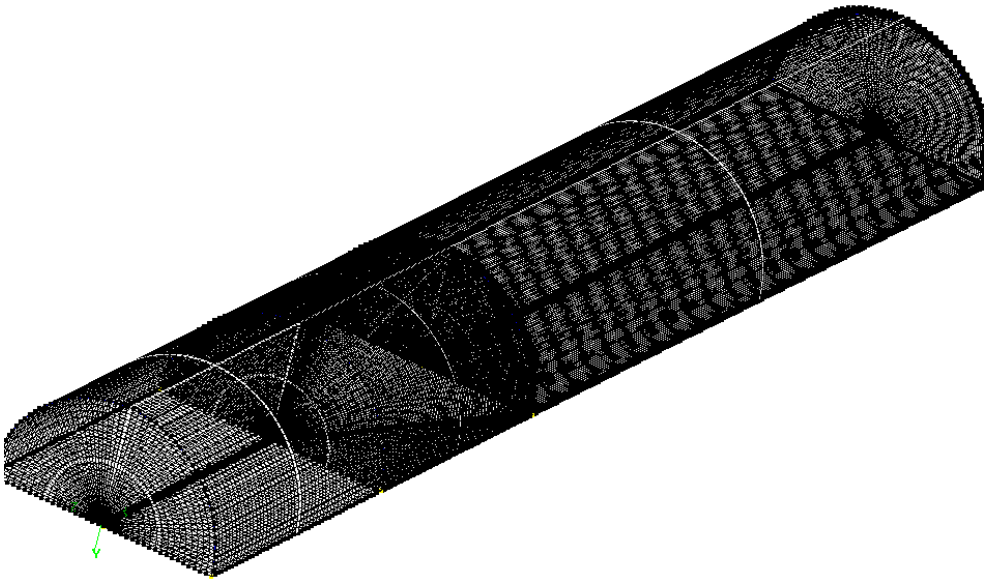

Figure 6. Structured Grid for Test Case.

4.3.2 LES Modeling

The LES model implemented utilizes the following parameters and boundary conditions:

- $\delta t=2.5 \times 10^{-4}$ s
- LDKM Subgrid Models
- Default Model Constants
- User Output 100HZ
- Fixed Velocity Inlet
- Fixed Pressure Outlet
- Random Fluctuations

4.4 Digital Particle Image Velocimetry

Digital Particle Image Velocimetry (DPIV) is a non-intrusive whole-flow-field technique providing instantaneous velocity vector measurements in a cross-

section of a flow. By using a 2D DPIV system two velocity components are measured, in the present case axial and radial components in the axisymmetric setup. The use of modern CCD cameras and dedicated computing hardware, provides the opportunity to measure velocity fields in essentially real time.

Details of the equipment utilized for this specific project include:

- Nd:YAG Laser : Continuum Surelite III@532nm, 340mJ/shot
- CCD Camera : Kodak Model ES 1.0
- Pulse Generator : Stanford Research Systems DG535
- PIV Software : TSI Insight ver.3.34

The laser, camera, and the associated sheet forming optics are illustrated in Figure 2. A schematic of the overall system is shown in Figure 7.

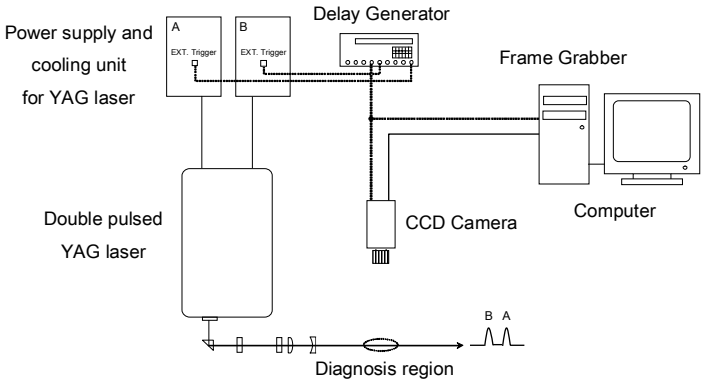

Figure 7. Digital Particle Image Velocimetry Diagnostic experimental setup.

A key requirement for DPIV is the presence of scattering centers in the flow. For the present study, nominally 2.0 micron alumina particles (MicroAbrasives GB1500) were utilized. They were introduced into the air stream approximately 500 mm upstream of the bluff body face using a slurry nebulization approach which is described in detail in Ikioka, Brum, and Samuelsen (1983). This method provides sufficient particle concentration and steady generation, key requirements for high quality DPIV results.

In DPIV, velocity vectors are calculated from the displacement of particles between two laser light pulses. The particles in the flow are illuminated in the diagnosis region with a laser light sheet. When the particle is illuminated, the scattered light image is captured by CCD camera. Through a technique called “frame straddling”, the Kodak CCD camera is able to obtain a second independent image from the scattered light from the second laser pulse. With the two separate images of the light scattered from the two consecutive laser pulses, the PIV software then establishes the displacement of particles using cross correlation methods, and through calibration of pixel spacing to physical distance, determines the velocity maps.

A cylindrical quartz is used for the flow measurement in the combustor and makes the flow in the combustor visible. However, light scattering from the surface of the quartz creates a challenge in terms of noise. This noise causes some errors in the vector field when the intensity of the surface scattering is comparable to the intensity of the light scattered by the particles. The software cannot discriminate between surface reflections and particle scattering. As a result, non-gloss black paper was carefully positioned on one side of quartz to mask any surface reflections from entering the camera.

A typical single image is shown in Figure 8. The size of this image is 107.9mm(H)*109.0mm(V). The scattering from the quartz on either the right or left edge of the particle field has been eliminated through the spatial filters and the scattering has been removed from the region of interest (i.e., the particle field). The bright part of the bottom is the flange around the bluff body which is the inlet plane. A substantial number of particles in the region of interest are noted as required for accurate image analysis.

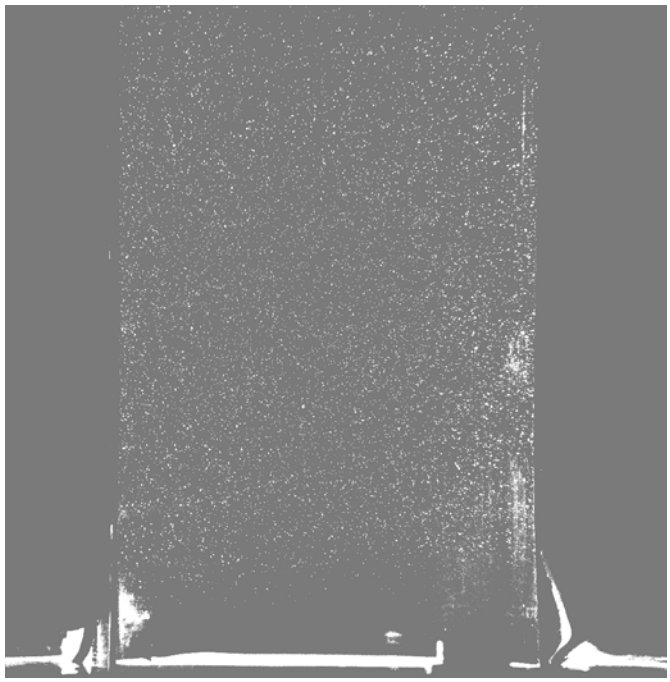

Figure 8. Typical Particle Image in the combustor.

4.5 Simulation Platform

Figure 9 illustrates the MPC Beowulf Cluster at UCI, which was utilized as the simulation hardware platform. The MPC (Massively Parallel Computing) Beowulf Cluster is available to all UCI Researchers and it consists of 16 full-time nodes and approximately 150 part-time PC Lab nodes. The 16 full-time nodes are dual-CPU Xeon 2.0GHz and Athlon 1.8GHz units, which are completely dedicated to the cluster. The other 150 part-time nodes are lab PCs located in different PC labs on UCI campus, which are used by UCI students in daytime and as part of the computing cluster at night (10:00PM-7:00AM) when they are free of use.

The MPC was continually upgraded throughout the duration of this project, and plans remaining include adding 16 dual CPU compute nodes and a GigE switch will be added to MPC. The 16 dual CPU nodes will use the new AMD 64 Bit Opteron nodes and four of them were put into use in early May and were utilized by this project. Each of the 16 additional nodes will have dual Opteron Model 240 - 1.4GHz CPU / 1MB L2 Cache, 1GB PC2700 DDR main memory, Broadcom NIC GIGE * 2, internal disk, CD and floppy. However, since the MPC cluster is not currently running the 64-bit Redhat9 linux OS, the Opteron nodes are restricted to 32-bit performance.

The operation system of MPC cluster is RedHat Linux9.0. At the UCICL offices, Exceed 7.0 X terminal simulator was utilized on a Windows XP machine since the experience with Linux was minimal. Xterm was typically used to launch tasks on the cluster.

The MPC Beowulf cluster uses PBS (Portable Batch System) to manage its task queue. All the tasks must be submitted to the head node and appointed to the computing nodes by the head node. The head node does the maintenance of the queue and balance the load of the different computing nodes. This mechanism is good for optimizing the usage of the computing capability of the whole cluster. In order to prevent individuals from claiming all the computing resource of the cluster for a unreasonably long time, a 24 hour time limit was applied to each task submitted to the PBS.

For the current LES project, the four new dual CPU Opteron nodes were utilized. The task was split into 8 parts and carried out by parallel runs within 24 hours. The software package we used was CFDACE+ Ver2002.2.24.

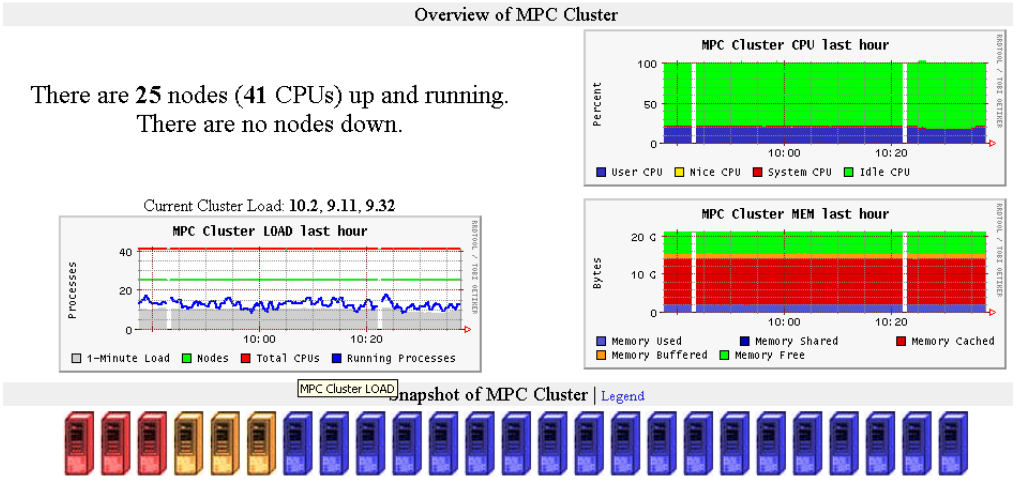

Figure 9. UC Irvine Beowulf Cluster.

5 Results

5.1 Software Implementation Experience

5.1.1 Installation

Installation of the CFDACE+ package was done under both Windows and Linux platforms. The Windows version of CFDACE+ was installed onto local lab PCs for CFD problems that required minimal computing power. For example, CFDACE+ has been used regularly to simulate cold flow aerodynamics simulation in various geometries using RANS. Most of these cases have about 600,000 unstructured cells and can be finished in a couple of hours. Geometries are imported from Solidworks or AutoCAD and grids are generated with CFDGeom. The simulations are run with CFDACE and results viewed with CFDView. If the result is not satisfactory, Solidworks is used to modify the design for next simulation. Using this approach, hundreds of simulations for various applications have been run. Until now, the Windows version of CFDACE+ works very well on local PCs with Windows XP Professional. The installation of the Windows version is also straightforward, and no major problems were encountered.

After learning about the MPC cluster, a Linux version of CFDACE+ with the parallel run capability was obtained and installation proceeded on the MPC Beowulf Cluster for LES simulation and other CFD cases demanding large amount of computation. This process was not straightforward and it took many weeks to get the software working. The problem was mostly caused by the license installation. It was found that, unfortunately, the license installation tool slm_admin couldn't install the license properly. So a licensing file (lservrc) was obtained and put directly into the licensing directory, which was successful.

Another issue encountered during the Linux installation is that license must be installed on the head node of the MPC cluster. At first, another machine (UCICL local PC) was identified to serve as a license server for convenience and control. However, we encountered license-accessing problems because all the computing nodes in the cluster must get licensing information from the head node.

In summary, getting the software installed and operable on the LINUX cluster proved to be challenging and required considerable assistance from CFDRC. In contrast, the Windows version was installed on a local PC without any issues.

5.1.2 Parallel Operation

Operation in parallel mode presented some issues related to the PBS structure. Initially, parallel operation in PBS system was attempted by using a host file to tell CFDACE+ what nodes should be used. This often caused conflict since we this essentially bypassed the queuing system. After consulting with CFDRC support, cfdace_mpi was operated in the PBS environment with the parameter – pbs, which proved to be successful.

5.1.3 Run CFDACE on X terminal

Because Linux OS is not supported in the UCICL local area network, in order to communicate with the MPC cluster, X terminal simulator Exceed7.0 was used on the Windows XP Lab PC. However, several problems were encountered when running

CFDACE+ remotely on Exceed7.0. The major problem is that the X simulator doesn't support OpenGL graphic extension well. CFDGEOM and CFDGUI crashed frequently when opening a grid file. XCFDGUI and XCFDGUI for X-window were both evaluated. These packages worked but the running speed was very slow in Exceed. To date, an acceptable method of running CFDACE+ smoothly in Exceed has yet to be identified. As a result, the DTF file is generated with the Windows version of CFDACE+ and then uploaded (via FTP) to the remote machine in the cluster. This is not very convenient because changing the DTF file cannot be done in the Linux environment remotely. Hopefully, CFDACE+ will improve the compatibility with X window simulator and run better in Exceed.

5.1.4 Time Limit

As mentioned above, the UCI MPC cluster administration applies a 24 hour time limit to each task submitted. As a result, only CFD cases that require less than 24 hours can be implemented. We have worked with the MPC cluster administrator to add nodes to the cluster, which will then be dedicated to our CFD simulations without limit. However, despite placing the order for 4 Opteron nodes, a desire on the part of the system administrator to consolidate orders to further reduce pricing led to delays and to date the units have not been received. Unfortunately, this time limit administration issue limited out ability to solve reacting flow LES cases and impacted out abilities to get good time resolution on cold flow cases. Once the machine orders are released and the units installed, we can then begin study of these more difficult cases.

5.2 Measured Flowfield

The diagnosis region in the combustor is shown in Figure 10. The full size of captured image is 107.9mm(H)*109.0mm(V) and the diagnosis region size is 74.3mm(H) * 98.5mm(V). The bottom of this region is 5.3mm above the bluff body face.

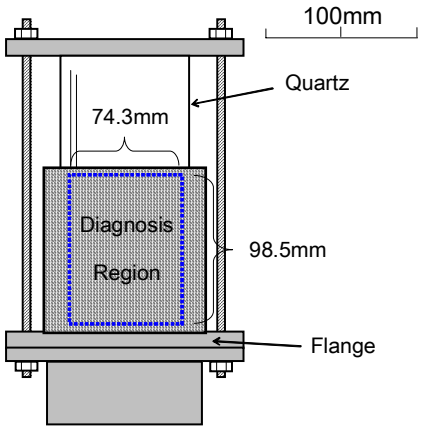

Figure 10. PIV Diagnosis Region in the combustor.

Tecplot v. 8.0 was utilized to conveniently manipulate and average the DPIV vector fields. Figure 11 shows the time averaged flowfield in the combustor as a result of averaging 100 images taken at a rate of 1 Hz. The results reveal an axisymmetric flow with strong recirculation as expected. The length of the recirculation zone is approximately 1 pipe diameter. Regions of high downstream velocity are apparent along the walls where the flow enters through the annulus between the bluff body and the wall.

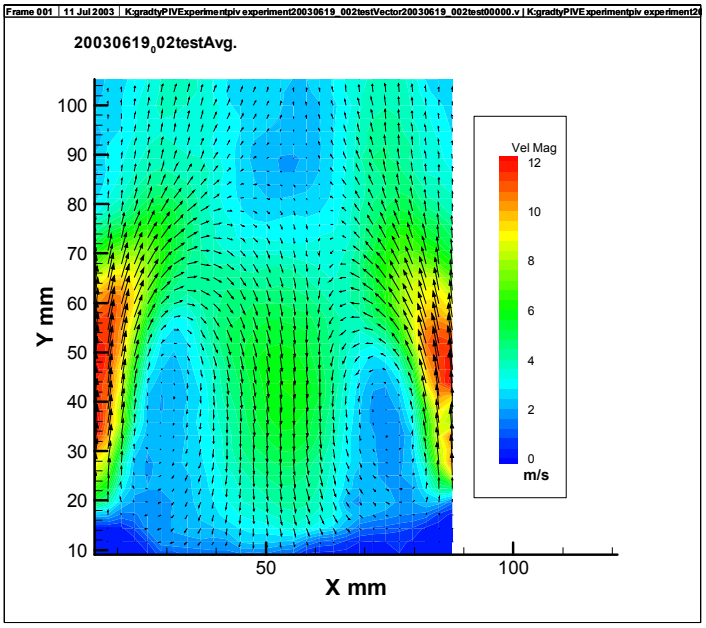

Figure 11. Time averaged Flowfield

In contrast to the symmetric and well-behaved time averaged behavior, the typical instantaneous behavior, as shown in Figure 12, features considerable irregularities and departures from the time averaged flow, which is again expected.

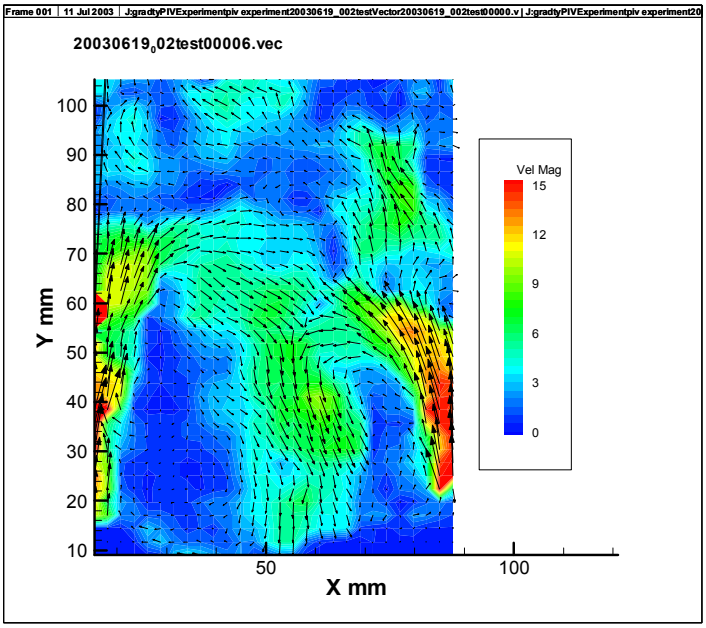

Figure 12. Instantaneous Flowfield

5.3 Predicted Flowfield

Due to challenges outlined above, significant LES results in terms of total physical time were not obtained for this project. Both RANS cases and LES cases were

run on the MPC cluster, but due to time limits and configuration issues, the LES operation was only recently accomplished, and with less than desired total solution time.

Figure 13 shows the flowfield predicted using steady state RANS. The trends are again as expected.

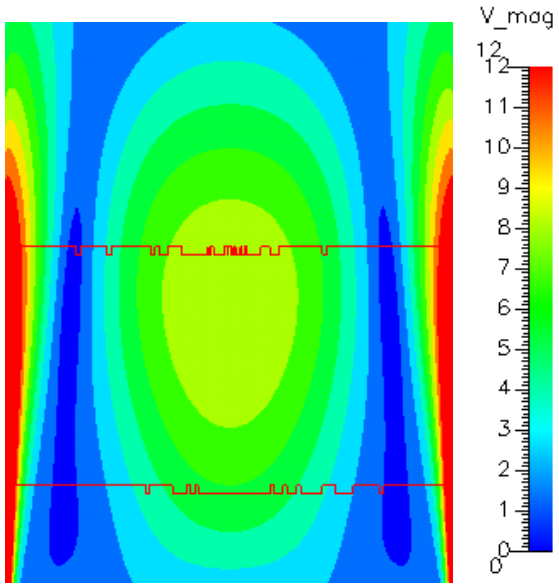

Figure 13. RANS Flow Field (Velocity Magnitude)

The time-averaged LES flowfield is illustrated in Figure 14. It is noted that this average is only based on 1 msec of time, so it not truly "time averaged."

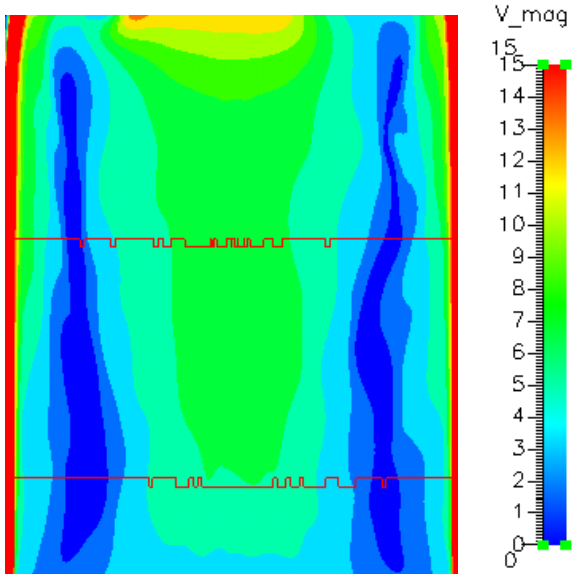

Figure 14. LES Average Flow Field (Velocity Magnitude)

5.4 Comparison Between Predicted and Measured Flowfield

5.4.1 Time Averaged V Velocity

The time averaged velocities from RANS and DPIV are shown in Figure 15. The general trends are similar for each case, yet the RANS solution shows a larger and longer recirculation zone.

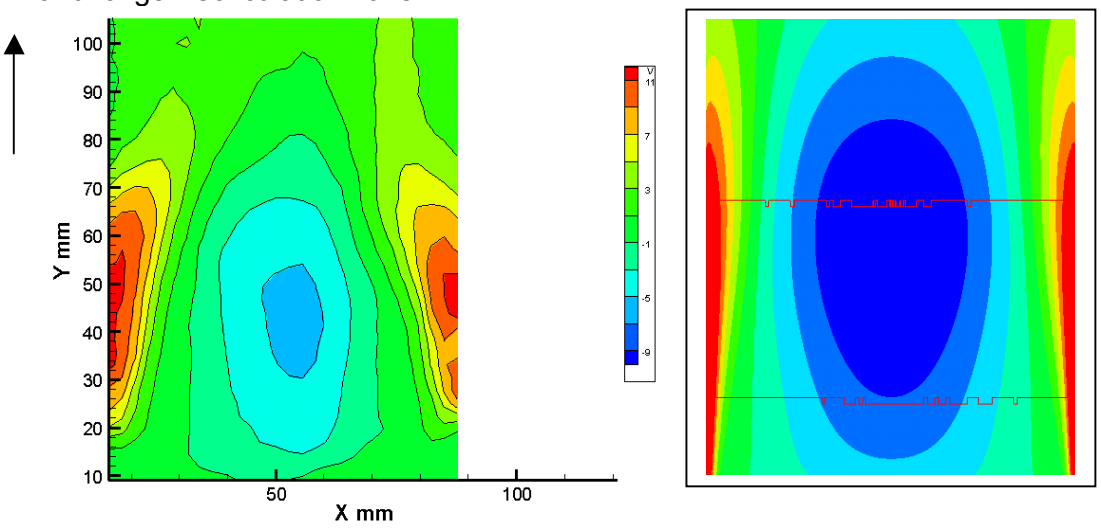

PIV RANS

Figure 15. Time Averaged V velocity

To provide more quantitative comparison, Figure 16 presents time-averaged profiles along the diameter of the flowfield at different axial distances of 10, 20, 30, and 40 mm downstream of the bluffbody face. At 10 mm, the experimental results appear somewhat asymmetric and have a lower magnitude recirculating velocity compared to the simulation. By 20 mm, however, the agreement between the experiment and simulation is good and this agreement remains satisfactory at the 30 and 40 mm axial distances as well.

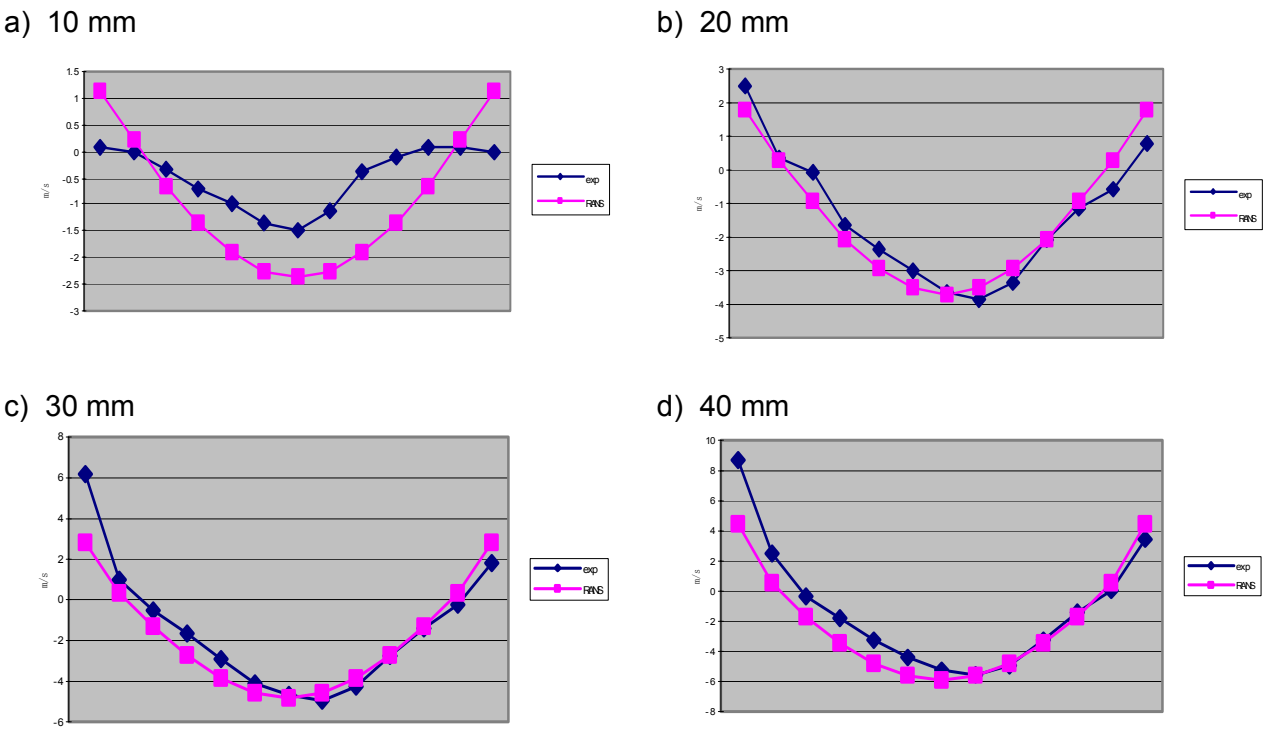

Figure 16. Comparison of RANS and DPIV Axial Velocities.

5.4.2 Time Resolved Axial Velocity

Figure 17 illustrates the instantaneous V velocity field (i.e., axial velocity) from the DPIV experiment and LES simulation. The flowfield is not driven by any external means, therefore the transient behavior is simply due to natural forces. Because the flow isn't driven, it is difficult to "synchronize" the snapshots from either technique. As a result, the comparison shown is not as illustrative as it might otherwise be. The results do show that the natural variation in the flowfield is captured by both DPIV and the LES and that the time-averaged view shown above in Figure 15 is only one interpretation of the flowfield. Time variant behavior at each point in the flow can be examined, but has not been at this point due to the limited LES total time (i.e., only 4 ms is available). To provide enough LES results, a much longer run time is needed, which is limited by the current 24 hour restriction on the cluster use.

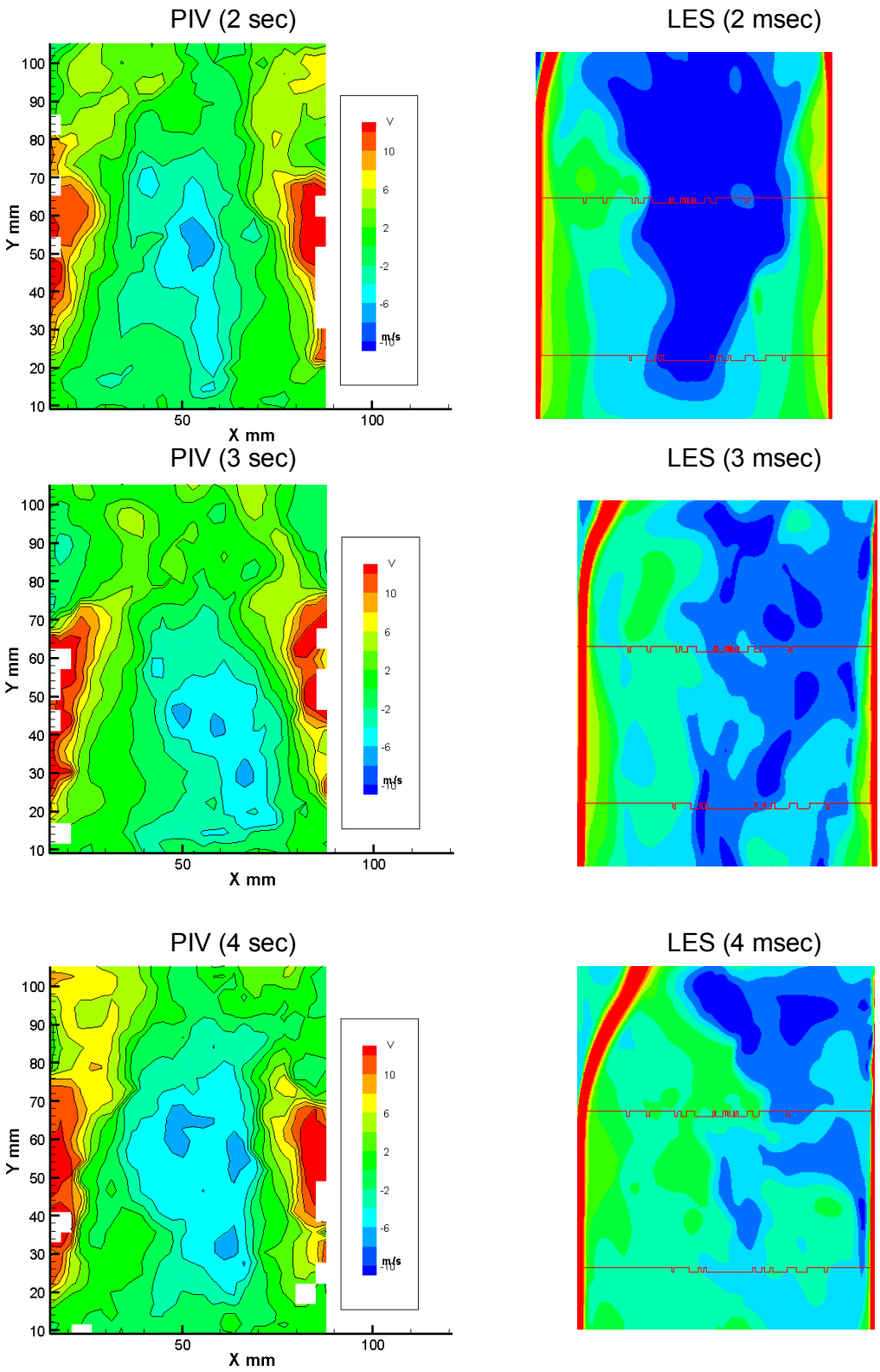

Figure 17. Comparison of Flowfield Snapshots from DPIV and LES.

6 Conclusions and Recommendations

6.1 Conclusions

- The implementation of the parallel operation of the software required some unanticipated issues to be overcome. In addition, some non-technical issues (e.g., time limits) created a non-ideal situation in which to fully evaluate the utility of the software.
- Once the various licensing and operational issues were overcome, the parallel operation of the code was achieved and provided some interesting, albeit limited results.
- The steady state result (RANS) shows some good correspondence with the PIV time average result.
- LES result shows the instantaneous fluctuation of the flowfield that RANS cannot provide us. However, we cannot do more detailed quantized comparison since we only have limited LES results caused by our current computing resource.

6.2 Recommendation

- A solution to overcome the time restriction issue was implemented during the project through a strategy to obtain nodes dedicated to use for parallel operation, but due to the desire to "pool" our node order with others on campus, the order has still not been placed at the time of this document.
- Once the nodes are in place, additional LES solution should be obtained and other quantities compared to the DPIV results such as turbulence levels and vorticity.
- While the total airflow was accurately known, the actual inlet conditions used in the simulation may have differed from the experiment. Additional characterization of the inlet conditions could improve comparisons.

7 References

L.A. Ikioka, R.D. Brum, and G.S. Samuelsen (1983).
LES Validation Study: Impinging Jets in Confined Crossflow, Dr Adrian Spencer (2002)
CFDACE Modules Manuals, CFDRC (2002)

Appendix

DTF Files (RANS and some LES) (on CD).

APPENDIX G

University of California, (Berkeley) Final Report

Final report Date: October-2003

LES Software for the Design of Low Emission Combustion System for Vision 21 Plants

J.-Y Chen
Department of Mechanical Engineering
University of California at Berkeley
Berkeley, CA 94720

Abstract

The complexity of turbulent combustion places severe demands on computer resources, as a wide range of turbulence-chemistry interactions needs to be included in modeling of advanced combustors. Research was conducted to develop accurate reduced chemistry for hydrogen, methane, and propane combustion in terms of their abilities in predictions of heat release, autoignition delay, and the accompany NOx. Approaches for further speed up in CFD with ISAT and ANN techniques are described and consultation on their uses were provided.

Development and Validation of Reduced Chemistry

Several reduced mechanisms have been developed and evaluated for methane-air, hydrogen-air, and propane-air combustion. These mechanisms were developed to provide accurate predictions in ignition delay, flame propagation speed, heat release rate, and pollutant formation, such as CO and NO_x.

Methane-Air Combustion

As the reaction rates in current detailed NO_x mechanisms contain large uncertainties, different NO_x mechanisms for rich and lean combustion were examined. For combustion chemistry, either GRI2.11 or GRI3.0 can be used as the base mechanism. Small differences were found in the predicted results for main flame characteristics. Recent experimental data from Dr. Robert Barlow at Sandia National Laboratories in Livermore have suggested that the NO_x mechanism contained in GRI3.0 gives high NO_x levels roughly by a factor of 2 in partially premixed laminar methane-air flames. GRI2.11 gives reasonable results in lean parts of flame but under-predicts the NO_x levels in the rich parts of flame. Computed results with a recently modified Miller's mechanism (denoted here as Miller2000) yield much improved NO_x levels for rich parts of the flame where re-burning process is dominant. Based on the above assessment, Table 1 summarizes the combinations of detailed mechanisms explored for different combustion regimes.

Table 1: Different combinations of combustion chemistry and NO_x mechanism

Combustion Chemistry	NO_x Mechanism	Application Regime
GRI2.11	GRI2.11	Lean to stoichiometric
GRI2.11	Miller2000	Rich
GRI3.0	Miller2000	Rich

Calculations were performed for the partially premixed Tsuji flames measured by Barlow and comparisons with the data were made. Shown in Figure 1 are comparisons of NO predictions by the three detailed mechanisms with data by Barlow revealing that in the lean side GRI2.1 agrees best with the data. On the rich side, GRI2.1+Miller2000 is seen best matched with the data. Based on this observation, two 15-step reduced mechanisms with identical species were developed based on GRI2.11+Miller2000 and GRI2.11. Figures 2 and 3 compare results obtained by the reduced chemistry with those by the detailed mechanisms and the data showing reasonably good agreement.

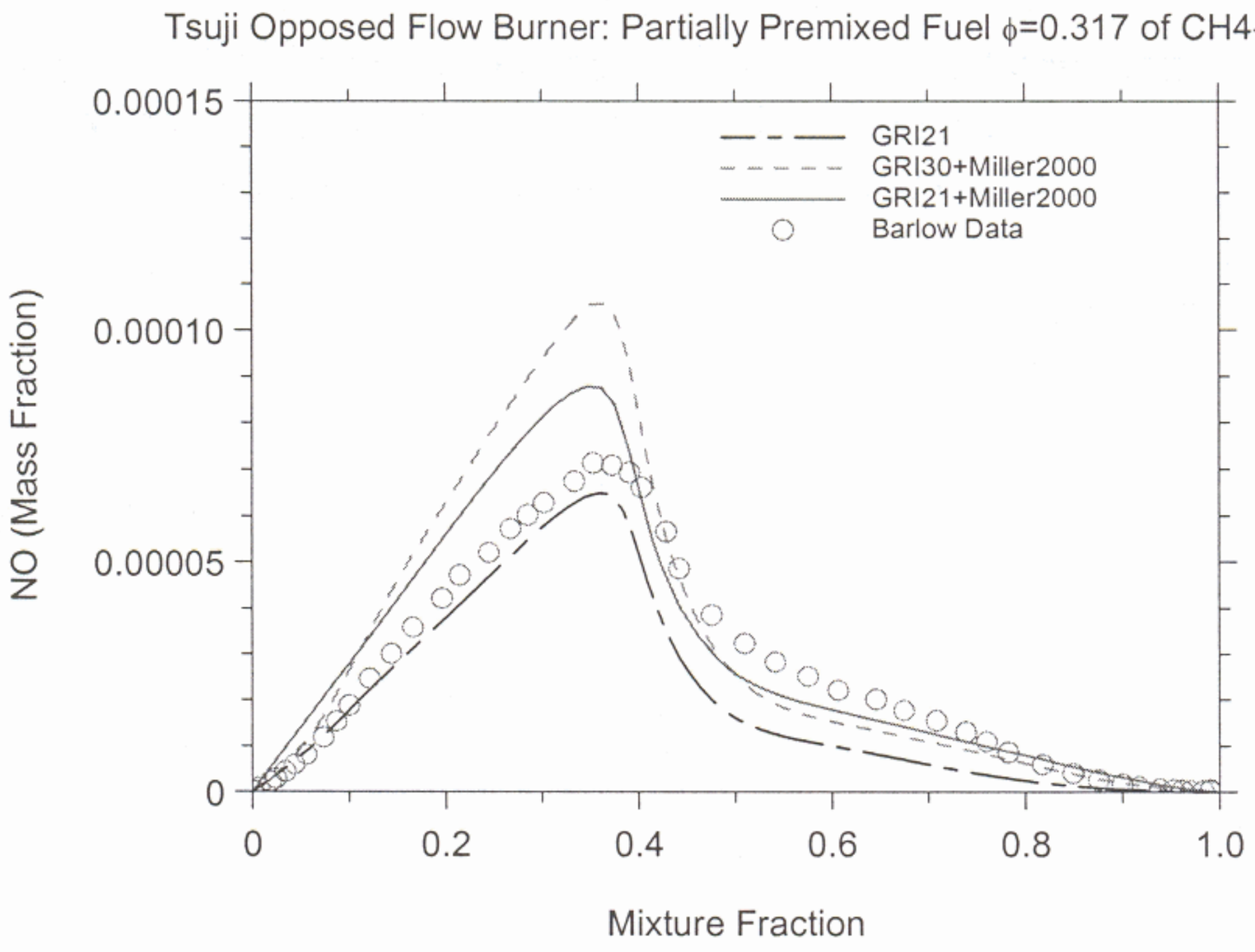

Figure 1 Comparison of NO predictions by three detailed mechanisms with data by Barlow showing that in the lean side GRI2.1 agrees best with the data. On rich side, GRI2.1+Miller2000 is seen best match with the data.

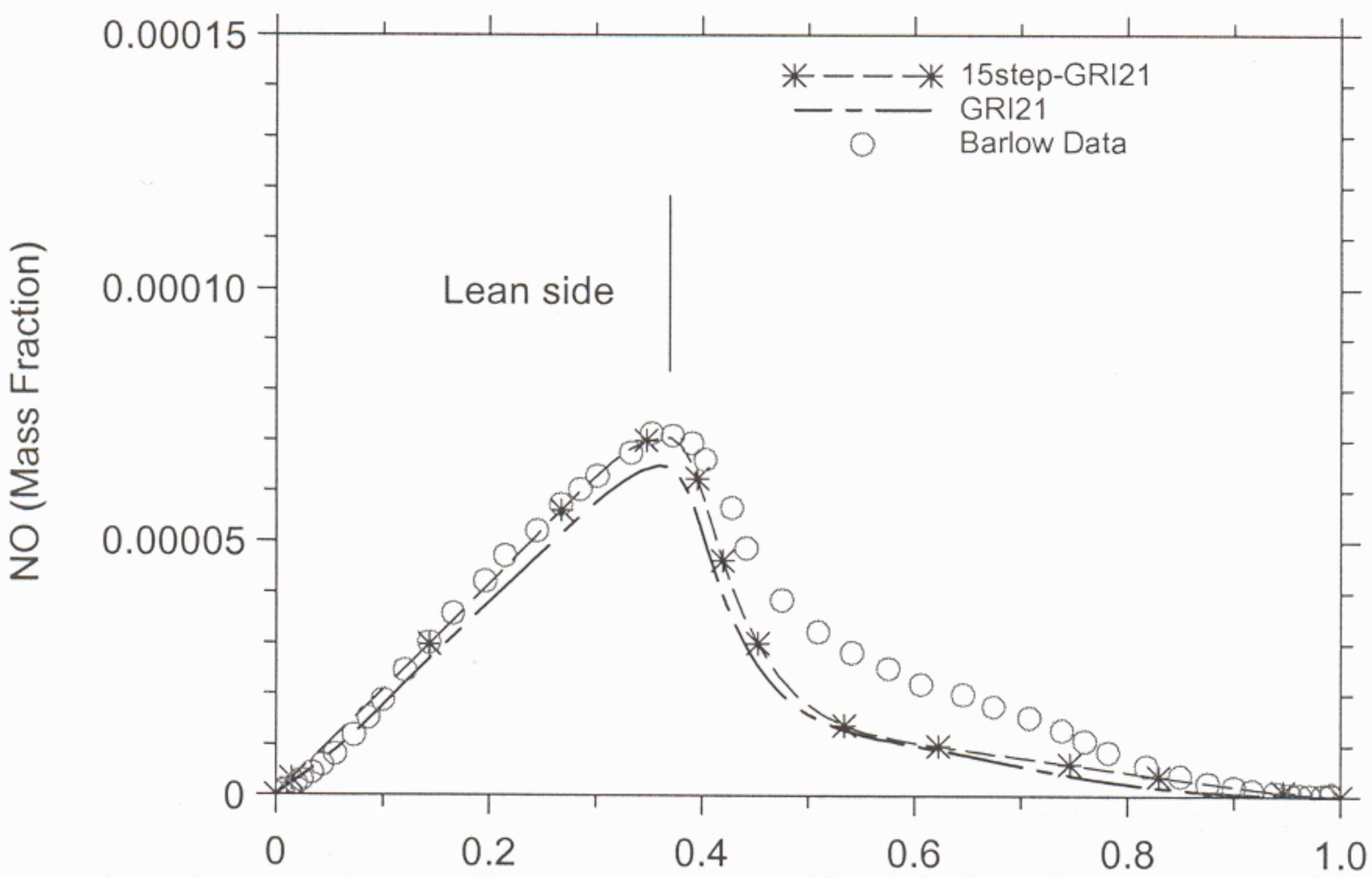

Figure 2 Comparison of NO predictions by a 15-step reduced chemistry with GRI2.11 and data by Barlow showing good agreement on the lean side.

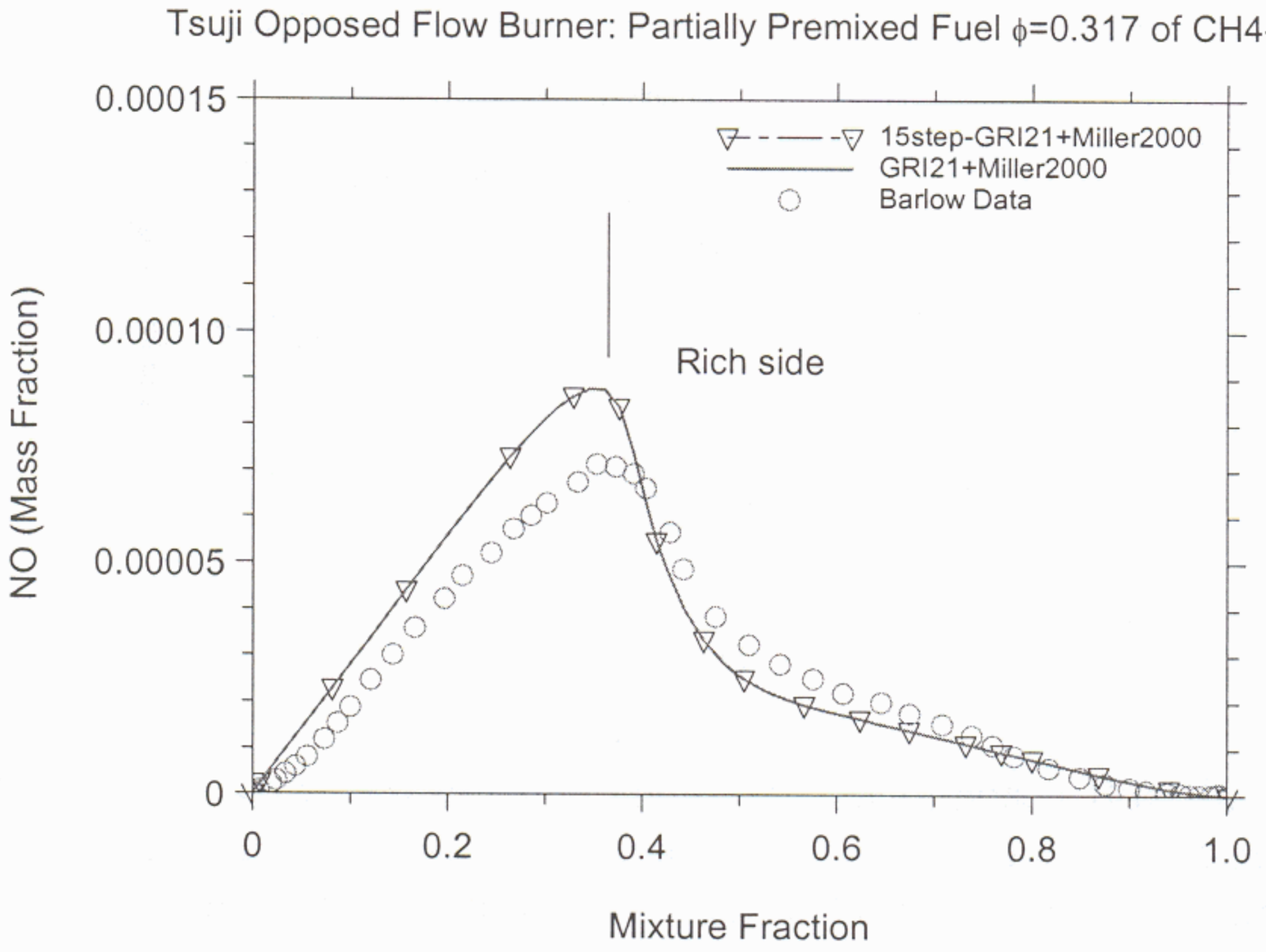

Figure 3 Comparison of NO predictions by a 15-step reduced chemistry with GRI2.11+Miller2000 and data by Barlow showing good agreement on the rich side.

Hydrogen-Air Combustion

For hydrogen-air combustion, a subset hydrogen mechanism of GRI2.11 was used as the base mechanism. The NO_x mechanism taken from Miller2000 was added to the base mechanism. A 7-step reduced chemistry was developed with this combined mechanism. Figures 4-7 assess the performances of the 7-step reduced mechanism showing overall good agreement with results obtained from the detailed mechanism.

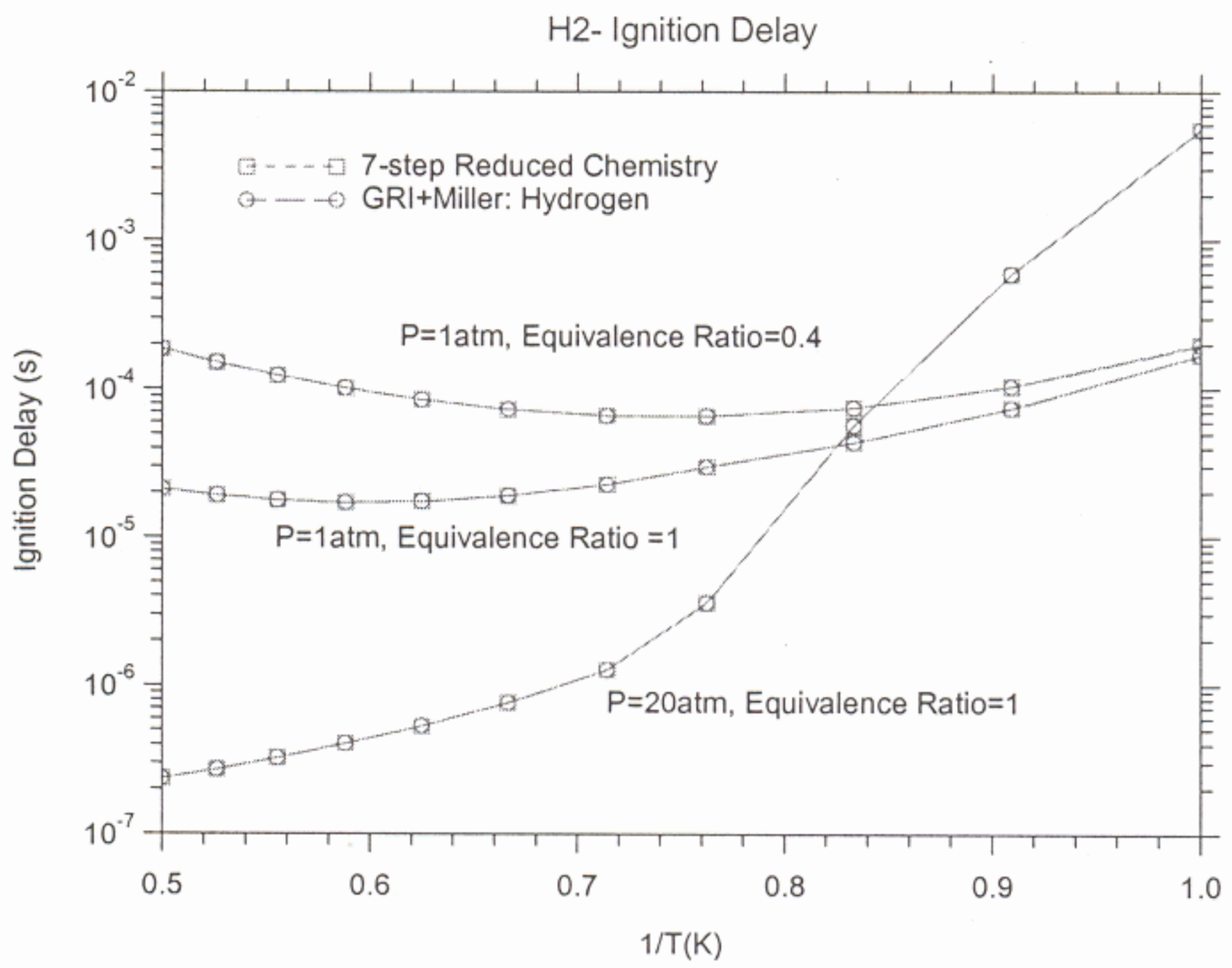

Figure 4 Ignition delay times under ambient and elevated pressures. Test cases include stoichiometric and lean mixture of equivalence ratio of 0.4. The 7-step reduced chemistry of H_2 predicts ignition delay in excellent agreement with those from the detailed mechanism based on GRI2.11 and NOx mechanism from Miller.

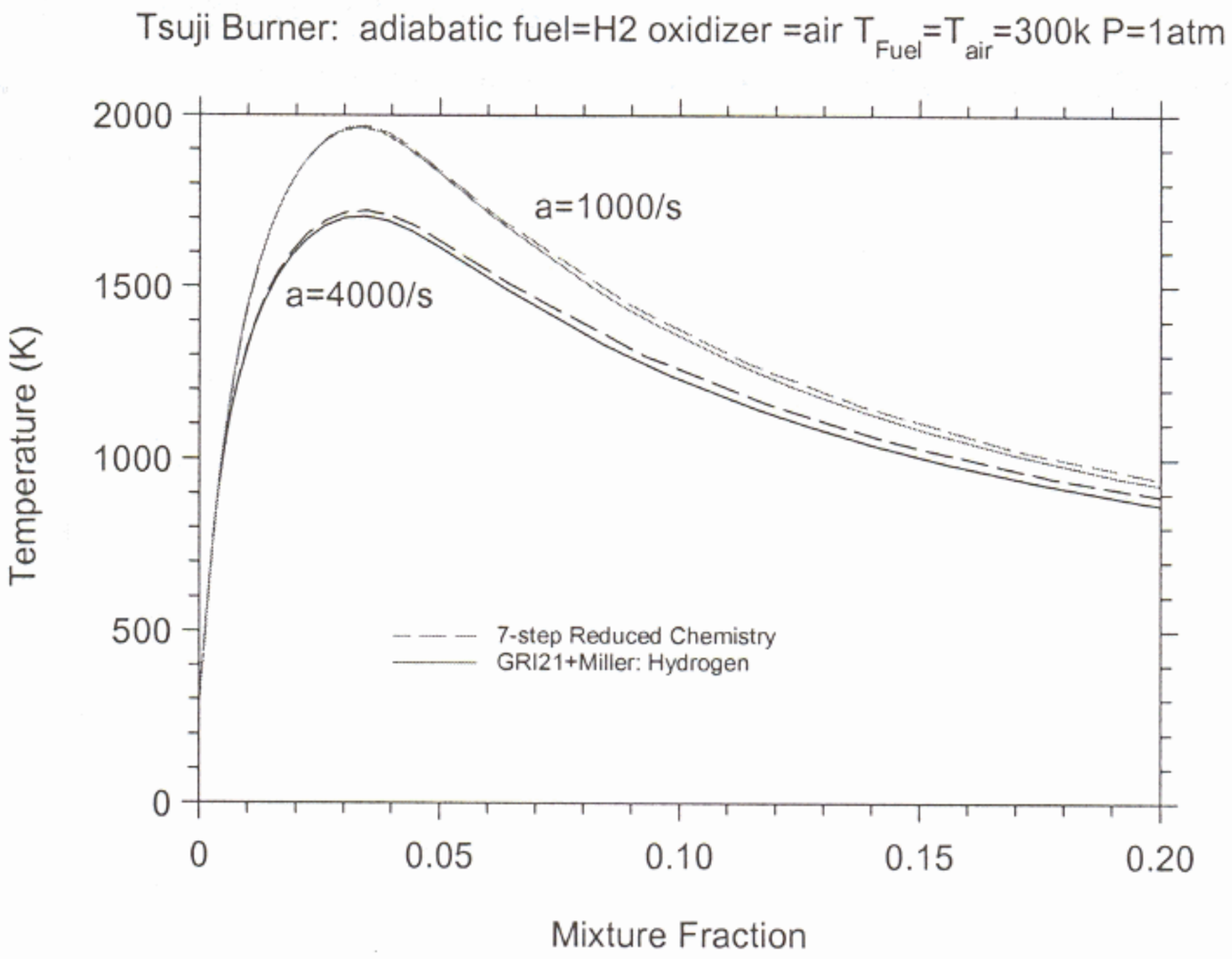

Figure 5 Validation of hydrogen reduced chemistry for opposed flow flames (Tsuji type burner) is carried at strain rates at 1,000/s and 4,000/s and the extinction limit is about 12,000/s. The predicted temperatures by the reduced chemistry and the detailed mechanism are in good agreement.

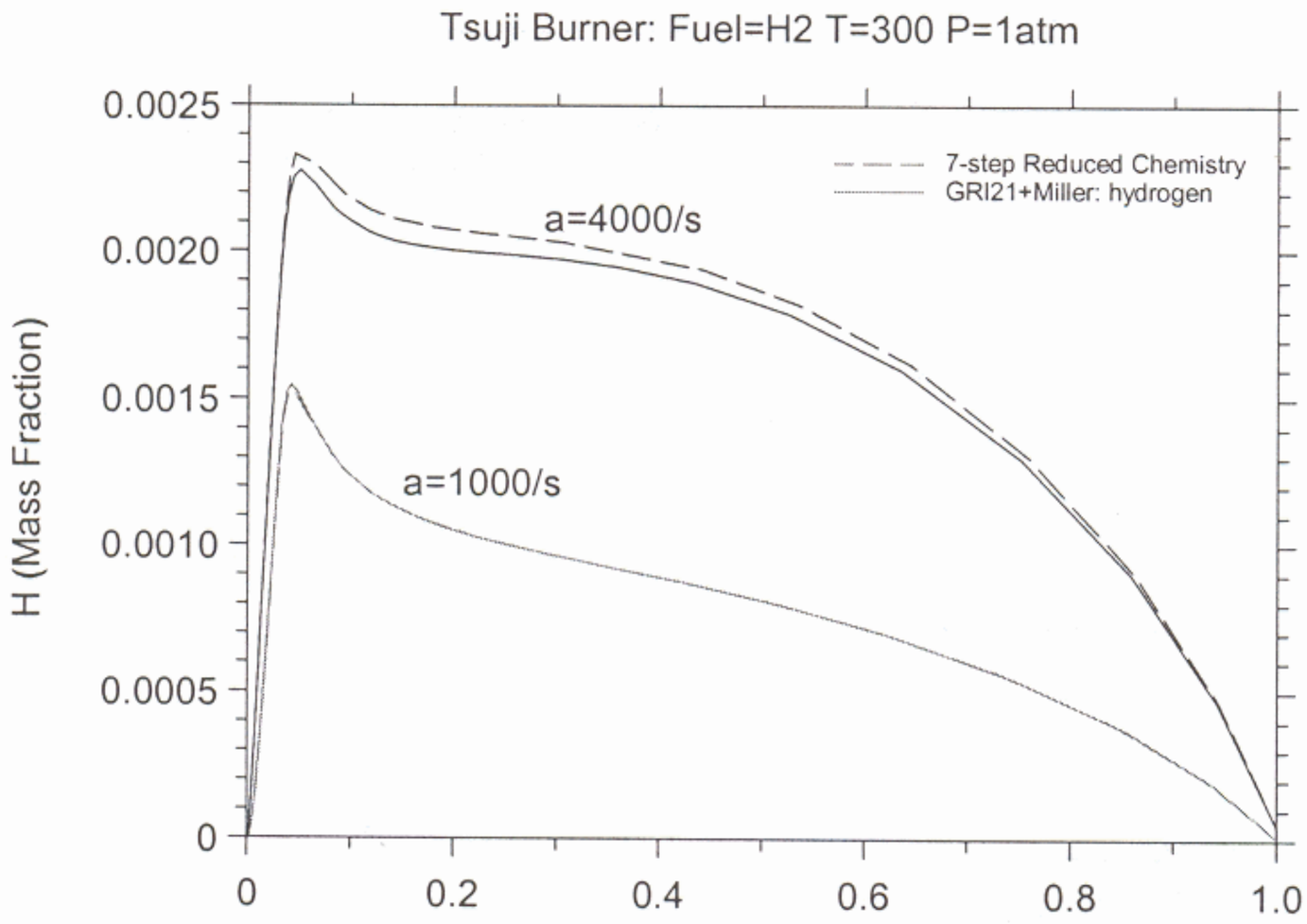

Figure 6 Validation of hydrogen reduced chemistry for opposed flow flames (Tsuji type burner) is carried at strain rates at 1,000/s and 4,000/s and the extinction limit is about 12,000/s. The predicted H radical concentrations by the reduced chemistry and the detailed mechanism are in good agreement.

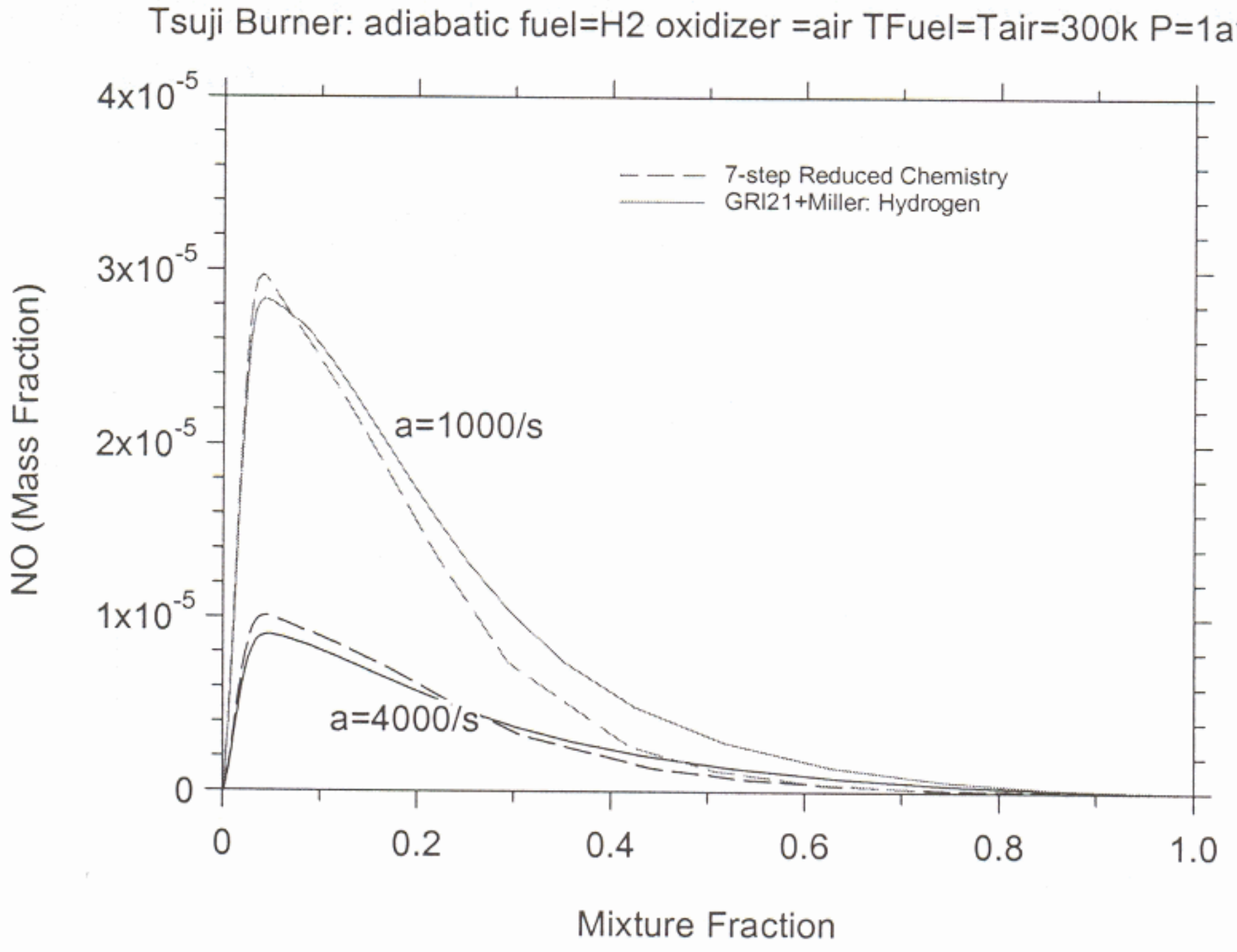

Figure 7 Validation of hydrogen reduced chemistry for opposed flow flames (Tsuji type burner) is carried at strain rates at 1,000/s and 4,000/s and the extinction limit is about 12,000/s. The predicted NO concentrations by the reduced chemistry and the detailed mechanism are in good agreement.

Propane-Air Combustion

A detailed propane-air combustion mechanism was compiled by CFDRC based on LLNL propane mechanism with NO_x chemistry. This mechanism was used for development of a 19-step reduced chemistry. The performances of this reduced chemistry were assessed first with PSR and results are presented in Figures 8 and 9.

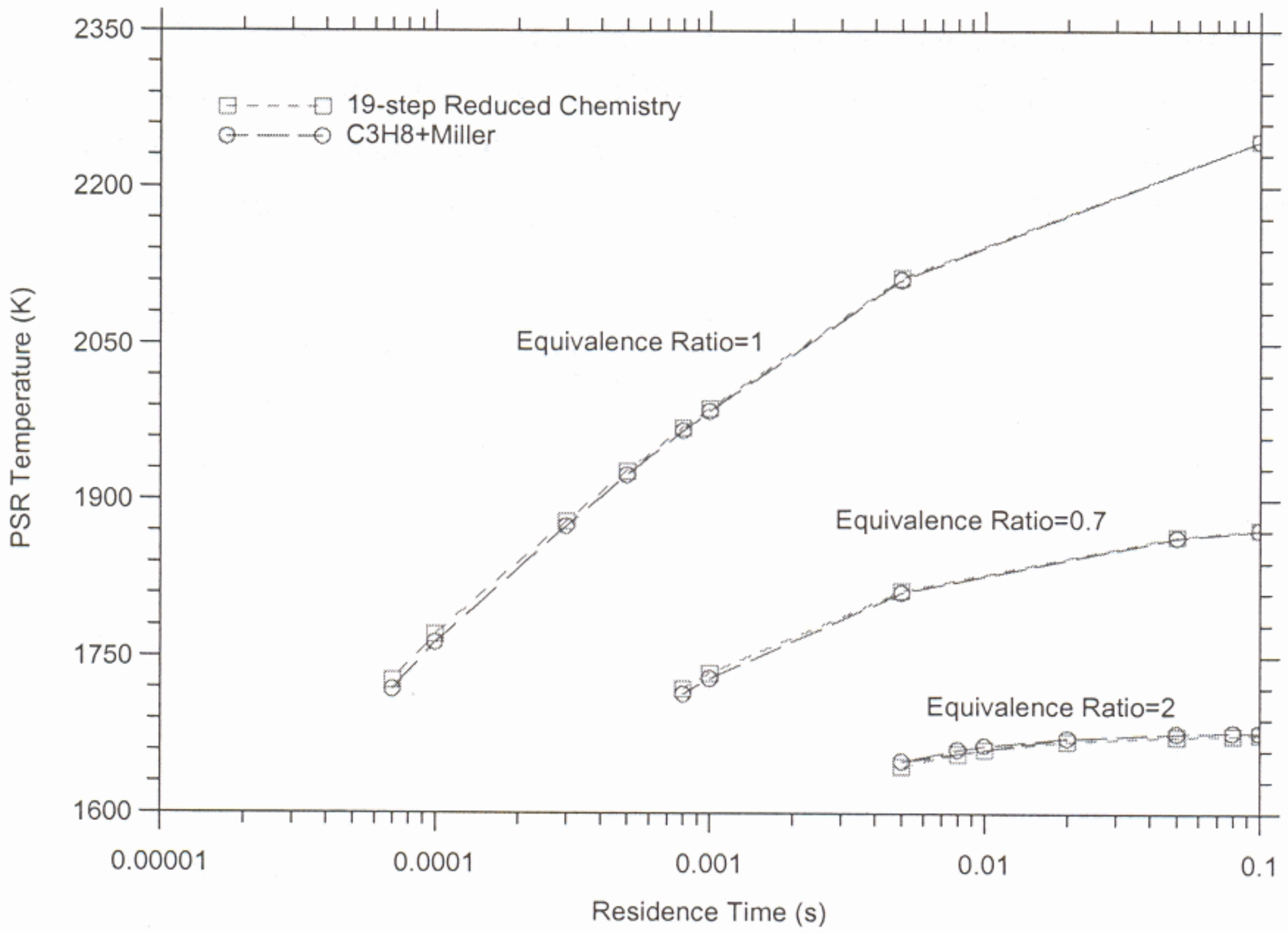

Figure 8 Comparison of predicted temperatures from a perfectly stirred reactor versus residence time for three different mixtures. The 19-step reduced chemistry gives temperatures within 10% of those from the detailed propane mechanism (from LLNL) and Miller's NOx mechanism.

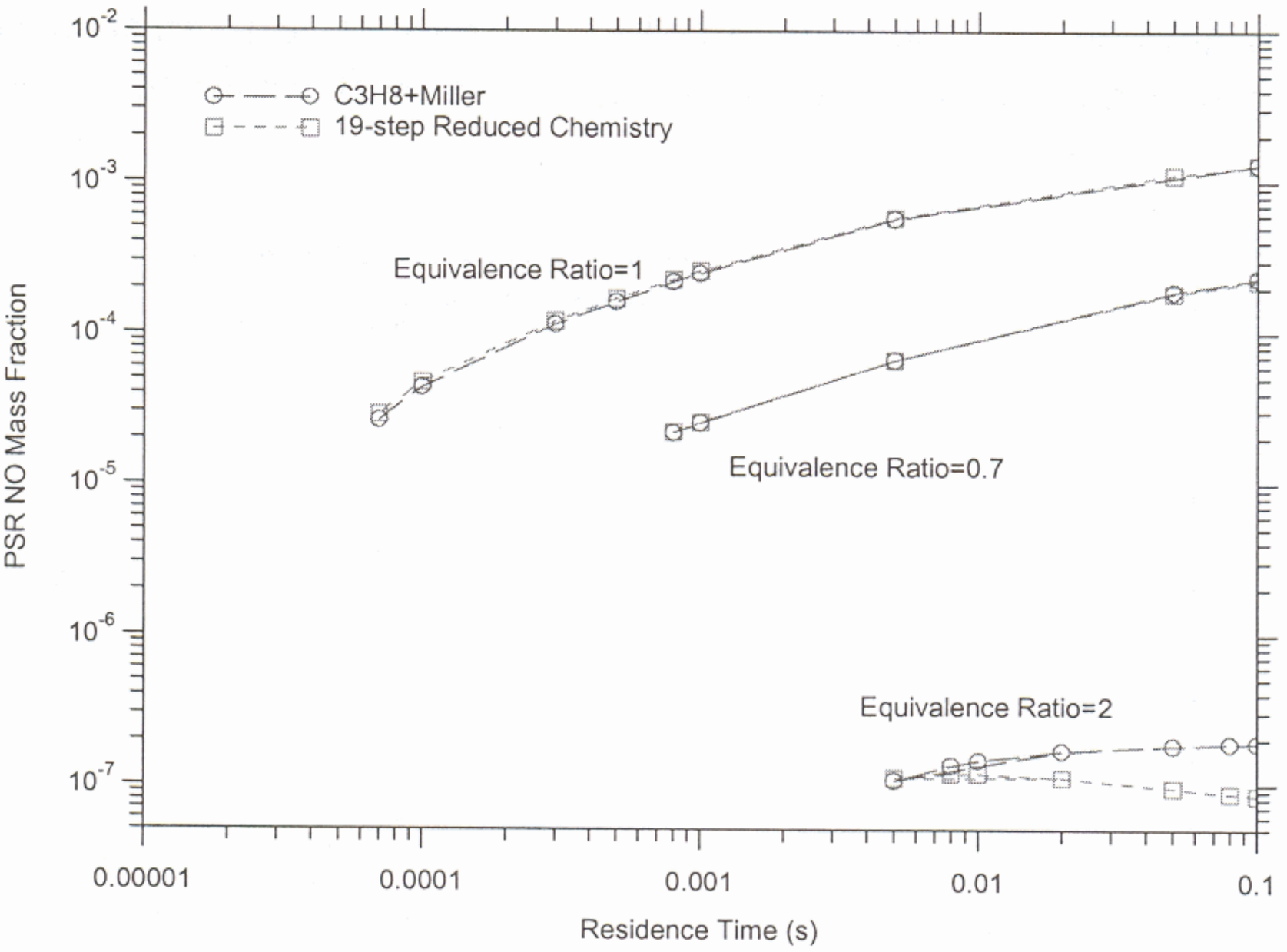

Figure 9 Comparison of predicted temperatures from a perfectly stirred reactor versus residence time for three different mixtures. The 19-step reduced chemistry predicts NOx level reasonable agreement with those from the detailed propane mechanism (from LLNL) and Miller's NOx mechanism. The worst case is seen for the rich mixture of equivalence ratio of 0.7; however, the NOx level is below 1ppm which is of negligible significance.

It is concluded from the comparisons that the 19-step performs very well for PSR over a wide range of residence times and equivalence ratios. Next, the reduced chemistry is tested for its accuracy in predicting autoignition delays. A detailed comparison is presented in Figures 10 and 11 showing good agreement with detail chemistry.

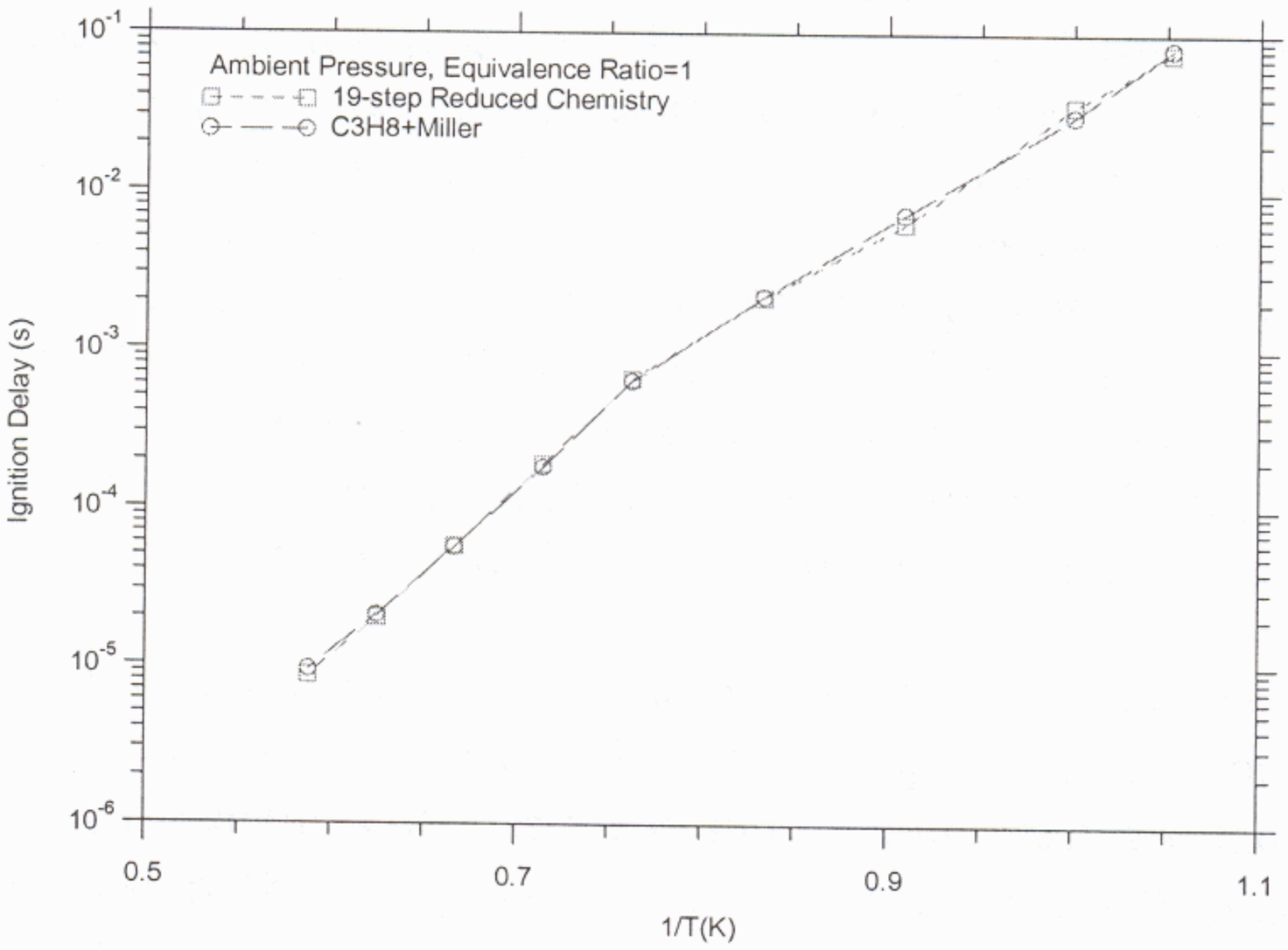

Figure 10 Comparison of ignition delay at ambient pressure versus temperature for stoichiometric mixture. The 19-step reduced chemistry predicts ignition delay in very good agreement with those from the detailed propane mechanism (from LLNL) and Miller's NOx mechanism.

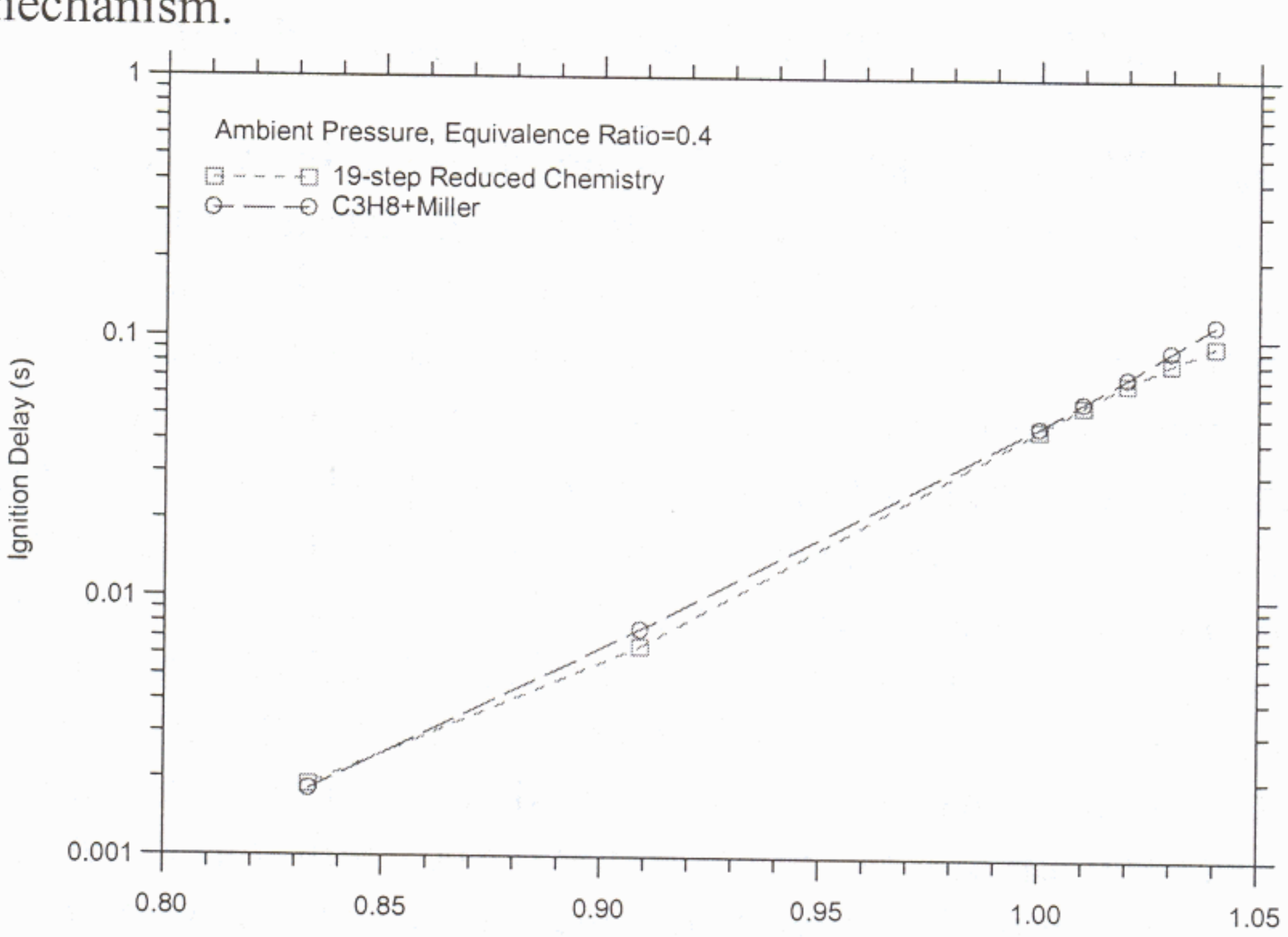

Figure 11 Comparison of ignition delay at ambient pressure versus temperature for a lean mixture of equivalence ratio of 0.4. The 19-step reduced chemistry predicts ignition delay in good agreement with those from the detailed propane mechanism (from LLNL) and Miller's NOx mechanism.

ISAT and ANN for Use in LES

Both memory and CPU time are the limiting factors to current applications of LES to predict complex chemical reactions. The use of reduced (or simplified) chemistry or simplification of chemical kinetics representation can alleviate these two factors as the total number of species is reduced. In addition to the use of reduced or simplified chemistry, additional speeding up can be achieved by using numerical methods for further decrease in CPU time. For example, several storage-based approaches have been developed in the past including In Situ Adaptive Tabulation (ISAT), Artificial Neural Networks (ANN) and polynomial fits. These techniques are suited for CFD using a fractional splitting scheme as the computed changes of chemical species over a certain period of time can be computed separately and stored for reuse later.

-ISAT: The essential idea of ISAT can be viewed as an inquiry process with the initial reactive scalars and time interval, Ψ^0, as the input and the changes of reactive scalars due to chemical reactions, $\Delta\phi$, as the output. An unstructured table (e.g., a binary tree) is constructed to store the changes of scalar properties, $\Delta\phi(\Psi^0)$. When an inquiry Ψ^q arrives, one locates the nearest point in the table, say, Ψ^p. If Ψ^q lies within an accuracy domain associated with Ψ^p (called the Ellipsoid Of Accuracy, EOA), the following linear approximation is used to calculate the changes of reactive scalars

$$\Delta\phi(\Psi^q) = \Delta\phi(\Psi^p) + \partial[\Delta\phi(\Psi^p)]/\partial\Psi \bullet (\Psi^q - \Psi^p).$$

The EOA is the region around Ψ^p such that $\varepsilon = \mathrm{Max}\{|\Delta\phi_I(\Psi^p) - \Delta\phi_I(\Psi^q)|/\phi_{i,nom}\} < \varepsilon_{tol}$, where ε is the maximum relative error, $\phi_{i,nom}$ is the value used for normalization, and ε_{tol} is a preset value for tolerance. If the point falls outside the EOA, a direct integration of chemical kinetics is performed and the outcome is used to evaluate ε. If ε is smaller than the preset value, the EOA is expanded to cover Ψ^q. If not, a new record is generated for Ψ^q. As the acceptable retrieval depends on ε_{tol}, the EOA decreases with decreasing value of ε_{tol} . In the PDF approach, an ISAT can be used and the results demonstrated for speeding up calculations by a factor of 20 –100 depending on the chemical mechanism and specific applications. As ISAT requires the computation and storage of Jacobian term $\partial[\Delta\phi(\Psi^p)]/\partial\Psi$ in building ISAT can be expensive in both CPU time and memory. For example, the memory requirement is about 50 MB for storing chemical kinetics with 20 species with an ISAT containing 10,000 nodes. Note that the memory requirement scales with the square of total number of species making ISAT quite expensive in terms of memory usage. Experiences with ISAT have revealed that the size of ISAT can grow with simulation especially for transient flames as chemical kinetics changes with time drastically. Dynamic trimming the ISAT is necessary for such applications and efficient programs must be developed to keep the computation task inexpensive. A recent analysis has revealed that the retrieval process places the most critical role in ISAT performances in term of CPU speed up factor. Improvements in binary search trees have shown further speed up as high as by a factor five under certain conditions.

-ANN: Applications of ANN for modeling combustion chemistry have been reported in many previous works with the intent of building ANN for the entire regime of turbulent combustion. However, it was found that the retrieved information can be inaccurate. Recent developments focus on fitting data in a local flame zone defined either by the mixture fraction or by the temperature. The inquiry Ψ^q, which may be specified by mixture fraction, reactive scalars, temperature, and time interval, is used to compute the changes of reactive scalars using a stiff solver. A large number of inquiries along with their changes are used to train the ANN. The outcomes are the weight values that are used for computing the output of each neuron according to

$$O_i^L = F\left(\sum_{j=1}^{n_{n,L}} w_{ij}^L O_j^{L-1} + \beta_i^L\right) \quad \text{for i} = 1,..,\text{n}_{\text{n.L}},$$

where O_i^L is the output of the *i-th* neuron of the *L-th* layer, w_{ij}^L represents the weight value for connecting the *j-th* neuron of the *(L-1)*-th layer and the *i-th* neuron of the *L*-th layer, β_i^L is the bias value, $n_{n,L}$ is the total number of neurons in the *L-th* layer, and F is the transfer function. Experiences using ISAT show that a large amount of storage may be needed if the chemical states are widely spread. ANN can be used for dramatically reducing the memory demands as sketched in Figure 12. Basically, data stored in ISAT is used to train ANN and the outcome is stored. This combined ISAT+ANN strategy is most useful for parametric studies as repeated calculations are performed with minor changes. The accuracy of ANN can be an issue that desires further studies. For example, past experiences revealed that the information retrieved from ANN can be erroneous if the inquiry point is way off the area that ANN has been trained. Certain strategies need to be developed so that the retrieved information is checked before it is used in the modeling. During the contract period, examples of ISAT and consultation were provided to CFDRC.

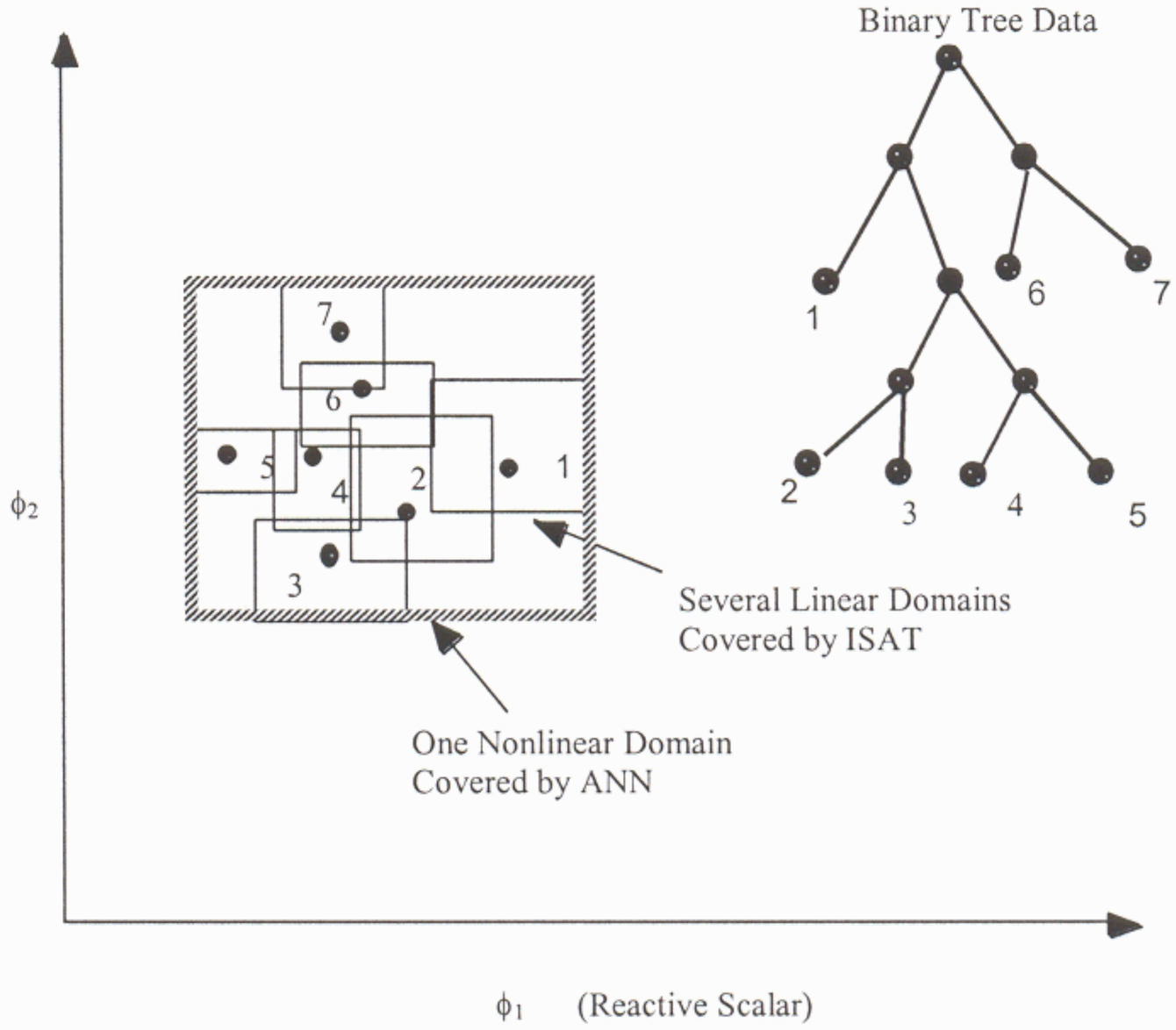

Figure 12 Artificial Neural Networks (ANN) can be used to fit ISAT for significant saving in memory. For instance, ANN can be used to include shaded area containing several domains of ISAT nodes from 1 to 7.

Summary

The complexity of sub-models required for modeling turbulence chemistry interactions in turbulent combustion can range from simple fast chemistry to one-dimension turbulence model. For LES, the demand of computer resources limits the degree of complexity in using these models. Approaches for speeding up computation for realistic chemical kinetics must be taken to make LES feasible for engineering problems. Various methods, including ILDM, QSSA, ANN, and others, will need further development in order to provide at least an order of magnitude of saving in memory requirement and computational speed. Combination of reduced chemistry with storage-based methods holds great potential to make the LES feasible with complex chemistry.